

**School of Chemical and Petroleum Engineering
Department of Petroleum Engineering**

**Shale Gas Prospectivity Studies in the Perth Basin,
Western Australia**

Hanieh Jafary Dargahi

**This thesis is presented for the Degree of
Doctor of Philosophy of
Curtin University**

May 2014

Declaration

To the best of my knowledge and belief this thesis contains no material previously published by any other person except where due acknowledgment has been made.

This thesis contains no material which has been accepted for the award of any other degree or diploma in any university.

Signature:

Date:

Summary

The Permian Carynginia Formation and the Late Triassic Kockatea Shale are prospective shale gas resources in the Perth Basin. A thorough knowledge of some of the key properties of these formations helps to better understand about the limits on the distribution and the volume of gas along with those reservoir characteristics having an effect on gas production and stimulation techniques. The properties included are stratigraphy, structure, lithofacies/rock types, hydrocarbon potential through identifying the organic carbon content and thermal maturity, reservoir quality, ability to fracture/effective fracture stimulation, and sweet spots.

The structural history of both formations is covered by the occurrence of the extension in the Early Permian. The thinning of Permian Carynginia Formation to the south indicates a limited sediment supply, whereas the thinning of Triassic Kockatea Shale to the north is interpreted by the non-deposition or the occurrence of Early Jurassic erosion. The dominance of argillaceous marine sediments in the Carynginia Formation suggests deposition under stable conditions of subsidence, along with the abundant accommodation space. The Kockatea Shale resulted from the deposition under marine transgression conditions. The marine Carynginia and Kockatea formations in the Northern Perth Basin correlate with their coeval continental deposits in the Southern Perth Basin.

The stratigraphic composition of both formations contains sandstone, siltstone and organic rich shale, and the formations have the dark organic-rich shales in the basal members. There is a deeper water shale member close to the base of Carynginia Formation which is overlain by a shallow water shelf limestone unit. The Basal Kockatea Shale (Hovea Member) is a distinct organic rich zone consisting of shelly storm beds, sandy siltstone, and fossiliferous mudstone.

Specific lithological facies were identified based on the external properties of the shale rocks which have been diagnosed on the available cored intervals. These properties consist of fabrics and the subsequent petrographical and mineralogical analyses such as x-ray diffraction (XRD) and Fourier transform infrared spectroscopy (FTIR). Petrographical analysis revealed the detailed textural relationship within the rock, in addition to the mineral composition in the preliminary identification of the depositional environment.

In terms of organic geochemistry, different shale attributes such as kerogen type, total organic carbon (TOC) content, thermal maturity, and formation thickness control the gas volume in the considered plays. Total organic content ranges from 1-15 wt% in the Carynginia Formation, and 1-4 wt% in the Kockatea Shale. Carynginia kerogen is type III with minor type II, whilst the mixed kerogen type II/III is diagnosed for the Kockatea Shale. The Kockatea's thickness varies from 50-1100 m, with thickest part in the Eastern Perth Basin. The Carynginia's thickest section in the Western Perth Basin, ranges from 50-650 m. Despite differences in the geochemical properties, both formations are predicted to be qualified shale gas reservoirs due to the desired organic richness, organic maturity and sufficient thickness in organic rich strata.

Petrophysical analyses present similar outcomes in terms of mineralogy/clay content and organic richness within shale intervals. Fracability of shale plays were identified with respect to their geomechanical characteristics (Young's Modulus and Poisson's Ratio), calculated on the acoustic slowness and bulk density well log measurements. Geological analyses on the brittleness of the shale plays through the proportion of clays-carbonates-quartz confirm the fragility trends in petrophysical studies across the Perth Basin.

To discern the favorable environments for depositing shale gas reserves, detailed internal stratigraphy of shale plays were established based on diagnosis of the lithofacies, cyclical stacking patterns, transgressive surfaces

of erosion (TSE), and condensed sections (CS's). The framework supports deposition mainly in a marine environment with minor regressions.

This study defines the stratigraphic zones within Kockatea and Carynginia formations that have the desired mineralogy, depositional environment, organic richness, kerogen maturity and natural fractures across the basin. The designation of the shale gas sweet spots of the Perth Basin is the ultimate aim which is obtained by mapping the key properties of shale plays including TOC, thermal maturity, thickness and fracability.

Acknowledgements

I owe a debt of gratitude to many people who helped me to flourish both academically and personally.

First I would like to thank my supervisor, Dr Reza Rezaee, for giving me the opportunity to study in Curtin University that has exposed me to numerous opportunities that brings me a bright future. I thank Reza for the guidance and freedom he has given me when I needed time to reschedule my research program.

I would like to thank the Curtin University Shale Gas Consortium sponsors, the Western Australia Department of Mines and Petroleum, Buru Energy, Carnarvon Petroleum, Norwest Energy, and Woodside for financial support that made my project a success. I acknowledge the use of equipment, scientific and technical assistance of the Curtin University Electron Microscope Facility, which has been partially funded by the University, State and Commonwealth Governments.

I greatly thank Dr Bobby Pejcic, for his kind help in analysing IR spectra of my samples. I greatly admire his passion for science. I would like to gratefully thank Dr Catherine Keally and Ms Elaine Miller for their kind help in the centre for material research of Curtin University, who helped me a lot in XRD quantitative phase analysis and SEM imaging. I wish to thank Mr Michael Verrall for his generosity to teach me how to analyse XRD clay fraction despite his busy schedule. My sincere thanks go to Mr Rao Danish for his cooperation in the electrofacies studies and Mr Roger Savage for editing this dissertation.

I would like to warmly thank, Dr Ali Saeedi, for his support in my lab studies. My heartfelt gratitude goes to my colleagues and the excellent staffs of the petroleum engineering department who made the work place very pleasant for me. Thanks for the amazing times we had together and I wish that our friendship be continued in the future.

I owe my profound gratitude to my beloved family for their continued support. My parents , Shahla and Davud, who raised me to everything I am today, my lovely sister and brother , Hedieh and Alireza, for the kind support and happiness they have brought to me during my life, and my wonderful partner, Cameron White, for his limitless support and kindness. I would like to dedicate this thesis to my cherished family without whom none of my success would be possible.

Table of Contents

Declaration	i
Summary	ii
Acknowledgements	v
List of Figures	xi
List of Tables	xvii
1. Introduction	1
1.1. Shale Gas resources in Australia	1
1.2. Background.....	3
1.3. General Characterisations of Shale Plays	4
1.3.1. Geologic Controls on Shale Gas Reservoirs.....	5
1.3.2. The Features of Organic Matter within Shale.....	7
1.3.3. Petrophysical Properties of Shale Gas Reservoirs.....	8
1.3.4. Mineralogical Variations of Shale Plays	10
1.3.5. Stratigraphic Concepts of Shale Gas Reservoirs	12
1.3.6. Depositional Environment of Shale Plays	14
1.4. The Scope	15
2. General Geology of the Perth Basin	16
2.1. Regional Setting	16
2.2. Stratigraphic Features	19
2.3. Structural Features.....	22
2.4. Prospective Shale Gas Formations	24
2.4.1. Geological Distribution and Thickness	27
3. Geological Studies	31
3.1. Visual Core Description	31
3.1.1. Results	32
3.2. Lithofacies Description	33
3.2.1. Black Shale	33
3.2.2. Pyritic Mudstone.....	34
3.2.3. Siliceous Mudstone.....	35
3.2.4. Calcareous Mudstone.....	36

3.2.5. Fossiliferous Mudstone.....	36
3.2.6. Bioturbated Mudstone	37
3.2.7. Wavy Laminated Deposit	37
3.2.8. Shaly-sandy Interlaminated Mudstone	39
3.2.9. Shaly Siltstone	39
3.2.10. Siliceous Calcareous Mudstone.....	39
3.2.11. Sandy-silty Interlaminated Deposit	40
3.3. Thin Section Petrography	42
3.3.1. Results	42
3.4. Scanning Electron Microscopy (SEM).....	45
3.4.1. Results	46
3.5. X-ray Diffraction Technique (XRD)	48
3.5.1. Results	50
3.5.2.1. XRD Whole Rock (XRD Bulk)	50
3.5.2.2. XRD Clay Fraction	53
3.6. Fourier Transform Infrared Spectroscopy (FTIR)	53
3.6.1. Techniques.....	53
3.6.2. Results	54
3.7. Depositional Settings.....	57
3.7.1. Carynginia Formation.....	58
3.7.2. Kockatea Shale	58
3.8. Fracability and Mineralogy	60
3.8.1. Results	61
4. Geochemical Studies	64
4.1. Total Organic Carbon (TOC)	64
4.1.1. Rock-Eval Pyrolysis	64
4.2. Kerogen Type	66
4.3. Thermal Maturity.....	68
4.3.1. Rock-Eval Pyrolysis (Tmax)	68
4.3.2. Vitrinite Reflectance Measurement (Ro)	70
4.4. Relative Hydrocarbon Potential (RHP)	71
5. Petrophysical Studies.....	74
5.1. Lithofacies in Non-cored Wells.....	74

5.1.1. Gamma Ray response of Lithofacies	75
5.1.2. Electrofacies	76
5.2. TOC from Logs	77
5.3. Fracability from Logs	81
6. Sequence Stratigraphy	85
6.1. Introduction	85
6.2. Parasequence Identification	88
6.3. Sequence Stratigraphic Framework.....	90
6.3.1. Stratigraphic Intervals of Hovea Member, Kockatea Shale	90
6.3.1.1. Stratigraphic Interval 1	90
6.3.1.2. Stratigraphic Interval 2.....	91
6.3.1.3. Stratigraphic Interval 3	91
6.3.1.4. Stratigraphic Interval 4.....	93
6.3.1.5. Stratigraphic Intervals 5	93
6.4. Areal Extend of Stratigraphic Intervals	93
7. Discussions, Conclusions, and Recommendations.....	96
7.1. Discussions and Conclusions	96
7.1.1. Thickness and Geographic Distribution	96
7.1.2. Lithofacies	97
7.1.3. Organic Richness and Kerogen Maturity	100
7.1.4. Fracability	101
7.1.5. Sequence Stratigraphy	101
7.2. Recommendations	103
References	104
Appendix	
A.1. XRD Clay Fraction Patterns	131
B.1. TOC Values of the Kockatea and the Carynginia Formations in the Perth Basin.....	135
B.2. Tmax and Remaining Potential Values of the Target Formations in the Perth Basin.....	136
B.3. The Vitrinite Reflectance Measurement for the Kockatea Shale and the Carynginia Formation	137

B.4. The Connection between the Kerogen Type and Maturity with Genetic Hydrocarbon and Depositional Environment	137
C.1. Gamma Ray Response of Lithofacies.....	138
C.2. Electrofacies of the Kockatea Shale	144
C.3. Electrofacies of the Carynginia Formation.....	149
C.4. Studied Cross Sections in the Kockatea Shale, Perth Basin.....	155
C.5. Correlation of the Electrofacies in the Kockatea Shale across the Perth Basin.....	156
C.6. Studied Cross Section for the Carynginia Formation	164
C.7. Correlation of the Electrofacies in the Carynginia Formation across the Perth Basin.....	165
C.8. TOC Values of the Kockatea and the Carynginia Formations in the Perth Basin, Acquired by Their Geomechanical Properties (Young's modulus and Poission's ratio) from Logs.....	167

List of Figures

Figure 1.1 The figure displays shale gas prospective areas in the Western Australia with two major potential basins of Perth in the southwest of Australian margin and Canning in the north part of Western Australia	2
Figure 1.2 The figure indicates shale characterising by breaks into parallel bedding along their thin laminae that commonly ranges in thickness less than one centimeter	5
Figure 1.3 Different pore throat and pore size within conventional and unconventional reservoirs, the graph shows finer pore throat for shale gas unconventional reservoir compared to tight gas reservoirs.	6
Figure 1.4 The graph illustrates the impact of kerogen type on gas sorption capacity within shale	8
Figure 1.5 Plotting mineralogic ternary diagrams for successful shale plays of North America such as Barnett Shale and Eagleford Shale, displaying higher amount of quartz or carbonate than clay minerals which makes them suitable for fracture stimulation	11
Figure 1.6 Schematic comparison of proximal and distal parasequences within shale succession	13
Figure 1.7 The figure shows different depositional environment along with their level of dissolved oxygen values	15
Figure 2.1 Basin subdivisions and tectonic elements of (the right) the onshore Northern Perth Basin, and (the left) the central and Southern Perth Basin.....	18
Figure 2.2 North-south stratigraphic features of the Perth Basin, displaying the petroleum system and accumulations within the basin, along with lithology and shifting the Permo-Triassic intervals form north towards south	21
Figure 2.3 North-south gravity model associated with structural section across the Perth Basin	23
Figure 2.4 Isopach maps of the Kockatea Shale (left) and Carynginia Formation (right).....	29
Figure 3.1 The location of studied wells containing available cores of the Kockatea Shale (red marks) and Carynginia Formation (blue marks), modified form Geoscience Australia website	32
Figure 3.2 Core photographs of lithofacies, displaying various sedimentary structures (A) black shale from Carynginia Formation at the depth of 2275.54-2275.68 m, Woodada Deep-1 (B) pyrite nodule (yellow arrow) and streaks of white crystalline calcite (red arrows) within black shale from	

Kockatea Shale at the depth of 3817.10-3817.20 m, Redback-2 (C) pyritic mudstone lithofacies with greenish brown colour from Carynginia Formation at the depth of 2278.81-2278.90 m, Woodada Deep-1 (D) higher magnification of Pyrite nodule from Kockatea Shale at the depth of 3798.24-3798.33 m, Redback-2 (E)pyrite vein within pyritic mudstone from Carynginia Formation at the depth of 3800.55-3800.67 m, Woodada Deep-1 (F) the replacement of pyrite in fossils (yellow arrows) from Carynginia Formation at the depth of 2285.27-2285.40 m, Woodada Deep-1 (G) core photo of siliceous mudstone from Kockatea Shale at the depth of 3832.75-3832.80 m, Redback-2. The bright colour within cores displays siliceous into gray brown clay matrix (H) calcareous mudstone from Kockatea Shale at the depth of 3804.23-3804.37 m, Redback-2 (I) the sparry calcite replaced burrow structure (yellow arrow) from Carynginia Formation at the depth of 2823.65-2823.75 m, Woodada Deep-1 35

Figure 3.3 Core photographs of lithofacies display (A) the compacted thin-walled brachiopods within fossiliferous mudstone from Kockatea Shale at the depth of 3794.81-3794.90 m, Redback-2 (B) Shelly fragmented mudstone from Carynginia Formation at the depth of 276.21-276.33m, Jurien-1 (C) bioturbated mudstone with burrowing structure (yellow arrows) which cut the deposited lamination at the depth of 2369.30-2969.43 m, Woodada deep-1 (D) bioturbated mudstone, the bioturbation has largely destroyed the initial depositional environment from Carynginia Formation at the depth of 2478.64-2478.72 m, Jingemia-4. (E) horizontal bedded and bioturbated sandstone from Carynginia Formation at the depth of 1619.57-1619.77 m, Dongara-23 (F) bioturbated sandstone from Carynginia Formation at the depth of 1495.76-1495.84 m, Beharra-2 (G) bioturbated and burrowed mudstone from Carynginia Formation at the depth of 2378.86-2378.98, Woodada Deep-1 (H) wavy laminated deposit, the photo indicates lenticular wavy lamination structure in siltstone (red arrows) from Carynginia Formation at the depth of 1655.32-1655.46 m, Dongara-12 (I) convolute bedded and lenticular bedded sandstone from Kockatea Shale at the depth of 1424.80-1424.92 m, Cliff Head-4. 38

Figure 3.4 Core photographs displaying (A) the interlaminations of shale and fine-grained sandstone related to shaly-sandy interlaminated mudstone from Kockatea Shale at the depth of 91.44-91.55 m, Jurien-1(B) parallel and crossed-bedded sandstone from Carynginia Formation at the depth of 1724.61-1724.81 m, Dongara-1(C) parallel bedded medium to coarse-grained sandstone from Carynginia Formation at the depth of 1494.30-1494.39 m, Beharra-2 (D) core photo of shaly siltstone lithofacies showing the lithofacies in form of silt laminations within shale from Kockatea Shale at the depth of 2267.13-2267.19 m, Arrowsmith-1(E) the light to dark gray interlaminations of siliceous calcareous mudstone from Kockatea Shale at the depth of 1975.40-1975.64 m, Hovea-3 (F) the skeletal components filled

by sparry calcite (red arrows) within siliceous calcareous mudstone at the depth of 1972.74-1972.97 m, Hovea-3 (G) the interlamination of sandstone and siltstone related to sandy-silty interlaminated deposit from Kockatea Shale at the depth of 1414.95-1415 m, Cliff Head-4 (H) the lenticular structure of sandstone in siltstone for sandy-silty interlaminated deposit lithofacies from Kockatea Shale at the depth of 1413.64-1413.78 m, Woolmulla-1 41

Figure 3.5 Thin section photomicrographs of (a) Black shale that displaying the lithofacies composition; clay minerals (dark brown), fine grained quartz (white), mica (light brown). The photo is taken with plain polarized light at a low magnification of 2.5x from Kockatea Shale at the depth of 3819.32 m, Redback-2 (B) pyritic mudstone, showing an opaque framboidal pyrite, crossed polarized light at high magnification of 20x from Kockatea Shale at the depth of 3798.82 m, Redback-2 (C) siliceous mudstone, representing high values of detritus quartz in silt and coarser sizes taken at a low magnification of 2.5x with plain polarized light from Kockatea Shale at the depth of 2233.30, Yardarino-1 (D) Calcareous mudstone, illustrates the detrital and autochthonous calcite with minor silica content into the clay matrix, captured with plain polarized light at a low magnification of 2.5x from Kockatea Shale at the depth of 3821.67 m, Redback-2 (E) fossiliferous mudstone, displaying brachiopod arms within clay matrix along with phosphatic Oolitic, taken with crossed polarized light with magnification of 2.5x from Kockatea Shale at the depth of 3792.55 m, Redback-2 (F) the photomicrograph showing a Lower Triassic foraminifera, taken with plain polarized light with magnification of 10x from Kockatea Shale at the depth of 3805.92 m, Redback-2 (G) bioturbated mudstone, there is no special character for this lithofacies thin section image, captured with crossed polarized light at magnification of 5x from Carynginia Formation at the depth of 2374.86 m, Woodada Deep-1 (H) wavy laminated deposit, the image displaying a wavy structure in the lithofacies at a low magnification of 2.5x with plain polarized light from Carynginia Formation at the depth of 1682.04, Dongara-1 (I) shaly siltstone, the photomicrograph indicates the scattering of silt in shale. The image is taken with plain polarized light at a low magnification of 2.5x from Kockatea Shale at the depth of 2725.04 m, ejarno-1 (J) shaly-sandy interlaminated mudstone, displaying the obvious lamination of shale and fine-grained sandstone, the image is taken with plain polarized light at low magnification of 2.5x from Kockatea Shale at the depth of 2938.55 m, North Erregulla-1(K) siliceous calcareous mudstone, the photomicrograph illustrates the presence of carbonate and quartz components; quartz particles represents poor sorting and roundness, captured with plain polarized light at magnification of 10x from Kockatea Shale at the depth of 2233.30-2233.31 m, Yardarino-1(L) sandy-silty interlaminated deposit, thin section petrography indicates special alignment

within lithofacies. The image is taken with crossed polarized light at a low magnification of 2.5x from Kockatea Shale at the depth of 1414.97m, Cliff Head-4..... 44

Figure 3.6 The SEM images of (A) black shale, the image showing the scattering of clays in Kockatea Shale at the depth of 3819.32-3819.36 m, Redback-2 (B-C) pyritic mudstone which displaying rhombohedral structure of pyrite, in terms of recognition of pyrite SEM is undoubtedly the most successful way. The images are taken from Kockatea Shale at the depth of 3798.82-3798.87 m, Redback-2 (D) siliceous mudstone, ascertaining a special alignment in clays, red arrow showing rhombohedral pyrite crystals. The SEM image is taken from Kockatea Shale at the depth of 3832.75-3832.80 m, Redback-2 (E) Calcareous mudstone, showing the lithofacies without any especial alignment. Depth of 3834.5-3834.55 m, Redback-2 (F) Fossiliferous mudstone, the distribution of fossils and pyrite displaying in the image from Kockatea Shale at the depth of 3792.55 m, Redback-2 (G) Bioturbated mudstone, the turbulence is nearly recognizable in the image, at the depth of 2374.84-2374.87 m, Woodada Deep-1(H) wavy laminated deposit, due to identifying this lithofacies based on its structure, the possibility of seeing the wavy structure at the image scale rarely happens, the photo is taken from Carynginia Formation at the depth of 1682.00-2682.04 m, Dongara-1 (I) shaly-sandy interlaminated mudstone from Kockatea Shale at the depth of 2938.5310-2938.5463 m, North Erregulla-1(J) Shaly siltstone, displaying the distribution of silicate and clays within lithofacies, the photo is captured from Kockatea Shale at the depth of 2725.00-2725.05 m, Ejarno-1 (K) siliceous calcareous mudstone, showing the scattering of silica and carbonate components together in the lithofacies. The photo is taken from Kockatea Shale at the depth of 2233.30-2233.31 m, Yardarino-1(L) sandy-silty interlaminated deposit displaying kaolinite within matrix at the depth of 1414.95-1415 m, Cliff Head-4 47

Figure 3.7 The stages of XRD sample preparation 49

Figure 3.8 Selected 2-theta region showing phase identification in the sample of fossiliferous mudstone lithofacies 51

Figure 3.9 Infrared spectra of shale samples..... 55

Figure 3.10 Vertical distribution of lithofacies within the Carynginia Formation (left), and the Kockatea Shale (right) 60

Figure 3.11 The figure shows presence of recrystallized quartz and detrital quartz within Calcareous mudstone lithofacies from the Kockatea Shale at the depth of 3834.5 m, Redback-2 62

Figure 3.12 clay-quartz-carbonate ternary diagram displaying mineral composition in various lithofacies, lithofacies with higher quartz content are more brittle than clayed shales 63

Figure 4.1 The distribution of TOC within the Kockatea Shale (left), and the Carynginia Formation (right) across the Perth Basin.....	65
Figure 4.2 Van Krevelen diagrams of Kockatea Shale (A) and Carynginia Formation (B)	67
Figure 4.3 TOC versus Remaining Hydrocarbon Potential, displaying different types of kerogen as a function of thermal maturity.....	67
Figure 4.4 The schematic figure indicates the relationship between vitrinite reflectance, depth and max with various zones of a typical reservoir (modified from Glorioso et al., 2012)	68
Figure 4.5 Tmax versus depth for shale samples of the Kockatea and the Carynginia in the Perth Basin	69
Figure 4.6 The figure display the highest organic maturity of Kockatea Shale (left), and Carynginia Formation (right) in the center and north of the Perth Basin (based on Tmax data)	71
Figure 4.7 Plot of Ro versus depth for shale samples of the Kockatea and the Carynginia formations at the Perth Basin	72
Figure 5.1 Core photograph of Redback-2; relevant gamma-ray response and evaluated TOC profile with grain size from core which demonstrates high variation in the vertical successions of the organic-rich shale intervals.	78
Figure 5.2 Sonic and resistivity curves fitting to calculate $\Delta\log R$ (modified from Glorioso et al., 2012)	80
Figure 5.3 The determination of kerogen maturity through combining of resistivity and neutron-density logs	80
Figure 5.4 The brittleness trend within the Kockatea Shale (left), and the Carynginia Formation (right) across the Perth Basin.....	84
Figure 5.5 Variability in the brittleness index of Redback-2 (left) and Arrowsmith-2 (right), the brittleness index derived from shear sonic)	84
Figure 6.1 Example of (A) upward-increasing gamma ray parasequence, mainly consists of pyritic mudstone lithofacies (B) interval of constant gamma ray parasequence, mainly contains fossiliferous mudstone lithofacies and (C) upward-decreasing gamma ray parasequence, mostly occurred due to the presence of calcareous mudstone, from Hovea Member of the Kockatea Shale, Redback-2	87
Figure 6.2 Aggradational and progradational systems in the Hovea Member of Kockatea Shale, Redback-2	89
Figure 6.3 Sequence stratigraphic frameworks for the Hovea Member of the Kockatea Shale from Redback-2, five stratigraphic intervals have been detected with correlation of gamma-ray log, stacking patterns of lithofacies,	

Relative Hydrocarbon Potential and TOC. The acquired match is reasonable in most parts. TR: Transgressive event of relative sea level, RE: Regressive event of relative sea level, FS: Flooding surface, TSE: Transgressive surface of erosion, and S.L: Sea level interval 92

Figure 6.4 Cross-section AB throughout north-south of Dandaragan Trough Sub-basin, Perth Basin. All stratigraphic intervals are presented in the selected wells at the Hovea Member; there are similar gamma-ray patterns for the upper part of the Kockatea Shale..... 94

Figure 7.1 The Distribution of black shale, bioturbated mudstone, siliceous mudstone and shaly siltstone (Kockatea Shale) in the Perth Basin 99

Figure 7.2 The sweet spots in the Kockatea Shale (left) and the Carynginia Formation (right). 102

List of Tables

Table 2.1 Shale gas reservoir properties in the Permian Carynginia Formation and the Triassic Kockatea Shale within the Perth Basin	26
Table 3.1 List of the wells containing examined cores of the shale plays through the Perth Basin	33
Table 3.2 The geological features of the lithofacies within the Kockatea and the Carynginia formations.....	34
Table 3.3 Selected samples for core plugging acquired from Northern Perth Basin.....	42
Table 3.4 Summary of geological properties in the lithofacies acquired by thin section petrography	43
Table 3.5 Phase abundance of identified mineral phases from Kockatea shale and Carynginia Formation	52
Table 3.6 Recognition of clay minerals based on the wavenumbers from transmission IR spectrum.....	54
Table 3.7 The list of identified clay groups by XRD bulk, XRD clay fraction and FITR	57
Table 3.8 Brittleness index for individual lithofacies	62
Table 4.1 TOC content of different lithofacies identified within the Kockatea and the Carynginia formations	65
Table 4.2 the status of lithofacies in relevance to organic richness and the rate of environmental oxygen.....	73
Table 5.1 The brittleness index acquired by geomechanical parameters of Young's modulus (E) and Poisson's ration (ν)	83
Table 7.1 The various properties of different lithofacies in the target formations, Perth Basin	98

Chapter 1: Introduction

1.1 Shale gas resources in Australia

The success of shale gas resources in the US energy industry has drawn the attention of Australia's energy industry to these types of reservoirs. The increasing costs associated with the petroleum industry and the anticipation of a decrease in Western Australia's domestic gas supply below demand by 2016 have caused the serious concerns about the future of WA's energy security (Haworth, 2013).

Geologically, Western Australia shows very different characteristics to other parts of the country, especially New South Wales and Queensland where coal seam gas (CSG) is the target. However, the WA's shale gas resources exceed the entire CSG resources in Australia, which are the basis of the LNG export projects in Queensland (Medd, 2012). Kuuskraa (2007) compare recoverable shale gas resources in different parts of Australia.

The commercial production of gas from shales in Australia has entailed a careful consideration of the presence of a comprehensive and stable regulatory regime for supporting large scale shale production, along with related environmental, health and safety concerns (Csiro, 2012).

Globally, Australia is ranked sixth in terms of shale gas resources (1.2 Tm² or 396 Tcf technically recoverable shale gas), total 8155 Gm³ or 288 Tcf of risked recoverable shale gas is estimated within Western Australia (U.S. Energy Information Administration, 2011).

There are considerable shale gas potentials in the thick Paleozoic and Mesozoic successions of the WA basins. Perth Basin Paleozoic successions include shales of the Permian Carynginia Formation, as well as potentially prospective Triassic shales of Kockatea Shale. In the Canning Basin, these successions are composed of Ordovician Goldwyer, Devonian Gogo, and Carboniferous Laurel formations.

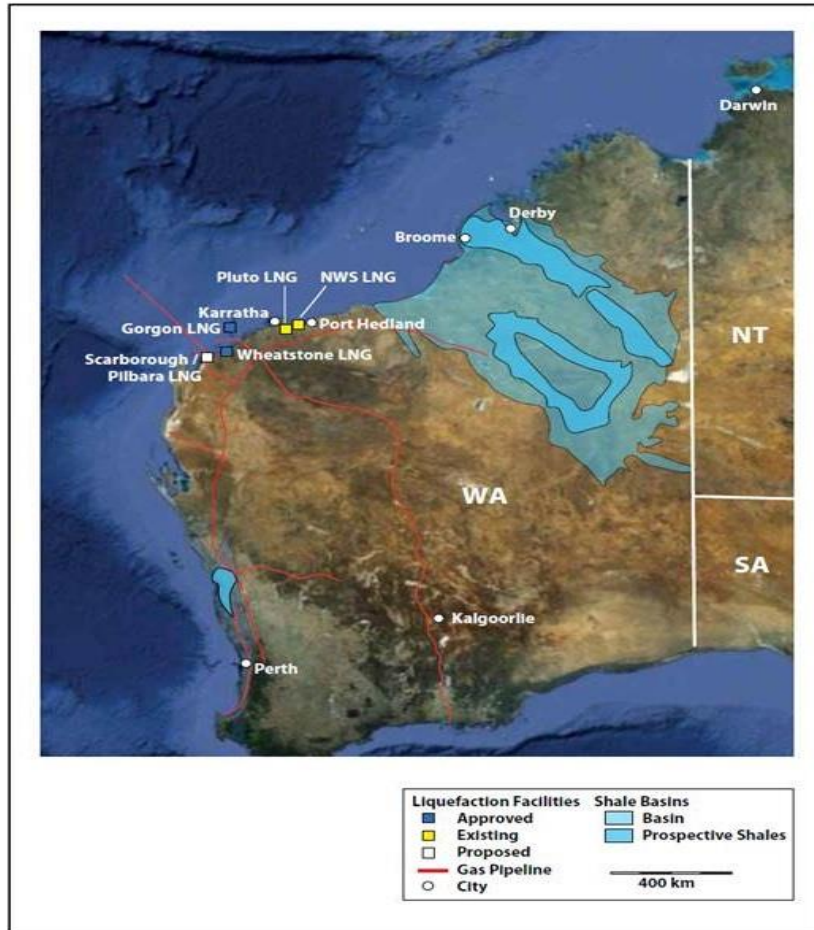


Figure 1.1: The figure displays shale gas prospective areas in Western Australia with two major potential basins of Perth in the southwest of Australian margin and Canning in the north part of Western Australia (source: PWA, Sep 2012).

The prospective areas of shale gas of Western Australia are shown in figure 1.1. The U.S. Energy Information Administration (2011) estimates 1670 Gm³ or 59 Tcf of risked recoverable shale gas for Perth Basin and 6484 Gm³ or 229 Tcf for Canning Basin. The Canning Basin with nearly 125,000 km² shale gas rock is considered to have a larger areal extent than Texas (Triche, 2012). Table 1 compares the potential of shale gas in the target formations between Western Australia and the United States of America. Despite the large shale gas potential at Canning Basin, Perth Basin is considered to have the most prospective shale gas potential in the near future due to its accessibility to the current infrastructure, pipelines, and Perth gas market (Triche, 2012). The Permian Carynginia Formation and the Triassic Kockatea Shale have been assessed as holding about 1670 Gm³ or

59 Tcf) of recoverable resource and 5663 Gm³ or 200 Tcf of gas-in-place (U.S. Energy Information Administration, 2011).

A Prospective Area Success factor (PAS) of 70% and Play Success Factor (PSF) of 60% were estimated for both the Kockatea and Carynginia Formations by U.S. Energy Information Administration (2011), which brings a 42% Composite Success Factor for the Perth Basin.

1.2 Background

The high possibility of prospective shale gas reserves in Western Australia has motivated the industry to come to explore these resources. However, there are major issues with exploring unconventional resources in Australia due to the lack of modern drilling rigs capable of deep and horizontal drilling (Haworth, 2013).

Western Australia has only started to develop the unconventional petroleum industry since 2005. A total of 15 wells have been drilled targeting unconventional reservoirs, and seven of these wells experienced fracture stimulation. However no horizontal drilling and no production have so far been achieved (Haworth, 2013).

The Kockatea Shale at Arrowsmith-2 well (300 km north of Perth, 50 km south of Dongara) had successful tests in terms of shale gas concepts. The well was drilled 400m from the Arrowsmith-1 well that produced (4 million Scf/d or 113000 m³/d) gas from the Carynginia Formation in 1960s (Haworth, 2013).

The primary target of the Arrowsmith-2 was the Carynginia Formation which has the thickness of 250 meters in the proximity of the well. The formation is laterally extensive. The thickness of 200 m potential shale gas intervals with high geographical spread is known for the Kockatea Shale.

In 2012, hydraulic fracturing was performed on three wells of Arrowsmith-2, Woodada Deep-1, and Senecio-2 in Northern Perth Basin. Stimulated zones in Woodada Deep-1 were in the upper and middle part of the Carynginia Formation. About 2.83 percent stimulation fluids have been

recovered from Kockatea Shale at Arrowsmith-2 (Jonasson, 2013). The stimulation at Senecio-2 was in tight sandstone reservoirs (Wagina and Dongara formations).

1.3 General Characterisations of Shale Plays

Shale is an organic rich fine-grained sedimentary rock (Joseph et al., 2005) which is generally deposited in quiet and low energy water. Shales are significantly important in petroleum exploration and production because of their multiple roles as source and cap rocks (Al Bazali et al., 2005). Due to low permeability, the gas within shale releases slowly. However, covering millions of acres and hundred feet thickness of shale layers in a particular basin makes this drawback negligible. The most prolific shales are sufficiently large that their wells can continue the gas production steadily for decades (Kalantari-Dahaghi and Mohaghegh, 2011).

Shale gas is a natural gas trapped in shales, which is expected to become the world's primary energy supply in the future. Shale gas plays are considered to be self-contained source reservoir petroleum systems (Schmoker, 1995). These systems are grouped into different types (Jarvie et al., 2007), in which our target shale intervals are classified as integration plays that have both unconventional and conventional gas production (Talukdar, 2009).

Producing gas from shales is highly dependent on the factors such as high gas generation and retention, shale fractures and seals for shale sequences.

The advances in hydraulic fracturing and horizontal drilling, as well as the rising cost of natural gas made shale gas production economically conceivable in recent decades (Arthur et al., 2008). Lewis et al (2004) believe that the low risk from shale gas wells compensates mostly the enormous expenditure of using these advanced technologies in producing gas from shale plays.

The profitability of shale gas plays is calculated based on the profitability of the net present value (NPV) of the cash flow, the internal rate of return (IRR) of the simulated well and the required breakeven price to obtain the least return on investment (Duman, 2012). Therefore, it is important to

define whether or not the natural gas produced from shale reservoirs is profitable or not.

There are noticeable uncertainties in determining gas recovery and matrix permeability of shale gas development (Pearson et al., 2012). However, the factors such as low matrix permeability, initial fractures, the network's conductivity and network fracture spacing create a unique solution for the production of shale gas (Cipolla et al., 2009). Wide variability in lithology, geologic setting, matrix lithofacies, production mechanism, along with local heterogeneity in cm-scale lead to the singular nature of each shale play (Chong et al., 2010). Lewis et al (2004) believe that diagenesis, sedimentary and structural history causes a substantial variety in reservoir characteristics such as lithology and mineralogy. The precise prediction of the fracture distribution within the network is another difficulty due to the complexity of fracture growth in the shale gas reservoirs (Cipolla et al., 2009).

1.3.1 Geologic Controls on Shale Gas Reservoirs

Shale gas reservoirs are geographically extensive units with high organic matter, low matrix permeability, and widespread gas saturation (Singh, 2008). Lithologically, shale is a fine-grained detrital sedimentary rock which splits into thin and parallel layers (Figure 1.2).



Figure 1.2: The figure indicates shale characterising by breaks into parallel bedding along their thin laminae, that commonly ranges in thickness less than one centimeter (Blatt et al., 1996) (Source: OWNI.eu News, Augmented).

Depending upon the amount of organic matter within shales, their colour varies (Potter et al., 1980). The rock is commonly composed of clay size

mineral particles and silt. Shale is considered to have the lowest grain-size in terms of petroleum reservoir.

Figure 1.3 displays a continuum pore throat size represented by petroleum reservoirs, from higher than 2 μm in conventional reservoirs, to 2-0.03 μm in tight sand, and 0.1-0.005 μm in shale gas (Nelson, 2009). The small pore-throat size enables shales to retain a significant quantity of gas (Ghori, 2013). The retained gas and flow characteristics are either uniquely trapped to nano scale pore size distribution and they serve clay content and organic matter as gas sorption sites and named as an adsorbed gas (Kalantari-Dahaghi and Mohaghegh, 2011), or are stored as a free gas in rock pores and natural fractures. These various storage mechanisms affect the speed and quality of gas production (Holditch and Lee, 2005). The organics and clays impart an anisotropic fabric to gas shales that impacts on their transport and mechanical properties (Sondergeld et al, 2010).

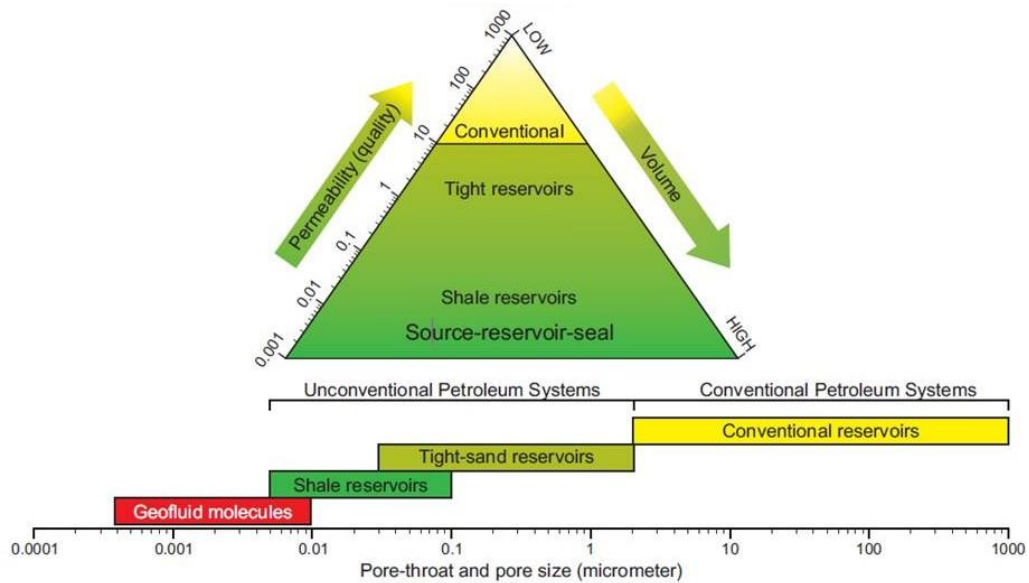


Figure 1.3: Different pore throat and pore size within conventional and unconventional reservoirs, the graph shows finer pore throat for shale gas unconventional reservoir compared to tight gas reservoirs (adapted from Ghori, 2013).

The key factors such as amount of organic matter, mineralogy, rock texture, diagenesis, pore size distribution, reservoir pressure and temperature control

the relative magnitude of adsorbed versus free gas (Bustin et al., 2008a, 2008b).

1.3.2 The Features of Organic Matter within Shale

The models described by Passey et al (1990) and Jarvie (1991) divide the reservoir into three separate parts, which are liquid hydrocarbons, solid rock matrix, and solid organic matter. The solid organic matter is defined as kerogen which is the residue of microbial debris preserved under anoxic conditions (Khalid et al, 2010) and it produces hydrocarbons when heated. Kerogen forms at low temperature with biogenic decay as well as abiogenic reactions of the organic matter. The production and following retention of the organic matter control the degree of their accumulation in the shales, particularly with marine shales (Singh, 2008). The type of hydrocarbon produced (oil or gas) is predictable with respect to the kerogen type. Figure 1.4 represents a connection between the sorption capacity and kerogen types in the shale rocks.

As described by Tissot (1977), the gas is produced in two forms, biogenic gas (by the action of anaerobic micro-organisms during the early diagenetic phase of burial) and thermogenic gas (by thermal breakdown of kerogen and hydrocarbons during the catagenesis phase of the evolution of organic matter). The presence of a desirable volume of in-situ gas requires a sufficient amount of organic matter within shales. Shale gas is considered to have total organic carbon (TOC) content between 2 wt% < TOC <20 wt% (Singh, 2008).

Organic rich shales could have been deposited in the aquatic environment such as marine, lacustrine, lake, or in associated mires and swamps along the margins of seas or lakes (Passey et al., 2010). These organic rich sediments can develop over hundreds of metres to a considerable thickness; however, there is high heterogeneity on short vertical scale (Bohacs, 1998b; Bohacs et al., 2005; Guthrie and Bohacs, 2009) due to their geologic and biotic conditions during deposition.

Passey et al (2010) suggest that the basic building blocks of the organic-rich shale intervals match to well-defined stratigraphic architectures, so that the basic unit is considered a parasequence (genetically related beds and bedsets) or its equivalent. The precise characterization of these parasequences help in understanding the depositional environment using the stacked depositional patterns into parasequence sets, and ultimately exploring shale intervals with great gas potential.

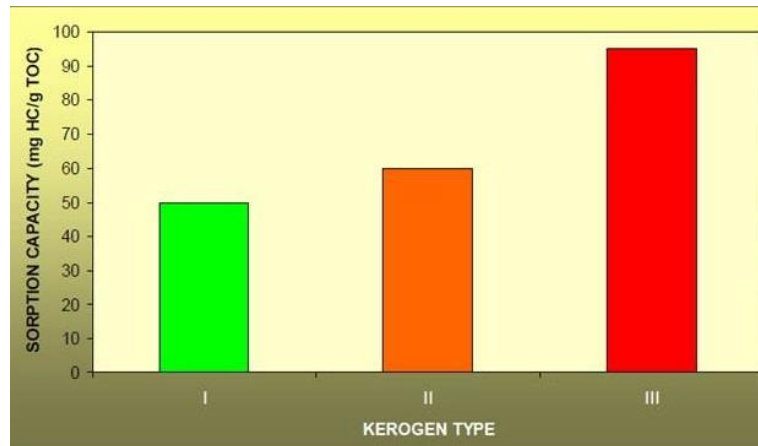


Figure 1.4: The graph illustrates the impact of kerogen type on gas sorption capacity within shale (adopted from Jarvie et al, 2004).

The complex and non-linear interactions of production, destruction, and dilution control the accumulation of organic matter in a depositional environment. The organic matter enrichment can be expressed by the relation:

$$\text{Organic matter enrichment} = \text{Production} - (\text{Destruction} + \text{Dilution}) \text{ (Bohacs et al., 2005)}$$

The desired organic matter enrichment occurs where organic matter destruction is minimized, production is maximized, and dilution is optimized, in the area where the accommodation can accumulate significant thickness of sediments.

1.3.3 Petrophysical Properties of Shale Gas Reservoirs

Petrophysical properties refer to the physical and chemical rock characteristics as well as their interactions with fluids (Tiab and Donaldson,

2004). Numerous petrophysical techniques have been developed from conventional source rocks to characterise organic rich shales. The influential petrophysical properties such as rock composition/mineralogy, porosity, permeability, TOC content, and gas saturation can characterise well where the typical analytical techniques are integrated with a full suite of well logs (Sondergeld et al., 2010). There is less certainty in the results obtained from the merging of analytical analysis and well logs in the heterogeneous shale intervals than conventional sandstone reservoirs according to Passey et al (2010) and Sondergeld et al (2010). The uncertainties might be caused by the complex pore volume connectivity and low-matrix permeability in the gas-bearing shale reservoirs.

The variation in key characteristics between mature organic rich rocks and overmature shale gas intervals (such as the presence of pores within organic matter along with intergranular matrix porosity, the fluid type, and rock mineralogy/rock composition) challenges the generalization of developed well log techniques used in conventional sandstone/carbonate reservoirs when applied to shale gas plays. For instance, gamma ray is a critical well log for separating fine-grained shale intervals in conventional reservoirs. This capability is decreased shale reservoirs where the entire petroleum system, namely source, reservoir, and seal, is composed of fine grained rocks (Passey et al., 2010).

The total gamma ray spectrum contains three common components of naturally occurring radiation, namely potassium (K), thorium (Th), and uranium (U), in shales and sands. In shale plays which are deposited under lacustrine conditions, the total gamma ray curve indicates the overall clay content within rock without demonstrating high TOC content (Bhuyan and Passey, 1994). These systems have low amounts of uranium, and there is mostly no relationship between TOC and uranium (Bohacs and Miskell-Gerhardt, 1998, Bohacs, 1998b). In a marine setting, the uranium content is useful due to its relation to organic matters (Passey et al., 2010).

The presence of organic matter in shale causes a light bulk density due to the low density of organic matter compared to matrix minerals, a high

resistivity because of the non-conductive nature of organic matter, an increase in transit time of acoustic logs (sonic log), an increase in neutron porosity, and high gamma-ray content due to high uranium levels within the organic matter. There is also an increase in porosity on the common porosity curves with the presence of organic matter (Sondergeld et al., 2010).

As described by Passey et al (1990), the organic matter content can be petrophysically estimated by the $\Delta\log R$ technique (combined sonic-resistivity method). To apply the method to shale plays, similar clays and conductive minerals such as pyrite are required in the calibration intervals, as well as available LOM data to predict TOC (Sondergeld et al., 2010). The technique is discussed in the geochemical section.

In terms of porosity, the density log is a combined response from the organic matter, matrix density and porosity, and hence doesn't present the actual porosity in shale (Hoeve et al., 2010). Krushin (1997) and Loucks et al (2009) suggest that the porosity networking in gas shale is mostly associated with the TOC due to larger pore throats in the organics.

1.3.4 Mineralogical Variations of Shale Plays

Variable mineral composition in shale gas reservoirs made the petrophysical analyses of the reservoir challenging. Gas shales are mainly formed from quartz, carbonate and clays. The contribution percentage of these minerals associated with organic matter properties directly impact on the rock quality, in-situ gas and hydraulic fracturing protocols (Sondergeld, et al., 2010). Passey et al (2010) indicate the compositional fields outlined for some producing shale plays in North America on the ternary diagram plot based on total carbonate, total clay, and quartz (see figure 1.5). Having less than 50 wt% total clay, and conversely a great amount of quartz and carbonate leads to this assumption that the fracture stimulation would work successfully in the shale plays. However, Ross and Bustin (2008) express that carbonate-rich facies might be problematic for fracturing and completions due to the fact that the shales enriched with carbonates have the potential ineffective rock mechanical properties (low Young's modulus and high Poisson's ration).

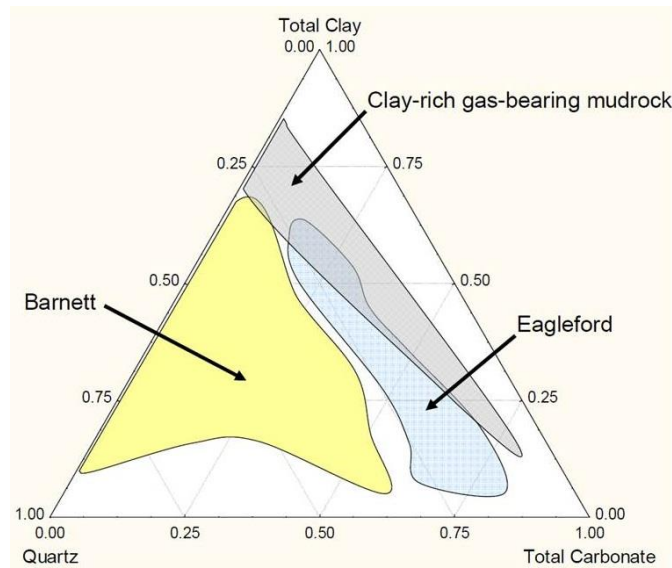


Figure 1.5: Plotting mineralogic ternary diagrams for successful shale plays of North America such as Barnett Shale and Eagleford Shale, displaying higher amount of quartz or carbonate than clay minerals which makes them suitable for fracture stimulation (Passey et al., 2010).

The intensity of the influence of quartz on the fracture stimulation is related to the type of deposited quartz (Passey et al., 2010). Detrital quartz is considered to be less effective in terms of stimulation, where recrystallized biogenic opaline silica forms the most effective quartz component (Jarvie et al., 2007) due to it having a continuous framework containing quartz cement. Detrital quartz can also increase the brittle behaviour of shales where the extra-basinal detrital quartz is cemented by silica formed by smectite-clay illitization during diagenesis (Thyburg et al., 2009) according to the reaction that is expressed by Boles and Frank (1979): $\text{Smectite} + \text{K}^+ = \text{Illite} + \text{Silica} + \text{H}_2\text{O}$.

The relationship between brittleness and mineral composition within shale plays is presented by Wang and Gale (2009):

$$\text{Brittleness Index (\%)} = \frac{\text{Quartz}}{\text{Quartz} + \text{Carbonates} + \text{Clays}}$$

Apart from determining the production potential through fracturing, maximising potential gas capacity can also be controlled by mineral composition given that they are mainly affected by the effective porosity and free gas capacity. There should be a dialectic relation between total

porosity and quartz content since clay rich shales tend to have higher porosities in comparison with their silica rich counterparts (Ross and Bustin, 2008).

1.3.5 Stratigraphic Concepts of Shale Gas Reservoirs

Even in the desirable conditions of accumulating organic matter, there are systematic variations in the characteristics and distribution of potential source rocks in several lateral and vertical scales (Bohacs, 1990, 1993, 1998b; Schwalbach and Bohacs, 1992; Creaney and Passey, 1993; Bessereau and Guillocheau, 1995; Bohacs et al., 2005). The depositional environment and stratal stacking control these variations. Passey et al (2010) suggest that the depositional processes arising from the environment lead to the formation of the basic building blocks of the geologic records, namely stratal surfaces and lithofacies package, These controlled stratal stacks represent a hierarchy in their facade. Each physiographic setting cumulates specific lateral and vertical distributions of lithofacies recorded in their stratal stacking, character, organic matter content and mineralogy. The distribution of these lithofacies is represented in parasequence-scale packages, and systematically forms depositional sequences that enable us to recognise the variations particularly in the marine depositional system. The identification of the characteristic lithofacies accordingly is beneficial in characterising the stratal stacking, mineralogy and organic matter content of depositional sequences. Similar to the systematic change vertically in rock characters that is controlled by accumulating the parasequence stratal unit, the proximity of the sediment supply to these accumulations leads to the systematic changes in rock properties laterally (Guthrie and Bohacs, 2009). Figure 1.6 compares the proximal and distal parasequences, and indicates the thicker sequence in proximal area. As described by Passey et al (2010), the thickness of fine-grained sandstone or siltstone increases slowly on a centimetre scale in this section. There is an upward rise in bioturbation and skeletal phosphorous content, and conversely an upward fall in radiolarian abundance of both distal and proximal parasequences.

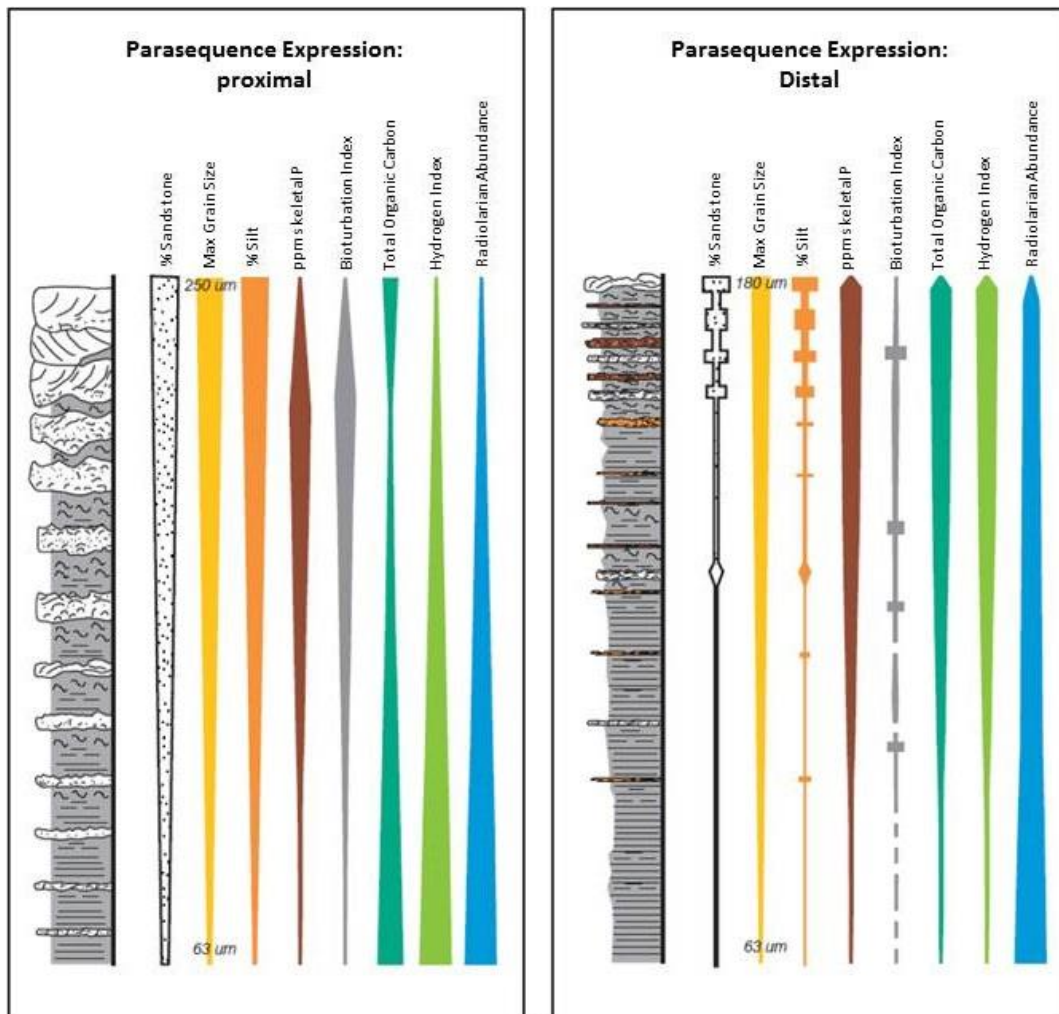


Figure 1.6: Schematic comparison of proximal and distal parasequences within shale succession (adapted from Passey et al., 2010).

Unlike proximal area which shows an upwardly decreasing TOC, there is an upwardly increasing tendency at the distal area in terms of TOC content. Structurally, the planar-parallel, current bedding as well as the horizontal burrows are dominant in these two sequences. The radiolarian abundance reduced towards the top of the sequences. Lateral burrowing raises in intensity upward in the distal and proximal parasequences, together with the increase in intensity and diversity of vertical burrowing in the distal area. In this area, the coarser grained biogenic carbonate originated from the benthic area are dominant at the top of the sequence whereas biogenic carbonate and silica with pelagic origin are less abundant at the top. Depending on the source of organic matter, hydrogen Index (HI) content varies. In the distal area, the high TOC originating from algae resulted in high HI, whilst the

high TOC originating from coal and wood in the proximal area leads to the low inherent HI. The gradual transition is presented for the parasequence sets in the intermediate position of distal and proximal areas (Passey et al., 2010).

The relative changes in the organic production, destruction, and dilution control the patterns of variations in organic matter enrichment of distal and proximal setting within coeval strata. The observations suggest that the dilution processes controls the organic matter enrichment in the proximal area (Bohacs et al., 2005). Passey et al (2010) suggest that maximum organic-carbon content generally occurs in the basal transgressive systems tract and decreases gradually to background levels at the maximum-flooding downlap surface.

1.3.6 Depositional Environment of Shale Plays

The depositional setting directly controls key factors in shales such as organic-richness, texture and rock composition. According to Potter et al (1980), the organic matter preserved in shales depends on the dissolved oxygen level in the water. The relation of oxygen deficient environment and TOC content is displayed at figure 1.7 according to Rhoads and Morse (1971). The variation in salinity and temperature prevent aerated water circulation and form density stratification within water (Singh, 2008), which reduce the oxygen level (Olausson, 1961).

The basin direction can be identified with respect to lateral changes in sedimentary fabric from dysaerobic to anaerobic. The deep marine basins might not be so specified in terms of lithological facies due to the long distance from the coastal sedimentary supply (Byer, 1997). The presence of well-developed lamination indicates the deposition under an anaerobic environment with low energy conditions. The bioturbation structure in sedimentary rocks formed by benthic organisms represents the deposition under the poor bottom oxygenation conditions (O'Brien and Slatt, 1990).

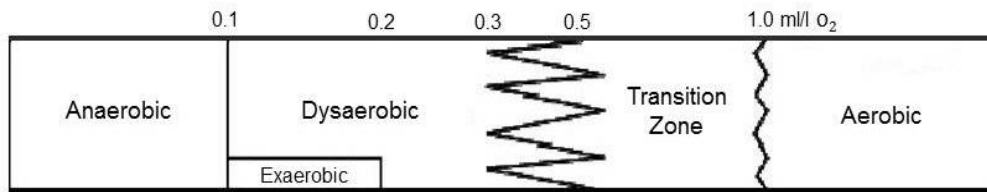


Figure 1.7: The figure shows different depositional environments along with their level of dissolved oxygen values (adapted from Singh, 2008, after Rhoades et al., 1991).

1.4 The Scope

This study evaluates the geological, geochemical and petrophysical properties of the Kockatea and the Carynginia formations as prospective shale gas potential in the Perth Basin, based on different analytical techniques. The fundamental research objective is to identify sweet spots, where the formations have the greatest shale gas potential and can produce gas in commercial levels with drilling. This is achieved through mapping of key shale properties such as thickness and geographic distribution, organic richness and kerogen maturity, as well as lithofacies and fracability.

General purposes of the research:

- Establish a lithofacies scheme using visual core descriptions
- Evaluate petrographical and mineralogical rock properties of the key shale beds in the basin.
- Determine the brittleness index in the target formations
- Establish a sequence stratigraphic framework
- Determine the lithofacies in the non-cored wells
- Examine the organic potential of appropriate facies in the basin
- Create a general outline from hydrocarbon maturity of the area
- Verify areas with the greatest gas potential in the Perth Basin
- Use as a valuable guideline of shale gas potential for the consequent projects in the future

The database includes well completion reports, core data, and Rock-Eval data which was provided by the Department of Mines and petroleum (DMP) as a part of the onshore Perth Basin studies.

Chapter 2: General Geology of the Perth Basin

2.1 Regional Setting

The Perth Basin is a deep north-south trending trough which extends along the southernmost 700 km of the western Australian coast (Crostella and Backhouse, 2000), encompassing both the onshore (covers 45,000 km²) and offshore (98,000 km²) (Boreham et al., 2000). The eastern margin of the basin is delimited by the north-south trending Darling fault, which has more than 15 kilometres of lateral movement on the western, down side (Jones, 1976). The contact between the Perth Basin and the Archaean Yilgarn Block is marked by the Darling Fault. To the southwest, a narrow belt of Proterozoic gneiss and granulite in the Leeuwin Block bounds the basin (McPherson and Jones, 2005). The basin is separated from the Carnarvon Basin in the north by a ridge of shallow basement rocks named Northampton Complex (Rabnawaz, 2009; Iasky and Mory, 1993), which encompasses the oldest unit in the Perth Basin on its eastern side (Hocking, 1991). According to Crostella and Backhouse (2000), the stratigraphy of the Southern Perth Basin contains sediments of Permian-Holocene overlying Precambrian basement.

Structurally, the basin is a complex rift-sag with two main tectonic phases: a southwesterly Permian extension; and, a north-westerly Early Cretaceous transtension during break-up. Dextral and sinistral movements are identified during these phases along the Darling Fault. The basin is divided by basement-related regional faults that were frequently reactivated by subsequent tectonic events creating wrench-induced anticlines, horizontal displacements, and further faults (Crostella, 1995).

Owad-Jones and Ellis (2000) express that the Darling fault and a series of bounded troughs by transfer faults form the dominant tectonic framework in the onshore part of the basin. The faults are throwing to either the east or west and mostly having north to northwest trends. The large east-west

trending cross-faults are seen within the basin (McPherson and Jones, 2005). Figure 2.1 shows the main subbasins and tectonic lineaments in the north, centre and south of the Perth Basin.

The main Permian depocentre is placed on the northeastern margin of the Dandaragan Trough in the onshore Northern Perth Basin. The Houtman/Abrolhos sub-basins in the northern offshore, the Bunbury Trough in the onshore Southern Perth Basin, and the Vlaming Sub-basin in the offshore part of the basin formed the other important subbasins within the basin (Bradshaw et al, 2000). A limited sediment supply is indicated by a thinning of the Permian section towards south to the Dandaragan Trough. Mory and Iasky (1996) state that the Permian setting began with melting of ice sheets of the Gondwana along with the deposition of fluvio-glacial-glacial-proglacial marineshelf sediments in the eastern and central part of the basin. This marine transgression is continued by a regression, with deposition of conglomerate and sand in the lower deltaic proglacial environment (High Cliff Sandstone) and alluvial coarse-grained coalesced prograding into a proglacial marine embayment (Irwin River Coal Measures). Returning to proglacial marineshelf conditions leads to the formation of argillaceous marine Carynginia Formation with a minor regressive pulse and the coal seams which suggest abundant accommodation space associated with sustained subsidence during the Early Permian. It appears that a period of rifting followed by trough infill occurred during the Permian. It appears that a period of erosion and uplift was predominant in the Late Permian. This uplift that was interrupted by a period of extension in the east-north-east (Harris, 1994) is related to the commencement of rifting in the Offshore Perth Basin (Marshall et al, 1989, Quaife et al, 1994).

The Early Triassic Kockatea Shale followed the late Permian tectonic activity with the occurrence of marine transgression. Subsequently, a long-lasting regressive phase of fluvial deposition expanded in the basin and continued until the Early Jurassic. The Woodada Formation acts as a thin transitional unit that connects the overlying Upper Triassic Lesueur Sandstone with the underlying marine Kockatea Shale (Mory and Iasky, 1996).

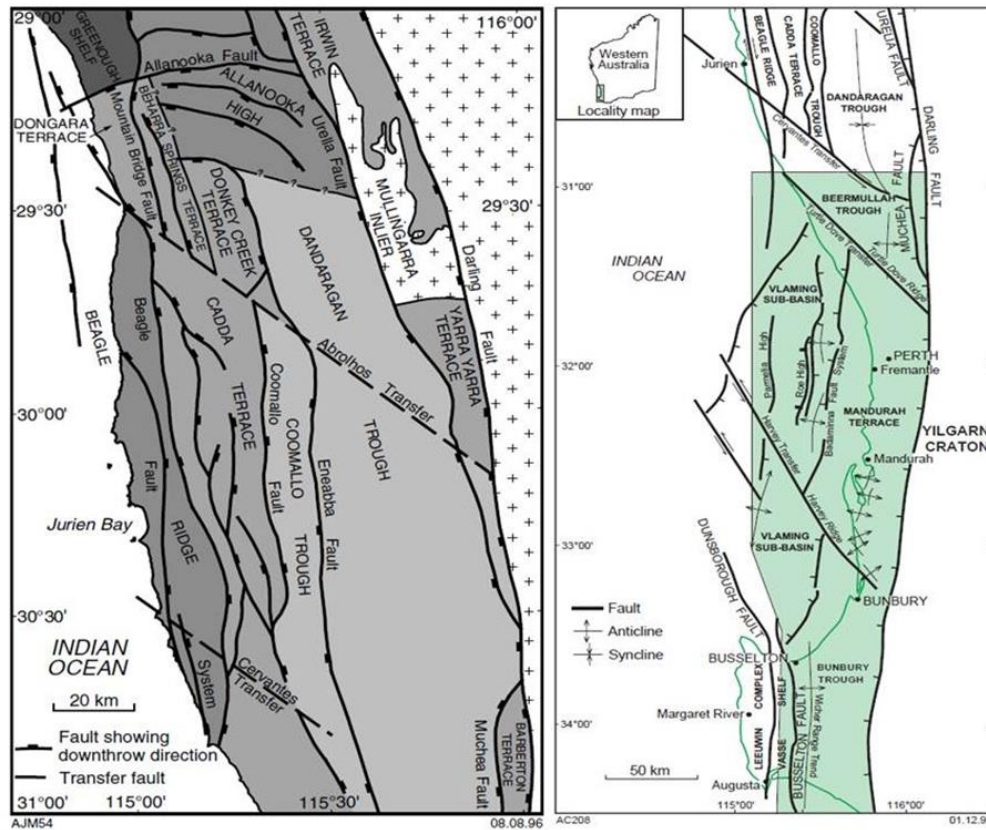


Figure 2.1: Basin subdivisions and tectonic elements of (the right) the onshore Northern Perth Basin (from Mory and Iasky, 1996), and (the left) the central and Southern Perth Basin (modified from Crostella and Backhouse, 2000).

The significant thickening of the Lesueur Sandstone in the southeast indicates a dramatic movement on the Darling fault during the late Triassic. There was an active ridge during deposition of the Lower Jurassic fluvial Eneabba Formation and the marginal marine Cattamarra Coal measures.

The onset of rifting along the southern margin of Australia, prior to the occurrence of Neocomian breakup of Gondwana is interpreted by the abrupt change in sedimentation in the Middle Jurassic and high thickness of the Middle Jurassic to the Lower Cretaceous sequence (Scott, 1991). A period of trough infill is suggested by a thickening of the Triassic and Lower Jurassic units towards the south along the axis of the Dandaragan Trough.

Vitrinite reflectance modelling developed by Mory and Iasky (1996) displays the major heating event between the Late Jurassic and the Early Cretaceous that is coincident with rifting followed by the separation of

Australia from Greater India. The increase of geothermal gradient during this period might have resulted from crustal thinning and mantle upwelling before separation (Middleton, 1982; Iasky and Mory, 1994). The final breakup of Australia and Great India occurred in the Mid Neocomian-Early Cretaceous (Early Valanginian) that developed deeply seated wrenching transfer faults, anticlines, and strike-slip movements (Crostell and Backhouse, 2000). The most important break in the basin succession occurred during this breakup, which is commonly referred as the Main Unconformity or the Breakup Unconformity (Woodside Offshore Petroleum, 1988).

2.2 Stratigraphic Features

The oldest sedimentary unit in the Perth Basin is the fluvial Tumblogooda Sandstone (Hocking, 1991) which is present in a structural low adjacent to the uplifted Precambrian basement (Cadman et al., 1994) in the north of the basin, and on the eastern side of the Northampton Complex (Mory and Iasky, 1996). Despite the common belief in the lack of Devonian and carboniferous sediments at the Perth Basin, Ingram (1967) and Backhouse (1993) suggest the indirect evidence of Devonian age, coming from reworked microfloras in the Lower Permian Nangetty Formation and the Upper Cretaceous Otorowiri Member. The record of carboniferous sediment is restricted to the Coolcalalaya Basin, according to the North Broken Hill Ltd report on shallow drilling in the Coolcalalaya subbasins (1981).

The Permian succession in the basin consists of nine formations over approximately 2,600 meters sediments (McPherson and Jones, 2005). A north-south trending trough was generated down the basin's axis by initial phases of rifting in the Early Permian period. In the Northern Perth Basin, the trough was preliminarily filled by a glacial unit, namely the Nangetty Formation (Mory and Iasky, 1996), overlain by a marine shale of Holmwood Shale (Figure 2.2). Playford et al (1976) believe that a regression in the Artinskian caused the sedimentation of shallow marine sands, which were covered by a paludal and fluvial coal measure sequence (Irwin River Coal Measures). The Carynginia Formation was

deposited after returning shallow marine conditions in the Late Artinskian (Cadman et al., 1994). In the Late Permian period, an alluvial fan delta system (Wagina Sandstone) expanded towards the west from the Darling fault into the Northern Perth Basin. According to Bergmark and Evans (1987), these sediments were sourced from uplifted sequences of Artinskian and earlier successions to the east and northeast of the Dandaragan Trough with slight contributions from the Northampton Block and likely the eastern flank of the Beagle Ridge. A fluvial to coal-swamp depositional environment dominated in the Southern Perth Basin during the Permian time (Cadman et al., 1994).

Despite the high comparability of the Lower Permian successions between the Northern and Southern Perth Basin, the marine Carynginia Formation in the north part changed into the Ashbrook Sandstone, which was deposited under continental conditions (Figure 2.2). The thickness of the Upper Permian sequences peaks to 300 meters in the northern part, whilst this thickness reaches 1000 metres in the Southern Perth Basin. Permian successions are the oldest sedimentary rocks in the southern part of the basin (Crostell and Backhouse, 2000).

The Late Permian-Early Triassic sediments are mostly continuous in the Southern Perth Basin, whereas the stratigraphic gap is locally presented in the Upper Permian (Dongara Sandstone, Beekeeper Formation, or Wagina Formation) with the overlying Lower Triassic Kockatea Shale (Mory and Iasky, 1996; Crostell and Backhouse, 2000). This discontinuity might be due to the particular tectonic framework in the Northern Perth Basin. Based on Marshal et al (1989), the rifting which had begun in the Late Palaeozoic had established a series of shallow basement highs and en-echelon rifts in the northern part during the Early Triassic.

The increase in the relative sea level resulted in the widespread marine transgression within the basin from the north, as well as the broad deposition of the Basal Triassic sandstone in the various environments from fluvial to shallow marine. In the Early Triassic, the major movements on the Urella and Darling Faults along with the continuous subsidence led to the

deposition of marine sequence (Kockatea Shale) throughout most of the Northern Perth Basin. The continental Sabina Sandstone is the equivalent of Kockatea Shale in the south, and it gradually expands northwards. The fluvialite deposition dominated in the Middle Triassic time and created Lesueur Sandstone (Cadman et al., 1994). According to Playford et al (1976), movement on the Urella and Darling Faults steadily continued from the Middle Triassic to the Middle Neocomian Period.

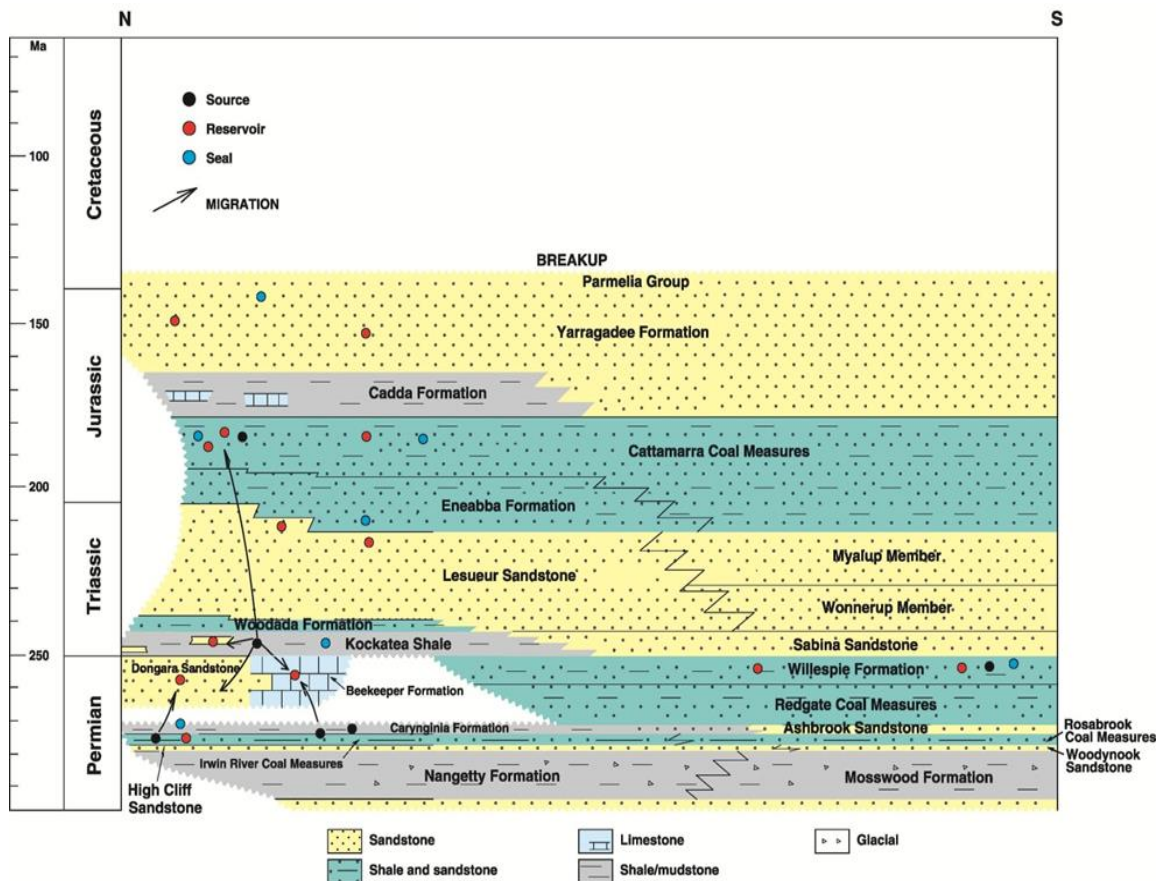


Figure 2.2: North- south stratigraphic features of the Perth Basin, displaying the petroleum system and accumulations within the basin, along with lithology and shifting the Permo-Triassic intervals from north towards south (adopted from Owad-Jones and Ellis, 2000).

A thick Jurassic sequence extends across the wide area of the Perth Basin. It mainly consists of continental deposits (Cockleshell Gully Formation), with the exception of the thin marine transgressive Cadda Formation which is limited to the Northern and part of central Perth Basin (Crostellla and Backhouse, 2000). The Cadda Formation becomes non-marine and

arenaceous in the central and Southern Perth Basin (Cadman et al., 1994). In the Middle Jurassic, major rifting related to the Urella and Darling Faults corresponds to the main Gondwanaland breakup event during the Oxfordian (Hall & Kneale, 1992); it coincides with the high depositions of Yarragadee Formation into the subsiding grabens and troughs of the basin (Cadman et al., 1994).

In Neocomian, a period of post uplift and erosion formed the intra-Neocomian breakup unconformity (Falvey and Mutter, 1981) which specifies the end of rifting and the beginning of the drift phase (the final segregation of Australia and India). According to Cadman et al (1994), Tertiary succession occurred under stable and passive margin conditions in the Abrolhos and Vlaming subbasins.

2.3 Structural Features

The structural setting of the Perth Basin was studied in the northern part by Mory and Iasky (1996) through analysing aeromagnetic, gravity, outcrop mapping and seismic data, and from geological and geophysical data in the central and southern part by Le Blanc Smith (1993), Le Blanc Smith and Kristensen (1998). A detailed insight into the structural history of the region is enabled where the Permian strata are influenced by low amplitude folding and extensive faulting. Crostella and Backhouse (2000) suggest that all deformations are formed by the Early Neocomian breakup tectonism.

The structures occurred initially during the Early Permian extension and were reactivated by Early Cretaceous transtension within the continental breakup of Australia and India. The wrench induced anticlines, horizontal displacements, and extensive faulting across the basin were resulted from the Early Cretaceous breakup (Owad-Jones and Ellis, 2000). It is assumed that an intracontinental rift containing non-marine sediments formed the pre-breakup Perth Basin. Bradshaw et al (2000) express that the faulted, mainly continental Permian-Early Cretaceous succession is mostly overlain by a relatively undeformed Mid-Neocomian and younger succession of paralic, continental and marine start.

The north trending Darling Fault System is the most significant structural feature in the basin which originated in the Archaean shear zone (Blight et al., 1981). Followed by its reactivation during the Proterozoic basin (Baxter and Harris, 1980), and its rejuvenation during the Early Permian and likely the Late carboniferous, that resulted in the formation of the Perth Basin. There is thick Permian to Neocomian succession in the west part of the fault plane, along with significant strike-slip movements indicated by the linearity of the fault (Crostella and Backhouse, 2000).

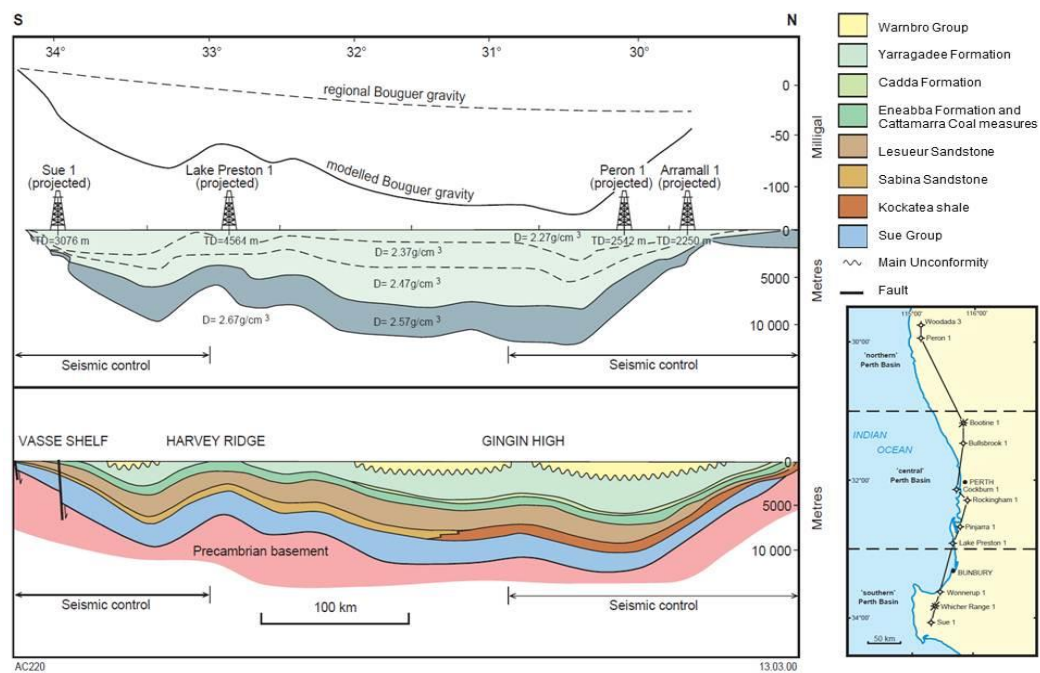


Figure 2.3: North-south gravity model associated with structural section across the Perth Basin (modified from Crostella and Backhouse, 2000).

The Busselton and Dunsborough Faults are also construed as rift faults controlling the Western Perth Basin. These faults are sub-parallel to the Darling Fault within the Bunbury Trough.

The Badaminna Fault is also related to the development of the Perth Basin, associated with the faults which separated the offshore Vlaming Sub-basin from the Bunbury Trough and Mandurah Terrace. The fault was mostly activated during the Early Jurassic as well as the Late Tithonian-Aptian. The Early Neocomian tectonism formed other structural features of the basin

which peaked in the breakup of Australia and Great India (Crostella and Backhouse, 2000).

Figure 2.3 illustrates the gravity model and structural variations from the north to the south in the basin. The prospective diagram at the basement displayed the deep trough in the south which rises gradually to the north. Westward, the trough goes up across the main faults onto the Beagle Ridge. Eastward, the deepest part of the Dandaragan Trough upwarps gradually against the Darling Fault system and creates a boundary with the Yilgarn Craton (to gain further knowledge about the structural history of the northern, central and Southern Perth Basin, please refer to Mory and Iasky (1996) and Crostella and Backhouse (2000) for further information. According to Crostella and Backhouse (2000) the basin grows progressively wider during the Triassic and Jurassic in the Northern Perth Basin, where the intervention of Early Triassic- Middle Jurassic marine sediments occurred and the fluvial- to alluvial-plain Triassic and Jurassic deposits thickened.

The regional cross sections across the Perth Basin have been studied by Seggie (1990), Blyth (1994), Enterprise Oil (1994), Crostella (1995), Stagg et al (1999), Song and Cawood (2000) and Crostella and Backhouse (2000).

2.4. Prospective Shale Gas Formations

The high potential of distributed conventional source rocks of the Perth Basin consists of the Permian, Triassic, and Jurassic, significantly the condensed sequence at the Hovea Member of the Triassic Kockatea Shale (Thomas, 1979, 1982, 1984; Thomas and Brown, 1983; Summers et al, 1995). The presence of un-faulted fine grained Kockatea Shale in the same depth with the main objectives forms an effective seal for the faulted structures. The Carynginia Formation locally presents a seal for the Irwin River Coal Measures. The seal potential increases to the south due to less intense faulting and the thickest stratigraphic section (Mory and Iasky, 1996).

The petroleum systems within the Perth Basin are specified as Gondwanan and Transitional (Bradshaw et al, 1994; GeoMark and AGSO, 1996). The gas-prone Permian Carynginia source beds with a TOC of more than 11 wt% and the oil-prone Triassic Kockatea Shale source beds with a TOC up to 2 wt% form the Gondwanan petroleum system (Thomas, 1984; Thomas and Barber, 1994). The main oil-prone source beds of the Transitional petroleum system are within the fluvial-lacustrine shale facies in the Jurassic Cattamarra Coal Measures and the Yarragadee Formation with TOC up to 27 wt%, and 2 wt%, respectively (Thomas, 1984).

Given the importance of structural development in the conventional systems, the Dandaragan Trough and the Donkey Creek Terrace are considered as to have poor conventional hydrocarbon potential because of their low structural expansion (Mory and Iasky, 1996). In contrary, this lack of structural development doesn't make any disadvantages for the unconventional resources, and the Dandaragan Trough is the most prospective area for the shale gas potential in the Northern Perth Basin.

Plotted maturity maps by Thomas and Brown (1983), displays an acceptable maturity level for hydrocarbon in the Kockatea and Carynginia shales throughout the most of the basin. The Kockatea Shale is highly mature in the Dongara Trough and the area where it is deeply buried. However, the formation represents less maturity in the flanks of the Beagle Ridge and Dongara Saddle where shale layers are partly replaced by shallow marine limestone. The Permian Carynginia Formation and The Triassic Kockatea Shale consider being in the mature gas window mostly in the centre of the basin (U.S. Energy Information Administration, 2011).

The estimated recoverable natural gas for the Carynginia and Kockatea Shales is about 1671 Gm³/59 Tcf (U.S. Energy Information Administration, 2011). The resource concentration of 107 Bcf/m², risked recoverable resources of 29 Tcf, and risked gas-in-place of 98 Tcf are estimated for the Carynginia Formation, whereas Kockatea Shale is estimated to have 110 Bcf/mi² of resource concentration, 100 Tcf risked total gas in place, along with 30 Tcf of risked recoverable resource (Table 2.1).

Table 2.1: Shale gas reservoir properties in the Permian Carynginia Formation and the Triassic Kockatea Shale within the Perth Basin (modified form U.S. Energy Information Administration, 2011).

Basic Data	Basin/Gross area	Perth Basin	
	Shale Formation	Carynginia Shale	Kockatea Formation
	Geologic Age	Upper Permian	Lower Triassic
Resource	GIP Concentration (Bcf/mi ²)	107	110
	Risked GIP (Tcf)	98	100
	Risked Recoverable (Tcf)	29	30

The Carynginia Formation is a restricted marine deposit (McLoughlin, 1993), and consisting mainly of interbedded sandstone and siltstone with minor shale above the Irwin River Coal Measures (Mory and Iasky, 1996). There is a deeper water shale member close to the base of Carynginia Formation which is overlain by a shallow-water, shelf limestone unit. The disordered quartzite, granitoids, and gneiss boulders present in the lower part of Carynginia Formation have been attributed to proglacial ice-rafting processes. The sandstone and conglomerate presented in outcrops consist of internal cross laminae, lenticular and reworked sediments formed by storm and wave into hummocky cross-stratification and symmetrical ripples. Coating of large ripples by small pebble sized materials indicates that storm activity has removed the fine grained materials (Mory and Iasky, 1996).

In Northern Perth Basin, the Carynginia Formation has a conformable contact with its underlying Irwin River Coal Measures. There is an angular unconformity between Carynginia Formation and its upper layers such as the Wagina and Dongara Sandstones, and the Beekeeper Formation. Crostella and Backhouse (2000) suggest that the formation shifts to Ashbrook Sandstone towards the south.

The Lower Triassic Kockatea Shale is believed to be the main oil source rock and the hydrocarbon flow seal in the Perth Basin (Thomas, 1979; U.S. Energy Information Administration, 2011). The unit consists of dark shale, micaceous siltstone, and minor limestone and sandstone. Cross-bedding, tool marks and tails as well as large undulose asymmetric ripples have been observed in outcrops of the unit (Mory and Iasky, 1996). The formation thickness generally increases to the south, reaching its peak at 1060 meters. However, the activities that occurred in the Early Triassic along the Beagle

Faults and Mountain Bridge have reduced Kockatea Shale's thickness on the Northern part of Beagle Ridge and Dongara Terrace, which formed a local depocentre near the Beharra springs field (Mory and Iasky, 1996). An average thickness of 700 meters is estimated for the Kockatea Shale by the U.S. Energy Information Administration (2011). The most prospective part of Kockatea Shale is its organic-rich basal shale (Hovea Member) that averages 2% TOC in comparison with an overall average of 0.8% TOC for the entire formation. Lithologically, the member is a distinct organic rich zone, consisting of shelly storm beds, sandy siltstone, and fossiliferous mudstone. The evidence indicates the deposition of this member under shallow water conditions during the earliest stage of a marine transgression (U.S. Energy Information Administration, 2011).

In terms of the stratigraphic relationships, the unit is disconformably overlain by Cattamarra Coal Measures, Eneabba Formation, and Lesueur Sandstone, and it overlies Dongara Sandstone in the north. The Kockatea Shale unconformably overlies Precambrian basement in the west of Mount Hill (Mory and Iasky, 1996). In the Southern Perth Basin, the marine Kockatea Shale correlates with the continental Sabina Sandstone.

According to Crostella and Backhouse (2000), the fine-grained sandstone and siltstone of the Middle-Upper Triassic Woodada Formation presents a transition unit between the overlying continental Lesueur Sandstone and the underlying marine Kockatea Shale in the Northern Perth Basin. The Woodada Formation has not been presented in the south, and the entire Middle-Upper Triassic succession has been dedicated to the Lesueur Sandstone.

2.4.1 Geological Distribution and Thickness

Having sufficient knowledge about the distribution of the Permian Carynginia Formation and the Triassic Kockatea Shale is considered a preliminary step in exploring shale gas reservoirs within these formations. This target can be achieved through studying the stratigraphy and structure of the Perth Basin during the Permo-Triassic period, as well as drawing the isopachs of the target formations to determine how the thickness changes.

According to Mory and Iasky (1996), the main depocentre of Permian is located on the northeastern margin of the Dandaragan Trough. The greatest thicknesses of the Permian sediments are within the Bunbury Trough and the Vasse Shelf, and the Mandurah Terrace for the Triassic sediments. The thinning of the Permian sediments westward to the Beagle Ridge- Dongara Saddle indicates the presence of high basement during the Early Permian, and the coeval thinning south towards the Dandaragan Trough indicating a limited sediment supply. The Permian sedimentation started in fluvial to glacial to proglacial marine shelf settings across the central and eastern Perth Basin (Mory and Iasky, 1996). In the Southern Perth Basin, the sedimentation was continuous during the Late Permian- Early Triassic, whereas there is a stratigraphic gap in the Uppermost Permian in the northern part.

A maximum thickness of 300 m is identified in the Northern Perth Basin during the Upper Permian, and the thickness reaches nearly 1000 m in the southern part during this time. The thickness of Permian sequence increases eastward to the Darling Fault (Iasky, 1993) which might be the result of the controlling of the sedimentation by the fault. The reduced thickness towards the south illustrates a limitation in the offshore extension (Crostell and Backhouse, 2000).

The Early Permian Carynginia Formation is 240 m thick in its type section located in the Carynginia Gully. The unit reaches 328 m thickness in Cadda-1. The formation is correlated with the Ashbrook Sandstone in the south part of the basin, with a significant change from a marine shale (Carynginia Formation) in the Northern Perth Basin into the continental sandstone (Ashbrook Sandstone) in the south. The correlation of the unit with the Mingenew Formation (Playford et al., 1976; Archbold, 1988) is limited to fault blocks along the Urella fault system (please refer to Mory and Iasky (1996) for further information).

In the Northern Perth Basin, after depositing of the Irwin River Coal Measures, a marine transgression occurred during the Early Permian, and this condition appears to have continued to the Early Triassic since the

related sequences are marine. Conversely, the Permian and the Early Triassic rocks are utterly continental in the Southern Perth Basin. Crostella and Backhouse (2000) express that there is no sedimentation gap between the Permian and the Triassic sequences.

The Triassic Kockatea Shale is less than 12 m thick in its type locality near the junction of the Kockatea Creek and Greenough River. The unit overlies the Permian Carynginia Formation with an unconformable contact, and the Dongara Sandstone in the Northern Perth Basin. The Kockatea Shale thickens towards the south. The Early Triassic activity along the Beagle faults and Mountain Bridge caused the thinning on the northern part of the Beagle Ridge and Dongara Terrace (Mory and Iasky, 1996). The Lower Triassic Kockatea Shale in the Northern Perth Basin has changed to the continental Sabina Sandstone in the southern part which thickens northwards, whilst the thickness of the coeval Kockatea Shale in the northern part increases southwards.

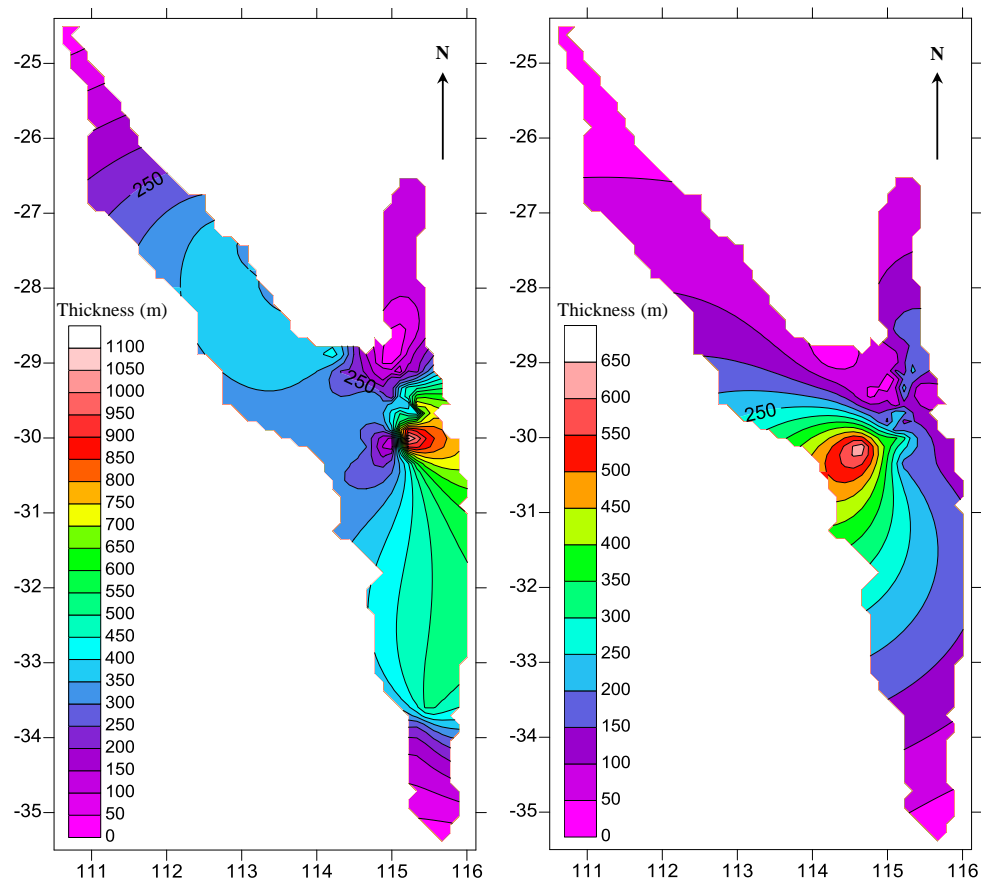


Figure 2.4: Isopach maps of the Kockatea Shale (left) and Carynginia Formation (right).

The thickening of the Triassic sequences along the axis of the Dandaragan Trough likely indicates a period of trough infill. There is an increase in the Triassic east of the Beagle Fault System and Mountain Bridge showing growth along the Beagle Ridge. The thinning of the Kockatea Shale onto the Dongara Saddle and the northern part of the Beagle Ridge represents the Early Triassic growth along the ridge. The thinning to the north suggests non-deposition or erosion at the location of the edge of the basin or near the Northampton Complex (Mory and Iasky, 1996). The isopach maps of the units show depositional thinning to the south, along with parts of the north and centre of the basin, whereas the thickest parts of the Carynginia Formation to be westwards. The Kockatea Shale has the highest thickness in the east-north of the basin (Figure 2.4).

Chapter 3: Geological Studies

Geological properties of a shale gas reservoir are different from conventional reservoirs which are relying on geologic traps to retain the gas in place (Zahid et al., 2007). A shale gas system is a self-contained source-reservoir system with low risk potential in terms of completion due to having thick zones, large lateral extents and consistent properties (Khalid et al., 2010).

3.1 Visual Core Description and Lithofacies Identification

Any geological study and rock analysis begins with studying the rocks, the outcrops, cores and cuttings. Initial identification of depositional processes and lithofacies were acquired through studying on long conventional cores of 42 wells throughout the Perth Basin (see figure 3.1). Table 3.1 is a list of cores studied for the prospective formations.

Facies refers to the rock unit forming under certain sedimentary conditions. Facies is normally characterised by all the geological properties reflecting its origin and differentiating it from adjacent rock units (Oilfield glossary, 2013). The designation of lithofacies has a significant effect on devising completion strategies because some lithofacies are more desirable for gas recovery due to their organic content and suitability to create an extensive network of induced fractures into a matrix (Cardot, 2006; Fisher et al, 2005; Johnston, 2004). The lithofacies with siliceous composition, high organic content, and a low amount of unconfined compressive strength are considered favourable to gas recovery (Jacobi et al., 2008). The lithofacies of the Kockatea Shale and the Carynginia Formation were identified based on lithology, colour, rock composition, grain size and distribution, sedimentary structure, and the nature of underlying and overlying contacts. The depositional environment were simultaneously studied for their lithofacies properties and detecting index minerals that reflect certain

environmental conditions, e.g. pyrite depositing under low energy conditions with reduced circulation.

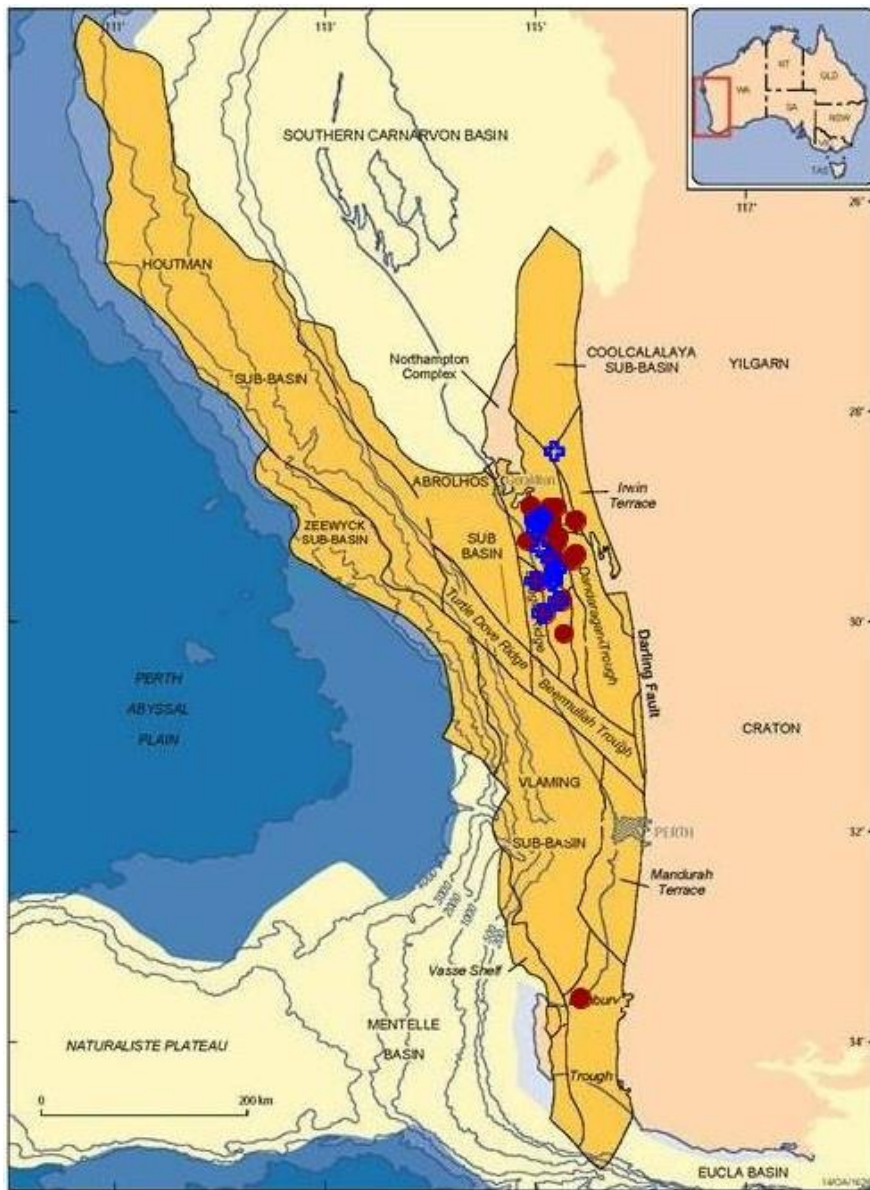


Figure 3.1: The location of studied wells containing available cores of the Kockatea Shale (red marks) and Carynginia Formation (blue marks), modified from Geoscience Australia’s website.

3.1.1 Results

Studying of continuous cores of Kockatea and Carynginia formations leads to the recognition of eight common lithofacies, in addition to three lithofacies of shaly siltstone, siliceous calcareous mudstone, and sandy-silty interlaminated deposit that have only been recognised in the Kockatea

Shale. Defining lithofacies is based on the broad range of geological parameters that differentiate them from each other. Table 3.2 displays different characteristics within each lithofacies.

Table 3.1: List of the wells containing examined cores of the shale plays through the Perth Basin.

Kockatea Shale	Sub-basins	Depth of core	Carynginia Formation	Sub-basins	Depth of core
Woolmulla-1	Dandaragan Trough	1311.8-1999.8	Woolmulla-1	Dandaragan Trough	2293.9-2809.3
Yardarino-1	Dandaragan Trough	2056.8-2234.8	Yardarino-1	Dandaragan Trough	2366.2-2373.5
Jurien-1	Beagle Ridge	91.44-268.22	Jurien-1	Beagle Ridge	275.2-552.3
BMR 10 Dongara	Beagle Ridge	30.48- 979.3	BMR 10 Dongara	Beagle Ridge	1005.8-1164.3
Hovea-3	Dandaragan Trough	1968.5-1993.0	Abbarwardoo-1	Dandaragan Trough	482.5-499.9
Donkey Creek-1	Dandaragan Trough	3741.1-3745.4	Woodada-2	Dandaragan Trough	2281.0-2363.1
Arrowsmith-1	Dandaragan Trough	2264.9-2681.3	Woodada-3	Dandaragan Trough	2440.0-2451.2
Eneabba-1	Dandaragan Trough	3418.9-3905.1	Beekeeper-1	Dandaragan Trough	2781.0-2792.9
Beharra Springs-2	Dandaragan Trough	3341.3-3355.5	Arrowsmith-2	Dandaragan Trough	2781.0-2835.2
Mt Adams-1	Dandaragan Trough	3340.8-3344.5	Dongara-12	Dandaragan Trough	1663.1-1670.9
Mondara-4	Dandaragan Trough	2813.3-2816.6	Dongara-1	Dongara Saddle	1681.2-1716.9
Centella-1	Dandaragan Trough	2940.0-2955.7	Dongara-2	Dongara Saddle	1682.2-1688.2
Redback-2	Dandaragan Trough	3788.0-3835.3	Dongara-3	Dongara Saddle	1604.1-1608.7
Senecio-1	Dandaragan Trough	2708.0-2729.6	Dongara-11	Dongara Saddle	1712.3-1733.4
North Erregulla-1	Dandaragan Trough	2798.9-2943.1	Dongara-23	Dongara Saddle	1613.2-1623.0
Mt Horner-1	Dandaragan Trough	1398.4-1404.2	Jingemia-4	Beagle Ridge	2474.2-2482.1
Mt Horner-7	Dandaragan Trough	1239.3-1239.7	Beharra-2	Beagle Ridge	1493.7-1501.9
Eurangoa-1	Dandaragan Trough	1572.5-1607.0	Jingemia-4	Beagle Ridge	2474.2-2482.1
Ejarno-1	Dandaragan Trough	2723.0-2725.9	Woodada Deep-1	Beagle Ridge	2272.0-2380.0
Dongara-24	Dandaragan Trough	1460.0-1531.2			
Dongara-25	Dandaragan Trough	1456.0-1685.5			
Dongara-27	Dandaragan Trough	1481.7-1485.3			
Dongara-4	Dongara Saddle	1661.1-1687.9			
Narkarino-1	Dongara Saddle	491.45-493.23			
Cadda-1	Beagle Ridge	1698.3-1702.3			
Cliff Head-4	Abrolhos sub-basin	1414.0-1430.0			
Whicher Range-1	Bunbury Trough	3737.4-3740.5			

3.2 Lithofacies Description

3.2.1 Black shale

The lithofacies mainly contains black organic-rich mudstone (Figure 3.2A). The facies is likely deposited in relatively deep and low energy water due to settling of its fine-grained components. The dark colour of the facies suggests high organic content, confirming the deposition under calm conditions in the anaerobic environment. In Hovea-3, the lithofacies contains micrite and glauconite that indicates the dominance of reduced conditions (Hendricks and Ross, 1941). Thick crystalline calcite veins are sporadically seen within the lithofacies (Figure 3.2B) representing the post-depositional process (Thomas et al., 2002).

3.2.2 Pyritic mudstone

The facies refers to a pyrite-rich mudstone (Figure 3.2C). The abundance of pyrite in this lithofacies is a sign of reduced conditions during its sedimentation, which is desired for preserving organic matter within fine-grained rocks. Pyrite nodules and pyrite veins within other lithofacies, particularly black shale, are likely formed after deposition in the diagenesis stage and hence are considered as post depositional structures (Figures of 3.2D and 3.2E). Fossils can be also replaced by pyrite as a result of the use of oxygen by aerobic bacteria (Figure 3.2F). In some intervals of the Carynginia Formation, pyritic mudstone appears with scattered particles of mica along quartz inclusions such as Woodada Deep-1 to a depth of 2280.36-2280.50 m.

Table 3.2: The geological features of the lithofacies within the Kockatea and the Carynginia formations.

Carynginia Formation	Kockatea Shale	Lithofacies	Composition	Colour	Grain size and grain distribution	Sedimentary structure	Nature of underlying and overlying contacts
		Black shale	Clays, slightly silty, with pyrite	Black	Fine-grained, Uniform	Massive	Gradual boundaries
		Pyritic mudstone	Clays with abundant pyrite	Greenish brown	Fine-grained Uniform	Massive, Pyritic nodules and veins	Gradual boundaries
		Siliceous mudstone	Silica, slightly silty and micaceous with rare pyrite	Gray black	Fine-grained Non-uniform	Massive, siliceous lamina and lenticulars	Distinguishable boundaries
		Calcareous mudstone	Clays, detrital and autochthonous calcite, and quartz	Brownish gray	Fine-grained Non-uniform	Massive Strong Reaction with dilute HCl acid	Distinguishable boundaries
		Fossiliferous mudstone	Clays, slightly silty	Gray black	Fine-grained Non-uniform	Compacted thin-walled fossils	Very distinguishable boundaries
		Bioturbated mudstone	Clays, siltstone and sandstone	Gray	Fine-medium grained Non-uniform	Massive, Bioturbation and burrows	Very distinguishable boundaries
		Wavy laminated deposit	Clays, siltstone and sandstone	Brownish gray	Fine-grained Non-uniform	Wavy and convolute laminations	Very distinguishable boundaries
		Shaly-sandy interlaminated mudstone	Interlaminations of shale and sandstone	Brownish light gray	Fine-medium grained Non-uniform	Laminated	Very distinguishable boundaries
		Shaly siltstone	Siltstone and shale	Brownish gray	Fine-grained Non-uniform	Laminated	Distinguishable boundaries
		Siliceous calcareous mudstone	Clays, Silica and calcite	Light to dark grey	Fine-grained Non-uniform	Massive Reaction with dilute HCl acid	Gradual boundaries
Sandy-silty interlaminated deposit	interlamination of sandstone and siltstone	Brown	Fine-medium grained Non-uniform	Laminated	Distinguishable boundaries		

3.3.3. Siliceous Mudstone

The lithofacies is one the most common lithofacies within Permo-Triassic intervals and is a moderately hard gray black lithofacies (Figure 3.2G).

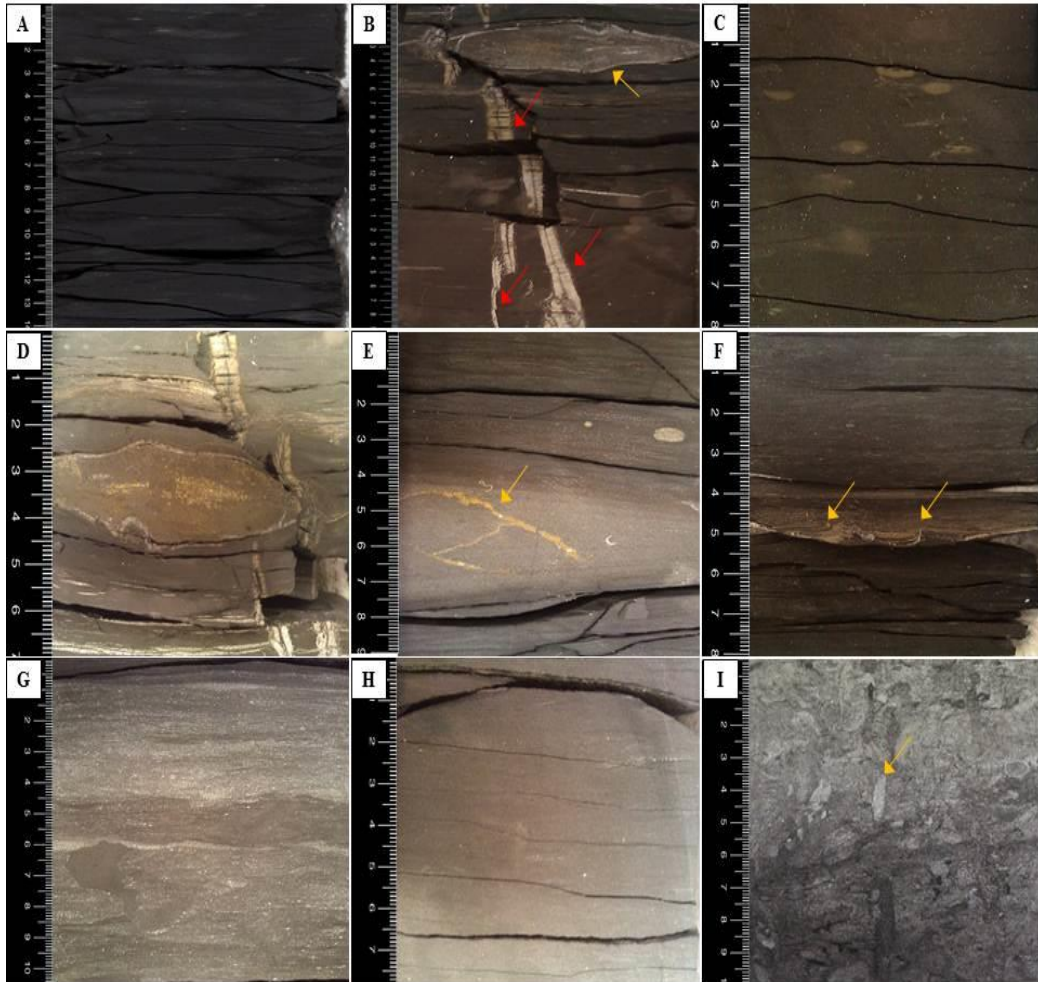


Figure 3.2: Core photographs of lithofacies, displaying various sedimentary structures (A) black shale from Carynginia Formation at the depth of 2275.54-2275.68 m, Woodada Deep-1 (B) pyrite nodule (yellow arrow) and streaks of white crystalline calcite (red arrows) within black shale from Kockatea Shale at the depth of 3817.10-3817.20 m, Redback-2 (C) pyritic mudstone lithofacies with greenish brown colour from Carynginia Formation at the depth of 2278.81-2278.90 m, Woodada Deep-1 (D) higher magnification of Pyrite nodule from Kockatea Shale at the depth of 3798.24-3798.33 m, Redback-2 (E)pyrite vein within pyritic mudstone from Carynginia Formation at the depth of 3800.55-3800.67 m, Woodada Deep-1 (F) the replacement of pyrite in fossils (yellow arrows) from Carynginia Formation at the depth of 2285.27-2285.40 m, Woodada Deep-1 (G) core photo of siliceous mudstone from Kockatea Shale at the depth of 3832.75-3832.80 m, Redback-2. The bright colour within cores displays siliceous into gray brown clay matrix (H) calcareous mudstone from Kockatea Shale at the depth of 3804.23-3804.37 m, Redback-2 (I) the sparry calcite replaced burrow structure (yellow arrow) from Carynginia Formation at the depth of 2823.65-2823.75 m, Woodada Deep-1.

It is scarcely silty and micaceous with rare pyrite. Although the facies doesn't react with diluted hydrochloric acid, slight veins of white crystalline calcite can be observed in some parts. Lenticular and burrowed sedimentary structures are common within lithofacies, which suggests depositing under low to moderate energy conditions. The presence of silica rich laminae in some wells represents terms of low energy.

3.2.4 Calcareous Mudstone

The lithofacies is formed with combination of clay minerals, detrital and autochthonous calcite with negligible amounts of quartz (Figure 3.2H). Calcareous mudstone lithofacies has strong reaction with diluted hydrochloric acid. The presence of both detrital and autochthonous calcite together within lithofacies points to the entrance of clastic(s) particles into the environment after initial sedimentation of clays, quartz, and autochthonous calcite which might be caused by particular tectonic processes such as fluvial debris. In some parts within core samples, sparry calcite fills the probabilistic burrows (Figure 3.2I).

3.2.5 Fossiliferous Mudstone

Fossiliferous mudstone is a particularly significant facies in interpreting the depositional processes with respect to its marine records. There is a wide range of fossil variability within target intervals, but in particular brachiopods and foraminifers (observed through optical microscopy) are at highest percentages. Brachiopod has deposited at about 17.75 m in the Basal Kockatea Shale (Hovea Member) in the form of thin-walled compacted brachiopods in Redback-2, Dandaragan Trough (Figure 3.3A). Well-preserved fossils of brachiopods are presented in the shale member of Carynginia Formation at Woodada Deep-1. The assemblage of fossils shown in figure 3.3B indicates the dominance of initial high-oxygen environment which enabled the proliferation of aquatic organisms, following with marine depositional setting with anoxic conditions which caused mass death of faunas. Low energy conditions are suggested for the sediment as the environmental energy wasn't enough to spread the deposited faunas.

3.2.6 Bioturbated Mudstone

The lithofacies is mostly composed of mudstone with the layer turbulence from biota (Figure 3.3C). Since the preservation of organic matter needs static conditions, the likelihood of the reservoir potential for the layers with bioturbated lithofacies is improbable. The probable occurrence of the bioturbation in the various environmental conditions makes interpreting its depositional setting particularly complex. The environment setting of marine offshore transitional zone is considered for the core shown in figure 3.3D. The facies typically occurs in the low energy conditions in the bay, lagoonal and offshore environment. The bioturbated and horizontal bedded structures in figure 3.3E indicate the deposition under the shoreface environment with moderate energy conditions. Figure 3.3F illustrates bioturbated fine-grained sandstone with burrows in the core's surface, suggesting a marine offshore transitional zone as its depositional setting. Burrows as a kind of trace fossils within sedimentary facies, particularly the bioturbated mudstone facies, naturally cross-cut the deposited laminations due to their temporal relationship (Figure 3.3C). Figure 3.3G displays the bioturbated mudstone with long burrows within the facies that characterise depositing in the bay, lagoonal and offshore environment.

3.2.7 Wavy Laminated Deposit

The wavy laminated deposit is defined as wavy lamination of sandstone in fine grained mudstone (Figure 3.3H). However, the facies can be seen as a form of wavy sand laminations in siltstone (Kockatea Shale, Woolmulla-1). Top and basal surfaces of the lithofacies are highly differentiable. At Dongara-12, the structure is shown as lenticular wavy lamination (Figure 3.3H) which is an indicator of sudden change in energy level of depositional conditions. These kinds of conditions mostly occur in tidal habitats. In some areas, breaking waves or storms may produce convolute laminations (Pratt, 1998) which usually range from nearly 3- 25 cm in thickness. Figure 3.3I represents the convolute and lenticular bedded fine grained sandstone and mudstone that indicates the depositional setting of marine and transitional marine to tidal flat. The facies is normally found in the areas with low-

moderate energy conditions associated with variable current velocity such as marine shoals, tidal point bars, lagoons, splays, as well as offshore near a fair-weather wave base.

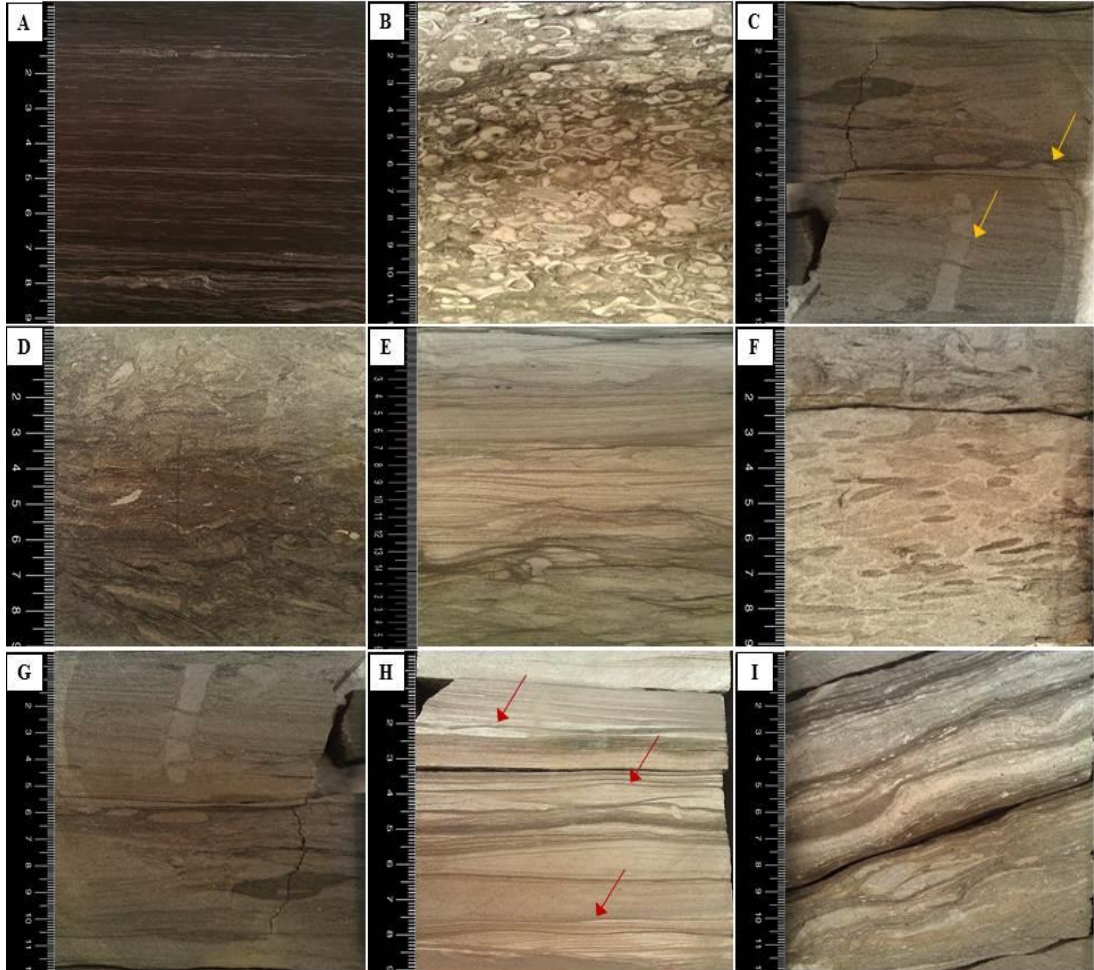


Figure 3.3: Core photographs of lithofacies display (A) the compacted thin-walled brachiopods within fossiliferous mudstone from Kockatea Shale at the depth of 3794.81-3794.90 m, Redback-2 (B) Shelly fragmented mudstone from Carynginia Formation at the depth of 276.21-276.33m, Jurien-1 (C) bioturbated mudstone with burrowing structure (yellow arrows) which cut the deposited lamination at the depth of 2369.30-2969.43 m, Woodada deep-1 (D) bioturbated mudstone, the bioturbation has largely destroyed the initial depositional features from Carynginia Formation at the depth of 2478.64-2478.72 m, Jingemia-4. (E) horizontal bedded and bioturbated sandstone from Carynginia Formation at the depth of 1619.57-1619.77 m, Dongara-23 (F) bioturbated sandstone from Carynginia Formation at the depth of 1495.76-1495.84 m, Beharra-2 (G) bioturbated and burrowed mudstone from Carynginia Formation at the depth of 2378.86-2378.98, Woodada Deep-1 (H) wavy laminated deposit, the photo indicates lenticular wavy lamination structure in siltstone (red arrows) from Carynginia Formation at the depth of 1655.32-1655.46 m, Dongara-12 (I) convolute bedded and lenticular bedded sandstone from Kockatea Shale at the depth of 1424.80-1424.92 m, Cliff Head-4.

3.2.8 Shaly-sandy Interlaminated Mudstone

Shaly sandy interlaminated mudstone lithofacies commonly refers to a facies with interlaminations of shale and sandstone (Figure 3.4A). The existence of this lithofacies represents a continuous change in sedimentary environment due to depositional processes variability. The lithofacies is very common at Carynginia Formation in the Dongara wells. Although the lithofacies does not suggest an appropriate reservoir for gas accumulation, its identification is certainly worthwhile in detecting depositional changing across the basin. The observed structure at figure 3.4B indicates depositing in the zones with moderate to high velocity currents such as the upper part of tidal deltas, fluvial and tidal point bars, channel bottoms, washovers, and distributary mouth bars. Marine shoreface (upper shoreface/beach) are suggested for the cross and parallel bedded sandstones of Dongara-11, whereas non-marine fluvial/channel environment is intended for parallel bedded structures in the sandstone of Beharra-2 (see figure 3.4C), and the structure occurs in a high energy environment such as channel, foreshore and aeolian.

3.2.9 Shaly Siltstone

The presence of silt in this lithofacies is either in a laminar form or is dispersed throughout the rock (Figure 3.4D). In some wells the lithofacies is composed of fossils and in some others pyrite. This lithofacies is absent in the Carynginia Formation. The constitutive particles of silt, together with a high abundance of clay minerals within the shale, predict a calm environment for the sedimentation of this facies. Although there is no evidence pointing to the presence of gas within the lithofacies, having dense and well-indurated texture along with high quartz content guarantees the successful fracture stimulation operations.

3.2.10 Siliceous Calcareous Mudstone

There is a relative welding of siliceous calcareous mudstone lithofacies in reaction with dilute hydrochloric acid due to sufficient proportions of calcite that differentiate it from siliceous mudstone lithofacies (Figure 3.4E). The

skeletal components within facies of siliceous calcareous mudstone and fossiliferous mudstone are mostly constituted from calcite (Figure 3.4F), resulting from a high amount of calcite within these lithofacies (about 4-40 wt% of the entire composition). Siliceous calcareous mudstone is noticeably present in the Early Triassic Kockatea Shale, whilst it is generally depleted in the Carynginia successions.

3.2.11 Sandy-silty Interlaminated Deposit

This lithofacies is non-shale lithofacies composed of interlaminated sandstone and siltstone (Figure 3.4G). In some areas, sandstone is observed in the form of lenticular structure in siltstone (Figure 3.4H). However sandy-silty interlaminated deposit doesn't suggest a favorable reservoir for unconventional gas accumulation; it shows changes in sedimentary conditions from shale facies to interlaminations of sandstone and siltstone. Similar to lithofacies of shaly siltstone and siliceous calcareous mudstone, the lithofacies is only present in the Kockatea Shale.

The depositional environments in this study are interpreted based upon the core comparison between Kockatea and Carynginia formations and the Cretaceous Gates Formation at British Columbia. Closer scrutiny in detecting depositional settings of lithofacies is acquired by optical and electron microscopic analyses (using polarized petrographic microscope and scanning electron microscope), X-ray diffraction (XRD) technique, and FTIR spectroscopy through identifying minerals, clay minerals, and fossils indicating certain environmental zones.

Petrographical and mineralogical analyses were studied on eleven samples taken from the areas within distinct lithofacies in the cores, and table 3.3 provides a brief summary of their core plugging description.

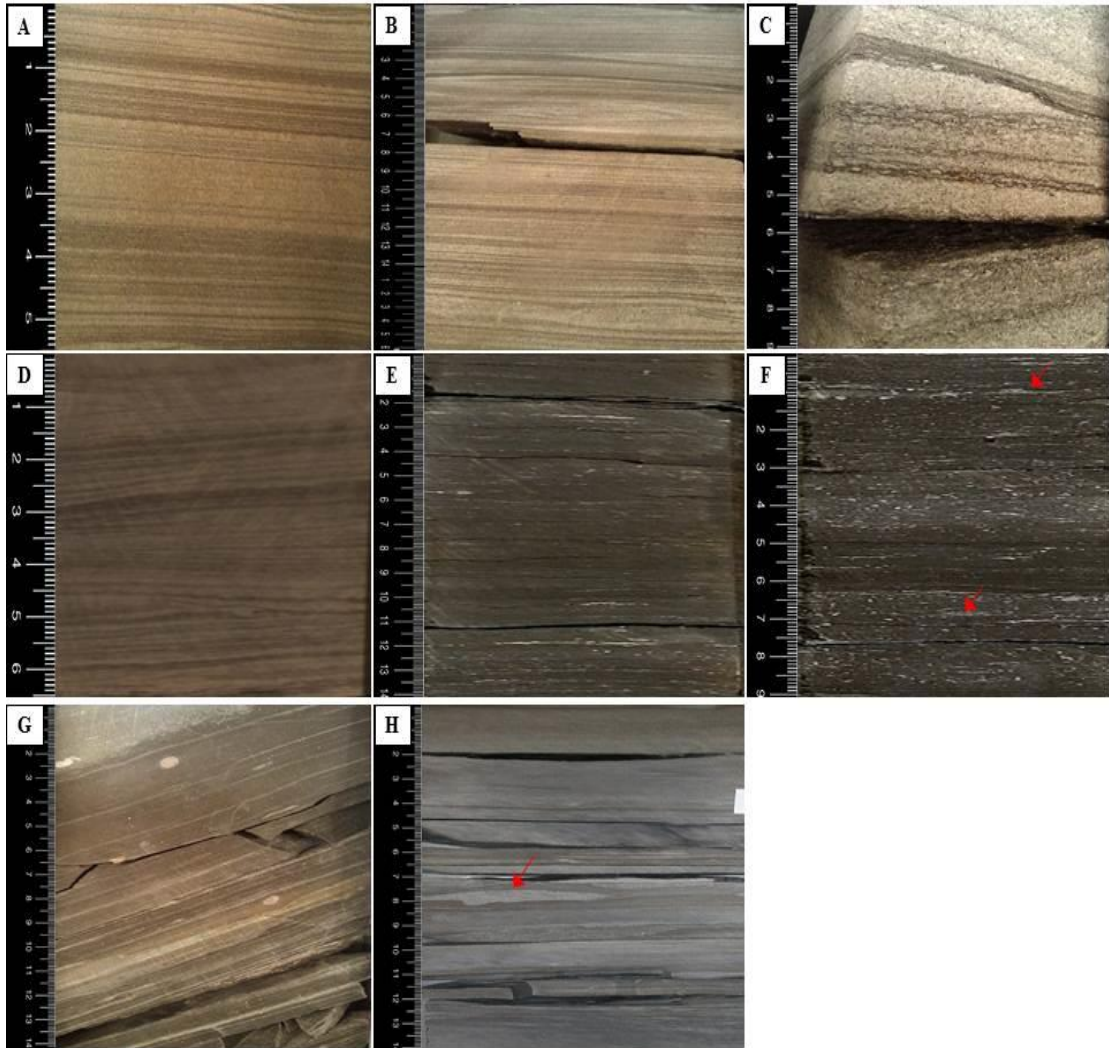


Figure 3.4: Core photographs displaying (A) the interlamination of shale and fine-grained sandstone related to shaly-sandy interlaminated mudstone from Kockatea Shale at the depth of 91.44-91.55 m, Jurien-1(B) parallel and crossed-bedded sandstone from Carynginia Formation at the depth of 1724.61-1724.81 m, Dongara-1(C) parallel bedded medium to coarse-grained sandstone from Carynginia Formation at the depth of 1494.30-1494.39 m, Beharra-2 (D) core photo of shaly siltstone lithofacies showing the lithofacies in form of silt laminations within shale from Kockatea Shale at the depth of 2267.13-2267.19 m, Arrowsmith-1(E) the light to dark gray interlamination of siliceous calcareous mudstone from Kockatea Shale at the depth of 1975.40-1975.64 m, Hovea-3 (F) the skeletal components filled by sparry calcite (red arrows) within siliceous calcareous mudstone at the depth of 1972.74-1972.97 m, Hovea-3 (G) the interlamination of sandstone and siltstone related to sandy-silty interlaminated deposit from Kockatea Shale at the depth of 1414.95-1415 m, Cliff Head-4 (H) the lenticular structure of sandstone in siltstone for sandy-silty interlaminated deposit lithofacies from Kockatea Shale at the depth of 1413.64-1413.78 m, Woolmulla-1.

Table 3.3: Selected samples for core plugging acquired from Northern Perth Basin.

Lithofacies	Well Name	Plug's Depth	Sub-basin
Black shale	Redback-2	3819.3 m	Dandaragan Trough
Pyritic mudstone	Redback-2	3798.8 m	Dandaragan Trough
Siliceous mudstone	Redback-2	3832.7 m	Dandaragan Trough
Calcareous mudstone	Redback-2	3834.5 m	Dandaragan Trough
Fossiliferous mudstone	Redback-2	3792.5 m	Dandaragan Trough
Bioturbated mudstone	Woodada Deep-1	2374.8 m	Dandaragan Trough
Wavy laminated deposit	Dongara-1	1682.0 m	Dandaragan Trough
Shaly-sandy interlaminated mudstone	North Erregulla-1	2938.5 m	Dandaragan Trough
Shaly siltstone	Ejarno-1	2725.0 m	Dandaragan Trough
Siliceous calcareous mudstone	Yardarino-1	2233.3 m	Dandaragan Trough
Sandy-silty interlaminated deposit	Cliff Head-4	1414.9 m	Abrolhos sub-basin

3.3 Thin Section Petrography

Thin sections were used for petrological and mineralogical observations to study the rock's microscopic features, mineral composition, and the textural relationship within the rock. The microstructure and structure presented in thin sections are able to reveal the origin of the rock (Pichler and Schmitt-Riegraf, 1997). Thin sections were prepared in a standard size (30 µm) from core plugs taken within each lithofacies and mounted on 50 mm microscope slides. Thin sections were viewed using a Nikon Eclipse LV100POL petrographic polarized microscope under two variant lighting conditions, plain polarized (PPL) and crossed polarized (XPL) lights.

The minerals were recognized using their textural characteristics and depositional properties. Grain size, sorting and mineral distribution were used to identify the depositional environment within each lithofacies.

3.3.1 Results

Thin section images illustrate detailed geological parameters that identify lithofacies such as grain size and its distribution, colour, sedimentary structure, as well as determining qualitative mineral composition. Geological parameters observed in thin section are summarised at table 3.4.

The analysis of black shale displays a dark matrix that indicates a high amount of organic matter. Brown colour within images refers to the constitutive clay minerals within lithofacies (see figure 3.5A). The opaque rhombohedral crystal of pyrite with black colour can be distinguished in the thin section image of pyritic mudstone at figure 3.5B. Petrographical image of siliceous mudstone illustrates high dispersion of poor sorted quartz within the clay matrix (see figure 3.5C).

Table 3.4: Summary of geological properties in the lithofacies acquired by thin section petrography.

Lithofacies	Mineral composition	Grain size	Grain distribution	Sedimentary structure	Special characteristics
Black shale	Clays, quartz, and mica	Very fine	Uniform	Not observed	Uniformly granulated
Pyritic mudstone	Pyrite, clays, sparry calcite	Fine-grained	Non-uniform	Sparry calcite filled vacant spaces	Black rhombohedral crystal of pyrite
Siliceous mudstone	Quartz, clay with biotite in the matrix	Fine-coarse grained	poorly sorted and have intense size differences	Not observed	Proximal particles, poor sorted and poor roundness
Calcareous mudstone	Clays, autochthonous and detrital calcite, glauconite	Fine-coarse grained	poorly sorted and have intense size differences	Not observed	Proximal particles, poor sorted and poor roundness
Fossiliferous mudstone	Clays, mica, quartz, pyrite	Fine-grained	Matrix uniform fossils are distributed as non-uniformly	Thin-wall compacted fossils within matrix	Thin-wall brachiopods, Calcareous foraminifer
Bioturbated mudstone	Clay, quartz, glauconite	Fine-grained	Non-uniformly distributed	Bioturbation	There are many cavity within matrix
Wavy laminated deposit	Quartz, mica, gypsum	Fine-grained	Uniformly distributed	Wavy lamination	High organic matter (dark colour) observed in the head of wave
Shaley-sandy interlaminated mudstone	Clays, quartz, mica, minor pyrite and calcite	Fine-medium grained	Non-uniformly distributed	laminated structure	continuous change in sedimentary environment
Shaley siltstone	Clays, quartz, mica	Fine-medium grained	Non-uniformly distributed	Not observed	A slight alignment is recognized
Siliceous calcareous mudstone	Clays, calcite, quartz, mica	Fine-coarse grained	poor-sorting quartz and have intense size differences	Not observed	Carbonate is more than silica. Clastic particles entered to the calm environment with already deposited clays
Sandy-silty interlaminated deposit	Quartz, mica, minor clays	Fine-grained	Non-uniformly distributed	Interlaminations of sandstone and silt	a clear alignment is recognized

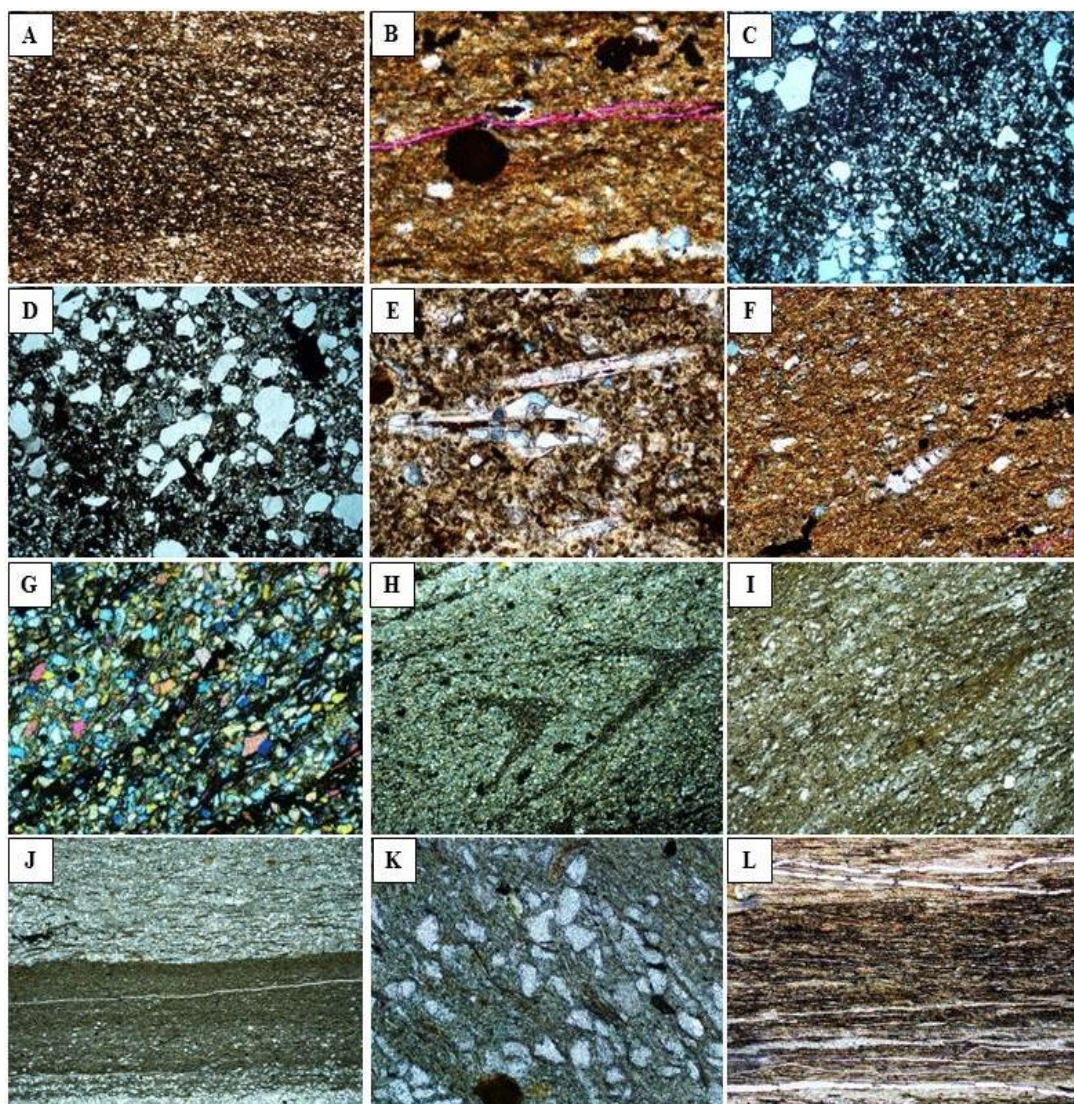


Figure 3.5: Thin-section photomicrographs of (A) Black shale that displaying the lithofacies composition; clay minerals (dark brown), fine grained quartz (white), mica (light brown). The photo is taken with plain polarized light at a low magnification of 2.5x from Kockatea Shale at the depth of 3819.32 m, Redback-2 (B) pyritic mudstone, showing an opaque framboidal pyrite, crossed polarized light at high magnification of 20x from Kockatea Shale at the depth of 3798.82 m, Redback-2 (C) siliceous mudstone, representing high values of detritus quartz in silt and coarser sizes taken at a low magnification of 2.5x with plain polarized light from Kockatea Shale at the depth of 2233.30, Yardarino-1 (D) Calcareous mudstone, illustrates the detrital and autochthonous calcite with minor silica content into the clay matrix, captured with plain polarized light at a low magnification of 2.5x from Kockatea Shale at the depth of 3821.67 m, Redback-2 (E) fossiliferous mudstone, displaying brachiopod arms within clay matrix along with phosphatic Oolitic, taken with crossed polarized light with magnification of 2.5x from Kockatea Shale at the depth of 3792.55 m, Redback-2 (F) the photomicrograph showing a Lower Triassic foraminifera, taken with plain polarized light with magnification of 10x from Kockatea Shale at the depth of 3805.92 m, Redback-2 (G) bioturbated mudstone, there is no special character for this lithofacies thin section image, captured with crossed polarized light at magnification of 5x from Carynginia Formation at the depth of 2374.86 m, Woodada Deep-1 (H)

wavy laminated deposit, the image displaying a wavy structure in the lithofacies at a low magnification of 2.5x with plain polarized light from Carynginia Formation at the depth of 1682.04, Dongara-1 (I) shaly siltstone, the photomicrograph indicates the scattering of silt in shale. The image is taken with plain polarized light at a low magnification of 2.5x from Kockatea Shale at the depth of 2725.04 m, Ejarno-1 (J) shaly-sandy interlaminated mudstone, displaying the obvious lamination of shale and fine-grained sandstone, the image is taken with plain polarized light at low magnification of 2.5x from Kockatea Shale at the depth of 2938.55 m, North Erregulla-1(K) siliceous calcareous mudstone, the photomicrograph illustrates the presence of carbonate and quartz components; quartz particles represents poor sorting and roundness, captured with plain polarized light at magnification of 10x from Kockatea Shale at the depth of 2233.30-2233.31 m, Yardarino-1(L) sandy-silty interlaminated deposit, thin section petrography indicates special alignment within lithofacies. The image is taken with crossed polarized light at a low magnification of 2.5x from Kockatea Shale at the depth of 1414.97m, Cliff Head-4.

Thin section petrography of calcareous mudstone is shown at figure 3.5D. Compacted thin-wall brachiopods surrounded by phosphatic fossils which according to Railsback (2012) are oolitic lithified in the clay matrix coupled with organic matter (Figure 3.5E). Some Lower Triassic foraminifers such as *Siphovalvulina variabilis* Septfontaines and *Paleomayncina termieri* (Hottinger) were also observed within the sample (Figure 3.5F). Thin section images of bioturbated mudstone and wavy laminated deposit are shown at figures 3.5G and 3.5H, respectively. The bioturbation structure cannot be clearly diagnosed in the presented thin section at figure 3.5G. However, it looks like something has shaped mineral aggregates; the black areas indicate the passages of the sediment- reworking organisms. Thin section petrography in shaly siltstone displays the dispersion of siltstone in shale (figure 3.5I). The thin section image of shaly-sandy interlaminated mudstone is displayed at figure 3.5J. Siliceous calcareous mudstone shows a higher proportion of carbonate in comparison with quartz within the lithofacies since carbonate is mixed with matrix (Figure 3.5K). Figure 3.5L displays sandy-silty interlaminated deposit.

3.4 Scanning Electron Microscopy (SEM)

A scanning electron microscope is used for surface topographic studies by using a focused beam to create various signals at the sample's surface. It has

high magnification, high resolution, and a large depth of field. Sample preparation for SEM analysis is challenging and depends highly on material properties. It is important that samples are vacuum compatible and sufficiently conductive to avoid charging. Small rock particles (3.5 mm×5 mm) were mounted to stub using carbon tape (dag), and then were coated with platinum which is inert and conductive. The specimens were imaged using a Zeiss EVO40 XVP scanning electron microscope under secondary electron (SE) detector with magnification between 1000 and 3000, and the image resolution of 1 μm and 10 μm based upon the diagnostic ability of the detailed specimens. SEM images were used to study rock composition and texture at the micro-nano scale.

3.4.1 Results

SEM analysis determined the exposure of different minerals in the lithofacies along with identifying nano-scale minerals such as clay minerals group. The SEM image of black shows the dispersion of clay minerals within the lithofacies (see figure 3.6A). The framboidal pyrite is brightly displayed through the electron microscope (Figures 3.6B and 3.6C). In contrast with siliceous mudstone that illustrates a particular orientation in the clay minerals along with scattered particles of silicate (Figure 3.6D), calcareous mudstone displays a random dispersal of calcite and silicate within the clay matrix (Figure 3.6E). The SEM image of fossiliferous mudstone indicates the distribution of fossils within lithofacies (Figure 3.6F).

Similar to petrographical analysis, there is no particular index for bioturbated mudstone using electron microscope since the sedimentary structures are visible in the larger scales. Nonetheless, the perturbation is partly shown in SEM image of the lithofacies at figure 3.6G. The SEM photographs are unable to display laminated structures in the lithofacies of wavy laminated deposit (Figure 3.6H), and shaley-sandy interlaminated mudstone (Figure 3.6I). SEM image of shaley siltstone illustrates how the components are mixed together (Figure 3.6J). The scanning electron microscopy confirms the existence of both carbonate and silicate in the

siliceous calcareous mudstone lithofacies (see figure 3.6K). In sandy-silty interlaminated deposit, SEM shows the dispersion of kaolinite in the matrix (Figure 3.6L).

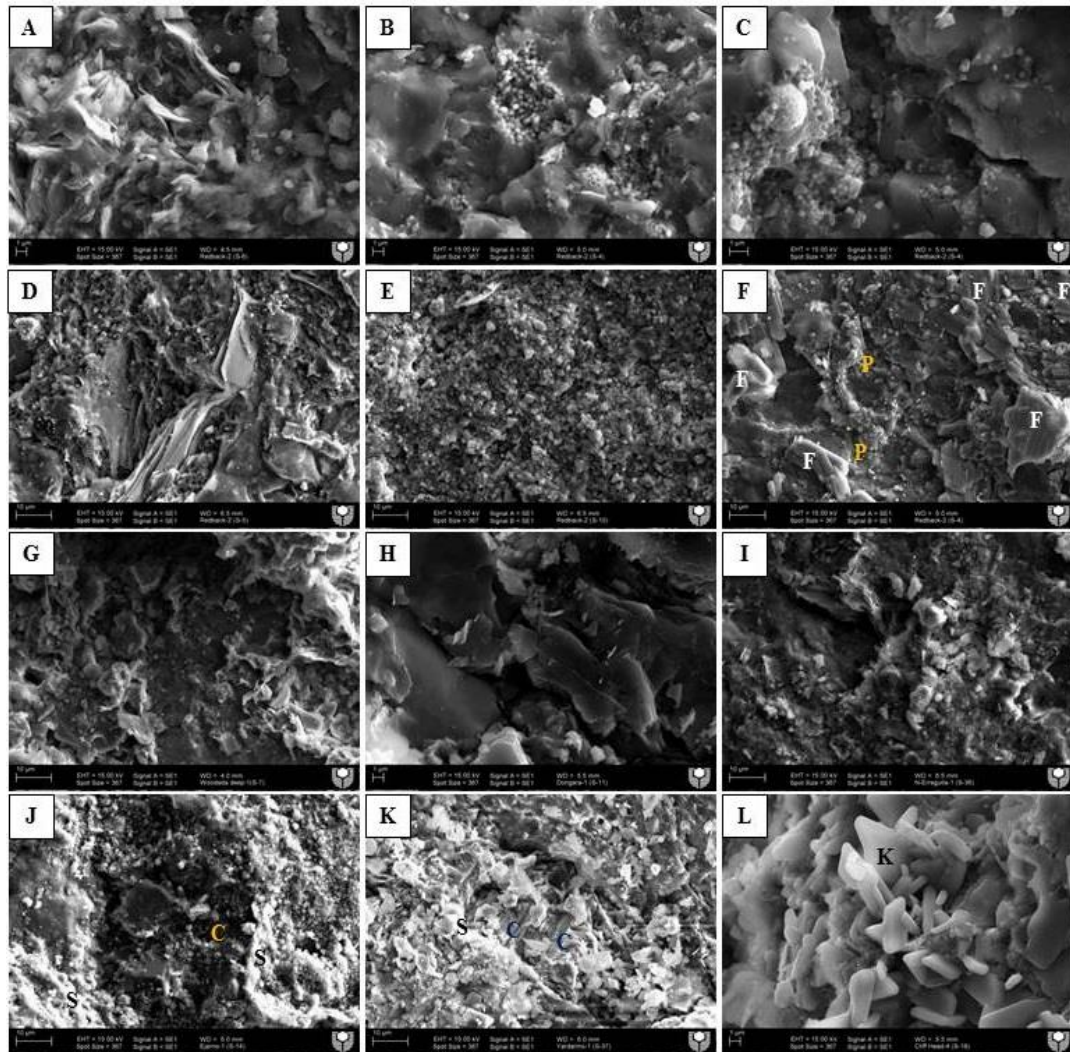


Figure 3.6: The SEM images of (A) black shale, the image showing the scattering of clays in Kockatea Shale at the depth of 3819.32-3819.36 m, Redback-2 (B-C) pyritic mudstone which displaying rhombohedral structure of pyrite, in terms of recognition of pyrite SEM is undoubtedly the most successful way. The images are taken from Kockatea Shale at the depth of 3798.82-3798.87 m, Redback-2 (D) siliceous mudstone, ascertaining a special alignment in clays, red arrow showing rhombohedral pyrite crystals. The SEM image is taken from Kockatea Shale at the depth of 3832.75-3832.80 m, Redback-2 (E) Calcareous mudstone, showing the lithofacies without any especial alignment. Depth of 3834.5-3834.55 m, Redback-2 (F) Fossiliferous mudstone, the distribution of fossils and pyrite displaying in the image from Kockatea Shale at the depth of 3792.55 m, Redback-2 (G) Bioturbated mudstone, the turbulence is nearly recognizable in the image, at the depth of 2374.84-2374.87 m, Woodada Deep-1(H) wavy laminated deposit, due to identifying this lithofacies based on its structure, the possibility of seeing the wavy structure at the image scale rarely happens, the photo is taken from Carynginia Formation at the depth of 1682.00-2682.04 m, Dongara-1 (I) shaly-

sandy interlaminated mudstone from Kockatea Shale at the depth of 2938.5310-2938.5463 m, North Erregulla-1(J) Shaly siltstone, displaying the distribution of silicate and clays within lithofacies, the photo is captured from Kockatea Shale at the depth of 2725.00-2725.05 m, Ejarno-1 (K) siliceous calcareous mudstone, showing the scattering of silica and carbonate components together in the lithofacies. The photo is taken from Kockatea Shale at the depth of 2233.30-2233.31 m, Yardarino-1(L) sandy-silty interlaminated deposit displaying kaolinite within matrix at the depth of 1414.95-1415 m, Cliff Head-4.

3.5 X-ray Diffraction Technique (XRD)

Historically, X-ray diffraction (XRD) methods have been used to identify the different types of minerals present in a rock (Gibbs, 1967; Bish and Post, 1993; Srodoń et al., 2001). The quantitative determination of mineral composition is a significant challenge. Various methods such as Rietveld analysis, pattern addition, and reference intensity ratio have been developed to address this issue. Quantitative XRD results can depend highly on the grain size and the mean particle size should ideally be less than 10 µm with a narrow size range (Tucker, 1988). Figure 3.7 shows the steps used for sample preparation. In this study, grinding was conducted using a McCrone micronizing mill for five minutes to avoid damaging the crystallites by strain and phase transformation by localized heating. This was also done to achieve a homogenous mix with the standard and to break up aggregates within the material to obtain a particle size of < 5.0 µm. In order to determine amorphous content Calcium Fluoride (-325 mesh, Sigma-Aldrich, Australia) was added as an internal standard (0.3 g CaF₂ and 3 g sample) before placing in the micronizing mill. The micronizing mill is a wet grinding process so acetone was used with the sample mixture. The slurry of the shale, fluorite, and acetone was allowed to dry at 70 °C. The prepared powder was packed in the cavity mount from its rear side in the manner described by Klug and Alexander (1974).

An XRD pattern from the micronized sample was measured using a Bruker-AXS D8 Advance Diffractometer with copper radiation and a LynxEye position sensitive detector. The data were collected from 7 to 120° 2θ with a nominal step size of 0.015° and a collection time of 0.7 seconds per step.

Crystalline phases were identified by using the Search/Match algorithm, DIFFRAC.EVA 2.1 (Bruker-AXS, Germany) to search the Powder Diffraction File (PDF4+ 2011 edition). Relevant crystal structures extracted for refinement were obtained from the Inorganic Crystal Structure Database (ICSD 2012/1). A divergent slit at 0.3 degrees, and a nickel Cu-K beta filter were used with primary Soller slits = 2.5°, secondary Soller slits = 2.5°, Receiving slit = 0.1 mm, detector slit = 1.0 mm. The crystalline phases were determined on an absolute scale using the Rietveld quantitative phase refinement technique (Rietveld, 1969), utilizing the Bruker-AXS TOPAS v4.2 software package.

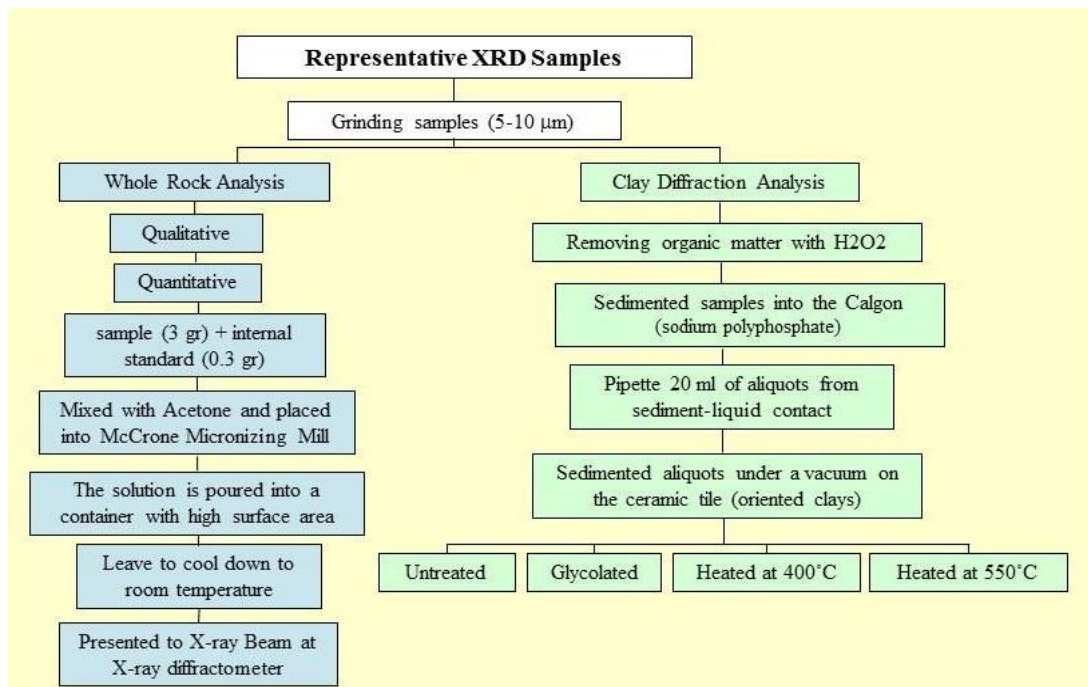


Figure 3.7: The stages of XRD sample preparation.

For clay diffraction analyses, the organic matter was removed by treating the shale samples with hydrogen peroxide (H₂O₂) as described by Hyeong and Capuano (2000). Calgon (sodium polyphosphate) was used as a base liquid to disperse the samples. Aliquots (20 ml) were extracted after 4h at 20°C temperature for the expected particle size of <2μm from the sediment-liquid contact and the suspension fluid was placed on a porous ceramic tile under suction. The oriented clay samples were treated in four different ways (i.e., air-dried, glycolated, heated at 400°C and heated at 550°C). Ethylene

glycol treatment was used for distinguishing chlorite from smectite where a possible overlap occurs. Glycolation causes the smectite to expand to a basal spacing of about 17 Å (Tucker, 1988).

3.5.1 Results

Two different XRD methods (i.e., whole-rock and clay fraction) were used to identify the clay minerals present in the various shale samples.

3.5.1.1 XRD Whole Rock (XRD Bulk)

Whole rock XRD analyses were performed on all samples. Figure 3.8 shows the XRD pattern of fossiliferous mudstone. Table 3.5 provides a summary of the minerals found and their abundance. Quartz was evident in all samples and the amount varied from 18 to 66 wt%. In terms of the clay mineralogy, kaolinite was found in most of the samples except for samples of siliceous mudstone and black shale. It is evident that the lithofacies of wavy laminated deposit and sandy-silty interlaminated deposit contained significant levels of kaolinite (≥ 30 wt%). Pyrite was present in most of the samples except for siliceous calcareous mudstone and shaley-sandy interlaminated mudstone.

XRD also detected various polytypes of muscovite (2M1 and 1M) and it was found that the lithofacies of siliceous mudstone, fossiliferous mudstone, pyritic mudstone and black shale comprised more than 30 wt% muscovite. There is the possibility of transforming smectite into mixed layers of illite-smectite, following by the transformation of illite to muscovite (Van De Kamp, 2008).

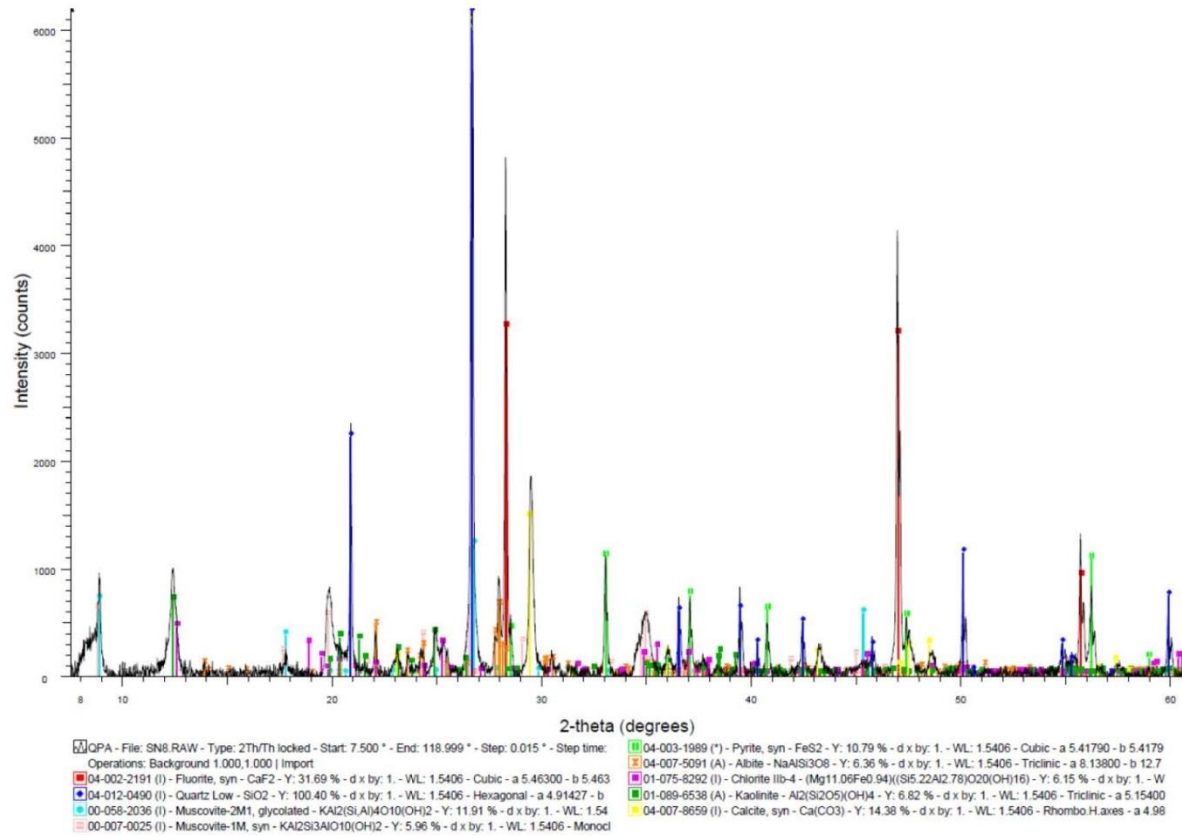


Figure 3.8: Selected 2-theta region showing phase identification in the sample of fossiliferous mudstone lithofacies.

Table 3.5: Phase abundance of identified mineral phases from the Kockatea shale and the Carynginia Formation.

Weight%											
Phase	BS	PM	SM	CM	FM	BM	WLD	ShSIM	ShS	SCM	SSID
Albite	6.1	7.1	7.3	7.4	10.3	12.5	-	-	-	-	-
Calcite	-	-	-	40	9.7	-	-	-	-	-	-
Calcite magnesium	-	-	-	-	-	-	-	-	-	10.0	-
Chlorite	7.1	2.8	6.1	-	1.6	-	-	-	-	-	-
Gypsum	-	3.9	-	2.1	-	2.1	2.4	-	-	1.1	4.3
Jarosite	-	-	-	4	-	3.9	7.2	-	3.6	-	3.2
Kaolinite	-	11.8	-	3.1	16.1	3.2	30	22	11.7	25	35
Microcline	-	-	-	2.1	-	-	12.8	18	7.4	15	7.7
Illite-smectite	41	35	32	-	35	-	-	-	-	-	-
Muscovite 1M	-	-	-	-	-	5.1	-	12.5	5.0	4.7	-
Muscovite 2M1	-	-	-	9.8	-	20	15.6	7.1	-	14.7	10.2
Pyrite	0.7	15	1.3	1.5	4.3	1.4	2.2	-	2.4	-	7.3
Quartz	42	18.2	50	27	20.2	46	22.4	34.8	66	20.7	16.8
Amorphous	3	6.2	3	3	2.8	5.8	7	5.6	3.9	8.8	15.4
Total	99.9	100	99.7	100	100	100	99.7	100	100	100	99.9

*Amorphous content determined by difference.

BS: black shale, PM: pyritic mudstone, SM: siliceous mudstone, CM: calcareous mudstone, FM: fossiliferous mudstone, BM: bioturbated mudstone, WLD: wavy laminated deposit ShSIM: shaly-sandy interlaminated mudstone, ShS: shaly siltstone, SCM: siliceous calcareous mudstone, SSID: sandy-silty interlaminated deposit.

A number of potential crystalline phases were detected in the lithofacies. The kaolin in lithofacies of ‘SSID’ and ‘WLD’ was highly disordered which makes data refinement difficult; therefore, its quality (wt %) could only be defined. A clear shift was shown in the <0 0 1> kaolin reflection in samples of ‘ShSIM’, ‘SM’, ‘CM’ and ‘WD1’, which have been accounted for by shifting the lattice parameters of software. There are many undefined peaks in all of the samples which were incorporated as wt% of the associated phases into the ‘amorphous contents’, shown at table 3.5. The muscovite phases in the data refinement show the best matches possible from the database. However, there is no ideal structure for these samples.

Overall, the XRD patterns are broad, with irregularity in some clay phases, and many overlapped peaks. The phases defined in table 3.5 give the best mathematical fit to phases.

3.5.1.2 XRD Clay Fraction

The platy behavior of clay minerals is well known and is responsible for causing problems due to preferred orientation which can lead to significant XRD errors. Whole rock XRD patterns can also be limited when determining clay mineral types and clay fraction analysis may be more reliable (Smith et al., 1987). Appendix A.1 shows XRD patterns for the samples studied with different treatments (air dried, glycolated, heated to 400°C, and heated to 550°C) and it is evident that different clay groups were detected. The clay minerals were identified based on the clay mineral identification flow chart from Starkey et al. (1984). The identified clay groups by XRD clay fraction are listed along with clay identification acquired by XRD bulk and FTIR at table 3.7.

3.6 Fourier Transform Infrared Spectroscopy (FTIR)

3.6.1 Techniques

Although XRD is a powerful technique, problems with preferred orientation and the presence of amorphous components can cause large quantitative errors. One recent study has shown that XRD over-predicts the quartz content in clay rich systems without clay separation (Sondergeld et al., 2010). Other techniques such as Fourier transform infrared spectroscopy (FTIR) have been extensively used for mineral identification (Povarennykh, 1978; Solomon and Miknis, 1980; Kaufhold et al., 2012). Matteson and Herron (1993) have shown that FTIR can provide chemical and mineral information on complex samples such as shales without the need for separating clays. Although FTIR is a powerful technique for mineral characterization, it does have some limitations with respect to clay quantification (Kaufhold et al., 2012), such as similar peak positions and overlap with many different types of clay that makes any reliable identification difficult.

A KBr pressed pellet was prepared for all samples. To reduce the infrared light dispersion on the particle surfaces, the samples were ground to 200 mesh. The ground shale sample (~2 mg) was dispersed in KBr (~200 mg)

and a Pike Technologies hand press was used to make a pellet. The pressed pellets were heated overnight at 120 °C prior to measurements to remove water features. All mid-infrared (MIR) measurements were made in transmission mode using a Vertex 70 FTIR spectrometer. Data was recorded in the 4000 to 400 cm⁻¹ range using a spectral resolution of 4 cm⁻¹ and a total of 16 scans were averaged for each sample spectra.

3.6.2 Results

To further understand the clay mineralogy, FTIR was used to characterise the shale samples. Figure 3.9 displays the infrared results, and table 3.6 summarises the wavenumbers for the main peaks detected in the spectra. The position and shape of the O-H and Si-O bands in the IR spectra is highly important in distinguishing different clay minerals (Madejová, 2003). According to Kaufhold et al. (2012), clay minerals can be identified by dividing the spectrum into the following five regions: (1) the hydroxyl stretching region (3450-3750 cm⁻¹) (2) carbonate region (1360-1580 cm⁻¹) (3) SiO₂ stretching region (975-1300 cm⁻¹) (4) smectite OH deformation (815-950 cm⁻¹), and (5) MeO deformation (450-580 cm⁻¹).

Table 3.6: Recognition of clay minerals based on the wavenumbers from transmission IR spectrum.

Lithofacies	Wavenumber (cm ⁻¹)	Identified Minerals
Black shale	3622, 3431, 1164, 1093, 1037, 798, 779, 693, 520, 474	Illite, montmorillonite
Pyritic mudstone	3695, 3621, 3397, 1094, 1032, 914, 828, 798, 778, 694, 672, 660, 629, 534, 473, 427	Kaolinite, montmorillonite, illite
Siliceous mudstone	3621, 3423, 1164, 1090, 1034, 798, 778, 693, 515, 473	Illite, montmorillonite
Calcareous mudstone	3621, 3421, 1164, 1090, 1036, 798, 778, 693, 515, 473	Montmorillonite, illite
Fossiliferous mudstone	3696, 3620, 3432, 1426, 1092, 1032, 914, 876, 829, 798, 778, 711, 695, 650, 535, 472, 429	Kaolinite, montmorillonite, illite
Bioturbated mudstone	3623, 3411, 1029, 797, 778, 693, 632, 532, 475	Montmorillonite, illite
Wavy laminated mudstone	3694, 3668, 3652, 3620, 3393, 1093, 1033, 1011, 938, 914, 796, 694, 631, 539, 472, 431	Kaolinite, montmorillonite, illite
Shaly-sandy interlaminated mudstone	3696, 3652, 3620, 3424, 1032, 1009, 913, 796, 778, 694, 646, 537, 471, 431	Kaolinite, montmorillonite, illite
Shaly siltstone	3694, 3651, 3620, 3424, 1165, 1091, 1037, 797, 778, 693, 515, 470	Kaolinite, montmorillonite, illite
Siliceous calcareous mudstone	3696, 3651, 3620, 3429, 1032, 1009, 939, 913, 878, 797, 778, 694, 537, 470, 430	Kaolinite, montmorillonite, illite
Sandy-silty interlaminated deposit	3696, 3655, 3620, 3395, 1010, 914, 799, 779, 696, 539, 473, 430	Kaolinite, montmorillonite, illite

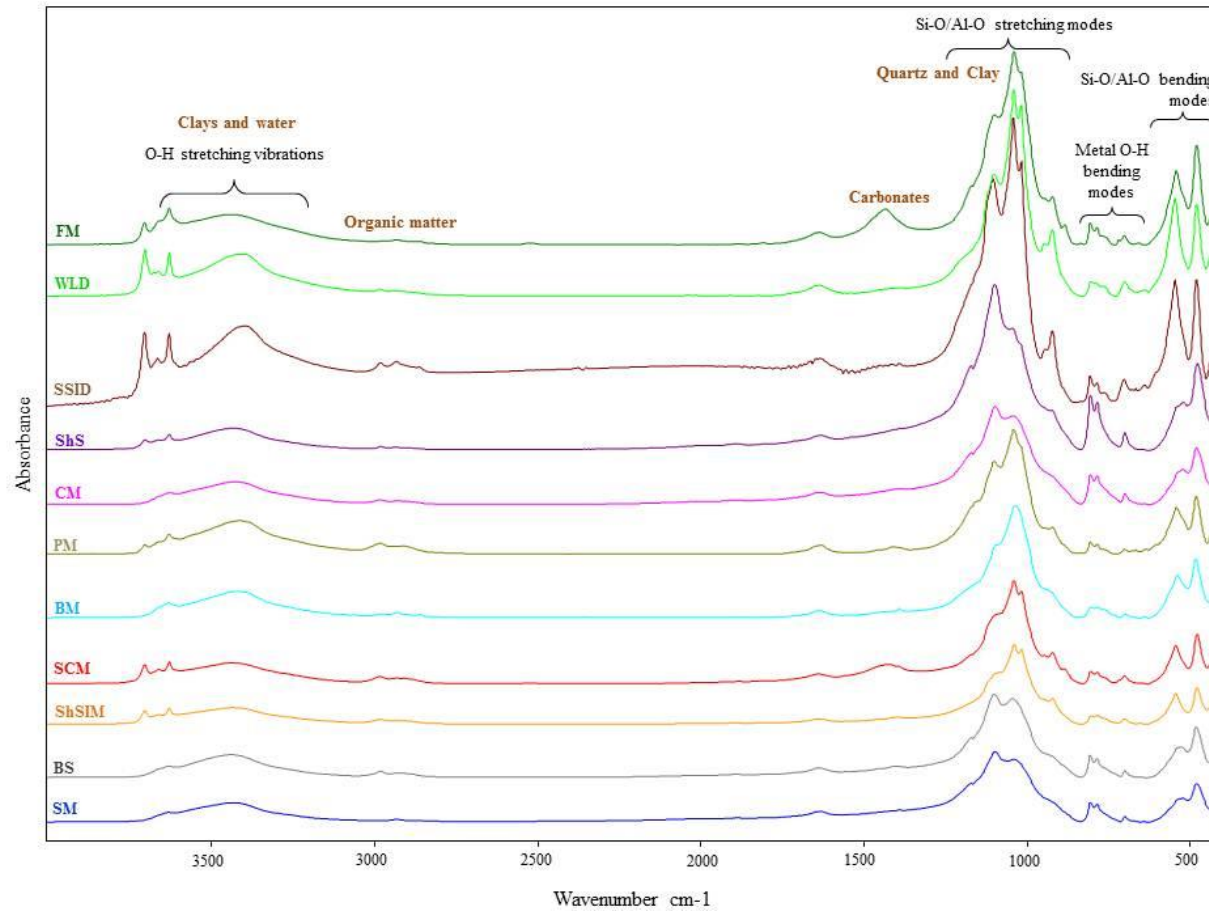


Figure 3.9: Infrared spectra of shale samples

Kaolinite can be easily detected from other clay mineral groups using FTIR and was one of the main clays detected in the shale samples. According to the IR spectra, most of the samples contained a significant amount of kaolinite except for lithofacies of siliceous mudstone, calcareous mudstone, bioturbated mudstone and black shale. This is somewhat consistent with the XRD results which revealed the absence or the presence of only very minor kaolinite content (<5 wt%) in lithofacies of siliceous mudstone, calcareous mudstone, bioturbated mudstone and black shale (see table 3.5). Unfortunately, no quantitative information was obtained on the amount of kaolinite (or any other phase) present in the shales by FTIR, since it requires the use of appropriate standards and the generation of a calibration curve. It is also evident from Figure 3.9 and table 3.6 that FTIR has detected a number of other clay minerals (possibly illite and montmorillonite). However, their peak positions are similar and they overlap with many different types of clays so that any reliable identification is difficult at this stage. Notwithstanding this, compositional information about other mineral components can be obtained, noting that the IR spectra also show absorption peaks due to quartz, carbonate and organic matter.

It is evident from Table 3.7 that some differences were observed in the identification of clay minerals by XRD and FTIR. The number of clay minerals found in the shale rocks by FTIR spectroscopy was considerably less compared to those obtained by XRD. The major clay components detected using FTIR were kaolinite, and possibly montmorillonite and/or illite. By contrast, XRD revealed the presence of these clay minerals along with chlorite. A number of other peaks were found in the XRD pattern, suggesting that various clay minerals may be present (i.e. possibly dickite and smectite) in the shale samples; however, further work is needed to confirm this. One reason for the lower number of clay minerals detected using FTIR is that significant peak overlap occurs in the IR spectra of the clays making it difficult to conclusively assign the bands to the different types. Another reason may be due to differences in the sensitivities/detection limit of XRD and FTIR for the various clay minerals.

Table 3.7: The list of identified clay groups by XRD bulk, XRD clay fraction and FTIR.

Lithofacies	XRD-Bulk	XRD-Clay	FTIR
Black shale	Chlorite, illite	Illite, chlorite, smectite	Illite, montmorillonite
Pyritic mudstone	Chlorite, kaolinite, illite	Illite, kaolinite, smectite	Kaolinite, montmorillonite, illite
Siliceous mudstone	Chlorite, illite	Chlorite, illite	Illite, montmorillonite
Calcareous mudstone	Kaolinite, illite	Kaolinite, chlorite, illite, smectite	Montmorillonite, illite
Fossiliferous mudstone	Chlorite, kaolinite, illite	Chlorite, illite	Kaolinite, montmorillonite, illite
Bioturbated mudstone	Kaolinite, illite	Kaolinite, illite, smectite	Montmorillonite, illite
Wavy laminated deposit	Kaolinite, illite	Kaolinite, illite, chlorite	Kaolinite, montmorillonite, illite
Shaly-sandy interlaminated mudstone	Kaolinite, illite	Kaolinite, illite	Kaolinite, montmorillonite, illite
Shaly siltstone	Kaolinite, illite	Kaolinite, illite	Kaolinite, montmorillonite, illite
Siliceous calcareous mudstone	Kaolinite, illite	Kaolinite, illite, smectite	Kaolinite, montmorillonite, illite
Sandy-silty interlaminated deposit	Kaolinite, illite	Kaolinite, chlorite, illite	Kaolinite, montmorillonite, illite

Both XRD and FTIR revealed significant differences in the mineral and clay composition between the eleven shale samples, suggesting that their physicochemical properties vary considerably. Smectite and illite with their hydrophilic properties are able to absorb a large amount of water and increase the wettability of the rock, whereas kaolinite is more likely to adsorb organic matter. Arduini et al. (2009) suggest that the presence of pore lining clays such as chlorite decrease the permeability of the reservoir rock. Kwon et al. (2004) have shown that illite is prone to blocking the pore spaces and this is more likely to have a high damaging effect on the permeability compared to other clay minerals. In general, rocks containing a high amount of clay minerals have less fracability relative to rocks with higher quartz and carbonate contents (Morris and Shepperd, 1982).

3.7 Depositional Settings

The depositional environments of the Carynginia and Kockatea shales were identified through the visual core description, along with their sedimentary structure and trace fossil assemblages.

3.7.1 Carynginia Formation

Some sedimentary structures in non-shale facies of Carynginia Formation such as hummocky cross-stratification, wave ripples, and sporadic conglomeratic lenses confirm the deposition of this formation under shallow marine environment with proglacial conditions in the Late Artinskian. U.S. Energy Information Administration (2011) believes that the depositional environment in Carynginia Formation tends to be a restricted marine. Open marine conditions are determined in the later phase of deposition. The deposition under anoxic environment with reduced circumstances is indicated for the lithofacies of black shale and pyritic mudstone within the Carynginia Formation. The wavy laminations of bedding displayed in the Carynginia Formation at Dongara-1 is considered to be a component of tidal dominated delta (Davis and Dalrymple, 2012), particularly in the areas with high sedimentation rate where the bedding is preserved well (Reineck and Singh, 1980). The turbulence of layers by biota makes the gas reservoir potential impossible for the layers, as static conditions are required for preserving organic matter. Bioturbation in the Carynginia Formation at Woodada Deep-1 demonstrates the domination of oxygenated bottom waters in the layers. Schieber (1994) states that bioturbation can be used as an oxygen indicator in the water column. There are burrows in the cores which cross-cut the deposited laminations because of their temporal differences. It seems that the organisms occupied the mudstone shortly behind the deposition and ahead of depositing of the overlying layers. Restricted (Morris, 1979) or dysaerobic (Byers, 1977) conditions are suggested for the bioturbated mudstone due to the presence of trace fossils as well as the disrupted shale fabrics and laminae, and the absence of body fossils (Schieber, 1994).

3.7.2 Kockatea Shale

The presence of foraminifers of *Siphovalvulina variabilis* Septfontaines and *Paleomayncina termieri* (Hottinger), in association with brachiopods in cores of the Hovea Member at Redback-2 reveal the deposition under deep marine conditions. The variant sizes of quartz and abundant clays observed

in thin-sections of Hovea Member (Basal Kockatea Shale) at figure 3.5C suggest the possibility of a calm pre-environment with the entering of detrital quartz particles later. The fragmentation of coarser grains into the fine-grained particles, along with the absence of fossil record indicates the dominance of high energy environment during the sedimentation. The authigenic and allogenic particles of quartz and carbonate with well sorting and roundness seen in the thin-section of the Kockatea Shale at Yardarino-1 suggest a high distance from the sediment supply. Due to it having authigenic quartz precipitation, it appears the sedimentation was under deep sea conditions (Muza and Wise, 1983).

The abundance of pyrite in the Hovea Member at Redback-2 illustrates the deposition under reduced circulation. Berner (1989) believes that most of the sedimentary rocks, especially marine sediments contain minimum traces of pyrite. Consequently, the mineral is widely used as an indicator for recognising various redox controlling cyclic transitions and sedimentary environments (Raiswell & Berner, 1985; Raiswell et al., 1988; Boesen & Postma, 1988; Raiswell et al., 1994; Wilkin et al., 1997; Suits and Wilkin, 1998). The rhombohedral crystals of pyrite form where sulfide has sufficient time to react with the precursor minerals (Roychoudhury et al., 2003). The main discussion on the black shale facies is related to their origins (shallow vs. deep-water). The facies are likely to have been deposited in the conductive conditions to preserve the organic matter within mudstone since the main constituent of black shale is the organic matter, consisting of depleting the dissolved oxygen in waters which is overlying the water/sediment interface (Arthur, 1994). The wavy lamination lithofacies in some core samples from the Kockatea Shale suggests a dominance of tidal delta for this unit in some parts of the basin. The core studies showing the dominance of mudstone facies indicate that the target shales are mostly deposited in relatively deep and low energy water. Figure 3.10 shows the vertical distribution of lithofacies in the Carynginia Formation at Woodada Deep-1 and in the Kockatea Shale at Redback-2.

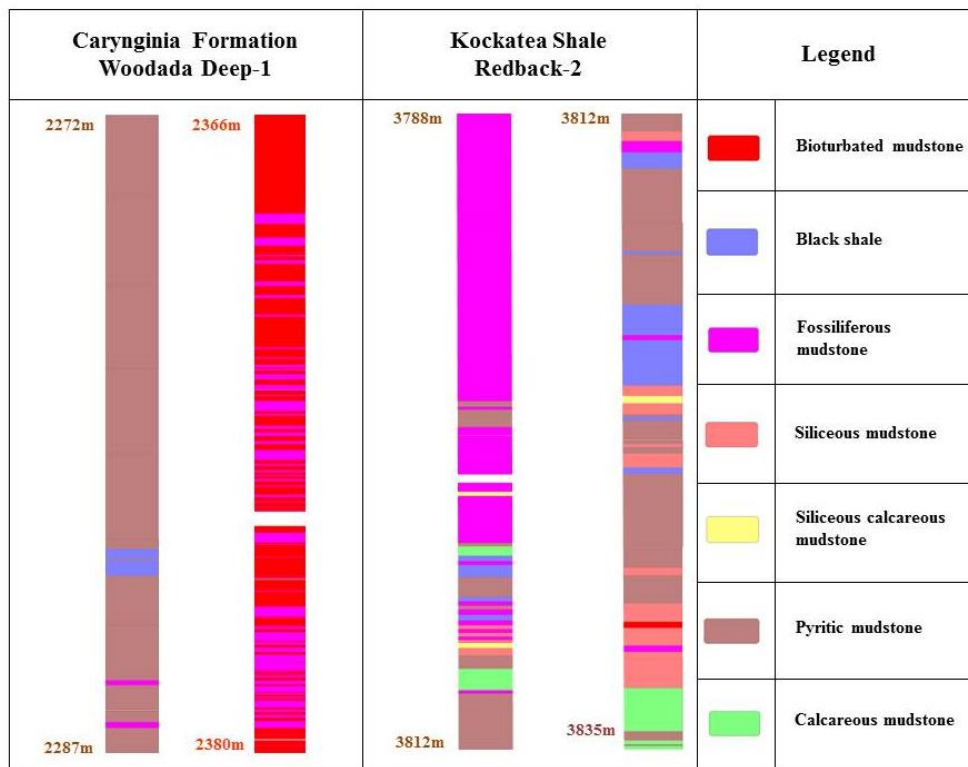


Figure 3.10: Vertical distribution of lithofacies within the Carynginia Formation (left), and the Kockatea Shale (right).

The currents, with a variety of velocities, affected some facies within the Kockatea and Carynginia formations. The evidence confirms the deposition of the Hovea Member (the most prospective part of Kockatea Shale) in the shallow water during the earliest phase of a marine transgression.

3.8 Fracability and Mineralogy

Fracability or the reservoir's ability to be efficiently fractured (Jaripatke, 2012) is a key to success in producing gas economically through inducing fractures within low permeability shale reservoirs. A number of geological factors impact the fracability of shale including mineral composition, sedimentary fabric, as well as presenting weakness planes (Mullen and Enderlin, 2012). Mineral variability indirectly influences hydraulic fracturing technique through the effect of different minerals on fracability (Sondergeld et al., 2010). This effect is calculated by revealing the relevance of mineralogical components and brittleness within the rock. The proportion of clay-carbonate-quartz defines the brittle index of the rock as:

Brittleness index (%) = quartz/ (clays+carbonates+quartz) (Wang and Gale, 2009).

In general, the siliceous component promises high fracability in comparison with more clay type minerals with high ductility. Nevertheless, it can be changed based on the rock's nature (BBY Ltd., 2010) so that unlike detrital quartz, recrystallized silica restricts the brittleness along developing continuous quartz cement within the pores (Passey et al., 2010; Jarvie et al., 2007). Neutral mechanical characteristics of carbonates also challenge carbonate-rich shales through avoiding the dispersion of fractures (Manger et al., 1991). The proportion of clay minerals, especially illite-smectite mixed layer clays which significantly reduce permeability, strongly influences the brittle behaviour of shale (Eichhubl et al., 2005). According to Khalid et al (2010) silica-rich zones are considered to have better long-term productivity from induced fractures compared to the clay content zones where fractures close in on themselves in a short duration. Petrophysical studies were conducted using various log data such as resistivity logs and dipole sonic logs to confirm the zones with greater fracability (discussed in chapter 5).

3.8.1 Results

The presence of recrystallized quartz along with detrital quartz at figure 3.11 threatens the legitimacy of equality of higher quartz with higher fracability. It should be said that recrystallized silica has the most effective role in reducing fractures by creating a continuous framework for quartz content (Passey et al., 2010). However, there is a negligible amount of recrystallized silica in the identified lithofacies of the target formations. The brittleness index is identified for individual lithofacies regarding their mineralogical contents obtained by XRD bulk analysis (Table 3.8), followed by plotting these acquired amounts on the ternary diagrams (Figure 3.12).

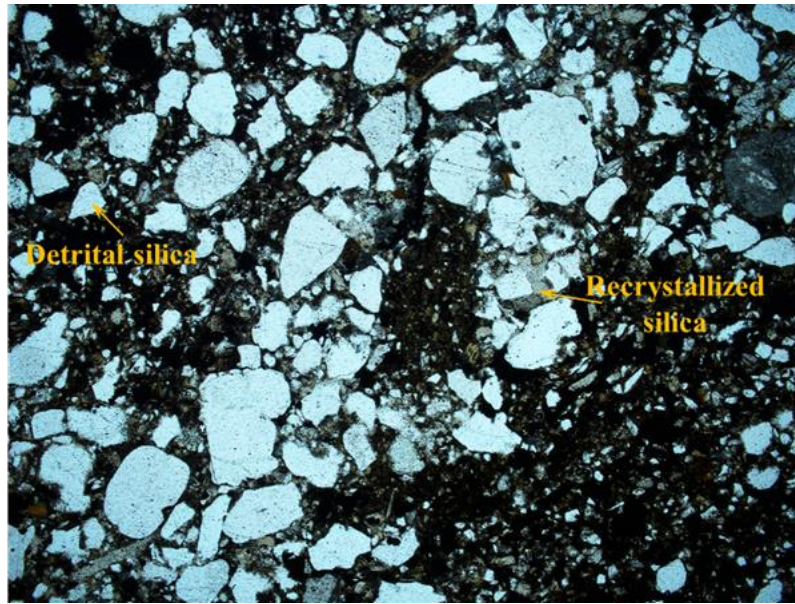


Figure 3.11: The figure shows presence of recrystallized quartz and detrital quartz within Calcareous mudstone lithofacies from the Kockatea Shale at the depth of 3834.5 m, Redback-2.

Table 3.8: Brittleness index for individual lithofacies within the target formations (based on Wang and Gale, 2009)

Lithofacies	Quartz	Carbonates	Clay minerals	Brittleness Index
Black shale	42	0	48.1	0.466
Pyritic mudstone	18.2	0	49.6	0.268
Siliceous mudstone	50	0	38.1	0.567
Calcareous mudstone	27	40	7.1	0.364
Fossiliferous mudstone	20.2	9.7	52.7	0.244
Bioturbated mudstone	46	0	7.1	0.866
Wavy laminated deposit	22.4	0	37.2	0.376
Shaly-sandy inter. mudstone	34.8	0	22	0.613
Shaly siltstone	66	0	15.3	0.812
Siliceous cal. mudstone	20.7	10	25	0.372
Sandy-silty inter. deposit	16.8	0	38.2	0.305

The ternary plot illustrates that the lithofacies of shaly siltstone, bioturbated mudstone, and siliceous mudstone with more than 50 wt% quartz enjoy more fracability compared to the lithofacies of siliceous calcareous mudstone, black shale, shaly-sandy interlaminated mudstone, wavy laminated deposit, sandy-silty interlaminated deposit, fossiliferous mudstone, and pyritic mudstone which have dominantly clays in their composition and

thus the least fracability. Moreover, the carbonate content is high in calcareous mudstone.

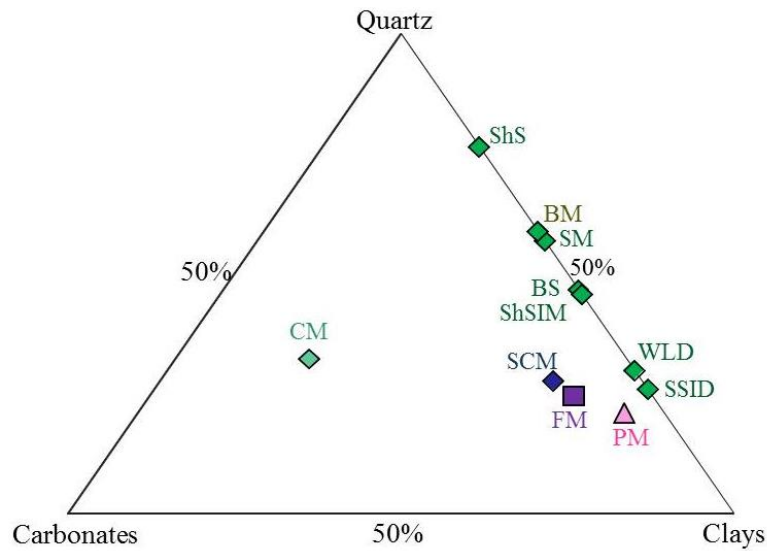


Figure 3.12: Clay- quartz-carbonate ternary diagram displaying mineral composition in various lithofacies, lithofacies with higher quartz content are more brittle than clayed shales.

BS: black shale, PM: pyritic mudstone, SM: siliceous mudstone, CM: calcareous mudstone, FM: fossiliferous mudstone, BM: bioturbated mudstone, WLD: wavy laminated deposit ShSIM: shaly-sandy interlaminated mudstone, ShS: shaly siltstone, SCM: siliceous calcareous mudstone, SSID: sandy-silty interlaminated deposit.

Chapter 4: Geochemical Studies

In addition to characterising petrologic and mineralogic features, the identification of potential shale plays depends on the adequate knowledge of the organic geochemistry of the shale layers. It is important to know whether favourable geologic zones, assessed by petrologic and mineralogic analyses, contain the least organic content (TOC) to be considered as a reservoir, and what type of organic compounds they are and what their level of maturity is. The amount of organic matter, kerogen type and its thermal maturity strongly affect the pores distribution, fluid saturation, in situ natural gas (Sondergeld et al., 2010), and their quality. Preliminary geochemical analyses including biomarker dispensation, rock-eval pyrolysis and vitrinite reflectance measurement on the Carynginia and Kockatea formations by Thomas and Barber (2004), showed a range of immature to the late mature intervals (Geological Survey of Western Australia, 2005). Geochemical parameters of prospective shale plays were studied through a variety of analytical techniques such as Rock-Eval pyrolysis, geophysical well-log response, and vitrinite reflectance measurement.

4.1 Total Organic Carbon (TOC)

4.1.1 Rock-Eval Pyrolysis

The technique is widely utilized to provide information about key geochemical parameters such as TOC, kerogen type, thermal maturity, and relative hydrocarbon potential (RHP). According to Sondergeld et al (2010) Rock-Eval is a combusting method which pyrolysize organic matter describing common peaks of S₁ (the liquid hydrocarbons distilled from the rock/volatilization at 300°C of existing HC), S₂ (the amount of convertible kerogen/pyrolysis of kerogen), and S₃ (the amount of inorganic carbon dioxide released/released of trapped CO₂). In fact the technique is used to

quantify productivity (production index), the kerogen conversion potential (hydrogen index) and the carbon dioxide in the rock (oxygen index). Peters (1986) promises an accurate measuring of TOC by Rock-Eval method when inorganic carbon is removed from carbonate prior to combustion. Rock-Eval data for the Kockatea Shale and the Carynginia Formation was provided by Department of Mines and Petroleum (DMP), and Figure 4.1 displays the areas with TOC content of 1-3 wt% for the formations of Kockatea and Carynginia in the Perth Basin.

Table 4.1: Average TOC content obtained from different lithofacies. Note that common lithofacies in two target formations vary slightly in terms of TOC content (TOC data provided by DMP).

Lithofacies	Black shale	Pyritic mudstone	Siliceous mudstone	Calcareous mudstone	Fossiliferous mudstone	Bioturbated mudstone
TOC-wt%	4.9	4.7	2.2	2.5	2.5	2.7
Lithofacies	Wavy laminated	Shaly-sandy interlaminated	Shaly siltstone	Siliceous cal. mudstone	Sandy-silty interlaminated deposit	
TOC-wt%	0.28	0.7	0.86	2.5	0.26	

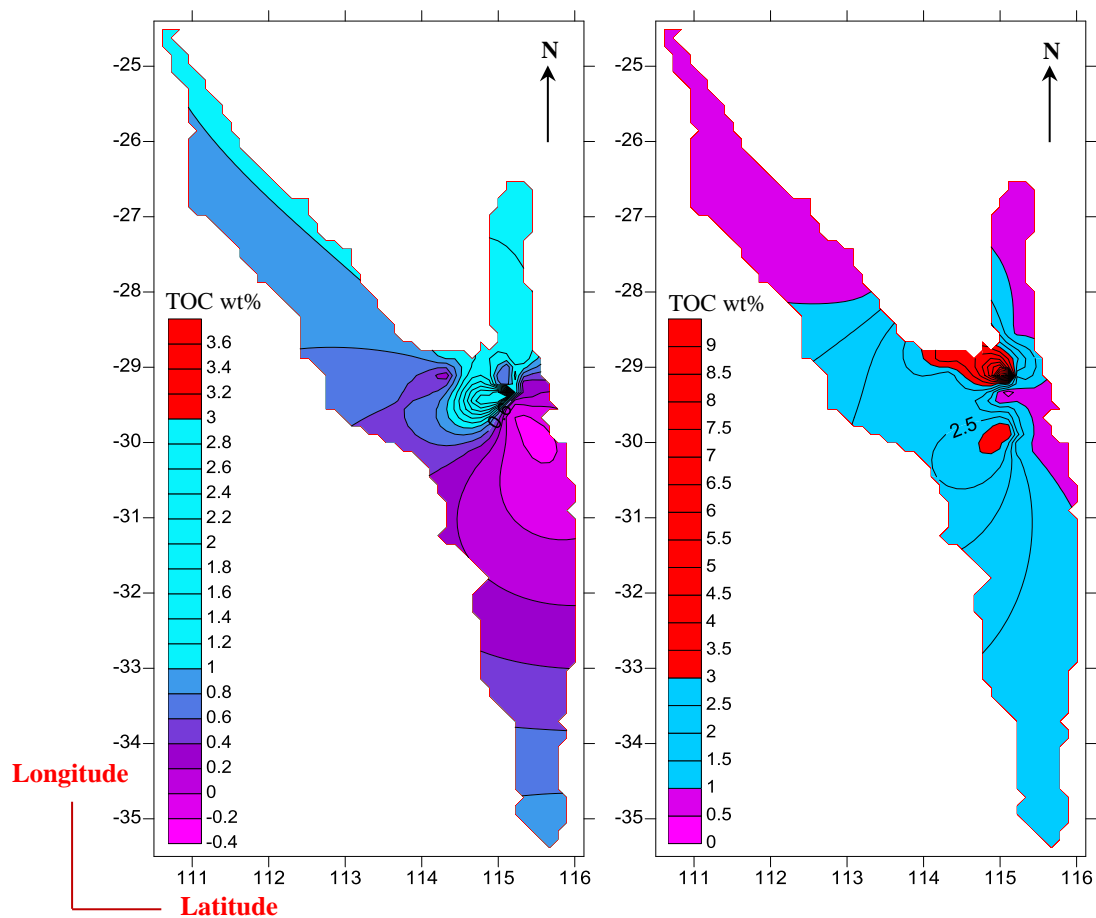


Figure 4.1: The distribution of TOC within the Kockatea Shale (left), and the Carynginia Formation (right) across the Perth Basin.

Appendix B.1 summarises the results of Rock-Eval technique for these two formations. There is lower TOC content in the Kockatea Shale compared to the Carynginia Formation which with TOC > 3 wt% is considered to have a reasonable shale gas potential.

It is crucial to carefully check the effects of mineral matrix on the organic matter when TOC < 1.5%, such that the presence of smectite and illite within the matrix leads to the adsorption of generated hydrocarbon through cracking of the kerogen on the clay minerals surfaces (Wu et al., 2012).

The estimation of TOC in various lithofacies revealed the highest TOC value within black shale, and the pyritic mudstone as a second lithofacies with a great organic-richness (Table 4.1).

4.2 Kerogen Type

The designation of kerogen type contributes to the identification of depositional settings, organic type, thermal maturity, and gas potential in the source rocks. Jarvie et al (2007) suggests that the amount and type of kerogen, as well as its thermal maturity impact on the amount of absorbed gas in kerogen. Kerogen type and the degree of maturation in the organic matter were estimated by cross-plotting some Rock-Eval parameters such as TOC versus HI on a Van Krevelan diagram (Figure 4.2). The diagram shows that the most plotted points of Carynginia Formation are located at gas-prone areas with type III kerogen, while the Kockatea Shale is mostly plotted in the oil and gas prone areas with a mixture of type II/III kerogen.

The diagram of TOC versus remaining hydrocarbon potential (S_2) at figure 4.3 confirms type III kerogen and a higher maturity in the Carynginia Formation. The presence of type II kerogen for the Kockatea Shale in this diagram is an indicator of depositing under marine conditions, compared to the Carynginia Formation which with most plotted points at the gas-prone area, reflects the deposition under the terrestrial or shallow marine conditions.

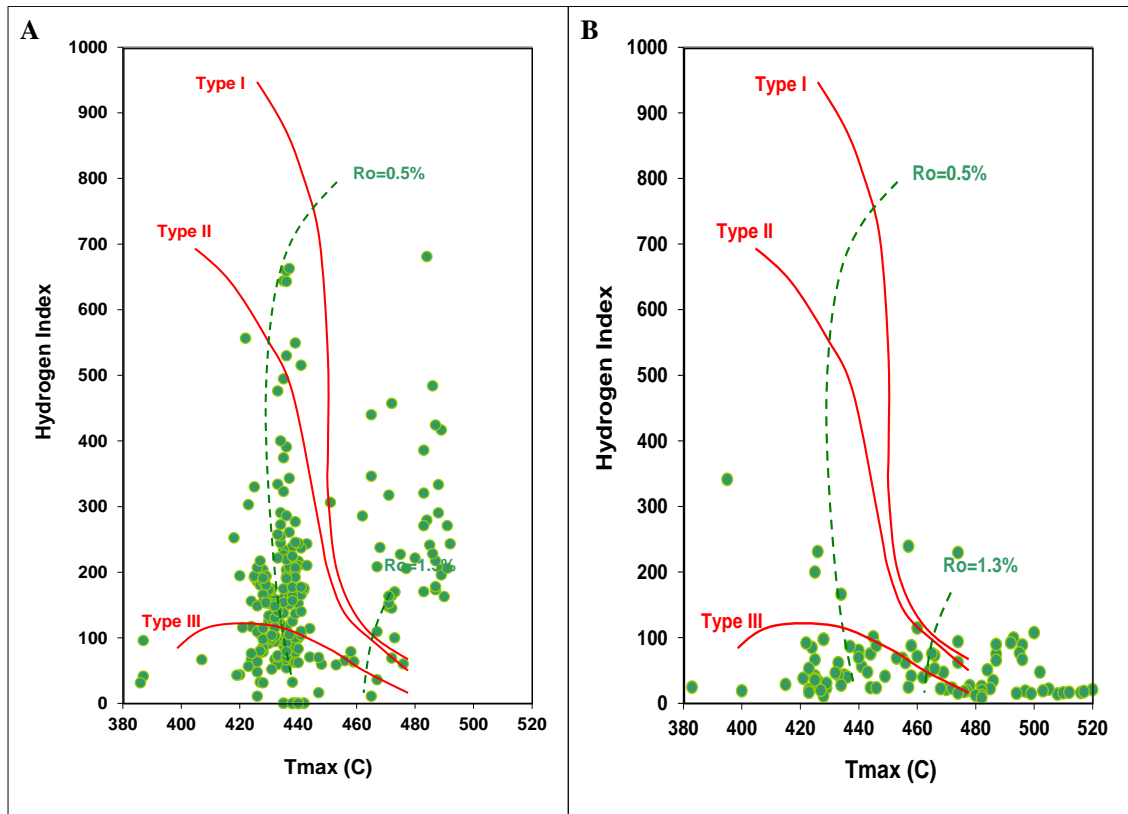


Figure 4.2: Van Krevelen diagrams of Kockatea Shale (A) and Carynginia Formation (B).

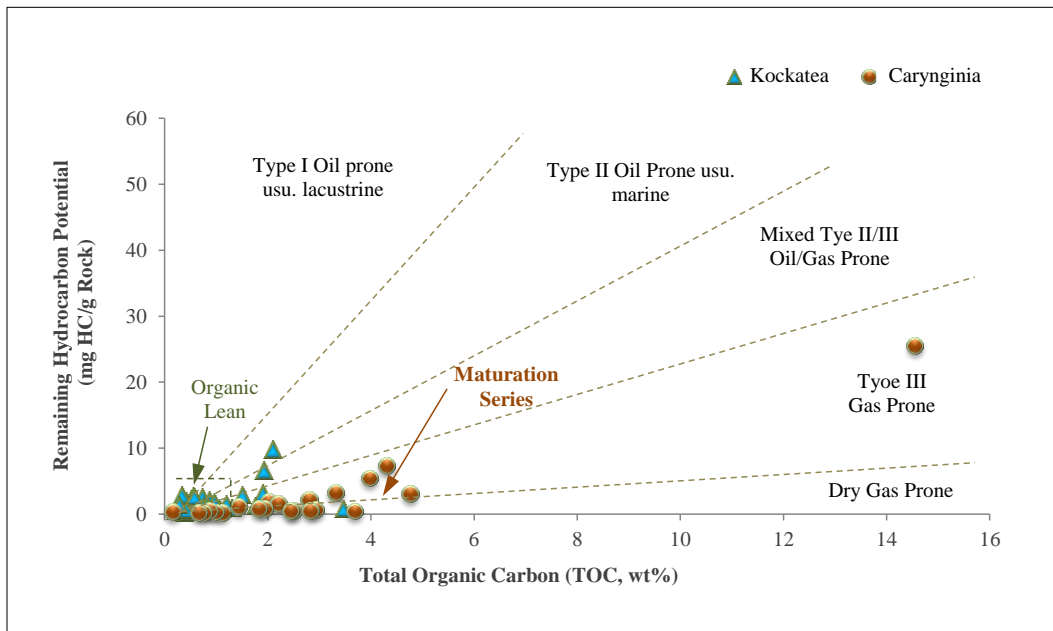


Figure 4.3: TOC versus Remaining Hydrocarbon Potential, displaying different types of kerogen as a function of thermal maturity.

4.3 Thermal Maturity

Thermal maturity refers to the degree of heating which has taken place for organic metamorphism to have processed into hydrocarbon. The parameter is commonly quantified by non-reversible special temperature-related, physical and chemical processes acting on the rock's components (Deaton et al., 1996). Shale thermal maturation can be identified by measuring vitrinite reflectance and Rock-Eval pyrolysis (Tmax). Figure 4.4 displays the relevancy of depth, vitrinite reflectance, and Tmax with different zones of hydrocarbon.

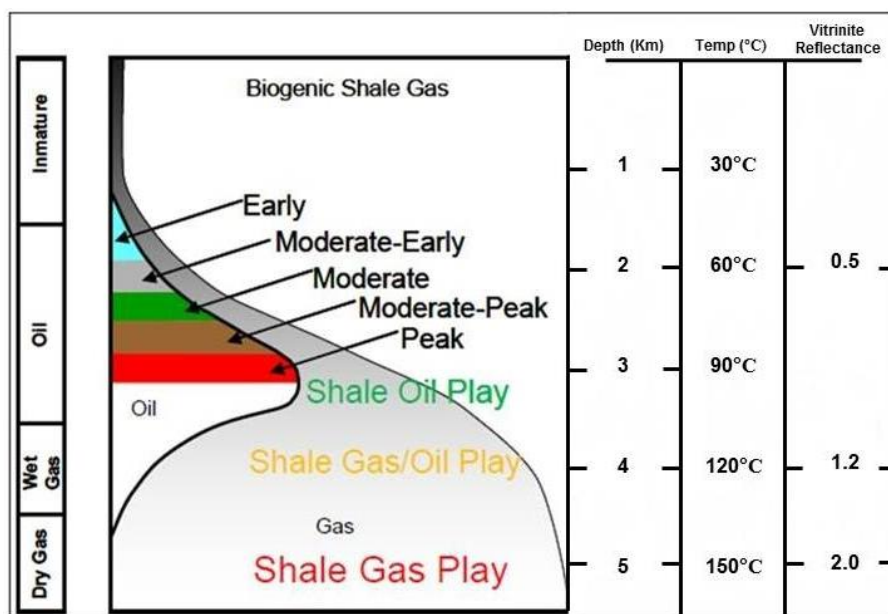


Figure 4.4: The schematic figure indicates the relationship between vitrinite reflectance, depth and max with various zones of a typical reservoir (modified from Glorioso et al., 2012).

4.3.1 Rock-Eval Pyrolysis (Tmax)

Thermal maturity is diagnosed based on Tmax or maximum temperature of decomposition of kerogen with respect to its relation with other geochemical properties such as TOC, remaining gas potential (S₂), and hydrocarbon index (HI). Tmax and S₂ data are available for the Kockatea Shale and the Carynginia Formation from 32 wells in the DMP reports, representing high organic richness along with immature to overmature

thermal maturity. The data at Appendix B.2 illustrates the highest Tmax within Kockatea Shale at wells of Jurien-1 and Woolmulla-1, whereas Wattle Grove-1 with the highest S₂ value of 9.84 shows the lowest Tmax. In the Carynginia Formation, the highest amount of Tmax is related to the wells of Jurien-1, Geelvink 1A and Woodada-6. Figure 4.5 displays the maturity of shale intervals in target formations through plotting Tmax versus depth.

Plot of Tmax data from studied wells on the basin's map highlights the areas with higher maturity in the Perth Basin, and the figure 4.6 indicates the greatest maturity of the Kockatea and the Carynginia formations in center of the basin. The diagram of TOC versus remaining gas potential- mg HC/g rock (Figure 4.3) implies higher maturation in the Carynginia Formation that is plotted in the gas-prone area with type III kerogen, whereas the Kockatea Shale is mainly plotted in oil and gas prone areas with mixed types II/III kerogen.

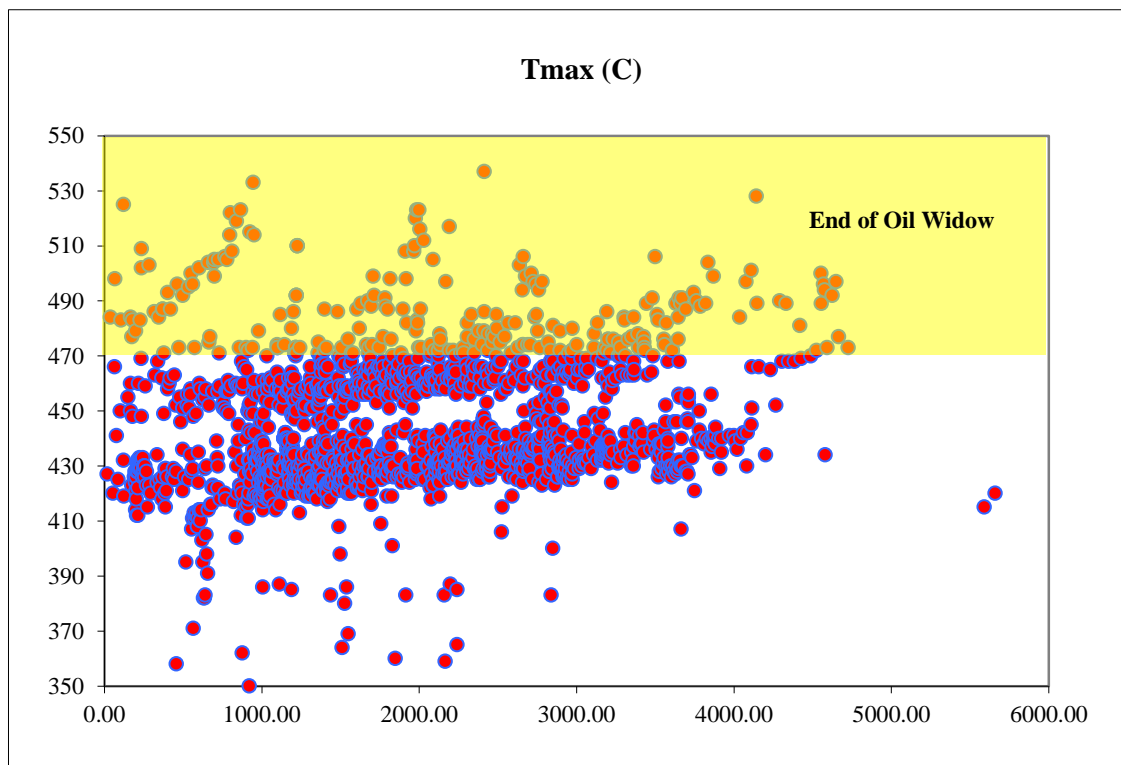


Figure 4.5: Tmax versus depth for shale samples of the Kockatea and the Carynginia in the Perth Basin.

4.3.2 Vitrinite Reflectance Measurement (Ro)

Vitrinite reflectance is the most popular approach, and it identifies the utmost paleotemperature reached by a source rock. The method is conducted by microscopic evaluation of kerogen which keeps track of the reflectivity of the particles. Thermal maturity is controlled by the preservation and the conversion of organic matter. In fact, the rate of decomposition of the organic matter highly affects the maturity windows. Indeed, gas generation is highly dependent on thermal histories and inherent decomposition rates (Jarvie et al., 2007). Waples & Marzi (1998) state that there is not universal correlation between the generation of hydrocarbon and the decomposition of vitrinite due to the kinetics of vitrinite and hydrocarbon generation overlap.

According to Burner and Smosna (2011), gas can be produced on a small scale at the commencement of thermal degradation of the kerogen ($R_o=0.5-0.6$). Nevertheless, the zone of $R_o < 1.0$ is mostly related to the low-gravity, low-sulfur, and slight condensate (Pollastro, 2007). It is at $R_o=1.1$ that oil in the shale starts to crack to condensate and gas (Hill et al., 2007). The level of maturity might be overestimated because of oil interacting with clay minerals or kerogen in the source rock which leads to it acting as catalyst (Burner and Smosna, 2011). The over-estimation of thermal maturity than measured by R_o could be because of the suppression of vitrinite reflectance (Comer et al., 1994). Applying a low amount of vitrinite to quantify maturity is another disadvantage of this procedure.

Jarvie et al (2007) suggest a relationship between the maturity of the organic-rich source rocks and their corresponding brittleness, which enables the identification of the feasible gas flow rate and the potential gas production from target shale plays. A geochemical database containing R_o information for the Kockatea and the Carynginia formations was used to interpret their thermal maturity (reported at Appendix B.3).

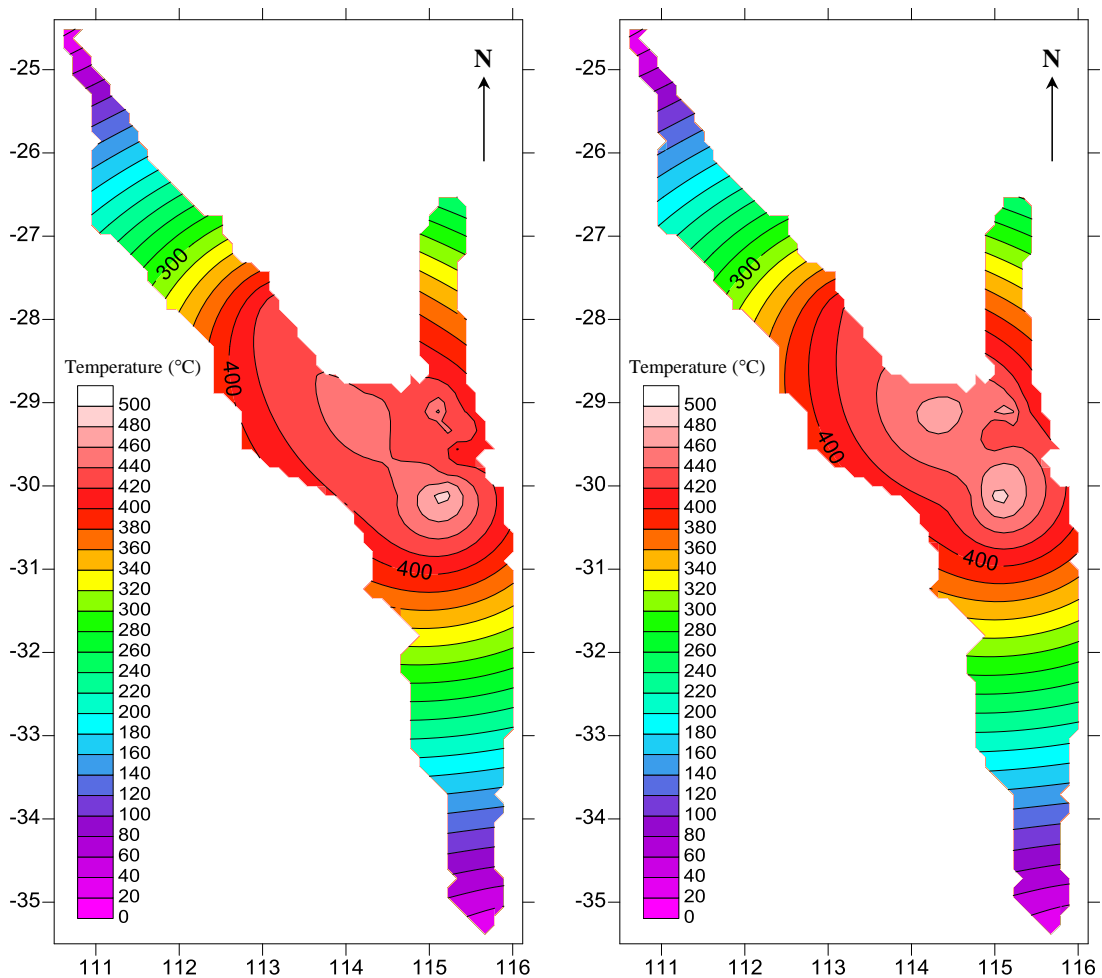


Figure 4.6: The figure display the highest organic maturity of Kockatea Shale (left), and Carynginia Formation (right) in the centre and north of the Perth Basin (based on Tmax data).

It is crucial to know about the kerogen type when measuring vitrinite reflectance (Glorioso et al., 2012). The depositional environment and the genetic hydrocarbon can be identified through determining the type and maturity of the kerogen (Talukdar, 2009). Appendix B.4 displays the relation of vitrinite reflectance to depositional settings and other geochemical parameters. Plotting Ro values of the target formations versus depth classifies the hydrocarbon's zones within samples based on the maceral type (Figure 4.7).

4.4 Relative Hydrocarbon Potential (RHP)

Relative hydrocarbon potential is a geochemical parameter acquired by pyrolysis with the formula of $(S_1+S_2)/TOC$. The parameter is critically

beneficial in developing a sequence stratigraphic framework, particularly in high frequency sequence stratigraphic analysis of shale gas systems (Abouelresh and Slatt, 2012). RHP is basically used as a paleoenvironmental indicator with the assumption that the maturity level of all samples is identical. Accordingly any change in S_1 and S_2 reflects changes in the quantity of preserved organic matter, not in the maturity level. A larger amount of organic matter will be preserved under anoxic conditions (highest S_2 peak) than under oxic conditions (least S_2 peak).

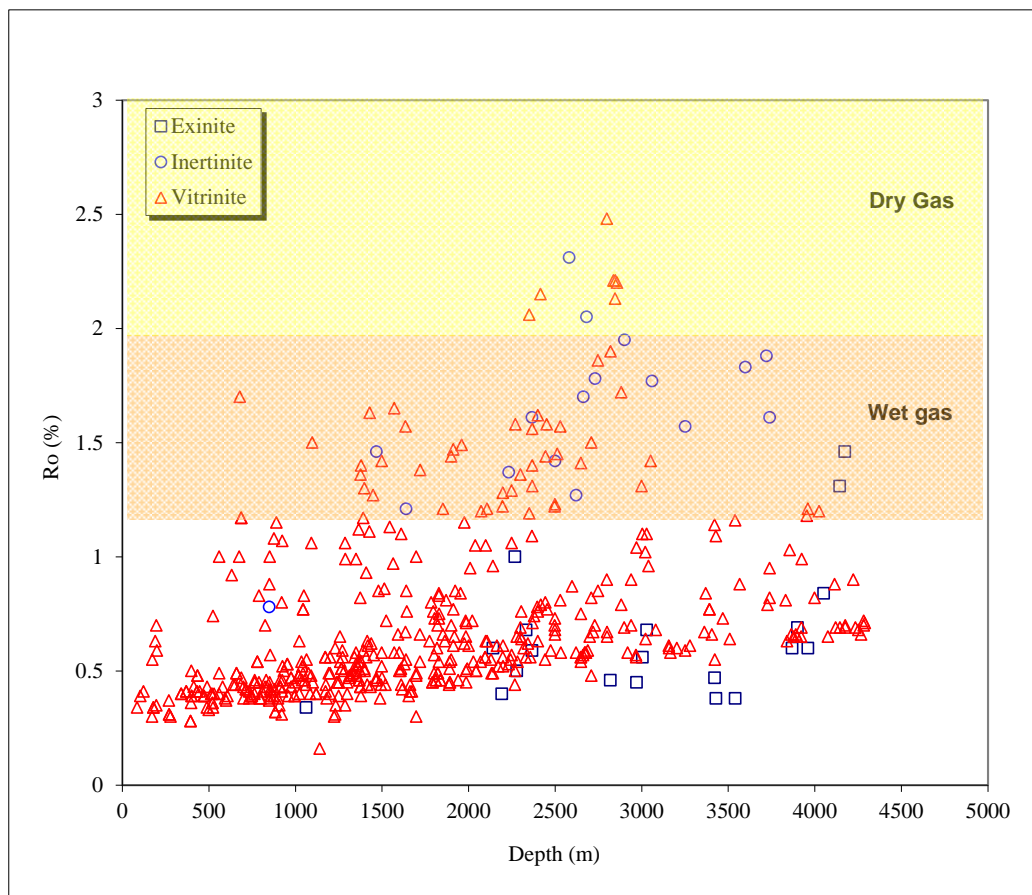


Figure 4.7: Plot of R_o versus depth for shale samples of the Kockatea and the Carynginia formations at the Perth Basin.

Hence the sediments deposited under oxic conditions have the smaller RHP value than for sediment deposited under anoxic conditions (Ghori, 2013).

Fang et al (1993) explain the concept of RHP pattern for detecting the organic facies sequence, in a manner that a decreasing upward RHP pattern suggests vertical organic facies changing from the features of anoxic to oxic

conditions, and conversely an increasing upward RHP pattern with vertical organic facies changing from the features of oxic to anoxic conditions. Table 4.2 illustrates the position of lithofacies with the amount of oxygen in the environment and organic richness. RHP can also be applied as an index of marine transgressions and regressions (Abouelresh and Slatt, 2012).

Table 4.2: The status of lithofacies in relevance to organic richness and the environmental oxygen.

Lithofacies	Features
Black shale Pyritic mudstone Bioturbated mudstone Fossiliferous mudstone Calcareous mudstone Siliceous calcareous mudstone Siliceous mudstone Shaly siltstone Shaly-sandy interlaminated mudstone Wavy laminated deposit Sandy-silty interlaminated deposit	<div style="display: flex; justify-content: space-around; align-items: center;"> <div style="text-align: center;">  Increase in the organic matter </div> <div style="text-align: center;">  Decrease in the oxygen within depositional environment  </div> </div>

Chapter 5: Petrophysical Studies

Petrophysical studies refer to the evaluation of chemical and physical rock properties along with their interaction with fluids by taking well log measurements. Petrophysical properties are commonly integrated with geological and geochemical and seismic measurements to give a comprehensive picture of the reservoir (Tiab and Donaldson, 2004), and to unlock retained hydrocarbons, which are mostly acquired by the combination of hydraulic fracturing and horizontal drilling (Jacobi et al, 2008, 2009). Numerous logging measurements are conducted in this approach to gain information about lithology, mineralogy, and stratigraphy. Petrophysical study classifies depositional facies through their mechanical and petrophysical characterizations, differentiates source rock intervals, quantifies total organic carbon (TOC), and defines the intervals with feasible fracture dispersion attenuation (Jacobi et al., 2008).

5.1 Lithofacies in Non-cored Wells

Due to insufficient core data for the target shales in the Perth Basin, a calibration of well log and core characteristics was conducted to identify lithofacies in the uncored wells. It is clear that the identification of lithofacies and lithostratigraphy in shales is not as simple as in carbonates and sandstones. Nevertheless, it is possible to relate various lithofacies stacking patterns to the stratigraphic changes in log character when a good match can be gained between core depth and log for a well (Slatt et al., 2011). Gamma ray log was used to detect the lithofacies and their stacking patterns in non-cored wells due to inadequate access to the other well logs in the study area. It is crucial to know that there is not a resolving power in gamma ray log to determine thin-bedded lithofacies in uncored wells; moreover, the fine scale stratigraphy can be missed by this method (Davis et al., 2006). Therefore, there is a noticeable uncertainty in relating well log-

derived characteristics with geological and laboratory-based petrophysical studies (Slatt et al., 2011).

However, the difficulties such as log to core depth correlation, deficient core representing all lithofacies, well log insensitivity to some bedding features and textures visible in core (Davis et al., 2006), and well log insensitivity to thin-beds can be dealt with by sufficient contrast in mineralogy and TOC content of under-studied lithofacies to affect gamma-ray log response (Slatt et al., 2011).

5.5.1 Gamma Ray Response of Lithofacies

Different lithofacies can be identified by establishing a classification model which separates the log data into sets of log responses, and these sets make it possible to characterise sediments and to discern them from each other (Serra and Abbott, 1980).

The gamma ray response of the identified lithofacies is shown at Appendix C.1. The facies of black shale displays high gamma ray value due to its high clay mineral content. Pyritic mudstone and siliceous mudstone depict a similar log trend. The presence of glauconite in the sandy-silty interlaminated deposit caused a surprising high gamma ray response. (refer to Appendix C.1); although the lithofacies does not contain shale facies, there is an increase in the amount of uranium (U) when the rate of glauconite is high within the lithofacies (Hesselbo, 1996). The gamma ray value varies in shaly-sandy interlaminated deposit, depending on the amount of clay minerals in the lithofacies. There is a considerable difference in the gamma ray value between siliceous calcareous mudstone and calcareous mudstone, such that the siliceous content reduces the log response in the siliceous calcareous mudstone. The lithofacies of fossiliferous mudstone, bioturbated mudstone, and wavy laminated deposit have a variable rate of gamma ray. Lower gamma ray value is displayed for shaly siltstone compared to the other lithofacies, but it is still $GR > 100$ (API). Having identified unique gamma-ray response of individual lithofacies, the next step is detecting these log responses in other wells (Shin and Philippe, 2000).

5.1.2 Electrofacies

The designation of lithofacies based on the analysis of the wireline logs is referred to as electrofacies which determines favorable log facies at cored and non-cored wells. In non-cored wells despite some challenges such as misclassification caused by missing well logs, electrofacies analysis is the most reliable way in determining desirable facies types in shale plays. The procedure allows log data to be integrated with geological observation through the zonation of electrofacies which establishes a criterion for extrapolating geological properties acquired from the cores (Zimmerle, 1995).

The electrofacies studies were conducted on eleven wells contained in the Kockatea and the Carynginia formations, and led to the recognition of six electrofacies for each formation. It is noteworthy that the individual electrofacies represents a particular gamma ray log response which is controlled by a variation in the mineralogical composition. Appendixes C.2 and C.3 show the identified electrofacies in the Kockatea Shale and Carynginia Formation.

In order to identify the lateral variation of electrofacies within wells, different cross sections were selected for the Kockatea Shale and the Carynginia Formation across the Perth Basin. Appendix C.4 illustrates the location of four cross sections for the Kockatea Shale. It is evident from the correlation of the electrofacies through cross sections that there is a variation in the electrofacies' thickness, which could be due to the complex structure of the basin and the deposition of sediments in the different tectonic phases. It clarifies the high thickness of electrofacies in the Dandaragan Trough, which has the maximum subsidence and accommodation space for sediments throughout the Perth Basin. Appendix C.5 displays the thickness variations in the electrofacies of the Kockatea Shale. In the cross section-A (CS-A), the highest thickness of the electrofacies is related to the Redback-2.

The electrofacies "E" is missed in the wells situated in the Beagle Ridge such as Robb-1 at CS-A and CS-C, and Jingemia-1 and Beharra-2 at CS-C,

which might be caused by the lack of conformity present in the border of Permo-Triassic intervals (Copper, 1967). Thickening of electrofacies in the CS-B from Dongara-8 to North Erregulla-1 suggests a thickening in the sediments from west to east in the Northern Perth Basin. Electrofacies “E” in CS-D was not present in the south of Dandaragan Trough and was replaced laterally by electrofacies “C”, particularly at Peron-1. In general, the correlations of the Kockatea’s electrofacies indicate an increase in their thickness in the Dandaragan Trough and Beagle Ridge from north to south (please refer to CS-C and CS-D at Appendix C.5).

A cross section was considered for checking the lateral variation of the identified electrofacies in the Carynginia Formation (Appendix C.6). In the correlation, the absence of electrofacies “B” in the Peron-1 (see Appendix C.7) can be explained by a shallowing of the massive limestone member (electrofacies E); increasing water depth during the deposition of the limestone member might be responsible for changing the facies from Woodada field southwards to Peron-1 (Lane et al., 1983). Study of the electrofacies indicates the variation in the lithology and thickness, as well as the absence or presence of the units across the Perth Basin.

5.2 TOC from Logs

The presence of TOC within potential source rocks impacts substantially on the well logs responses (Fertl and Chilingar, 1988). Olsen (1982) states that organic-rich black shale is detectable through anomalous high gamma ray and resistivity log signature. Nonetheless, the effectiveness of logging responses in determining TOC and thermal maturity of shale gas plays is subject to the complicated mineralogy of lithofacies which occur in shale gas intervals (Jacobi et al., 2008). A good example of this is the positive linear relationship between the uranium value and TOC value in the marine source rocks (Fertl and Rieke, 1980); however the high uranium can be related to its concentration in the authigenic and organogenic calcium phosphate such as apatite. Therefore, there is an uncertainty in detecting TOC empirically without taking into account lithofacies and mineralogical factors (Jarvie et al., 2005). Figure 5.1 illustrates the relation between

gamma-ray response, TOC value and the grain size in shale intervals of Redback-2.

Numerous methods are using to quantify TOC along with their corresponding kerogen maturities from well logs. The weight and volume percentage of TOC is directly related to the log responses, namely gamma ray and bulk density which are commonly applied to reservoirs with similar fluid phases and constant mineralogy (Jacobi et al., 2008). There are procedures using acoustic data and resistivity which are considered as being effectual in detecting TOC in shale plays (Passey et al., 1990; Fertl and Rieke, 1980).

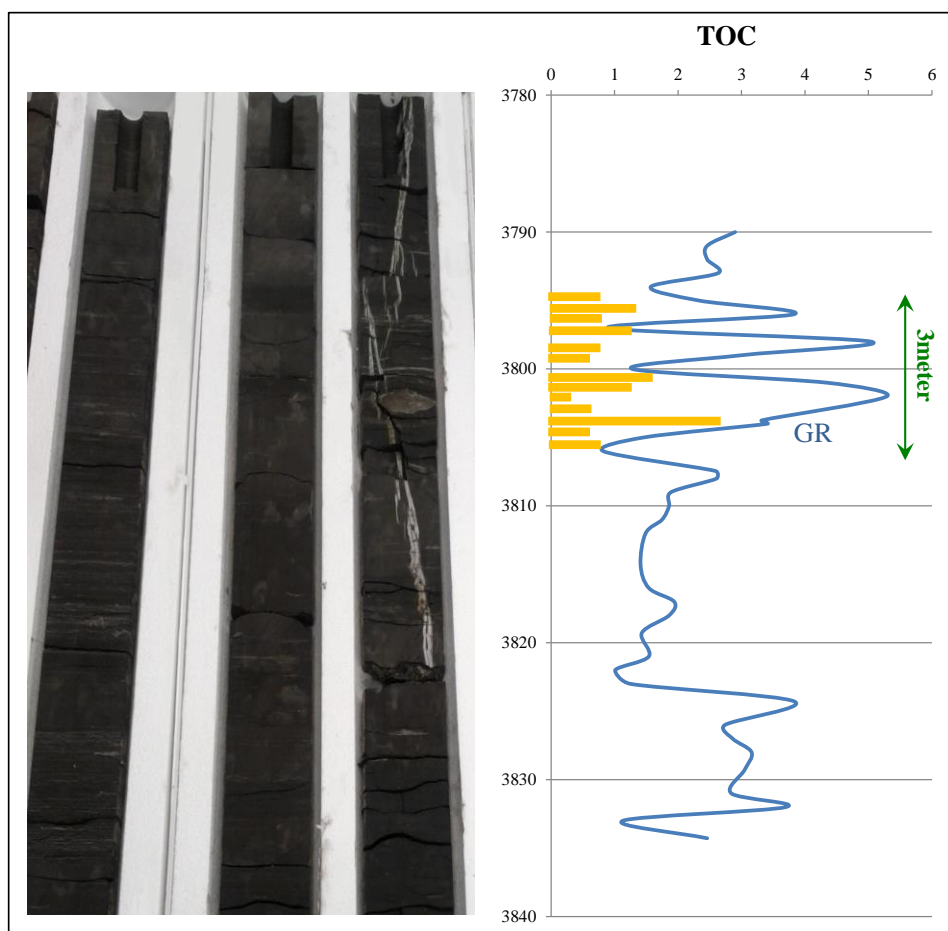


Figure 5.1: Core photograph of Redback-2; relevant gamma-ray response and evaluated TOC profile with grain size from core which demonstrates high variation in the vertical successions of the organic-rich shale intervals.

In the gas shale reservoirs without uranium-enriched clays, the uranium and gamma ray correlation technique can be used (Sondergeld et al., 2010).

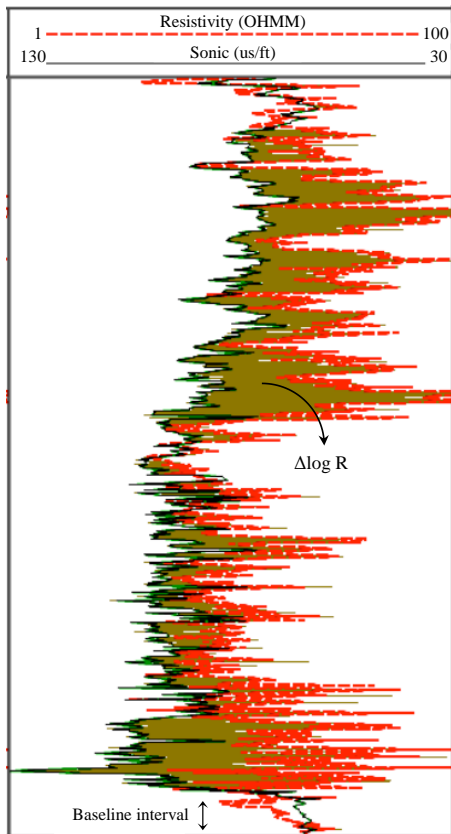
However, factors such as high heterogeneity in mineral composition, the possible percentage of uranium-enriched minerals, and insufficient log data have resulted in more use of the Delta Log R method as described by Passey et al (1990).

The method is comprised of calibrating the graphical variation of a porosity log curve, such as the sonic log, according to the resistivity log curve which allocates a value to the crossover, termed $\Delta\log R$. The $\Delta\log R$ is then calibrated against TOC with respect to the LOM (Level of Maturity, normally derived from R_o data). It is crucial that LOM and TOC should be acquired from formation samples derived from most locations of intervals of interest as applicable. A correlation between LOM and depth of target intervals is also established. Eventually, these correlations are used to measure TOC from $\Delta\log R$ in the non-cored wells (Glorioso et al., 2012). Figure 5.2 shows how the $\Delta\log R$ can be measured through the position of the sonic and resistivity logs towards each other. To measure TOC from logs, a correlation between $\Delta\log R$, TOC value must be established (Passey et al., 1990).

TOC was measured by the Passey method from formation samples derived from the Kockatea and the Carynginia formations across the Perth Basin, and showed a similar trend with the TOC acquired by rock-eval pyrolysis (Appendix C.8).

Despite the high performance in determining TOC, the $\Delta\log R$ method has some limitations such as under-predicting TOC in over mature shale gas systems, or in the presence of high amount of pyrite (Passey et al., 2010). The technique is highly dependent to the availability of maturity data (LOM or R_o) to deduce TOC content.

The maturity of organic matter can be identified by integrating neutron, density and resistivity logs (Figure 5.3).



Equation C.1:

$$\Delta \text{Log} R = \text{Log}_{10} \left(\frac{R}{R_{\text{baseline}}} \right) + (P \times (\Delta t - \Delta t_{\text{baseline}}))$$

P : Resistivity logarithmic cycle over transit time cycle

Equation C.2:

$$\text{TOC (w\%)} = \Delta \text{Log} R \times 10^{(2.297 - 0.1688 \times \text{LOM})}$$

LOM : level of maturity is achieved by Eq.3.

Equation C.3:

$$\text{LOM} = -5.9462R_o^2 + 16.653R_o + 0.3281$$

R_o : Vitrinite reflectance measurement

Figure 5.2: Sonic and resistivity curves fitting to calculate $\Delta \log R$ (modified from Glorioso et al., 2012).

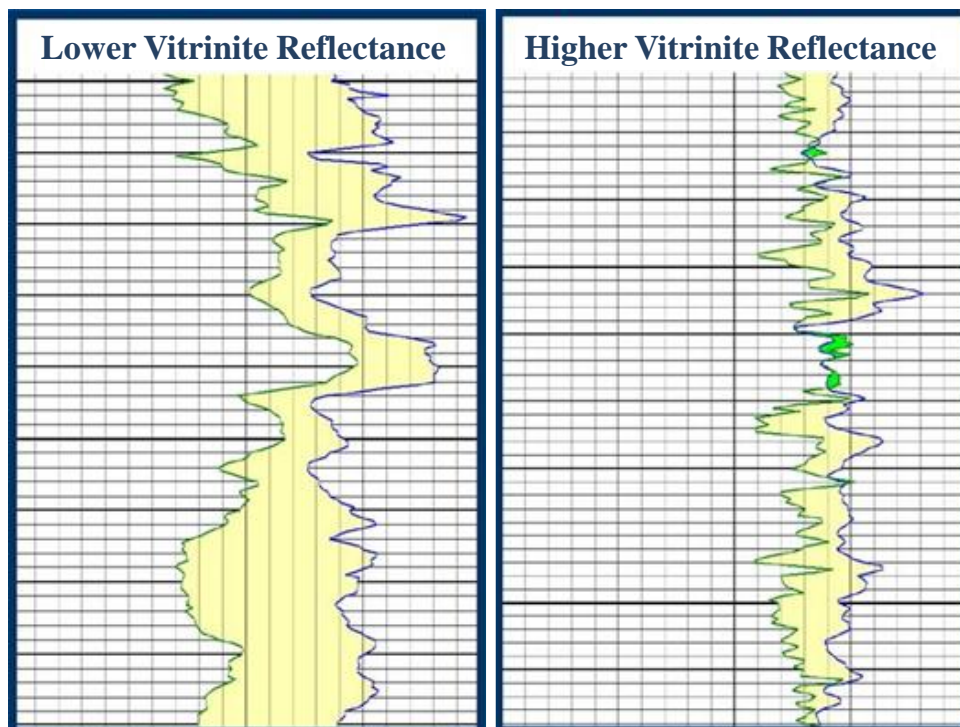


Figure 5.3: The determination of kerogen maturity through combining of resistivity and neutron-density logs (modified from Utley, 2012).

5.3 Fracability from Logs

Fracability is a subject of material fragility and ductility deduced from geomechanical properties of Young's modulus and Poisson's ratio (Enderlin et al., 2011). It is believed that certain rock types influence on fracture initiation, such as specific clays which cause very high fracture initiation pressure (Khalid et al., 2010). Enderlin et al (2011) states that the efficiency of fracture stimulation techniques is highly controlled by the heterogeneity of the rocks which is constrained by rock composition and mineral distribution, the existence and orientation of preexisting planes of weakness, and the nature of primary sedimentary fabric. A positive linear relationship is reported between the kerogen maturity and the corresponding fragility of the rock (Jacobi et al., 2008), which forms factors reflecting the viable gas flow rate and the expected gas productivity from a given well (Jarvie et al., 2007).

Generally shale gas reservoirs are present in quartz-dominated and carbonate-dominated lithofacies. Carbonate can also be detected in the form of nodules, cements and filling in fractures in the silicate-dominated systems. In the form of nodules, carbonate does not reduce permeability; however permeability can be affected by well distributed carbonate cements (Khalid et al., 2010). Contradictory, Jacobi et al (2008) believes that the cements within the fractures generate planes of weakness because of the fact that cements are not bonded to the grains of the rock wall. These planes of weakness reactive open and optimize further recovery of shale reserves when intersected by induced hydraulic fractures (Gale et al., 2007). However, these fractures are not considered as factors contributing to well productivity due to their rarity (Bowker, 2007; Montgomery et al., 2005).

In terms of heterogeneity there are factors that directly impact on the induced fracturing such as natural fractures, faults, and stress regime changes (Khalid et al., 2010).

Undoubtedly, the presence of natural fractures makes the initiation of induced fractures easier. This is due to presence of a preexisting natural fracture framework which brings about the planes of weakness; it allows the

induced fractures to break apart more conveniently. Furthermore, the abundance of natural fractures could be linked to the geometry and shape of the induced fractures. It is crucial to note that the success of induced fracturing based on the preexisting natural fracture depends on the extent of the fracture network (for more information, please refer to Khalid et al., 2010).

Faults are much more effective on the system than natural fractures. They detract the volume of fractured reservoir rocks through diverting the flow of fracture fluids. Faults lead to the entry of water into the Barnett from adjacent aquifers (Burner and Smosna, 2011). Steward (2007) claims that the wells near Karst and structural flexures are similarly disposed for being weak gas producers.

The brittleness index was petrophysically calculated for the shale samples of the Kockatea and the Carynginia formations in a manner described by Rickman et al (2008) and Grieser and Bray (2007). The values were measured by acoustic slowness and bulk density well log measurements; it is based on understanding of the rock strength under stress (Poisson's ratio, ν) and retaining a fracture (Young's modulus, E) when the rock fractures. These two components were calculated using the equations below:

Equation C.4
$$E (Pa) = \frac{\rho V_s^2 (3V_p^2 - 4V_s^2)}{V_p^2 - V_s^2}$$

Equation C.5
$$\nu = \frac{V_p^2 - 2V_s^2}{2(V_p^2 - V_s^2)}$$

Equations of C.6 and C.7

$$E_{brittle} = \frac{E - E_{min}}{E_{max} - E_{min}} \quad \nu_{brittle} = \frac{\nu - \nu_{max}}{\nu_{min} - \nu_{max}}$$

The brittleness index is calculated as follow

Equation C.8
$$BI_{sonic} = \frac{E_{brittle} - \nu_{brittle}}{2} \times 100$$

Castagna et al (1985) introduced an equation which estimates shear wave velocity through compressional wave velocity

Equation C.9
$$V_s = \frac{V_p - 1.36}{1.16}$$

Compressional wave velocity can be acquired by converting DT with the equation of:

Equation C.10
$$V = \left(\frac{1}{DT}\right) \times 304800 \quad V \text{ in m/s and DT in } \mu\text{sec/ft}$$

The brittleness index of target formations in the Perth Basin is summarised in table 5.1, and figure 5.4 displays the fracability trends in the Kockatea and the Carynginia formations throughout the Perth Basin.

Table 5.1: The brittleness index acquired by geomechanical parameters of Young's modulus (E) and Poisson's ration (ν).

Well Name	Formation	BI (%)	Well name	Formation	BI (%)
Centella-1	Kockatea	18.702	Hovea-4	Kockatea	18.183
Mt Horner-7	Kockatea	54.754	Hovea-11	Kockatea	39.178
Whicher Range-1	Kockatea	64.974	Jingemia-1	Kockatea	4.8746
Agonis-1	Kockatea	51.618	Jingemia-5	Kockatea	40.506
Apium North-1	Kockatea	52.251	Jingemia-8	Kockatea	1.861
Beekeeper-1	Kockatea	25.617	Jingemia-10	Kockatea	16.127
Corybass-1	Kockatea	43.566	Murrumbah-1	Kockatea	44.145
Erregulla-1	Kockatea	54.163	Snottygobble-1	Kockatea	37.747
Flying Foam-1	Kockatea	33.973	Strawberry Hill-1	Kockatea	29.899
Gairdner-1	Kockatea	45.652	Wonnerup-1	Kockatea	55.328
Geelvink-1A	Kockatea	44.531	Wye-2	Kockatea	33.594
Hovea-2	Kockatea	62.624	Xyris South-1	Kockatea	46.788
Jingemia-4	Kockatea	29.656	Jingemia-4	Carynginia	29.656
Dongara-12	Kockatea	47.013	Dongara-12	Carynginia	47.013
West White Point-2	Kockatea	35.007	West White Point-2	Carynginia	35.007
Warradong-1	Kockatea	51.185	Warradong-1	Carynginia	51.185

Due to insufficient well log data, few wells were only petrophysically analysed to measure their fracability. Figure 5.5 shows the brittleness variation in the wells of Redback-2 and Arrowsmith-2.

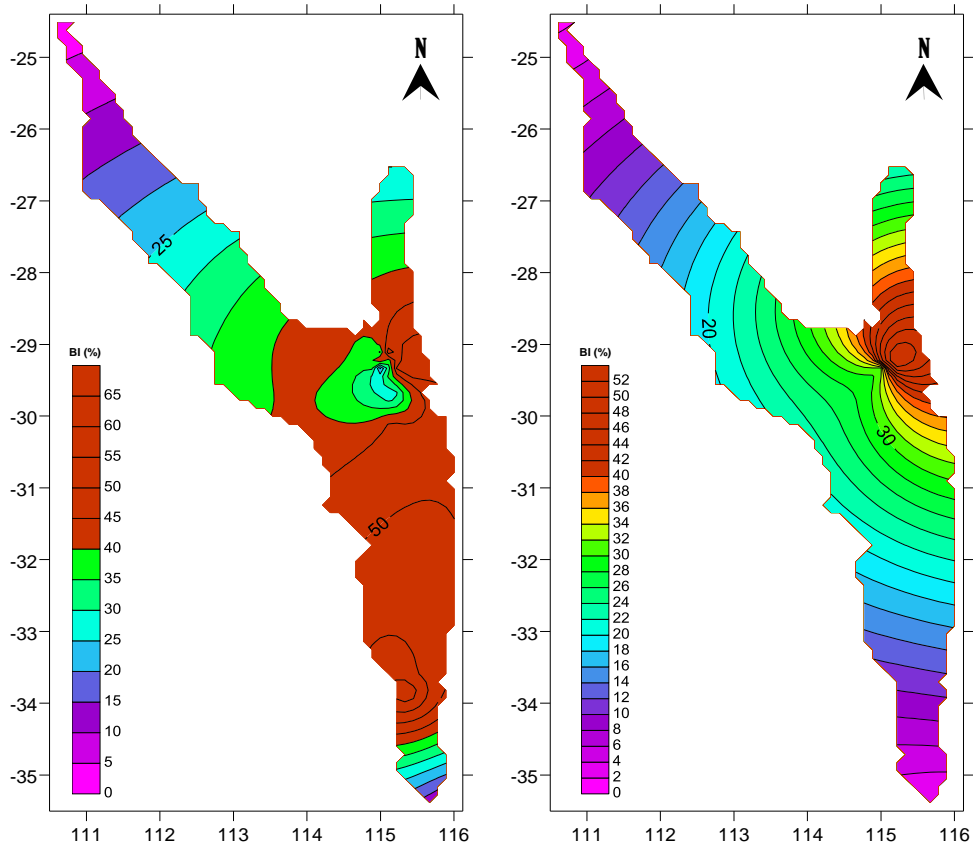


Figure 5.4: The brittleness trend within the Kockatea Shale (left), and the Carynginia Formation (right) across the Perth Basin.

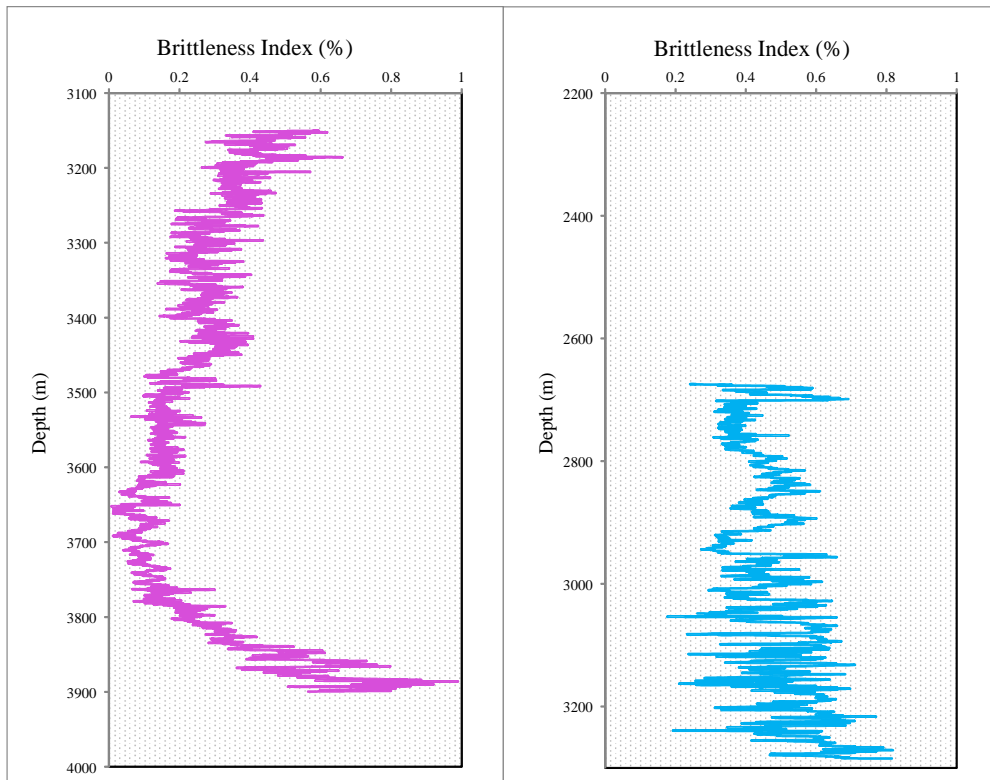


Figure 5.5: Variability in the brittleness index of Redback-2 (left) and Arrowsmith-2 (right), the brittleness index derived from shear wave sonic.

Chapter 6: Sequence Stratigraphy

6.1 Introduction

Sequence stratigraphy is the study of genetically related facies which demonstrates the record of depositional variation preserved in the rocks (Embry, 2007). It is referred to as the interaction of habitation space with sediments supply where eustatic sea level change and tectonic subsidence intensely affects the habitat (Singh, 2008). Sequence stratigraphy is able to predict the incidence, distribution and the features of organic-rich rocks that are being considered as shale gas reservoirs from basin-wide to field-wide scale (Passey et al., 2010; Guthrie and Bohacs, 2009; Bohacs and Lazar, 2010). It authorizes the subdivision of the basin to the system tracts through the detection of boundary and internal surfaces based upon actualistic (asymmetric) base level curves and depositional models. In fact, it pursuits to distinguish and correlate changes in depositional settings that reflect an individual base level cycle (Lash and Engelder, 2011). Hallam (1999) suggests that the concepts of sequence stratigraphy are beneficial in analysing both basin and global sea level changes; they also create a realistic model to adapt with geologic data (Leetaru, 2000).

Sequence stratigraphy is commonly applied for gas resources locked in shales in order to detect desirable internal gas source, recognise the best strata for artificial fracture operation and horizontal well placement, as well as regional to local correlations (Slatt et al., 2011).

The study of sequence stratigraphy in fine-grained shales is not as simple as coarse grained facies due to them being stratigraphically heterogeneous (Macquaker et al., 1998; Schutter, 1998; Almon et al., 2002; Paxton et al, 2006; Loucks and Ruppel, 2007; Singh, 2008; Mazzullo et al., 2009) and systematically variant (Sutton et al., 2004). Despite excellent insights into shales to check their depositional variety and effective environmental

factors on the depositional systems (Hester et al., 1990; Hickey and Henk, 2007; Loucks and Ruppel, 2007; Singh, 2008; Comer, 2009; Slatt et al., 2009a, 2009b, 2009c, and 2009d), there is negligible understanding of sequence stratigraphy in shales (Bohacs, 1998a). Having sufficient knowledge about the sediment supply, the delivery method, depositional rate and sediments type (coarse vs. fine, carbonates vs. clastics, detrital vs. biogenic) is crucial for establishing the sequence stratigraphic framework for the marine organic rich shale depositional system (Bohacs and Schwalbach, 1992).

There is a link between bottom energy level and water depth with depositing shales, such that the deposition of fine-grained shales implicates the calm water conditions, which in turn is representative of higher accommodation. High sedimentation would commonly present deeper water, higher preserved organic-matter, lower oxygen level, lower fossil abundance and diversity (Singh, 2008).

There are three different sequence types including Exxon-type sequences, Galloway's-type sequences, and Embry-type sequences. The Embry-type was conducted for this study, and it is commonly used for regional basin analysis due to the occurrence of subaerial unconformities at its boundaries, not within it. This type is based on the transgressive-regressive (T-R) events; the transgressive surface and the specified correlative conformity can be diagnosed in most occasions (Hallam, 1999). The terminology of transgressive-regressive sequence summarises sequence interpretations (Embry and Johannessen, 1992). Houseknecht and Bird (2004) state that a transgressive system tract overlain by a regressive system tract in a transgressive-regressive sequence, and a maximum flooding surface define their border.

The system tracts within the depositional sequences which are bounded by correlative conformities or unconformities render a reliable means to analyse sequence stratigraphy and to correlate marine facies accumulated in highstand system tracts (shelf environment) with those that are deposited in

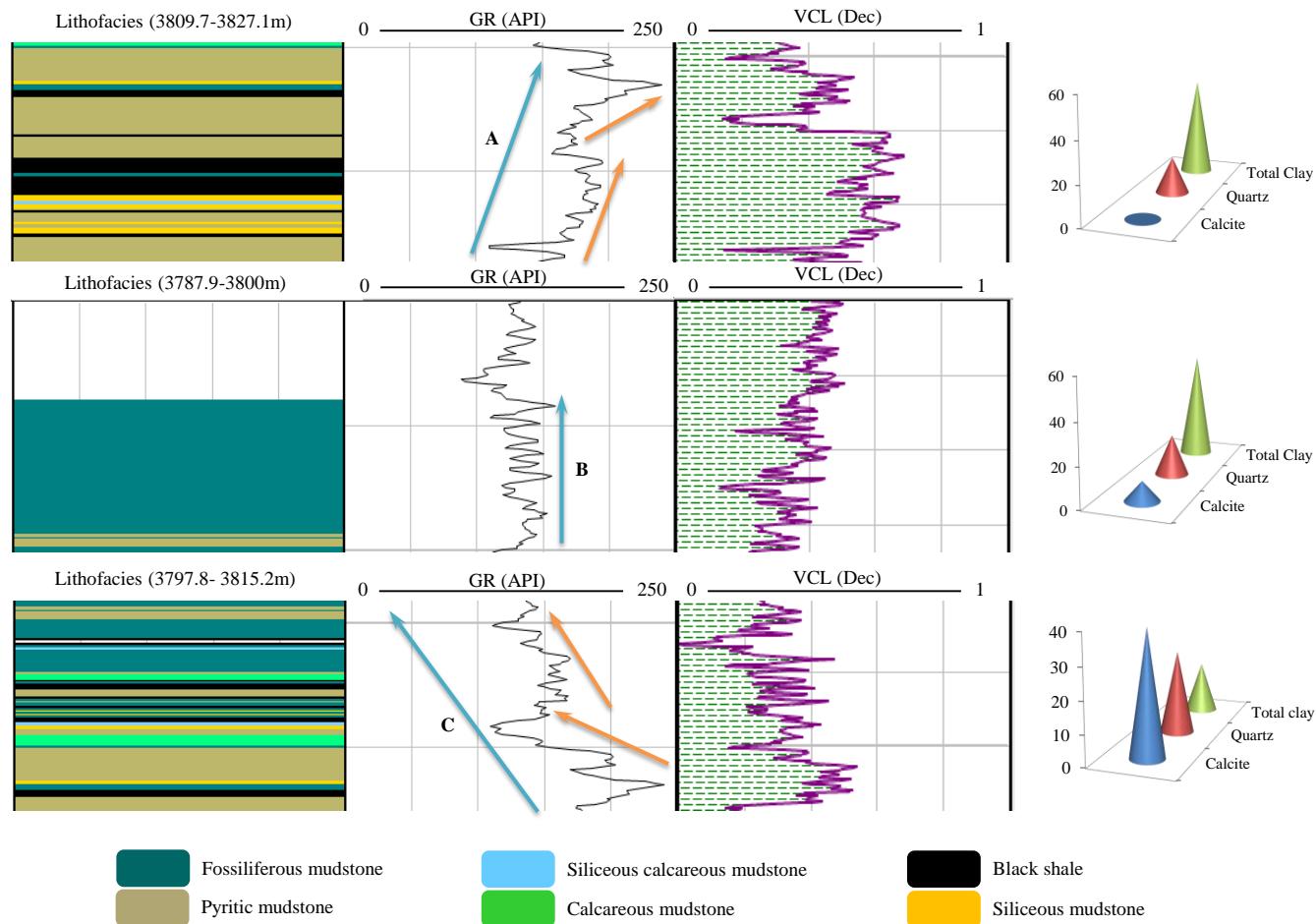


Figure 6.1: Example of (A) upward-increasing gamma ray parasequence, mainly consists of pyritic mudstone lithofacies (B) interval of constant gamma ray parasequence, mainly contains fossiliferous mudstone lithofacies and (C) upward-decreasing gamma ray parasequence, mostly occurred due to the presence of calcareous mudstone, from Hovea Member of the Kockatea Shale, Redback-2.

lowstand system tracts (slope and abyssal plain environment) (Mancini and Puckett, 2005).

It should be noted that a single character cannot be performed to make a stratigraphic interpretation. Different features control this interpretation, such as the identification of the cyclical stacking pattern of the lithofacies, sedimentologic criteria, TOC content, the oxygen level in the depositional environment, the determination of repeated and differentiable patterns in vertically stacked successions, and finally the recognition of parasequences and their sidelong continuity (Singh, 2008).

6.2 Parasequence Identification

The sequence stratigraphic framework was studied on the Hovea Member of the Kockatea Shale at Redback-2 through the diagnosis of the gamma ray patterns of the cored wells. The GR profile of Hovea Member reveals three gamma ray parasequences in the manner described by Singh (2008), upward-increasing gamma ray API intervals, intervals of constant API, and upward-decreasing gamma-ray API intervals (Figure 6.1).

It appears from the figure that upward-increasing gamma ray parasequence is composed of upward-increasing clay value with low amounts of quartz and calcite. Constant interval has uniformly low calcite value with upward-increasing quartz and clays. Upward-decreasing gamma ray parasequence is represented by high amounts of calcite and an upward-decreasing of clay content. The boundary of a parasequence is able to differentiate strata deposited in shallow water with high energy conditions from those accumulated in deeper water with low energy conditions (Bohacs, 1998a).

Van Wagner et al (1990) suggest that nearly all carbonate parasequences are aggradational, and most siliciclastic parasequences are progradational. Figure 6.2 differentiates the aggradational and progradational systems within the Hovea Member, Redback-2. A rhythmic periodicity is shown in progradational and retrogradational stacking patterns of the member.

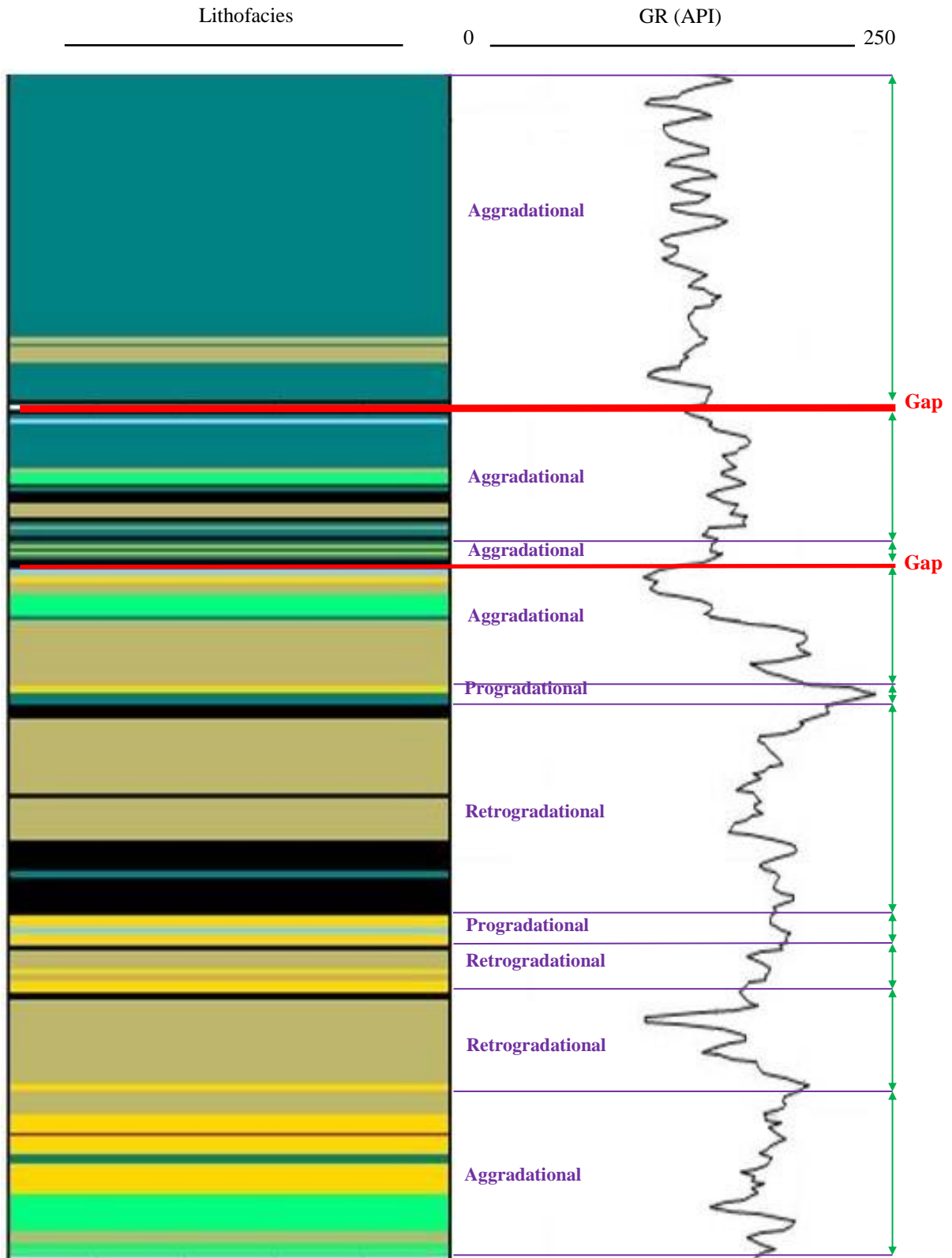


Figure 6.2: Aggradational and progradational systems in the Hovea Member of Kockatea Shale, Redback-2.

6.3 Sequence Stratigraphic Framework

The sequence stratigraphic framework of the Hovea Member is established based on diagnosis of the gamma ray parasequences on the gamma ray log patterns, the identification of various cyclical stacking patterns of lithofacies through key stratigraphic surfaces, such as transgressive surface of erosion (TSE) and flooding surface (FS), in association with sequential sea level change events which formed with a transgressive event (TR) and regression event (RE), and TOC value. Relative hydrocarbon potential ($RHP = S_1+S_2/TOC$) also helped in detecting the depositional environment of the lithofacies with respect to the amount of their environmental oxygen. The sedimentary environment predicted by RHP was integrated with those acquired by sequence stratigraphy through stratigraphic interval and gamma ray patterns. Five stratigraphic intervals containing complete or partial cycles of the TR and REs were identified from the gamma-ray log in the Hovea Member of the Kockatea Shale from Redback-2.

6.3.1 Stratigraphic Intervals of Hovea Member, Kockatea Shale

6.3.1.1 Stratigraphic Interval 1 (3,835.8–3,826.0 m)

This interval expresses the earliest transgression and regression sedimentation in the member, and contains two gamma ray patterns (GRPs), GRP-TR1 and GRP-RE, with an upward increasing gamma ray parasequence and an upward decreasing gamma ray parasequence, respectively (Figure 6.3). The boundary between the two gamma ray parasequence intervals is a distinct flooding surface (FS1), which demonstrates the change in the lithofacies related to deposition in different environments. The interval composes mostly pyritic and calcareous mudstone coupled with fossiliferous and bioturbated layers. Since there is not any calcite in the pyritic mudstone lithofacies, the high presence of this lithofacies at GRP-RE1 can be explained by the relative sea level undergoing a slow fall with an equal rate of eustatic fall and subsidence.

The TOC value decreases in the siliceous lithofacies compared to the pyritic mudstone.

6.3.1.2 Stratigraphic Interval 2 (3,826.0–3,808.3 m)

There is no distinct lithofacies change at the boundary between interval 1 and interval 2, but it can be distinguished by a slight rise in sea-level change. The sea-level rise can be confirmed by the lithofacies's change from pyritic mudstone to black shale. Similar to interval 1, this interval also contains two gamma ray patterns, GRP-TR2 and GRP-RE2. The difference is that GRP-TR2 consists of two upward increasing gamma ray patterns instead of just one. The black-shale lithofacies is associated with the highest gamma ray readings (Figure 6.3). The contact surface between GRP-TR2 and GRP-RE2 is another flooding surface (FS2). It is difficult to distinguish the TSE at the base of interval 2, as there are no changes in lithofacies. TOC values of the interval are not high in comparison with adjacent stratigraphic intervals.

6.3.1.3 Stratigraphic Interval 3 (3,808.3–3,800.3 m)

The base of this interval is a TSE with a sharp decrease in the gamma ray log response and the presence of the siliceous mudstone lithofacies (Figure 6.3). In TR3, there are two gamma ray patterns of upward increasing gamma ray parasequence, and an interval of constant gamma ray parasequence. The upward increasing gamma ray parasequence is composed of pyritic mudstone, black shale, and fossiliferous mudstone, while the constant GRPS is mostly fossiliferous mudstone. Similarly, GRP-RE3 is represented by the fossiliferous lithofacies; the low GR response in this lithofacies might be due to its high carbonate content. XRD results estimate 9.7% calcite for this lithofacies. The TOC curve displays high amounts of TOC in the interval.

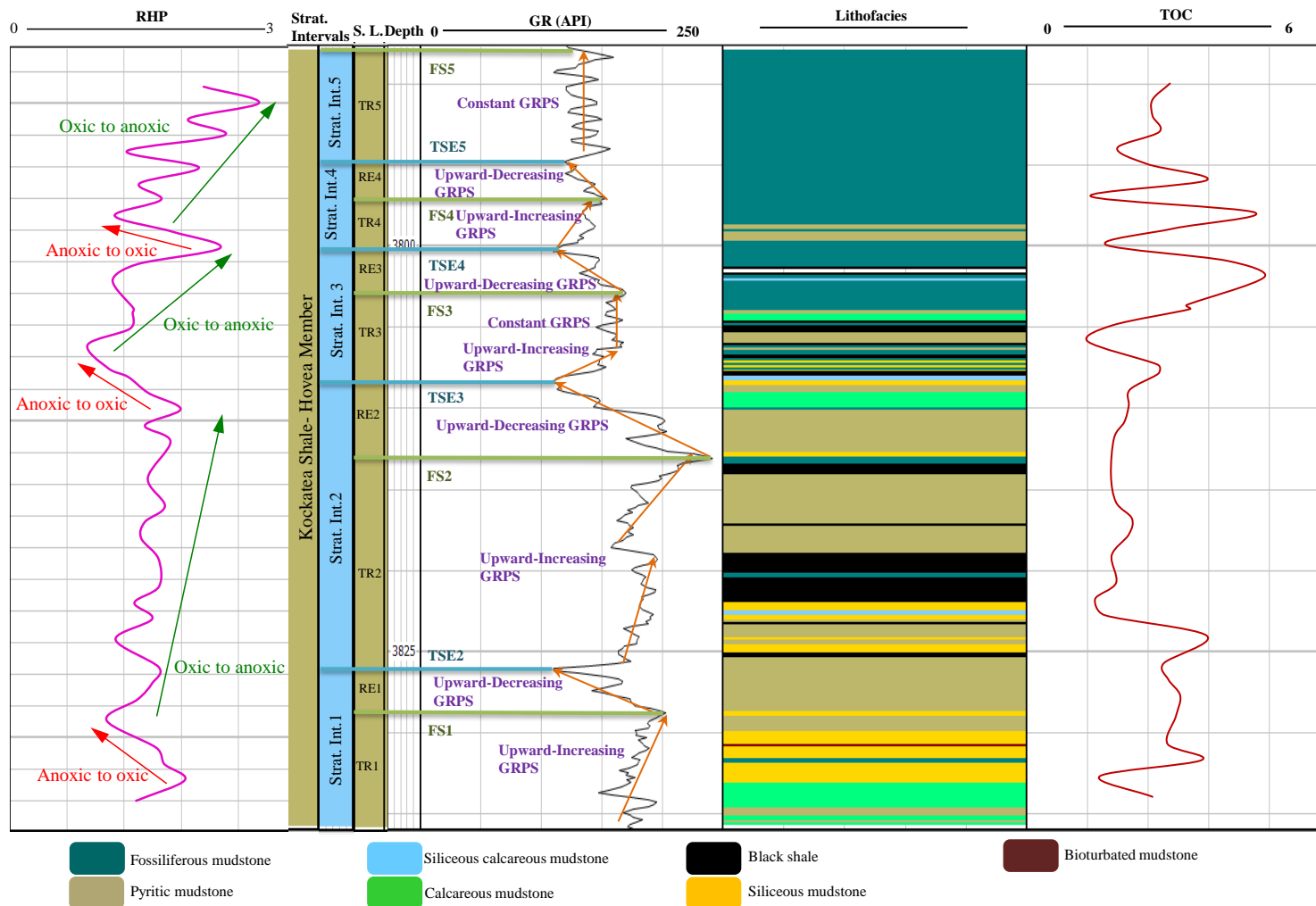


Figure 6.3: Sequence stratigraphic frameworks for the Hovea Member of the Kockatea Shale from Redback-2, five stratigraphic intervals have been detected with correlation of gamma-ray log, stacking patterns of lithofacies, Relative Hydrocarbon Potential and TOC. The acquired match is reasonable in most parts. TR: Transgressive event of relative sea level, RE: Regressive event of relative sea level, FS: Flooding surface, TSE: Transgressive surface of erosion, and S.L: Sea level interval.

6.3.1.4 Stratigraphic Interval 4 (3,800.3–3,794.8 m)

The interval starts with a slow rise in relative sea level. The TR4 in the interval is represented by fossiliferous mudstone at the base, and continues with pyritic mudstone and a repeat of the fossiliferous mudstone. The high amount of TOC in this interval is confirmed by the presence of phosphatic fossils (3,798 m). RE4 also consists of fossiliferous mudstone. The difference in the GR response can be described by the different compositions of the various fossils. As there is no change between the lithofacies at the boundary between GRP-TR4 and GRP-RE4, the possibility of the presence of a FS at this boundary is unlikely.

6.3.1.5 Stratigraphic Interval 5 (3,794.8–3,787.9 m)

This interval is composed of GRP-TR5 with the interval consisting of constant GR. The fossiliferous mudstone covers the whole interval.

Apart from an organic-richness measurement by TOC content, RHP was also compared with identified sequence stratigraphic intervals, GR log and lithofacies at Redback-2. Similar to TOC values, it shows main shifts at stratigraphic surfaces; major shifts in the RHP trend are situated at TSE and FS. Organic facies sequences can be identified from the RHP because the changes from anoxic to oxic conditions occur with a RHP increasing upward pattern, and changes from oxic to anoxic conditions occur along with a RHP decreasing upward pattern (Singh, 2008). The comparison of RHP with the sequence stratigraphic intervals acquired from the geological properties of the rocks shows good conformity.

6.4 Areal Extent of Stratigraphic Intervals

The lithofacies were correlated with the gamma ray responses at Redback-2, and then these recognised gamma ray patterns for the stratigraphic intervals were correlated with gamma ray logs of three other wells to study their lithofacies and stratigraphic intervals. After reviewing log data of various wells, a north–south transect through the Dandaragan Trough consisting of Redback-2, Beharra Springs South-1, Woodada-2, and Woodada-6 was

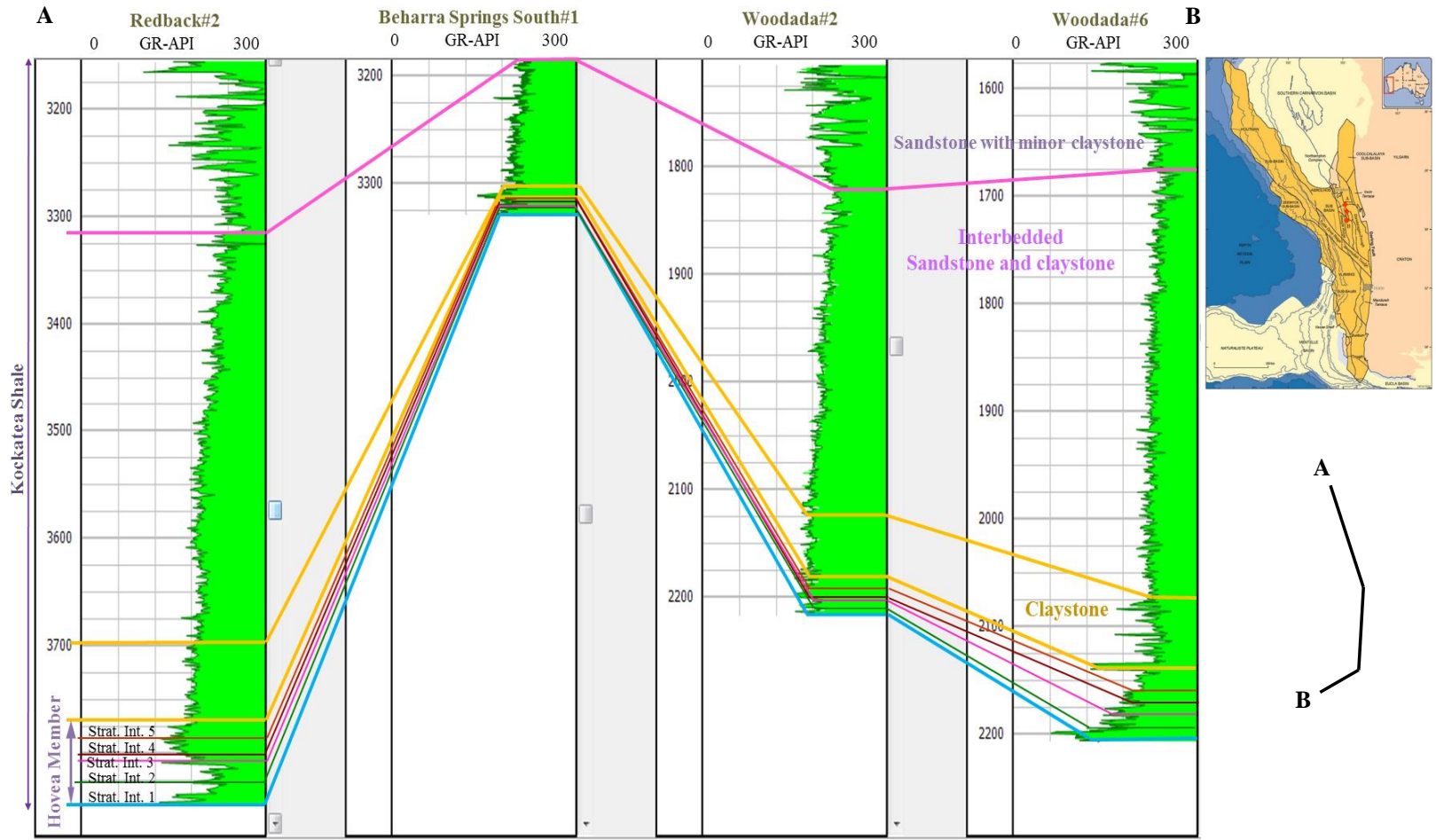


Figure 6.4: Cross-section AB throughout north-south of Dandaragan Trough Sub-basin, Perth Basin. All stratigraphic intervals are presented in the selected wells at the Hovea Member; there are similar gamma-ray patterns for the upper part of the Kockatea Shale.

created. In spite of the limited number of wells, the result reveals a detailed sequence stratigraphic framework for the Hovea Member in the Perth Basin. The cross-section shows that although the Hovea Member thins in Beharra Spring South-1 and Woodada-2, all lithofacies are still present across the trough (Figure 6.4). There is similarity in the gamma ray patterns of the selected wells, not a high gamma ray in all wells, which indicates the presence of various lithofacies across the Dandaragan Trough.

Chapter 7: Discussions, Conclusions and Recommendations

7.1 Discussions and Conclusions

The sweet spot areas of shale reservoirs at the Kockatea and the Carynginia formations, where well efficiency will be more economical, are identified through detailed geological, geochemical and petrophysical studies. This identification was conducted by defining different lithofacies, the type and quantity of their minerals, their organic richness and maturity, their fracability and eventually their distribution across the Perth Basin. General trends of thickness, TOC, thermal maturity and brittleness in the target formations are also accomplished for the study area.

Gamma ray response of lithofacies and detecting different electrofacies are carried out to understand the lithofacies and their lateral variations for the non-cored wells. Sequence stratigraphic framework is established for the Hovea Member at the base of the Kockatea Shale in Redback-2. This frame is then mapped with other wells to check its continuity. The following conclusions can be drawn from the discussed subjects in this study:

7.1.1 Thickness and Geographic Distribution

Thickness and geographic distribution of the main units are attained by assessing the basin's structure and stratigraphy during the Permo-Triassic period. The Permian Carynginia Formation is thickened in the Bunbury trough and Vasse Shelf and east towards the Darling Fault. The unit is thinner to the west onto the Beagle Ridge and Dongara Saddle. The Lower Triassic Kockatea Shale shows thickening along the Beagle Ridge and towards the south. The formation thins onto the Dongara Saddle, the northern part of the Beagle Ridge, and near the Northampton Complex. The

thickest part of the Carynginia Formation is shown westward by isopach maps, while the Kockatea Shale has the highest thickness towards the east.

7.1.2 Lithofacies

Detailed analysis of the long continuous cores of the target formations resulted in the recognition of eleven lithofacies in the Kockatea Shale and eight lithofacies in the Carynginia Formation. The lithofacies of shaly siltstone, siliceous calcareous mudstone and sandy-silty interlaminated deposit are only present in the Kockatea Shale. The criteria to differentiate lithofacies were the differences in lithology, mineral composition, colour, grain size and distribution, nature of underlying and overlying contacts, sedimentary structures and geochemical properties such as organic richness and kerogen maturity. Numerous techniques were conducted to characterise the lithofacies such as thin section petrography, SEM, XRD and FTIR for determining mineral composition, along with geochemical analysis in detecting TOC content and thermal maturity. Table 7.1 summarises different properties in the lithofacies, and figure 7.1 represents the distribution of some lithofacies in the Perth Basin.

The depositional environments were simultaneously studied by lithofacies properties observed on the cores, sedimentary structure, trace fossil assemblages and determining index minerals that reflect specific environmental conditions. The depositional environment of the Carynginia Formation is considered to be restricted marine, while it appears that the Kockatea Shale deposited under deep marine conditions due to the presence of a large number of thin-walled brachiopods and foraminifers of *Siphovalvulina variabilis* Septfontaines and *Paleomayncina termieri* (Hottinger). The identified sedimentary structures on the cores reveal various depositional environments in different wells. The pyrite is used as an indicator to identify variant redox controlling cyclic transition and sedimentary environments.

Table 7.1: The various properties of different lithofacies in the target formations, Perth Basin.

Lithofacies	Properties
Black shale	Lithology: clays, slightly silty, with pyrite and minor mica Depositional environment: relatively deep and low energy water Mineralogy: albite, chlorite, Illite-smectite, pyrite, quartz TOC (sum of two units): 4.9 wt.%, Thickness (at 42 studied wells): 8.11 m Brittleness Index: 0.466
Shaly siltstone	Lithology: Siltstone and shale Depositional environment: calm environment Mineralogy: Jarosite, kaolinite, montmorillonite muscovite, pyrite, quartz TOC (sum of two units): 0.86 wt.%, Thickness (at 42 studied wells): 18.35 m Brittleness Index: 0.812
Pyritic mudstone	Lithology: Clays, sparry calcite with abundant pyrite Depositional environment: reduced conditions Mineralogy: albite, chlorite, gypsum, kaolinite, illite-smectite, pyrite, quartz TOC (sum of two units): 4.7 wt.%, Thickness (at 42 studied wells): 37.84 m Brittleness Index: 0.268
Siliceous mudstone	Lithology: Silica, slightly silty and micaceous with minor pyrite Depositional environment: low to moderate energy conditions Mineralogy: albite, chlorite, illite-smectite, pyrite, quartz TOC (sum of two units): 2.2 wt.%, Thickness (at 42 studied wells): 45.19 m Brittleness Index: 0.567
Calcareous mudstone	Lithology: Clays, detrital and autochthonous calcite, and quartz Depositional environment: fluvial debris Mineralogy: albite, calcite, gypsum, jarosite, kaolinite, montmorillonite, muscovite, pyrite, quartz TOC (sum of two units): 2.5 wt.%, Thickness (at 42 studied wells): 43.38 m Brittleness Index: 0.364
Bioturbated mudstone	Lithology: clays, siltstone and sandstone Depositional environment: marine offshore transitional zone Mineralogy: albite, gypsum, jarosite, illite, montmorillonite, kaolinite, muscovite, pyrite, quartz TOC (sum of two units): 2.7 wt.%, Thickness (at 42 studied wells): 72.21 m Brittleness Index: 0.866
Fossiliferous mudstone	Lithology: clays, slightly silty Depositional environment: marine with anoxic conditions Mineralogy: albite, calcite, kaolinite, illite-smectite, pyrite, quartz TOC (sum of two units): 2.5 wt. %, Thickness (at 42 studied wells): 38.085 m Brittleness Index: 0.244
Wavy laminated deposit	Lithology: clays, siltstone and sandstone Depositional environment: marine and transitional marine to tidal flat Mineralogy: gypsum, jarosite, kaolinite, illite, montmorillonite, muscovite, pyrite, quartz TOC (sum of two units): 0.28 wt.%, Thickness (at 42 studied wells): 6.33 m Brittleness Index: 0.376
Siliceous calcareous mudstone	Lithology: clays, silica and calcite Depositional environment: Clastic particles entered to the calm environment with already deposited clays Mineralogy: calcite(mg), gypsum, kaolinite, smectite, muscovite, quartz TOC (sum of two units): 2.5 wt.%, Thickness (at 42 studied wells): 20.526 m Brittleness Index: 0.372
Sandy-silty interlaminated deposit	Lithology: interlamination of sandstone and siltstone Depositional environment: constant changing in environmental conditions Mineralogy: gypsum, jarosite, kaolinite, illite, montmorillonite, muscovite, pyrite, quartz TOC (sum of two units): 0.26 wt.%, Thickness (at 42 studied wells): 33.90 m Brittleness Index: 0.305
Shaly-sandy interlaminated mudstone	Lithology: interlaminations of shale and sandstone Depositional environment: the zones with moderate to high velocity currents Mineralogy: kaolinite, montmorillonite, illite, muscovite, quartz TOC (sum of two units): 0.7 wt.%, Thickness (at 42 studied wells): 104.79 m Brittleness Index: 0.613

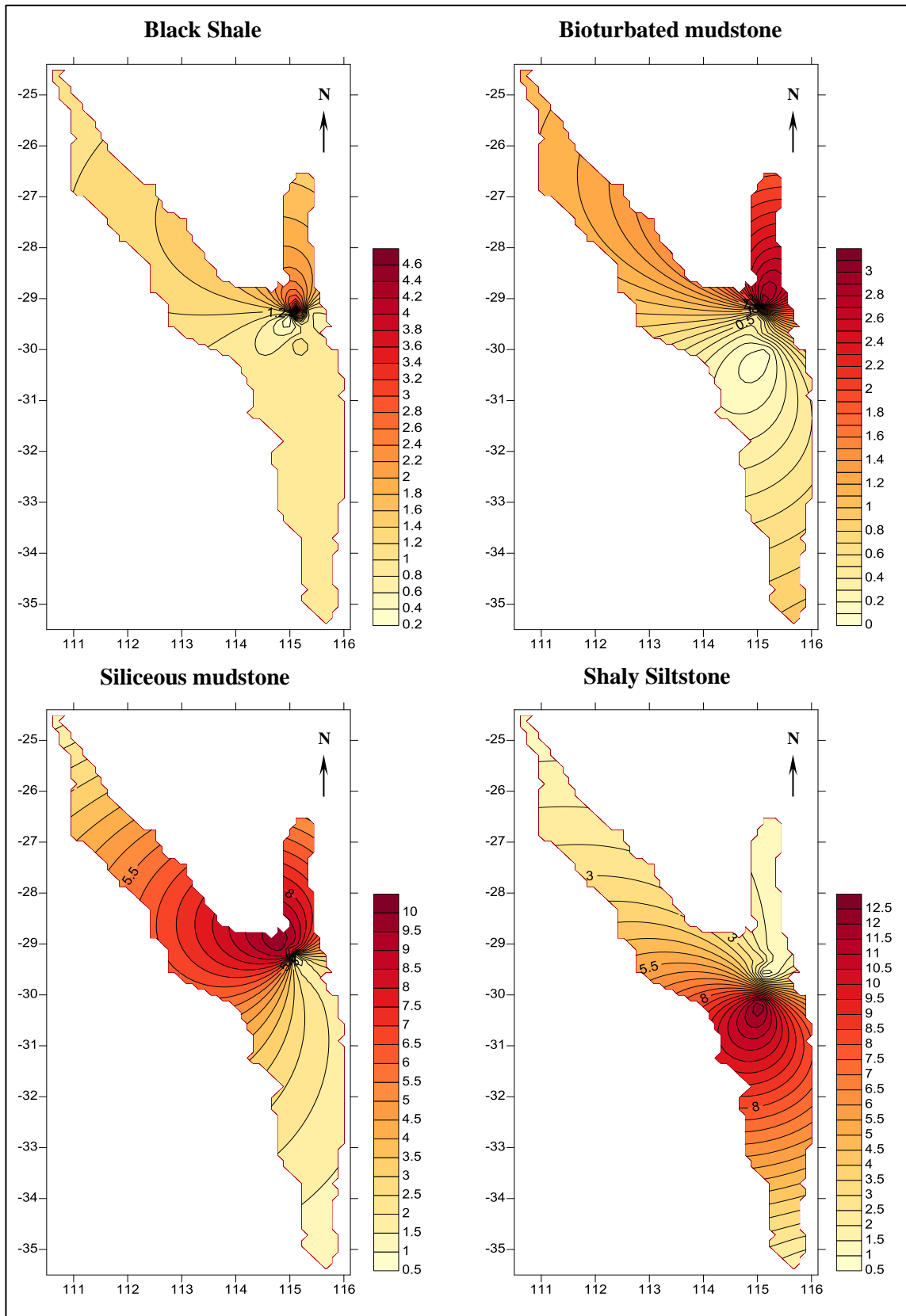


Figure 7.1: The Distribution of black shale, bioturbated mudstone, siliceous mudstone and shaly siltstone in the Perth Basin

In non-cored wells, different lithofacies were identified by the diagnosis of gamma ray response of lithofacies and electrofacies. Six electrofacies of A1, A, B, C, D, and E for the Kockatea Shale and A, B, C, D, E, and F for the Carynginia Formation were defined, each electrofacies showing a certain gamma ray log response controlled by mineral variability. The lateral variations of the electrofacies across the Perth Basin were identified through four selected cross sections for the Kockatea Shale and one cross section for the Carynginia Formation. The complex structure of the basin and the sedimentation under different tectonic phases lead to the thickness variation in the electrofacies. A lack of conformity in the border of Permo-Triassic intervals eliminated the electrofacies “E” in the Beagle Ridge. An increase is seen in the thickness of electrofacies within the Kockatea Shale in the Dandaragan Trough and Beagle Ridge from north to south. The lack of electrofacies “B” in the correlation of the identified electrofacies for the Carynginia Formation might be caused by a shallowing out of the limestone member and the deepening of water during the deposition of this member.

7.1.3 Organic Richness and Kerogen Maturity

Two techniques of rock-eval pyrolysis and the $\Delta\log R$ were conducted to quantify the organic richness within the Kockatea Shale and the Carynginia Formation. There is higher TOC content in the Carynginia Formation (TOC >3 wt. %) in comparison with the Kockatea Shale. The diagram of TOC versus HI confirmed the position of the Carynginia Formation in the gas-prone areas with type III kerogen. The Kockatea Shale is mainly plotted in the oil and gas prone areas with a mixture of type II/III kerogen. The diagram TOC versus S_2 also suggests type III kerogen for the Carynginia Formation, along with a higher maturity and deposition under restricted conditions due to locating plotted points at the gas-prone areas. The Kockatea Shale is considered to have been deposited under marine conditions due to plotting mostly in the areas with type II kerogen.

Thermal maturity was identified by pyrolysis (Tmax) and vitrinite reflectance measurements. Plotting Tmax value on the basin’s map shows the highest maturity of the formations in the centre of the basin. Organic

facies sequences were identified by RHP patterns, which act as an index for the marine transgressions and regressions.

7.1.4 Fracability

The presence of natural fractures, faults and stress regime changes directly affects the induced fracturing. However, a successful induced fracturing operation relies on the extent of the fracture network. The presence of faults, karst and structural flexures near the wells have negative effect on their productivity. The brittleness index was acquired from mineralogical and geomechanical properties, and high fracability has been shown in the centre of the basin for the Kockatea Shale and in the north-east in the Carynginia Formation.

7.1.5 Sequence Stratigraphy

The framework of sequence stratigraphy of the Basal Kockatea Shale has been identified using its gamma ray profiles, and it reveal three gamma ray parasequences: upward increasing gamma ray API intervals, intervals of constant API, and upward decreasing gamma ray API intervals. The parasequences' boundaries differentiate strata deposited in shallow water under high energy conditions from those deposited in deeper water under low energy conditions. A rhythmic periodicity is seen in retrogradational and progradational stacking patterns of the Hovea Member. Variant cyclical stacking patterns of lithofacies were identified through key stratigraphic surfaces, sea level changes, TOC value and RHP. Five stratigraphic intervals were determined from the gamma ray log in the Hovea Member of the Kockatea Shale from Redback-2.

By integrating the geological, geochemical, and petrophysical analyses conducted in different scales from logs to cores to nano-scale SEM images, this study indicates the highlighted areas in the figure 7.2 as the best area for investment in the shale gas reservoirs in the Kockatea and Carynginia formations at the Perth Basin.

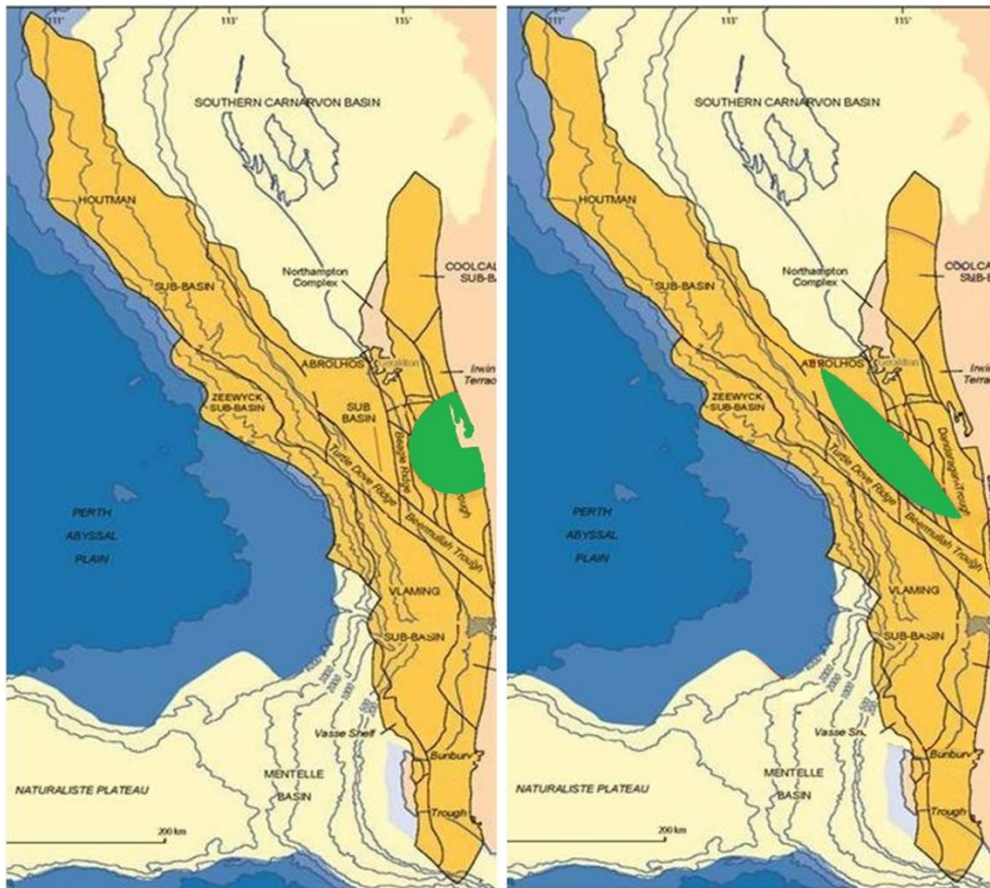


Figure 7.2: The sweet spots in the Kockatea Shale (left) and the Carynginia Formation (right).

7.2 Recommendations

1. It is recommended to study biostratigraphic properties of the lithofacies for more accuracy in detecting their depositional environment effectiveness for preserving organic matter.
2. The application of the analysis of redox-sensitive trace elements is recommended in order to reflect the oxygenation conditions in the TOC curve.
3. The identification of shale reservoir productivity cannot only rely on its geological and geochemical characteristics. These studies should be incorporated with key petrophysical properties such as porosity, permeability, and gas saturation.
4. It is beneficial that 3D seismic be integrated with the established stratigraphy in this study to acquire a much more precise sequence stratigraphic framework.
5. It is suggested to apply rock CT scanning to identify natural fractures, porosity, grain density, bulk volume of rock, and mineralogy.

Bibliography

- Abouelresh, M. O., & Slatt, R. M. (2012). Lithofacies and sequence stratigraphy of the Barnett Shale in east-central Fort Worth Basin, Texas. *AAPG Bulletin*, 96(1), 1-22.
- Almon, W. R., Dawson, W. C., Sutton, S.J., Ethridge, F. G., & Castelblanco, B. (2002). Sequence stratigraphy, facies variation, and petrophysical properties in deep-water shales, Upper Cretaceous Lewis Shale, south-central Wyoming: Gulf Coast Association of Geological Societies Transactions, 52, 1041-1053.
- AL-Bazali, T. M., Zhang, J., Chenevert, M. E., & Sharma, M. (2005). A rapid rigsite-deployable electrochemical test for evaluating the membrane potential of shales. Presented at the 2005 SPE Annual Technical Conference and Exhibition, Dallas, Texas. SPE 96098.
- Archbold, N. W. (1988). Permian brachiopod faunas of the Perth Basin, Western Australia: a study of progressive isolation. Australian Geological Society, Ninth Australian Geological Convention, Abstracts n21, 46-47.
- Arduini, M., Golfetto, F., & Ortenzi, A. (2009). The Chlorite-Bearing Reservoirs: Effects of the Main Petrographic Parameters on Reservoir Quality. Search and Discovery Article #50178. Posted 27/04/2009.
- Arthur, J. D., Bohm, B., & Layne, M. (2008). Hydraulic fracturing considerations for natural gas wells of the Marcellus shale. Presented at the Ground Water Protection Council 2008 Annual Forum, Cincinnati, Ohio, USA.
- Arthur, M. A. (1994). Marine black shales: Depositional Mechanisms and Environments of Ancient Deposits. *The Annual Review of Earth and Planetary Sciences*, 22, 499-551.

- Backhouse, J. (1993). *Wicherina 1: a palynological review*. Western Australia Geological Survey, Palaeontological Report 13 (unpublished).
- Baxter, J. C., & Harris, Y. L. (1980). The Darling Fault- diamond drilling results at Harrisons copper prospect: Western Australia Geological Survey, Annual Report 1979, 90-93.
- BBY limited, 2010. Perth Basin shale gas- unconventional upside.
- Bergmark, S. L., & Evans, P. R. (1987). Geological controls on reservoir quality of the northern Perth Basin. *Australian Petroleum Exploration Journal*, 27(1), 318- 330.
- Berner, R. A. (1989). Biogeochemical cycles of carbon and sulfur and their effect on atmospheric oxygen over Phanerozoic time. *Palaeogeography, Palaeoclimatology, Palaeoecology*, 75, 97-122.
- Bessereau, G., & Guillocheau, F. (1995). Stratigraphic séquentielle et distribution de la matière organique dans le Lias du bassin de Paris: *Académie des sciences (Paris), comptes rendu*, 316, 1271-1278.
- Bhuyan, K., & Passey, Q. R. (1994). Clay estimation from GR and neutron-density porosity logs, SPWLA 35th Annual logging Symposium, June 19-22, paper DDD.
- Bish, D. L., & Post, J. E. (1993). Quantitative mineralogical analysis using the Rietveld full-pattern fitting method, *American Mineralogist*, 78, 932-940.
- Blatt, H., & Tracy, R. J. (1996). *Petrology: Igneous, Sedimentary and Metamorphic*, 2nd ed., Freeman, 281–292. ISBN 0-7167-2438-3.
- Blight, D. F., Compston, W., & Wilde, S. A. (1981). The Logue Brook Granite: age and significance of deformation zones along the Darling Scarp: Western Australia Geological Survey, Annual Report for 1980, 124-132.

- Blyth, C. I. (1994). Beagle seismic survey interpretation report WA-22-P (North). Woodside Offshore Petroleum, PSLA 92/30 (unpublished).
- Boesen, C., & Postma, D. (1988). Pyrite formation in anoxic environments of the Baltic. *American Journal of Science*, 288, 575-603.
- Bohacs, K. M. (1990). Sequence stratigraphy of the Monterey Formation, Santa Barbara County: Integration of physical, chemical and biofacies data from outcrop and subsurface: SEPM, core workshop 14, San Francisco, Ca.
- Bohacs, K., & Schwabach, J. (1992). Sequence stratigraphy of fine-grained rocks with special reference to the Monterey Formation, in J. Schwabach and K. Bohacs, eds., *Sequence stratigraphy in fine-grained rocks: Examples from the Monterey Formation: Pacific Section SEPM*, 70, 7-19.
- Bohacs, K. M. (1993). Source quality variations tied to sequence development in the Monterey and associated formations, Southwestern California, in Katz, B.J., and Pratt, L.M., eds., *petroleum source rocks in a sequence stratigraphic framework: AAPG studies in geology*, 7, 177-204.
- Bohacs, K. M., & Miskell-Gerhardt, K. (1998). Well-log expression of lake strata; controls of lake-basin type and provenance, contrasts with marine strata. *AAPG annual meeting expanded abstracts*, Tulsa, Oklahoma, p. A78.
- Bohacs, K. M. (1998a). Introduction: Mudrock sedimentology and stratigraphy: Challenges at the basin to local scales, in J. Scheiber, W. Zimmerle, and P. Sechi, eds., *Shales and mudrocks: Basin studies, sedimentology and paleontology*: Stuttgart, Germany, Schweizerbart'sche Verlagsbuchhandlung, 1, 13-20.
- Bohacs, K. M. (1998b). Contrasting expressions of depositional sequences in mudstones from marine to non-marine environs, in Schieber, J., Zimmerle, W., and Sethi, P., eds., *Mudstones and shales, characteristics at the basin scale*: Stuttgart, Schweizerbart'sche Verlagsbuchhandlung, 1, 32-77.

- Bohacs, K. M., Grawbowski, G. J., Carroll, A. R., Mankeiwitz, P. J., Miskell-Gerhardt, K. J., Schwalbach, J. R., Wenger, M. B. & Simo, J. A. (2005). Production, destruction, and dilution- the many paths to source rock development, SEPM special publication 82, 61-101.
- Bohacs, K. M., & Lazar, O. R. (2010). Sequence stratigraphy in fine-grained rocks at the field to flow-unit scale: insights for correlation, mapping, and genetic controls, presented at Houston Geological Society, Applied Geoscience Conference, February 8-9, Houston.
- Boles, J. R. and Franks, S. G. (1979). Clay diagenesis in Wilcox Sandstones of Southwest Texas; implications of smectite diagenesis on sandstone cementation, *Journal of Sedimentary Petrology*, 49, 55-70.
- Boreham, C. J., Hope, J. M., Hartung-Kagi, B., & Van Aarssen, B. J. K. (2000). More sources for gas and oil in Perth Basin Study highlights potential for multiple petroleum systems, AGSO Research Newsletter.
- Bowker, K.A. (2007). Barnett shale gas production, Fort Worth Basin: issues and discussion, *AAPG Bulletin*, 91, 523-533.
- Bradshaw, M. T., Bradshaw, J., Murray, A. R., Needham, D. J., Spencer, L., Summons, R. E., Wilmot, J., & Winn, S. (1994). Petroleum systems in West Australian basins. In: Purcell, R.G. and Purcell, R.R. (eds), *The Sedimentary Basins of Western Australia. Proceedings of Petroleum Exploration Society of Australia, The Western Australian Basins Symposium*, Perth, WA, 93-118.
- Bradshaw, J., Bradshaw, B., Spencer, L., & Mackie, V. (2000). Geodisc Project 1- Regional Analysis, Stage 2 Basins - Perth Basin, Western Australia (Appendix 1 of report no. RPT06-0162), Australian Petroleum CRC.
- Burner, K. R., & Smosna, R. (2011). A Comparative Study of the Mississippian Barnett Shale, Fort Worth Basin, and Devonian Marcellus Shale, Appalachian Basin. U.S. Department of Energy. DOE/NETL-2011/1478.

- Bustin, A. M. M., Bustin, R. M., & Cui, X. (2008a). Importance of fabric on production of gas shale, the Society of Petroleum Engineers (SPE) 114167.
- Bustin, M. R., Bustin, A., Ross, D., Chalmers, G., Murthy, V., Laxmi, C., & Cui, X. (2008b). Shale gas opportunities and challenges. Search and Discovery Articles, AAPG Annual Convention, San Antonio, Texas.
- Byers, C. W. (1977). Biofacies patterns in euxinic basins: A general model: In Cook, H.E. and Enos, P., eds, Deep-water Carbonate Environments: Society of Economic Paleontologists and Mineralogists Special Publication 25, 5-17.
- Cadman, S. J., Pain, L., & Vuckovic, V. (1994). Perth Basin, W.A., Australian Petroleum Accumulations Report 10, Bureau of Resource Sciences, Canberra.
- Cardott, B. J. (2006). Gas shales tricky to understand: AAPG Explorer, 27(11), 48-49.
- Castagna, J. P., Batzle, M. L., & Eastwood, R. L. (1985). Relationships between compressional-wave and shear-wave velocities in clastic silicate rocks: Geophysics, 50, 571-581.
- Chong, K. K., Grieser, W. V., Passman, A., Tamayo, C. H., Modeland, N., & Burke, B. (2010). A Completions Guide Book to Shale-Play Development: A Review of Successful Approaches Towards Shale-Play Stimulation in the Last Two Decades. SPE133874: Canadian Unconventional Resources and International Petroleum Conference, 19-21 October 2010, Calgary, Alberta, Canada.
- Cipolla, C. L., Lolon, E. P., & Mayerhofer, M. J. (2009). Reservoir Modeling and Production Evaluation in Shale-Gas Reservoirs. IPTC13185: International Petroleum Technology Conference, 7-9 December 2009, Doha, Qatar.
- Cooper, R.E. (1967). Well completion report: Beharra-1 and Beharra-2, Western Australia. FPC (A) Perth Operational Geology. R.G. 514.

- Comer, J. B., Hamilton-Smith, T., & Frankie, W. T. (1994). Source rock potential, in N. R. Hasenmueller and J. B. Comer, eds., Gas potential of the New Albany Shale (Devonian and Mississippian) in the Illinois Basin: Gas Research Institute GRI-92/0391, Illinois Basin Studies 2, 47-57.
- Comer, J. B. (2009). The forms of quartz and dolomite in Woodford Shale of the southern mid-continent, U.S.A.: Indicators of paleoclimate, paleogeography, paleoceanography, and depositional processes (abs.): AAPG Mid-Continent Meeting, Book of Abstracts, 21.
- Creaney, S., & Passey, Q. R. (1993). Recurring patterns of total organic carbon and source rock quality within a sequence stratigraphic framework, AAPG Bulletin, 77, 386-401.
- Crostella, A. (1995). An evaluation of the hydrocarbon potential of the onshore northern Perth Basin. Western Australia. Perth: Geological Survey of Western Australia. Report, 43.
- Crostella, A., & Backhouse, J. (2000). Geology and petroleum exploration of the central and southern Perth Basin, Western Australia: Western Australia Geological Survey, Report 57, 85.
- CSIRO (The Commonwealth Scientific and Industrial Research Organisation), 2012. Shale gas production Shale gas porosity, permeability and production. Report: CESREfs018-12 Shale gas production.
- Davis, R. J., Blume, C. R., & Slatt, R. M. (2006). Reservoir characterization: Applications of electrical borehole images, in R.M. Slatt, N.C. Rosen, M. Bowman, J. Castagna, T. Good, R. Loucks, R. Latimer, M. Scheihing, and R. Smith, eds., Reservoir characterization: Integrating technologies and business practices, 26th Annual GCSSEPM Foundation Bob F. Perkins Research Conference, December 3-6, Houston, Texas, 465-512.
- Davis, R. A., Jr., & Dalrymple, R. W. (2012). Principles of Tidal Sedimentology. New York, Springer, 607 p.

- Deaton, B. C., Nestell, M., & Balsam, W. L. (1996). Spectral reflectance of conodonts: A step toward quantitative color alteration and thermal maturity indexes. *AAPG Bulletin*, 80(7), 999-1007.
- Duman, R. J. (2012). Economic Viability of Shale Gas Production in the Marcellus Shale; Indicating by Production Rates, Cost and Current Natural Gas Price” MS thesis, Applied Natural Resources Economics, Michigan Technology Institute.
- Eichhubl, P., D'Onfro, P. S., Aydin, A., Waters, J., & McCarty, D. K. (2005). Structure, petrophysics, and diagenesis of shale entrained along a normal fault at Black Diamond Mines, California-Implications for fault seal. *AAPG Bulletin*, 89(9), 1113-1137.
- Embry, A. F., & Johannessen, E. (1992). T-R sequence stratigraphy, facies analysis and reservoir distribution in the uppermost Triassic–Lower Jurassic succession, western Sverdrup basin, Arctic Canada, in T.O. Vorren, E. Bergsager, O.A. Dahl- Stamnes, E. Holter, B. Johansen, E. Lie, and T. B. Lund, eds., *Arctic geology and petroleum potential: Norwegian Petroleum Society Special Publication 2*, 121-146.
- Embry, A. (2007). Six impossible sequence boundaries before breakfast: A 50 year saga of unworkable methods and wishful thinking. A 2007 Ashton Embry presentation. Calgary, Canada <http://wildhorse.insinc.com/embry2007/> accessed on 23rd July 2008.
- Enderlin, M., Alsleben, H., & Breyer, J. A. (2011). Predicting fracability in shale reservoirs. Adapted from poster presentation at AAPG annual convention and exhibition, Houston, Texas, USA, April 10-13; Search and Discovery article#40783, posted 31/07/2011.
- Enterprise Oil Exploration Ltd., & Nippon Oil Exploration (Perth Basin) Ltd., 1994. Plum MSS final report. Part E. geo-physical interpretation (unpublished).
- Falvey, D. A., & Mutter, J. C. (1981). Regional plate tectonics and the evolution of Australia's passive continental margins. *BMR Journal of Australian Geology and Geophysics*, 6, 1-29.

- Fang, H., Jianyu, C., Yongchuan, S., & Yaozong, L. (1993). Application of organic facies studies to sedimentary basin analysis: A case study from the Yitong graben, China: *Organic Geochemistry*, 20(1), 27-42, DOI: 10.1016/0146-6380(93)90078-P.
- Fertl, W. H., & Rieke, H. H. (1980). Gamma ray spectral evaluation techniques identify fractured shale reservoirs and source rock characteristics, *Journal of Petroleum Technology*, 2053-2062.
- Fertl, W. H., & Chilingar, G. V. (1988). Total organic carbon content determined from well logs. SPE 15812 presented at 1986 SPE annual technical conference and exhibition, New Orleans, Louisiana, 5-8 October.
- Fisher, M. K., Wright, C. A., Davidson, B. M., Goodwin, A. K., Fielder, E. O., Buckler, W. S., & Steinsberger, N. P. (2005). Integrating fracture-mapping technologies to improve stimulations in the Barnett Shale. SPE paper 77441.
- Frantz, J. H. Jr., & Waters, G.A. (2005). Schlumberger Data & Consulting Services, and Valerie A. Jochen, Schlumberger. Operators re-discover shale gas value. Management Report, E& P. Copyright, Hart Energy Publishing.
- Gale, J. F. W., Reed, R. M., & Holder, J. (2007). Natural fractures in the Barnett Shale and their importance for hydraulic fracture treatments, *AAPG Bulletin*, 91, 603-622.
- Geological Survey of Western Australia. (2005). Prospectivity of acreage release areas L05-3 and L05-4 Northern Perth Basin. Western Australia.
- GeoMark & Agso. (1996). The oils of Western Australia, petroleum geochemistry and correlation. Propriety Report (unpublished), Canberra and Houston.
- Ghori, K. A. R. (2013). Emerging unconventional shale plays in Western Australia, the Australian Petroleum Production and Exploration (APPEA) Journal, 313-336.

- Gibbs, R.J., 1967. Quantitative X-ray diffraction analysis using clay mineral extracted from the samples to be analysed, *Clay Minerals*, 7(1), 79-90. DOI: 10.1180/claymin.1967.007.1.07.
- Glorioso, J. C., Rattia, A., & Repsol. (2012). Unconventional reservoirs: basic petrophysical concepts for shale gas, SPE/EAGE European unconventional resources conference and exhibition, Vienna, Austria, SPE 153004. DOI: 10.2118/153004-MS.
- Grieser, W. V., & Bray, J. M. (2007). Identification of Production Potential in Unconventional Reservoirs. Production and operations symposium, Oklahoma, U.S.A. Society of Petroleum Engineers: SPE-106623-MS. DOI: 10.2118/106623-MS.
- Guthrie, J. M., & Bohacs, K. M., (2009). Spatial variability of source rocks: a critical element for defining the petroleum system of Pennsylvanian carbonate reservoirs of the Paradox Basin, SE Utah. In W.S. Houston, L.L. Wray, and P.G. Moreland, eds., *the Paradox Basin revisited- new developments in petroleum systems and basin analysis*, RMAG 2009 special publication- the Paradox Basin, 95-130.
- Hall, P. B., & Kneale, R. L. (1992). Perth Basin rejuvenated. *Australian Petroleum Exploration Journal*, 32 (1), 33-43.
- Hallam, A. (1999). Evidence of sea level fall in sequence stratigraphy: examples from the Jurassic, *Geology*, 27, 343-346.
- Harris, L.B. (1994). Structural and tectonic synthesis for the Perth Basin, Western Australia., *Journal of Petroleum Geology* (Refid: 14253), 17, 129-156.
- Haworth, J. (2013). US Gas industry a learning opportunity for Western Australia, Petroleum and Geothermal Petroleum Division. Magazine: *Petroleum in Western Australia*, Western Australia's digests of petroleum exploration, development and production, 7.
- Hesselbo, S. P. (1996). Spectral gamma-ray logs in relation to clay mineralogy and sequence stratigraphy, Cenozoic of the Atlantic Margin, Offshore New Jersey. Through Mountain, G.S., Miller, K.G.,

Blum, P., Poag, C.W., and Twichell, D.C. (Eds.), Proceedings of the Ocean Drilling Program, Scientific Results, 150.

Hendricks, S. B., & Ross, C. S. (1941). Chemical composition and genesis of glauconite and celadonite. *Am. Mineral*, 26(12), 683-708.

Hester, T. C., Schmoker, J. W., & Sahl, H. L. (1990). Log derived regional source rock characteristics of the Woodford Shale, Anadarko Basin, Oklahoma: U.S. Geological Survey Bulletin, 1866-D, 1-38.

Hickey, J. J., & Henk, B. (2007). Lithofacies summary of the Mississippian Barnett Shale, Mitchell 2 T.P. ims well, Wise County, Texas: AAPG Bulletin, 91, 437-443, DOI: 10.1306/12040606053.

Hill, R. J., Zhang, E., Katz, B. J., & Tang, Y. (2007). Modeling of gas generation from the Barnett Shale, Fort Worth Basin, Texas: American Association Petroleum Geologists Bulletin, 91, 501-521.

Hocking, R.M. (1991). The Silurian Tumblagooda Sandstone, Western Australia: Western Australia Geological Survey, Report 27,124p.

Hoeve, M. V., Meyer, S. C., Preusser, J., & Makowitz, A. (2010). Basin-wide delineation of gas shale “sweet spots” using density and neutron logs; implications for qualitative and quantitative assessment of gas shale resources, AAPG Hedberg Conference, December 5-10, Austin, Texas.

Holditch, S. A., & Lee, W. J. (2005). Advances in technology; key to realizing potential of unconventional gas. U.S. Energy Information Administration (EIA).

Houseknecht, D. W., & Bird, K. J. (2004). Sequence stratigraphy of the Kingak Shale (Jurassic-Lower Cretaceous), National Petroleum Reserve in Alaska, AAPG Bulletin, 88(3), 279-302.

- Hyeong, K., & Capuano, R. M. (2000). The effect of organic matter and the H₂O₂ organic-matter-removal method on the δ D of smectite-rich samples, *Geochimica et Cosmochimica Acta*, 64, 3829-3837.
- Iasky, R. P. (1993). A structural study of the southern Perth Basin, Western Australia: Western Australia Geological Survey, Report 31, 56p.
- Iasky, R. P., & Mory, A. J. (1993). Structural and tectonic framework of the onshore northern Perth Basin, *Exploration Geophysics*, 24(3-4), 585-592.
- Iasky, R. P., & Mory, A. J. (1994). Structural and tectonic framework of the onshore northern Perth Basin. *Australian Society of Exploration Geophysicists Journal*, 24, 585-592.
- Ingram, B. S. (1967). Palynology of the Otorowiri Siltstone Member, Yarragadee Formation: Western Australia Geological Survey, Annual Report for 1966, 79-82.
- Jacobi, D., Gladkikh, M., LeCompte, B., Hursan, G., Mendez, F., Longo, J., Ong, S., Bratovich, M., Patton, G., & Shoemaker, P. (2008). Integrated petrophysical evaluation of shale gas reservoirs. CIGP/SPE Gas Technology Symposium 2008 Joint Conference, Calgary, Alberta, 16-19 June, SPE 114925, Society of Petroleum Engineers (SPE) 114925-MS.
- Jacobi, D., Breig, J., LeCompte, B., Kopal, M., Hursan, G., Mendez, F., Bliven, S., & Longo, J. (2009). Effective geochemical and geomechanical characterization of shale gas reservoirs from the wellbore environment: Caney and the Woodford Shale. Society of Petroleum Engineers (SPE) Annual Technical Conference and Exhibition, New Orleans, Louisiana, 4-7 October, SPE 124231.
- Jaripatke, O., Grieser, B., & Chong, K. K. (2012). A Review of Successful Approach towards Shale Play Stimulation in the Last Two Decades- A Completions Road Map to Shale Play Development. SPE130369. ISB: 978-1-55563-275-5.

- Jarvie, D. M. (1991). Total Organic Carbon (TOC) analysis, in Merrill, R.K., ed., *Treatise of petroleum geology: Handbook of petroleum geology, source and migration processes and evaluation techniques*. American Association of Petroleum Geologists (AAPG), 113-118.
- Jarvie, D. (2004). Evaluation of hydrocarbon generation and storage in the Barnett Shale, ft. Worth Basin, Texas, Humble Geochemical services, division of humble instruments and services, Inc.
- Jarvie, D. M., Pollastro, R. M., & Hill, R. J. (2004). Evaluation of hydrocarbon generation in Barnett shale ft. Worth Basin, Texas, Ref. Noble et al, 1997, P. 26, Special REG/PTTC Presentation. Humble Instruments & Services.
- Jarvie, D. M., Hill, R. J., & Pollastro, R. J. (2005). Assessment of the gas potential and yields from shales: the Barnett Shale model, in B. Cardott, ed., *Oklahoma Geological Survey Circular 110: unconventional gas of the southern mid-continent symposium*, March 9-10, Oklahoma City, OK, 37-50.
- Jarvie, D. M., Hill, R. J., Ruble, T. E., & Pollastro, R. M. (2007). Unconventional shale-gas systems: the Mississippian Barnett Shale of north-central Texas as one model for thermogenic shale-gas assessment, *AAPG Bulletin*, 91, 475-499.
- Johnston, D. (2004). Technological advances expand potential pay, *Oil and Gas Journal*, 51-59.
- Jonasson, K. (2013). Review of Petroleum Exploration, Production and Development in Western Australia in 2012. *Petroleum Resource Geologist; Resources Branch. Magazine: Petroleum in Western Australia, Western Australia's digests of petroleum exploration, development and production*, 7.
- Jones, D. K. (1976). Perth Basin. In: Leslie, R.B., Evans, H.J., and Knight, C.L. (eds), *Economic Geology of Australia and Papua New Guinea*, 3, Petroleum. Perth: Australasian Institute of Mining and Metallurgy, Monograph series, 7.

- Kalantari-Dahaghi, A., & Mohaghegh, S.D. (2011). A new practical approach in modelling and simulation of shale gas reservoirs: application to New Albany Shale. *International Journal of Oil Gas and Coal Technology*, 4(2), 104-133.
- Kaufhold, S., Hein, M., Dohrmann, R., & Ufer, K. (2012). Quantification of the mineralogical composition of clays using FTIR spectroscopy. *Journal of Vibrational Spectroscopy*, 59, 29-39.
- Khalid, S., Faurschou, K., Gorchynski, T., Zhao, X., & Marechal F. C., 2010. Mapping key reservoir properties along horizontal shale gas wells. The Canadian Unconventional Resources and international petroleum conference (CSUG), CSUG/SPE 137413. Calgary, Alberta, Canada.
- Klug, H. P., & Alexander, L. E. (1974). X-ray diffraction procedures for polycrystalline and amorphous material. Wiley, New York.
- Krushin, J. T. (1997). Seal capacity of nonsmectite shale, in R.C. Surdam, ed., seals, traps, and the petroleum system: AAPG Memoir 67, 31-47.
- Kuuskaa, V. (2007). A decade of progress in unconventional gas. *Oil and Gas Journal*, unconventional gas article #1 final. Arlington, Virginia: Advanced Resources International.
- Kwon, O., Kronenberg, A. K., Gangi, A. F., Johnson, B., & Herbert, B. E. (2004). Permeability of illite-bearing shale: 1. Anisotropy and effects of clay content and loading, *Journal of Geophysical Research*, 109, B10205, DOI: 10.1029/2004JB003052, 2004.
- Lane, C., Watts, K., & Ulmer, B. (1983). Well completion report, Peron-1. Highbay Oil (Australia) Ltd.
- Lash, G. G., & Engelder, T. (2011). Thickness trends and sequence stratigraphy of the Middle Devonian Marcellus Formation, Appalachian Basin: Implications for Acadian foreland basin evolution. *AAPG Bulletin*, 95(1), 61-103. DOI: 10.1306/06301009150.

- Le Blanc Smith, G. (1993). Geology and Permian coal resources of the Collie Basin, Western Australia: Western Australia Geological Survey, Report 38, 86p.
- Le Blanc Smith, G., & Kristensen, S. (1998). Geology and Permian coal resources of the Vasse River Coalfield, Perth Basin, Western Australia: Western Australia Geological Survey, Record 1998(7), 49p.
- Leetaru, H. E. (2000). Sequence Stratigraphy of the Aux Vases Sandstone: A Major Oil Producer in the Illinois Basin, AAPG Bulletin, 84(3), 399-422.
- Lewis, R., Ingraham, D., Percy, M., Williamson, J., Sawyer, W., & Frantz, J. (2004). New evaluation techniques for gas shale reservoirs. Reservoir Symposium 2004.
- Loucks, R. G., & Ruppel, S. C. (2007). Mississippian Barnett Shale: Lithofacies and depositional setting of a deep-water shale-gas succession in the Fort Worth Basin, Texas: AAPG Bulletin, 92, 579-601, DOI: 10.1306871 /11020606059.
- Loucks, R. G., Reed, R. M., Ruppel, S. C., & Jarvie, D. M. (2009). Morphology, genesis, and distribution of nanometer-scale pores in siliceous mudstone of the Mississippian Barnett Shale. *Journal of Sedimentary Research* 79, 848-861.
- Macquaker, J. H. S., Gawthorpe, R. L., Taylor, K. G., & Oates, M. G. (1998). Heterogeneity, stacking patterns and sequence-stratigraphic interpretation in distal mudstone successions: Examples from the Kimmeridge Clay Formation, U.K., in J. Scheiber, W. Zimmerle, and P. Sechi, eds., *Shales and mudrocks: Basin studies, sedimentology and paleontology*: Stuttgart, Germany, Schweizerbartsche Verlagsbuchhandlung, 1, 163-185.
- Madejová, J. (2003). FTIR techniques in clay mineral studies, a review. *Vibrational Spectroscopy*, 31, 1-10.

- Mancini, E. A., & Puckett, T. M. (2005). Jurassic and Cretaceous Transgressive-Regressive (T-R) Cycles, Northern Gulf of Mexico, USA. *Stratigraphy*, 2(1), 31-48.
- Manger, K. C., Oliver, S. J. P., Curtis, J. B., & Scheper, R. J. (1991). Geologic influences on the location and production of Antrim shale gas, Michigan Basin: SPE paper21854, Proceeding of Society y of Petroleum Engineers, Rocky Mountain Regional; Low permeability reservoirs symposium and exhibition, 511-519.
- Marshall, J. F., Lee, C. S., Ramsay, D. C., & Moore, A. M. G. (1989). Tectonic controls on sedimentation and maturation in the offshore north Perth Basin. *Australian Petroleum Exploration Journal*, 29(1), 450-465.
- Matteson, A., & Herron, M. M. (1993). Quantitative mineral analysis by fourier transform infrared spectroscopy - 1993 SCA Conference Paper Number 9308, Schlumberger-Doll Research Old Quarry Road, Ridgefield, Ct. 06877-4108.
- Mazzullo, S. J., Wilhite, W., & Woolsey, I. W. (2009). Petroleum reservoirs within a spiculite-dominated depositional sequence: Cowley Formation (Mississippian-Lower Carboniferous), south-central Kansas: *AAPG Bulletin*, 93, 1649-1689, DOI: 10.1306/06220909026.
- McLoughlin, S. (1993). Plant fossil distributions in some Australian Permian non-marine sediments. *Sedimentary Geology*, 85, 601-619.
- McPherson, A., & Jones A. (2005). Appendix D: Perth Basin geology review and site class assessment. In: Jones T, Middelman M & Corby N, comps. *Natural hazard risk in Perth, Western Australia: comprehensive report*. Geoscience Australia, 313-44.
- Medd, J. (2012). Shale: a New Energy Dawn? Principal Policy Officer Petroleum Division. Magazine: *Petroleum in Western Australia*, Western Australia's digests of petroleum exploration, development and production, 34.

- Middleton, M. F. (1982). Tectonic history from vitrinite reflectance: Royal Astronomical Society, *Geophysical Journal*, 68, 121-132.
- Montgomery, S. L., Jarvie, D. M., Bowker, K. A., & Pollastro, R. M. (2005). Mississippian Barnett Shale, Fort Worth Basin, North-Central Texas: gas-shale play with multi-trillion cubic foot potential, *AAPG Bulletin*, 89, 155-175.
- Morris, K. (1979). A classification of Jurassic marine shale sequences; an example from the Toarcian (Lower Jurassic) of Great Britain. *Paleogeography, Paleoclimatology, Paleocology*, 26, 117-126.
- Morris, K. A., & Shepperd, C. M. (1982). The role of clay minerals in influencing porosity and permeability characteristics in the Bridport Sands of Wytch Farm, Dorset. *Clay Minerals*, 17(1), 41-54. DOI: 10.1180/claymin.1982.017.1.05.
- Mory, A. J., & Iasky, R. P. (1996). Stratigraphy and structure of the onshore northern Perth Basin, Western Australia: Western Australia Geological Survey, Report 46.
- Mullen, M., & Enderlin, M. (2012). Fracability index- more than just calculating rock properties. SPE159755.
- Muza, J. P., & Wise, S. W., Jr. (1983). An authigenic gypsum, pyrite, and glauconite association in a Miocene deep sea biogenic ooze from the Falkland Plateau, Southwest Atlantic Ocean. Texas A & M University, Ocean Drilling Program, College Station, TX, United States, DOI: 10.2973/dsdp.proc.71.114.1983, 71(1), 361-375.
- Nelson, P. H. (2009). Pore-throat sizes in sandstones, tight sandstones, and shales. *AAPG Bulletin*, 93(3), 329-340.
- Noble, D. C., Park-Li, B., Henderson, W. B., & Vidal, C. E. (1997). Hypogene oxidation and late deposition of precious metals in the Pierina high-sulfidation deposit and other volcanic and sedimentary rock-hosted gold systems. IX Congreso Peruana de Geología, Resúmenes Extendidos, Sociedad Geológica del Perú, 1, 121-127.

- North Broken Hill Ltd. (1981). Temporary reserves 8057H–8076H, Coolcalalaya Sub-basin, via Geraldton, report for quarter ended 13th August 1981: Western Australia Geological Survey, M-series Open File M7444 A35991 (unpublished).
- O'Brien, N. R., & Slatt, R. M. (1990). *Argillaceous Rock Atlas*. Springer Verlag. 141.
- Olausson, E. (1961). Studies of Deep-Sea Cores. Reports of the Swedish Deep-Sea Expedition, 1947-1948(8), 353-391.
- Olsen, R. K. (1982). Factors controlling uranium distribution in Upper Devonian-Lower Mississippian black shales of Oklahoma and Arkansas, Dissertation, University of Tulsa, Tulsa, Oklahoma.
- Owad-Jones, D. L., & Ellis, G. K. (2000). Western Australia atlas of petroleum fields, Onshore Perth Basin: Petroleum Division, DMEWA, 1.
- Passey, Q. R., Creaney, S., Kulla, J. B., Moretti, F. J., & Stroud, J. D. (1990). A practical model for organic richness from porosity and resistivity logs. *AAPG Bulletin*, 74(12), 1777-1794.
- Passey, Q. R., Bohacs, K. M., Esch, W. L., Klimentidis, R., & Sinha, S. (2010). From oil-prone source rock to gas producing shale reservoir-geologic and petrophysical characterization of unconventional shale-gas reservoirs, the Society of Petroleum Engineers (SPE) 131350.
- Paxton, S. T., Cruse, A. M., & Krystyniak, A. M. (2006). Detailed fingerprints of global sea level change revealed in Upper Devonian/Mississippian Woodford Shale of south-central Oklahoma, *AAPG Search and Discovery Article* 40211.
- Pearson, I., Zeniewski, P., Gracceva, F., Zastera, P., McGlade, C., Sorrell, S., Speirs, J., & Thonhauser, G. (2012). *Unconventional Gas: Potential Energy Market Impacts in the European Union*, A report by the energy security unit of the European commission's joint research centre. Other contributors: Corina Alecu, Arne Eriksson, Peter Toft & Michael Schuetz, JRC Scientific and Policy Reports.

- Peters, K. E. (1986). Guidelines for evaluating petroleum source rock using programmed pyrolysis. *AAPG Bulletin*, 70(3), 318-329.
- Pichler, H., & Schmitt-Riegraf, C. (1997). *Rock-forming Minerals in Thin Section*. Original German Edition *Gesteinsbildende Minerals im Dünnschliff*, translated by L. Hoke. London, Cambridge University Press, 217 p.
- Playford, P. E., Cockbain, A. E., & Low, G. H. (1976). *Geology of the Perth Basin Western Australia*. Geological Survey of Western Australia, Bulletin 124.
- Pollastro, R. M. (2007). Total petroleum system assessment of undiscovered resources in the giant Barnett Shale continuous (unconventional) gas accumulation, Fort Worth Basin, Texas: *American Association Petroleum Geologists Bulletin*, 91, 551-578.
- Potter, P. E. Maynard, J. B., & Pryor, W. A. (1980). *Sedimentology of Shale*. Springer Verlag New York Inc. 305p.
- Povarennykh, A. S. (1978). The use of infrared spectra for the determination of minerals, *American Mineralogist*, 63, 956-959.
- Quaife, P., Rosser, J., & Pagnozzi, S. (1994). The structural and stratigraphic architecture of the offshore northern Perth Basin, Western Australia, in *West Australian Basins* edited by P. Purcell and R. Purcell: Petroleum Exploration Society of Australia Symposium, Perth, Proceedings, 811-822.
- Rabnawaz, U. (2009), *Acoustic logging for hydrogeology, Perth Basin, Western Australia*. Perth: Department of Exploration Geophysics, Curtin University. Report no. GPM 3/09.
- Raiswell, R., & Berner, R. A. (1985). Pyrite formation in euxinic and semi-euxinic sediments. *American Journal of Science*, 285, 710-724.

- Raiswell, R., Buckley, F., Berner, R. A., & Anderson, T. F. (1988). Degree of pyritization of iron as a paleoenvironmental indicator of bottom-water oxygenation. *Journal of Sedimentary Petrology*, 58(5), 812-819.
- Raiswell, R., Canfield, D. E., & Berner, R. A. (1994). A comparison of iron extraction methods for the determination of degree of pyritisation and the recognition of iron-limited pyrite formation. *Chemical Geology*, 111(1-4), 101-110.
- Reineck, H. E., & Singh, I. B. (1980). *Depositional sedimentary environments*. Springer-Verlag, Berlin, Heidelberg, New York, 551 p.
- Rickman, R., Mullen, M., Peter, E., Grieser, B., & Kundert, D. (2008). A practical use of shale petrophysics for stimulation design optimization: all shale plays are not clones of the Barnett Shale. SPE 115258, presented at 2008 SPE Annual technical conference and exhibition, Denver, Colorado, 21-24 September, 2008.
- Rietveld, H.M. (1969). A profile refinement method for nuclear and magnetic structures. *Journal of Applied Crystallography*, 2, 65-71.
- Rhoades, D. C., & Morse, I. W. (1971). Evolutionary and ecologic significance of oxygen-deficient marine basins, *Lethaia* 4, 413-428.
- Rhoades, D. C., Mulslow, S. G., Gutschik, R., Baldwin, C. T., & Stolz, J. F. (1991). The dysaerobic zone revisited: a magnetic facies? In: R.V. Tyson and T. H. Pearson (editors), *Modern and ancient continental shelf anoxia*. Geological Soc. Spec. Publication 58, 187-199.
- Ross, D. J. K., & Bustin, R. M. (2008). Characterising the shale gas resource potential of Devonian-Mississippian strata in the Western Canada sedimentary basin: application of an integrated formation evaluation, *AAPG Bulletin*, 92(1), 87-125.
- Roychoudhurya, A. N., Kostkab, J. E., & Cappellen, P. V. (2003). Pyritization: a palaeoenvironmental and redox proxy reevaluated. *Estuarine, Coastal and Shelf Science*, 57, 1183-1193.

- Scott, J. (1991). The occurrence of oil-prone source rocks in continental half-grabens. *PESA (The Petroleum Exploration Society of Australia) Journal*, 18, 47-53.
- Schieber, J. (1994). Evidence for high energy events and shallow water deposition in the Chattanooga Shale, Devonian, central Tennessee, USA, *Sedimentary Geology*, 93, 193-208.
- Schmoker, J. W. (1995). Method for assessing continuous-type (unconventional) hydrocarbon accumulations. National assessment of United States oil and gas resources—Results, methodology, and supporting data: U.S. Geological Survey Digital Data Series 30.
- Schutter, S. R. (1998). Characterization of shale deposition in relation to stratigraphic sequence systems tracts, in J. Scheiber, W. Zimmerle, and P. Sechi, eds., *Shales and mudrocks: Basin studies, sedimentology and paleontology*: Stuttgart, Germany, Schweizerbartsche Verlag-sbuchhandlung, 1, 79-108.
- Schwalbach, J. R., & Bohacs, K. M. (1992). Sequence stratigraphy in fine-grained rocks: examples from the Monterey Formation: SEPM, Pacific Section, Guidebook 70, 80 p.
- Seggie, R. (1990). Geological cross-section of the North Perth Basin. Bureau of Mineral Resources, Geology and Geophysics and Australian Petroleum Industry Research Association, Record 199/65.
- Serra, O., & Abbott, H. T. (1980). The contribution of logging data to sedimentary sedimentology and stratigraphy, SPE-9270: Society of Petroleum Engineers, presented at 55th Annual Technical Conference and Exhibition [Dallas], preprint, 19 p. Later published in 1982, *Society of Petroleum Engineers Journal*, 22(1), 117-131.
- Shin, J. Y., & Philippe, R. (2000). A new tool for electro-facies analysis: Multi-Resolution Graph Based Clustering. Society of Petrophysicists & Well Log Analysts. SPWLA 41st Annual Logging Symposium.

- Singh, P. (2008). Lithofacies and sequence stratigraphic framework of the Barnett Shale, Northeast Texas. PhD thesis. Norman, Oklahoma: University of Oklahoma.
- Slatt, R. M., Singh, P., Philp, R. P., Marfurt, K. J., Abousleiman, Y., & O'Brien, N. R. (2009a). Workflow for stratigraphic characterization of unconventional gas shales: 2008 Society of Petroleum Engineers Shale Gas Production Conference, Fort Worth, Texas, SPE Paper 119891, 1-17.
- Slatt, R. M., Singh, P., Philp, R. P., Marfurt, K. J., Abousleiman, Y., O'Brien, N. R., & Eslinger, E. V. (2009b). Workflow for stratigraphic characterization of unconventional gas shales: Gulf Coast Association of Geological Transactions, 59, 699-710, DOI: 10.2118/119891-MS.
- Slatt, R. M., Singh, P., Philp, R. P., Saison, A., Abousleiman, Y., O'Brien, N. R., & Eslinger, E. V. (2009c). Workflow for stratigraphic characterization of unconventional gas shales (abs.): Geological Society of America, Abstracts with Programs, 412, 12.
- Slatt, R. M., Singh, P., Borges, G., Perez, R., Portas, R., Vallejo, J., Ammerman, M., Coffey, W., & Eslinger, E. (2009d). Reservoir characterization of unconventional gas shales: Example from the Barnett Shale, Texas, U.S.A. (abs.): AAPG Search and Discovery article 30075: http://www.searchanddiscovery.com/documents/2009/30075slatt/ndx_slatt.pdf (accessed September 21, 2009).
- Slatt, R. M., Philp, P. R., Abousleiman, Y., Singh, P., Perez, R., Portas, R., Marfurt, K. J., Madrid-Arroyo, S., O'Brien, N., Eslinger, E. V., & Baruch, E. T. (2011). Pore-to-regional-scale integrated characterization workflow for unconventional gas shales, in J. Breyer, ed., Shale reservoirs-Giant resources for the 21st century: AAPG Memoir 97, 1-24.
- Smith, G. L. B. (1993). Geology and Permian coal resources of the Collie Basin, Western Australia. Western Australia Geological Survey, Report 38, 86p.

- Smith, D. K., Johnson, G. G., Scheible, W., Wims, A. M., Johnson, J. L., & Ullmann, G., (1987). Quantitative X-ray powder diffraction method using the full diffraction pattern. *Powder Diffraction*, 2, 73-77.
- Smith, G. L. B., & Kristensen, S. (1998). Geology and Permian coal resources of the Vasse River Coalfield, Perth Basin, Western Australia: Western Australia Geological Survey, Record 1998/7, 49p.
- Solomon, P. R., & Miknis, F. P. (1980). Use of fourier transform infrared spectroscopy for determining oil shale properties- fuel, 59, 893-896.
- Sondergeld, C. H., Newsham, K. E., Comisky, J. T., & Rice, M. C. (2010). Petrophysical considerations in evaluating and producing shale gas resources, the Society of Petroleum Engineers (SPE) 131768, 23-25, Pittsburgh.
- Song, T., & Cawood, P. A. (2000). Structural styles in the Perth Basin associated with the Mesozoic breakup of Greater India and Australia, *Tectonophysics* (Refid: 12771), 317, 55-72.
- Srodoń, J., Drits, V. A., McCarty, D. K., Hsieh, J. C. C., & Eberl, D. D. (2001). Quantitative x-ray diffraction analysis of clay-bearing rocks from random preparations, *Clays and Clay Minerals*, 49(6), 514-528.
- Stagg, H. M. J., Willcox, J. B., Symonds, P. A., O'Brien, G. W., Colwell, J. B., Hill, P. J., Lee, C-S., Moore, A. M. G., & Struckmeyer, H. I. M. (1999). Architecture and evolution of the Australian continental margin, *AGSO Journal of Australian Geology and Geophysics* (Refid: 12772), 17(5/6), 17-33.
- Starkey, H. C., Blackmon, P. D., & Hauff, P. L. (1984). The routine mineralogical analysis of clay-bearing samples. U.S. Geological Survey, Bulletin 1563.
- Steward, D. B. (2007). The Barnett Shale play: phoenix of the Fort Worth basin, a history: Fort Worth Geological Society and North Texas Geological Society, 202 p.

- Suits, N. S., & Wilkin, R. T. (1998). Pyrite formation in the water column and sediments of a meromictic lake. *Geology (Boulder)*, 26(12), 1099-1102.
- Summers, R. E., Boreham, C. J., Foster, C. B., Murray, A. P., & Gorter, J. D. (1995). Chemostratigraphy and the composition of oils in the Perth Basin, Western Australia: *APEA Journal*, 35(1), 613-632.
- Sutton, S. J., Ethridge, F. G., Almon, W. R., Dawson, W. C. and Edwards, K. K. (2004). Textural and sequence-stratigraphic controls on sealing capacity of Lower and Upper Cretaceous shales, Denver basin, Colorado *AAPG Bulletin*, 88(8), 1185-1206.
- Talukdar, S. C. (2009). Application of geochemistry for shale gas assessment. Weatherford Laboratories: Weatherford Laboratories.
- Thomas, B. M. (1979). Geochemical analysis of hydrocarbon occurrences in the northern Perth Basin, Australia. *American Association of Petroleum Geologists, AAPG Bulletin* 63, 1092-1107.
- Thomas, B. M. (1982). Sand plant source rocks for oil and their significance in Australian sedimentary basins. *APPEA Journal*, 22, 164-178.
- Thomas, B.M., & Brown, S. A. (1983). Hydrocarbon generation in the northern Perth Basin: *APEA Journal*, 23(1), 64-74.
- Thomas, B. M. (1984). Hydrocarbons, source rocks and maturity trends in the northern Perth Basin, Australia, in *Petroleum geochemistry and basin evolution* edited by G. Demaison, and R. J. Morris: American Association of Petroleum Geologists, *AAPG Memoir* 35, 341-403.
- Thomas, B. M., & Barber, C. J. (1994). A re-evaluation of the hydrocarbon habitat of the northern Perth Basin. *The APPEA Journal*, v. 44, 59-92.
- Thomas, D. B., Nance, R. D., & Murphy, J. B. (2002). Deformation of the Macumber Formation, Antigonish Basin, Nova Scotia: implications for the Ainslie Detachment. *Atlantic Geology*, 38(2- 3), 1-10.

- Thomas, B. M., & Barber, C. J. (2004). A re-evaluation of the hydrocarbon habitat of the northern Perth Basin. *The APPEA Journal*, 44(1), 13-57.
- Thyburg, B., Jahren, J., winje, T., Bjorlykke, K., & Faleide, J. I. (2009). From mud to shale: rock stiffening by micro-quartz cementation, *EAGE First Break*, 27, 53-59.
- Tiab, D., & Donaldson, E. C. (2004). *Petrophysics*. Elsevier press, second edition, ISBN 0-7506-7711-2. MA, United States.
- Tissot, B. P. (1977). The application of the results of organic chemical studies in oil and gas exploration. In "Developments in petroleum geology", 1, 53-82. Applied Science Publishers, London.
- Triche, N. (2012). Wave of the future? Petroleum Geologist Resources Branch, Shale gas in Western Australia –Magazine: Petroleum in Western Australia, Western Australia's digests of petroleum exploration, development and production, p. 20.
- Tucker, M. (1988), *Techniques in Sedimentology*. Black Well Scientific Publications, Oxford OX2 0EL.
- Utley, L. (2012). Unconventional Petrophysical Analysis in Unconventional Reservoirs Putting the Puzzle Together in Gas Shales. *Petroleum software techniques-Utley petrophysics*.
- Van De Kamp, P. C. (2008), Smectite-illite-muscovite transformations, quartz dissolution and silica release in shales, *Clays and Clay Minerals*, 56(1), 66-81.
- Van Wagoner, J. C., Mitchum, R. M., Campion, K. M., & Rahmanian, V. D. (1990). Siliciclastic sequence stratigraphy in well logs, cores and outcrops: concepts for high resolution correlation of time and facies: *AAPG Methods in Exploration Series*, (7), 53 p.

- Wang, F. P., & Gale, J. F. W. (2009). Screening criteria for shale-gas systems: Gulf Coast Association of Geological Societies Transactions, 59, 779-793.
- Waples, D. W., & Marzi, R. W. (1998). The universality of the relationship between vitrinite reflectance and transformation ratio: Organic Geochemistry, 28(6), 383-388.
- Wilkin, R. T., Arthur, M. A., & Dean, W. E. (1997). History of water column anoxia in the Black Sea indicated by pyrite. Earth and Planetary Science Letters, 148(3-4), 517-525.
- Woodside Offshore Petroleum. (1988). A review of the petroleum geology and hydrocarbon potential of the Barrow–Dampier Sub-basin and environs, in The North West Shelf, Australia edited by P. G. PURCELL and R. R. PURCELL: Petroleum Exploration Society of Australia; North West Shelf Symposium, Perth, Proceedings, 115-128.
- Wu, L. M., Zhou, C. H., Keeling, J., Tong, D. S., & Yu, W. H. (2012). Towards an understanding of the role of clay minerals in crude oil formation, migration and accumulation. Earth Science Reviews, 115(4), 373-386.
- Zahid, S., Bhatti, A. A., Khan, H. A., & Ahmad, T. (2007). Development of unconventional gas resources: stimulation perspective. In Production and Operations Symposium. Oklahoma City, Oklahoma, U.S.A.
- Zimmerle, W., (1995). Petroleum sedimentology. Published by Ferdinand Enke Verlag, Kluwer Academic Publisher, Netherland. ISBN 0-7923-3418-3.

Web References

Clastic Depositional Environments: Reconstruction of the Cretaceous Gates Formation A wave dominated shoreline, northeastern British Columbia- core displays. Last accessed at Sep 2013. <<http://www.eos.ubc.ca/resources/slidesets/clastic/clastic.html>>.

Geoscience Australia. (2012). Last updated at May 2012 <<http://www.ga.gov.au/energy/province-sedimentary-basin-geology/petroleum/offshore-southwest-australia/perth-basin.html>>.

Oilfield glossary. (2013). Schlumberger last accessed at Aug 2013. <<http://www.glossary.oilfield.slb.com/en/Terms/f/facies.aspx>>.

Railsback, L.B. (2012). An Atlas of Pressure Dissolution Features (disponível em <http://www.gly.uga.edu/railsback/PDFimage0107.html>).

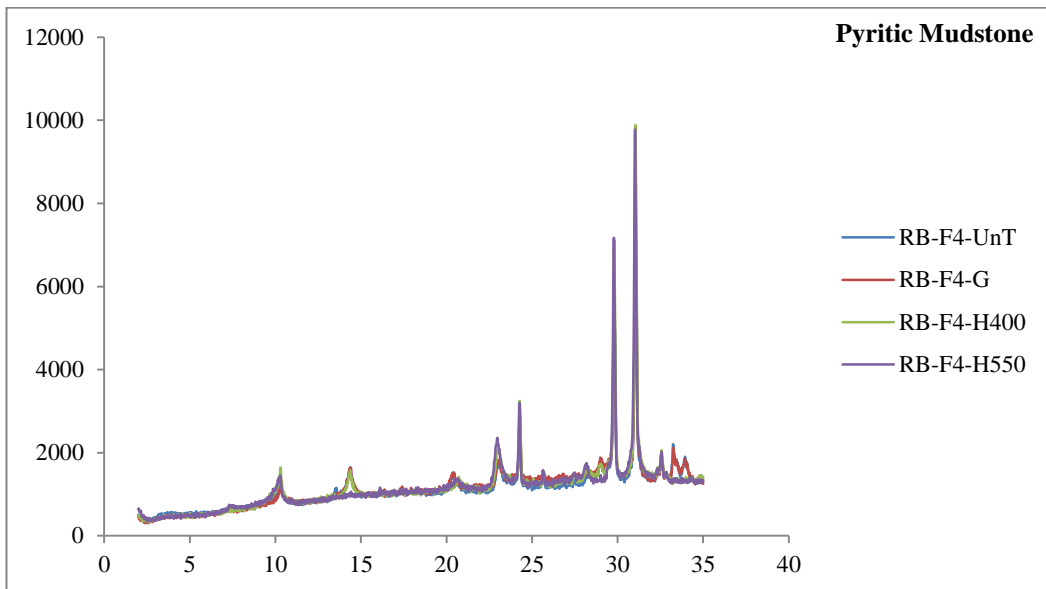
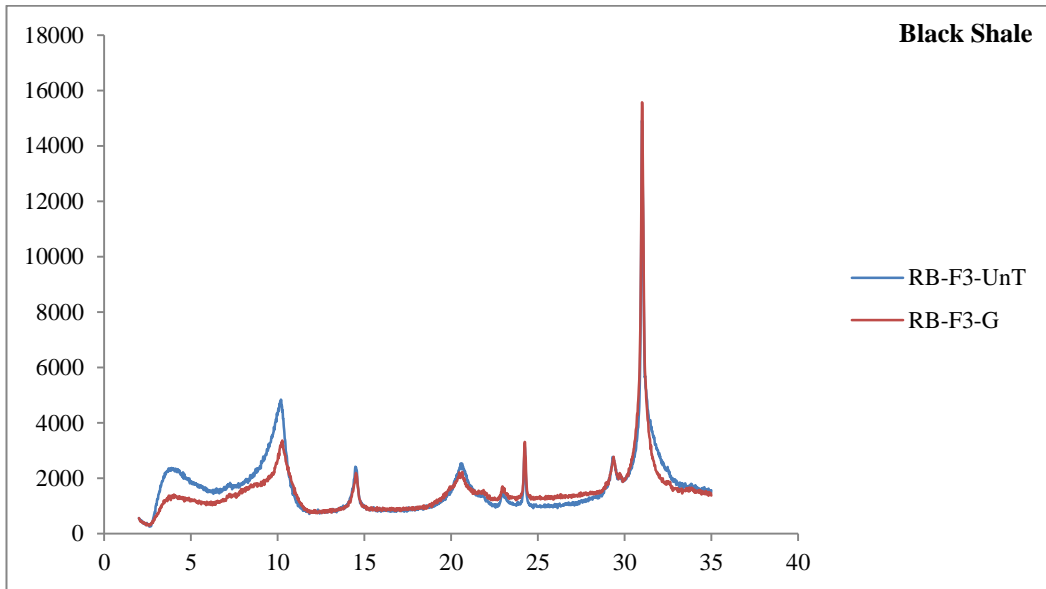
U.S. Energy Information Administration, (2011). World shale gas resources: an initial assessment of 14 regions outside the United States. Accessed 7 July 2011. <<http://www.eia.gov/analysis/studies/worldshalegas/pdf/fullreport.pdf>>.

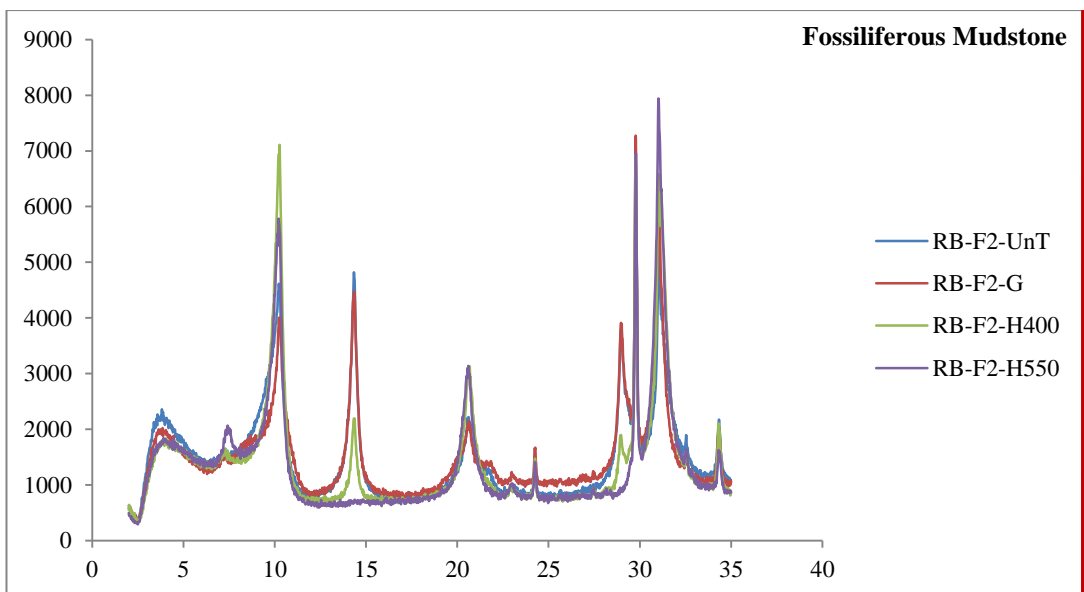
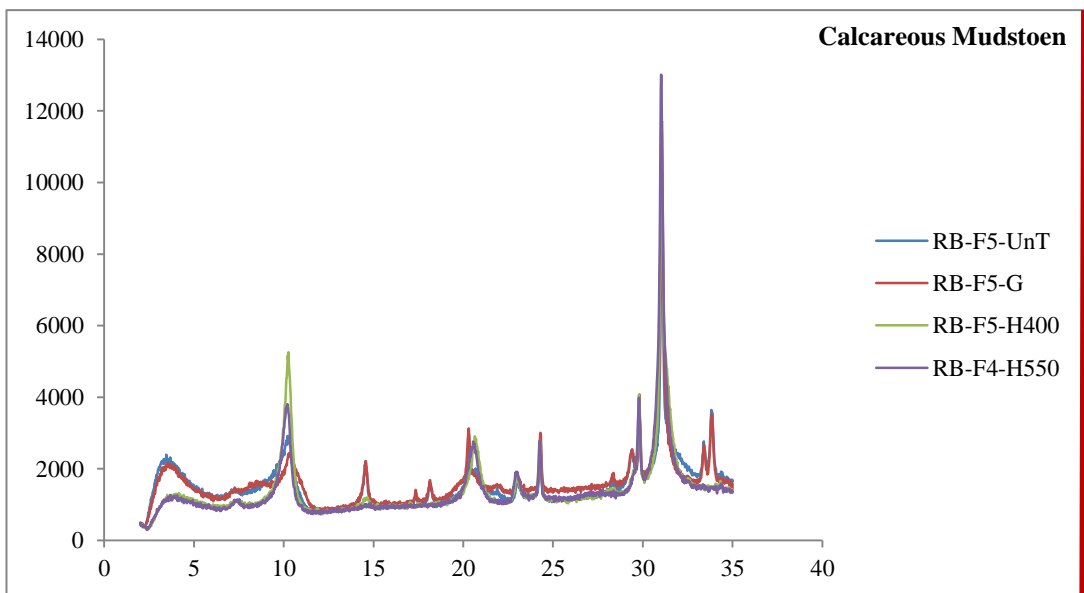
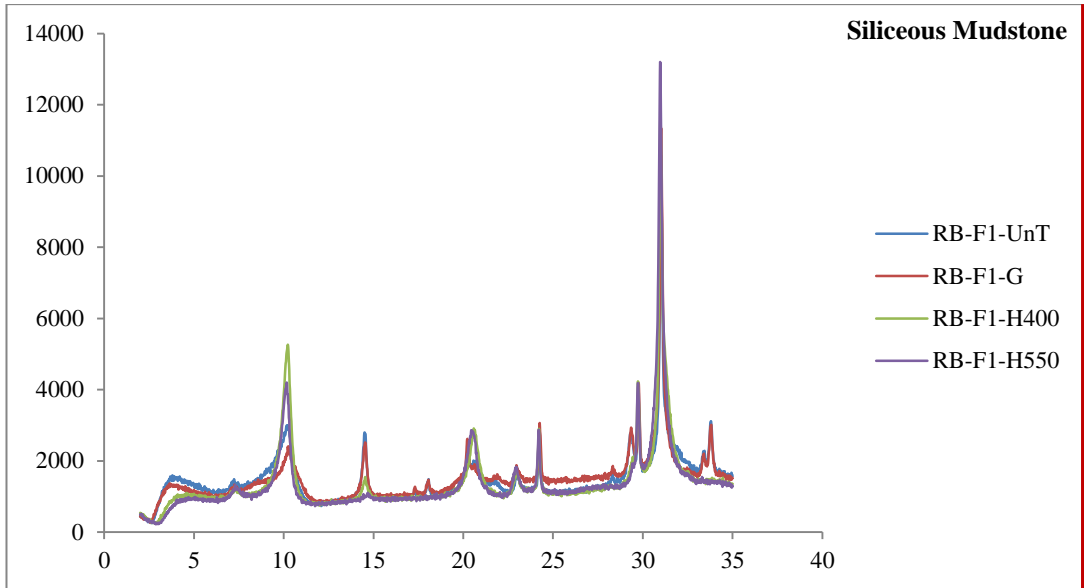
Every reasonable effort has been made to acknowledge the owners of copyright material. I would be pleased to hear from any copyright owner who has been omitted or incorrectly acknowledge

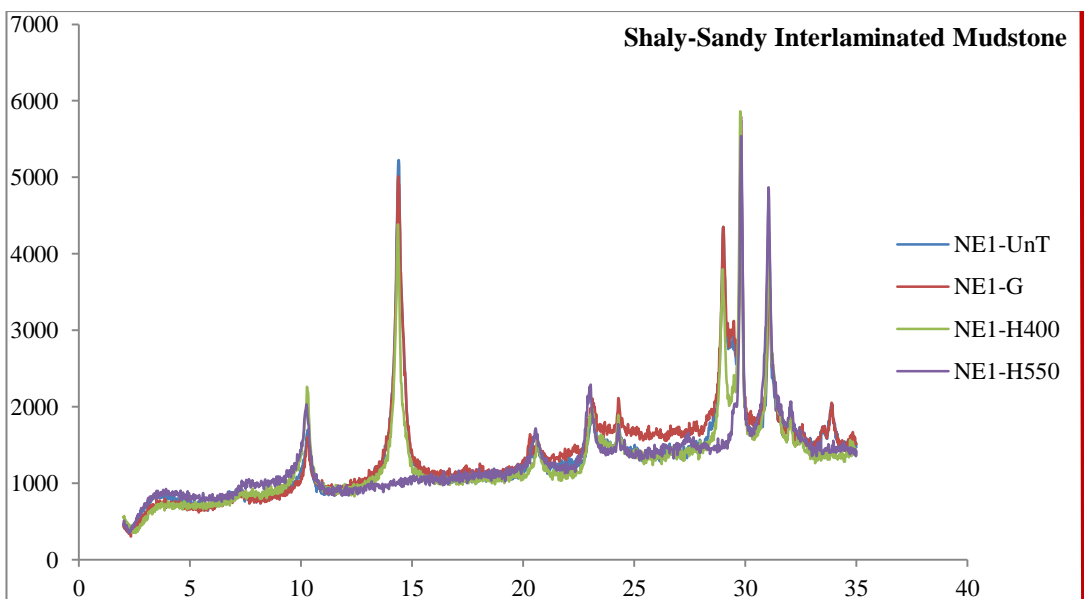
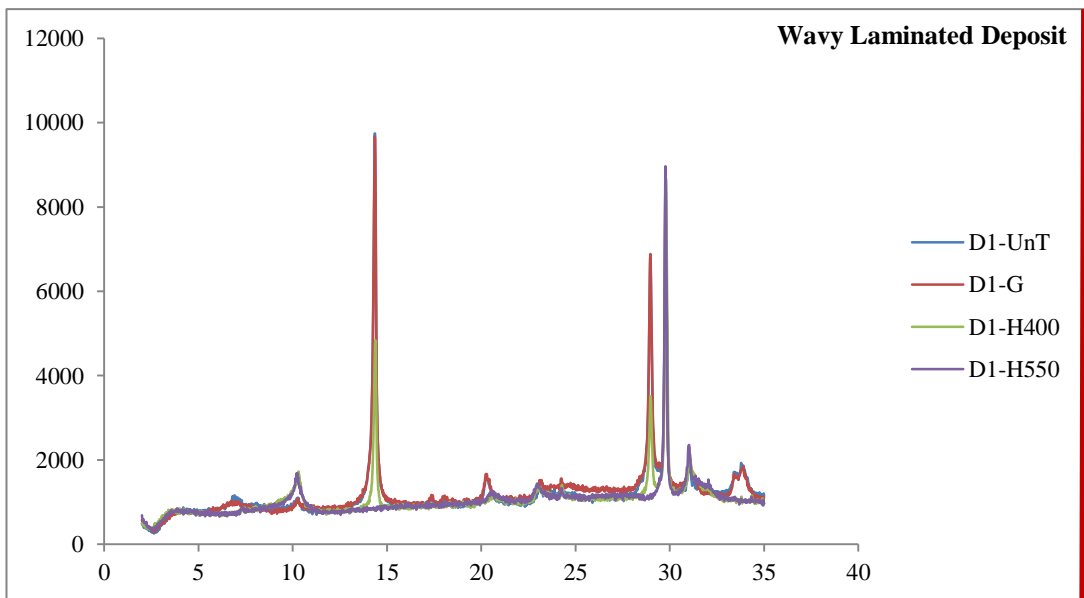
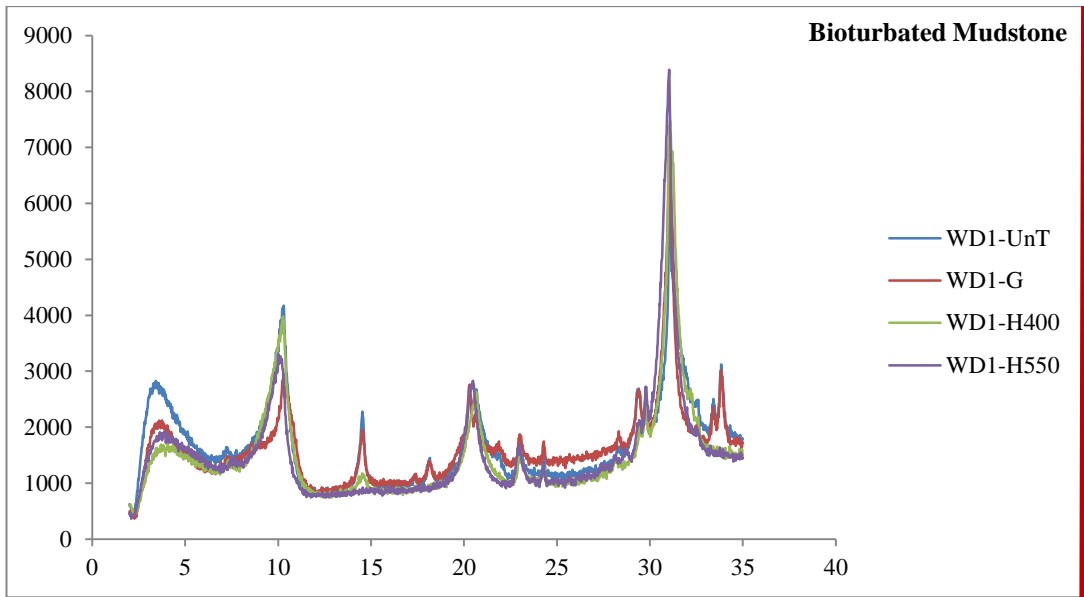
Appendix

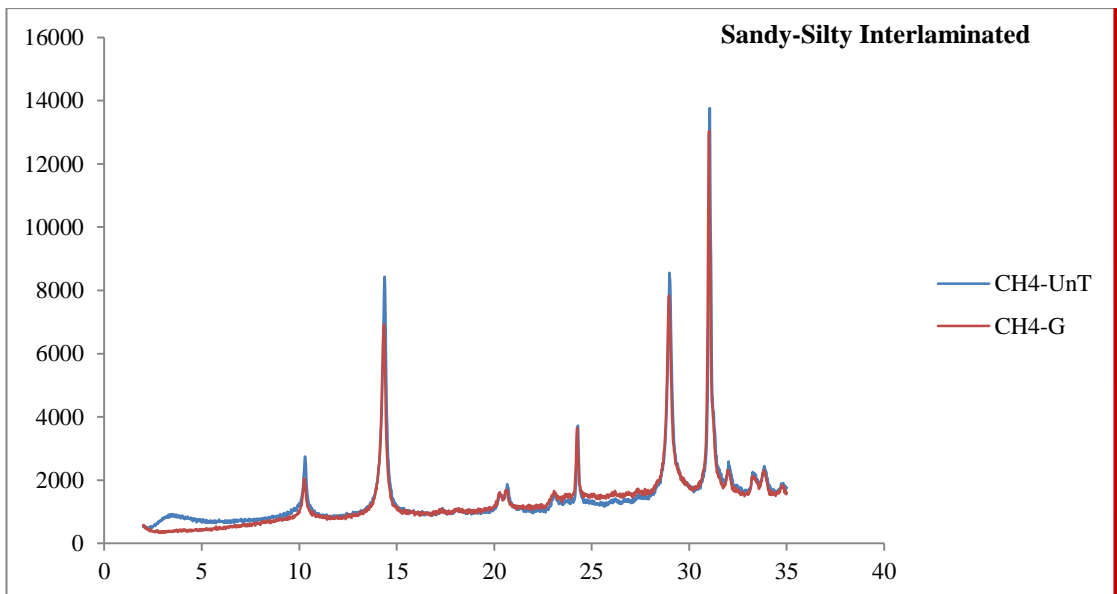
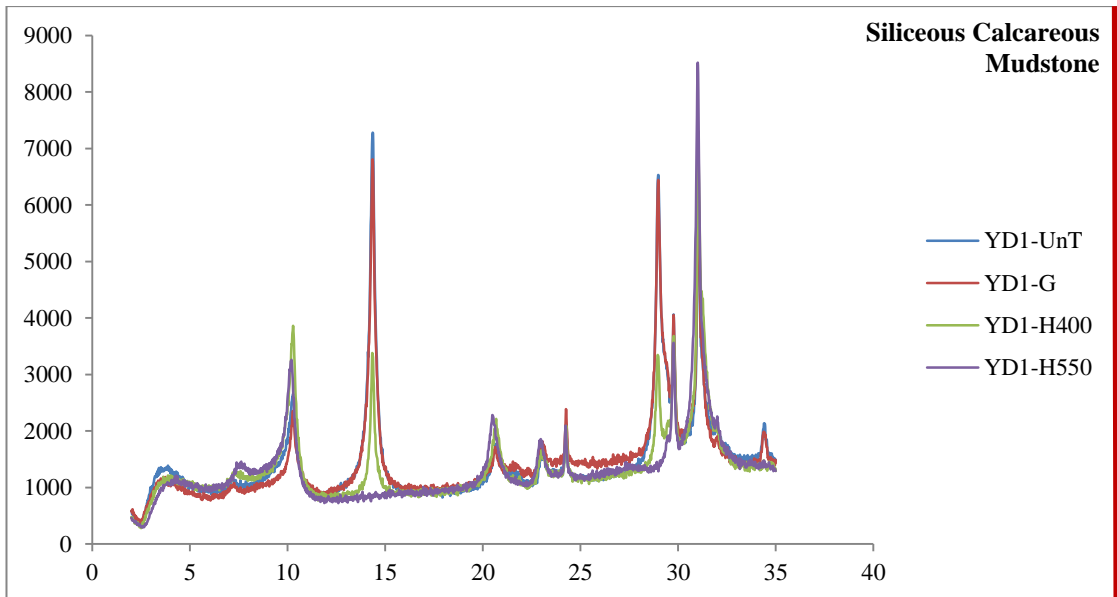
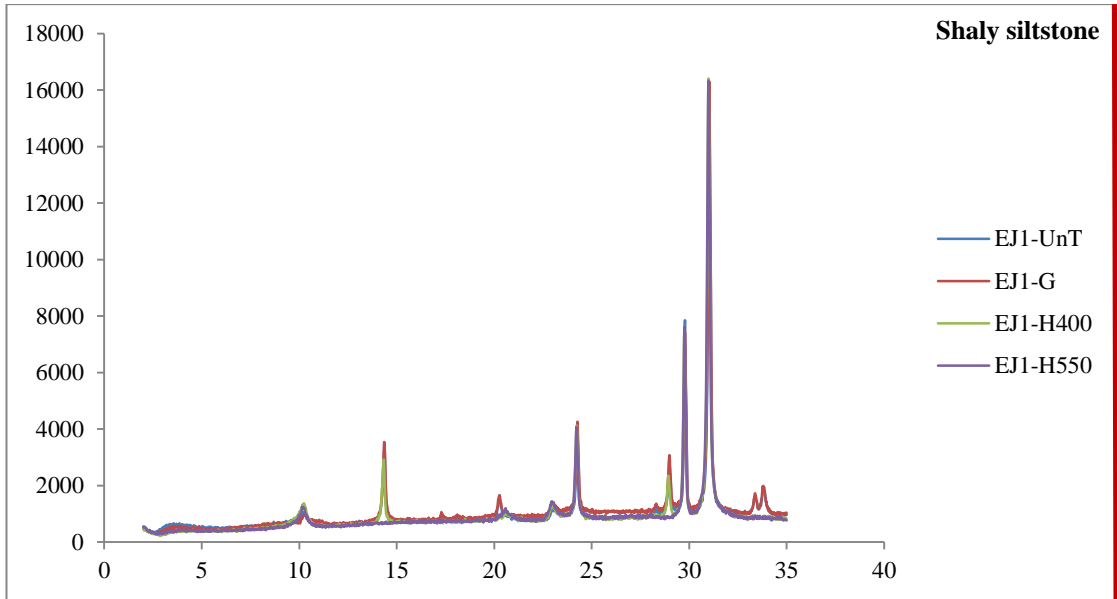
Appendix A.1

XRD clay fraction patterns









Appendix B.1

TOC values of the Kockatea and the Carynginia formations in the Perth Basin

Well name	Formation	Number of samples	TOC-mean	Well Name	Formation	Number of samples	TOC-mean
Jurien-1	Kockatea	10	0.51	Jurien-1	Carynginia	39	2.80
Woolmulla-1	Kockatea	30	0.41	Woolmulla-1	Carynginia	14	1.11
Yardarino-1	Kockatea	47	3.46	Yardarino-1	Carynginia	2	0.99
Mungarra-5	Kockatea	6	1.34	Mungarra-5	Carynginia	4	1.32
Mt Horner-1	Kockatea	12	1.50	Mt Horner-1	Carynginia	9	14.55
Eurangoa-1	Kockatea	13	1.05	Eurangoa-1	Carynginia	14	4.31
Mt Adams-1	Kockatea	27	1.90	Mt Adams-1	Carynginia	2	0.87
Beharra-2	Kockatea	9	0.36	Beharra-2	Carynginia	2	0.75
Mondarra-1	Kockatea	9	0.38	Mondarra-1	Carynginia	2	0.15
Narlingue-1	Kockatea	13	0.21	Narlingue-1	Carynginia	9	4.76
Heaton-1	Kockatea	10	1.92	Heaton-1	Carynginia	6	1.43
South-Turtle Dove 1B	Kockatea	74	0.55	South-Turtle Dove 1B	Carynginia	47	2.93
Geelvink 1A	Kockatea	35	0.41	Geelvink 1A	Carynginia	4	2.02
Batavia-1	Kockatea	23	0.51	Batavia-1	Carynginia	2	3.97
Woodada-5	Kockatea	16	0.53	Woodada-5	Carynginia	11	2.50
Woodada-6	Kockatea	9	1.30	Woodada-6	Carynginia	5	3.69
Robb-1	Kockatea	5	0.53	Robb-1	Carynginia	2	2.20
Peron-1	Kockatea	13	0.61	Peron-1	Carynginia	19	2.82
Depot Hill-1	Kockatea	5	0.60	Depot Hill-1	Carynginia	7	1.93
Diamond Soak-1	Kockatea	8	0.38	Diamond Soak-1	Carynginia	4	2.45
Leander Reef-1	Kockatea	20	0.73	Leander Reef-1	Carynginia	10	1.82
Wittecarr-1	Kockatea	45	0.33	Wittecarr-1	Carynginia	11	0.65
Central Yardarino-1	Kockatea	17	0.57	Central Yardarino-1	Carynginia	6	3.32
Eneabba-1	Kockatea	25	0.74	Abbarwardoo-1	Carynginia	5	0.95
Mt Hill-1	Kockatea	2	1.75	Woodada-2	Carynginia	2	1.65
Arrowsmith-1	Kockatea	8	0.60	Conder-1	Kockatea	4	0.96
Cadda-1	Kockatea	2	0.54	Connelly-1	Kockatea	3	0.42
Erregulla-1	Kockatea	24	0.47	Eleven mile-1	Kockatea	20	0.84
North Erregulla-1	Kockatea	13	0.86	Rakrani-1	Kockatea	8	0.28
Strawberry Hill-1	Kockatea	6	1.19	Livet-1	Kockatea	12	0.28
Wattle Grove-1	Kockatea	7	2.09				

Appendix B.2

Tmax and Remaining potential values of the target formations in the Perth Basin

Well name	Formation	S ₂	Tmax	Well Name	Formation	S ₂	Tmax
Jurien-1	Kockatea	2.32	483.4	Jurien-1	Carynginia	2.15	492.08
Woolmulla-1	Kockatea	0.78	488.0	Yardarino-1	Carynginia	0.31	425.00
Yardarino-1	Kockatea	0.87	443.4	Mt Horner-1	Carynginia	25.5	474.00
Mt Hill-1	Kockatea	1.12	454.0	Eurangoa-1	Carynginia	7.30	456.80
Mt Horner-1	Kockatea	2.94	462.2	Beharra-2	Carynginia	0.30	426.00
Arrowsmith-1	Kockatea	0.43	428.7	Mondarra-1	Carynginia	0.36	432.00
Eurangoa-1	Kockatea	0.90	461.7	Narlingue-1	Carynginia	3.13	465.00
Mt Adams-1	Kockatea	3.15	449.9	Heaton-1	Carynginia	1.13	465.50
Erregulla-1	Kockatea	0.41	437.8	South Turtle Dove 1B	Carynginia	0.71	428.00
Beharra-2	Kockatea	0.34	424.4	Geelvink 1A	Carynginia	1.90	474.00
North Erregulla-1	Kockatea	2.16	436.1	Batavia-1	Carynginia	5.48	454.66
Mondarra-1	Kockatea	0.27	433.7	Woodada-5	Carynginia	0.52	462.00
Strawberry Hill-1	Kockatea	1.56	434.7	Woodada-6	Carynginia	0.49	478.80
Narlingue-1	Kockatea	0.60	462.0	Robb-1	Carynginia	1.53	440.00
Heaton-1	Kockatea	6.66	435.2	Peron-1	Carynginia	0.55	469.60
South-Turtle Dove 1B	Kockatea	2.76	439.6	Depot Hill-1	Carynginia	0.86	426.14
Geelvink 1A	Kockatea	2.01	452.7	Diamond Soak-1	Carynginia	0.57	426.75
Batavia-1	Kockatea	1.32	439.2	Leander Reef-1	Carynginia	0.88	446.94
Woodada-5	Kockatea	0.79	439.5	Wittecarr-1	Carynginia	0.28	421.50
Woodada-6	Kockatea	0.92	435.1	Central Yardarino-1	Carynginia	3.26	442.20
Robb-1	Kockatea	1.00	438.6	Wittecarr-1	Kockatea	2.89	439.33
Peron-1	Kockatea	0.64	443.4	Conder-1	Kockatea	1.78	422.42
Depot hill-1	Kockatea	0.66	422.0	Conelly-1	Kockatea	0.72	428.00
Diamond Soak-1	Kockatea	0.59	424.7	Eleven Mile-1	Kockatea	1.16	429.75
Leander Reef-1	Kockatea	2.60	433.8	Central Yardarino-1	Kockatea	2.62	437.00
Wattle Grove-1	Kockatea	9.84	425.0	Eneabba-1	Kockatea	1.21	395.65

Appendix B.3

The vitrinite reflectance measurement for the Kockatea Shale and the Carynginia Formation

Well name	Formation	Ro-Mean	Well Name	Formation	Ro-Mean
Eneabba-1	Kockatea	0.88	Yardarino-1	Carynginia	0.59
Yardarino-1	Kockatea	1.37	Diamond Soak-1	Carynginia	0.56
Erregulla-1	Kockatea	0.64	Robb-1	Carynginia	1.65
Beharra-2	Kockatea	0.50	Peron-1	Carynginia	1.49
Mondarra-1	Kockatea	1.07	Depot Hill-1	Carynginia	0.57
Strawberry Hill-1	Kockatea	1.93	Wattle grove-1	Carynginia	0.64
Diamond Soak-1	Kockatea	0.48	Wittecarr-1	Carynginia	1.91
Geelvink 1A	Kockatea	0.67	Central Yardarino-1	Carynginia	0.77
Robb-1	Kockatea	0.86	Geelvink 1A	Carynginia	1.31
Peron-1	Kockatea	0.85	Wattle Grove-1	Kockatea	0.85
Depot Hill-1	Kockatea	0.52	Wittecarr-1	Kockatea	1.54
Central Yardarino-1	Kockatea	0.71	Condor-1	Kockatea	0.62

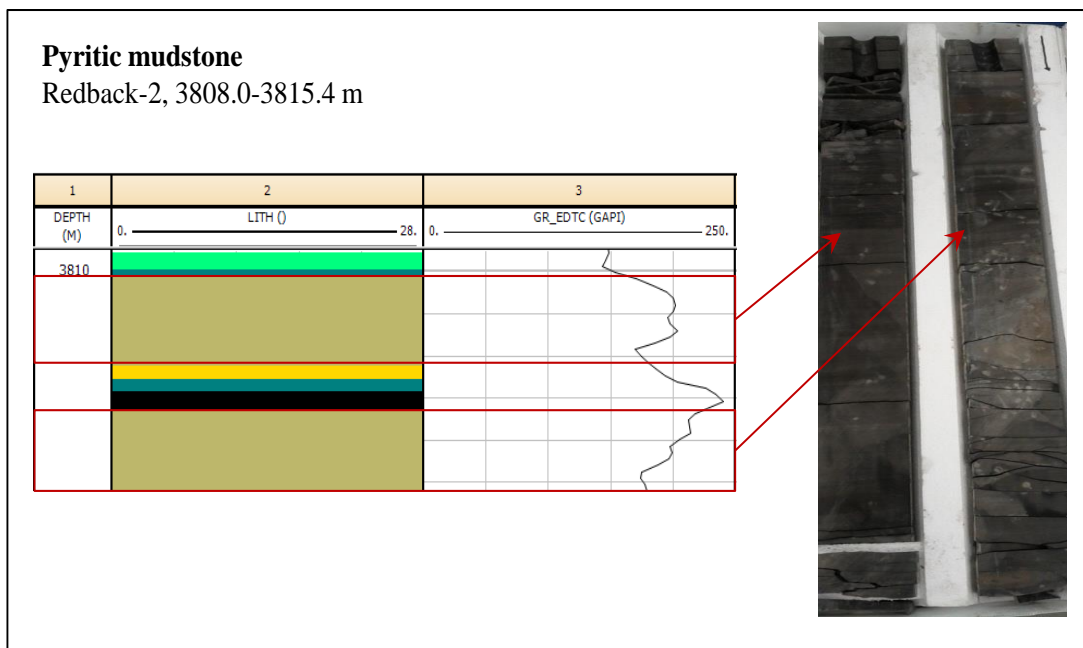
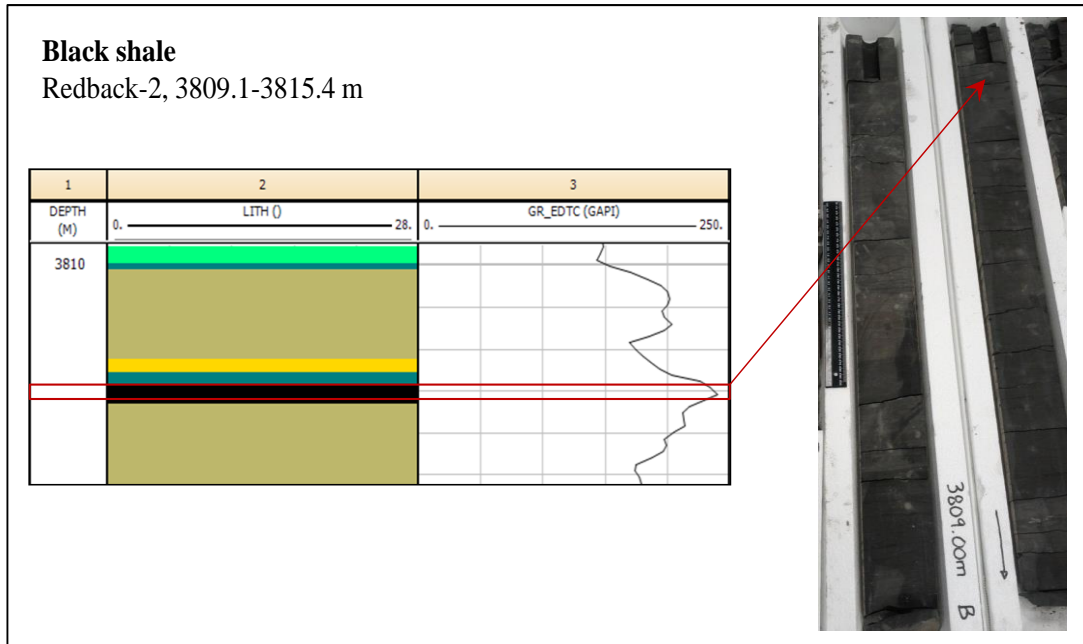
Appendix B.4

The connection between the kerogen type and maturity with genetic hydrocarbon and depositional environment

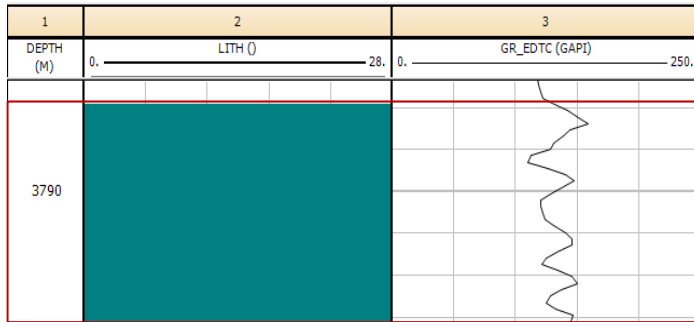
Kerogen Type	Maceral Composition	HI (mg HC/g rock)	Thermal Maturity	Genetic Hydrocarbon	Environment
Type I	Algal & Amorphous	>700	0.60-0.90 0.90-1.30 1.30-2.60	Oil Gas/ condensate	Highly anoxic Lacustrine & shallow marine, lagoonal
Type II	Amorphous & structured lipids	400-700	0.50-0.90 0.90-1.30 1.30-2.60	Oil Gas/ condensate	Anoxic marine basin Lacustrine & subtidal supratidal
Type II/III	Mixed OM amorphous & Vitrinite	200-400	0.60-1.00 1.00-3.00 1.30-2.60	Oil & Gas Gas condensate	Swamp & delta complexes, low to medium anoxic lagoon
Type III	Mainly Vitrinite	50-200	0.60-1.00 1.00-2.60	Mainly gas condensate/ Gas	Brackish water swamps
Type IV	Inertinite	<50	No source of HC	Little gas if any	Oxic swamp and oxic marine basins

Appendix C.1

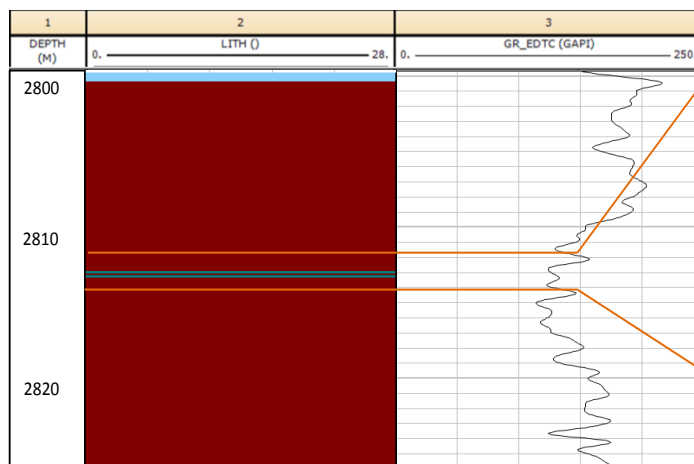
Gamma-ray response of lithofacies



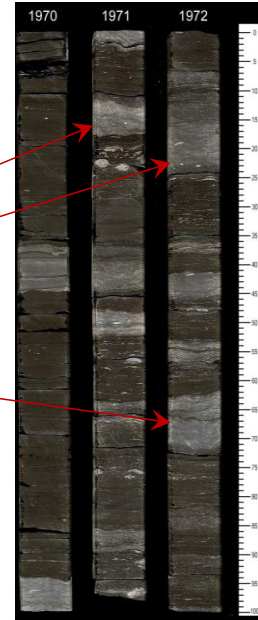
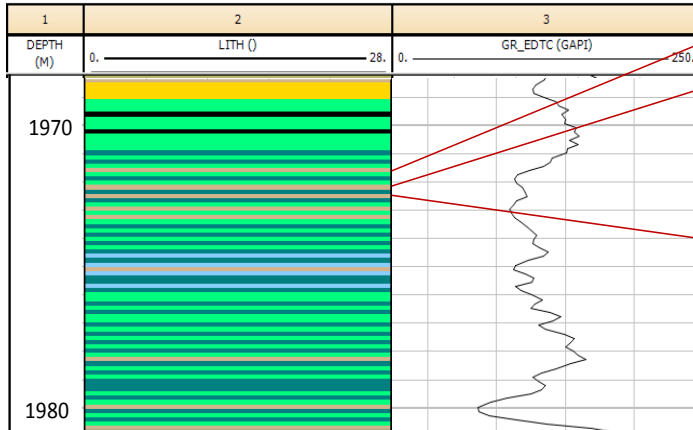
Fossiliferous mudstone
Redback-2, 3787.9-3793.1 m



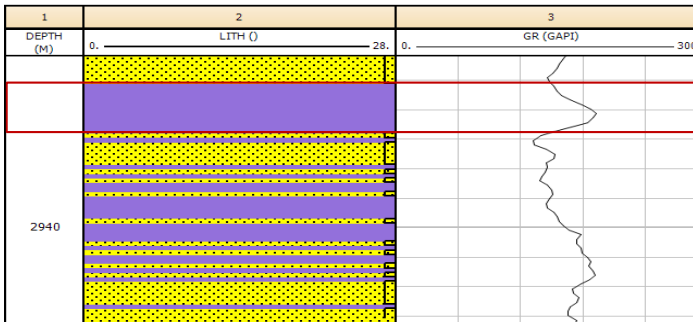
Bioturbated mudstone
Arrowsmith-2, 2798.8-2825.87 m



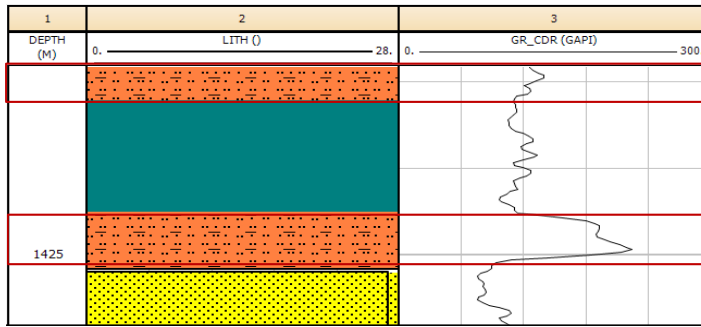
Wavy laminated deposit
Hovea-3, 1968.5-1980.6 m



Shaly-sandy interlaminated mudstone
North Erregulla-1, 2934-2943.3 m



Sandy-silty interlaminated deposit
Cliff Head-4, 1413.9-1430.2 m



Appendix C.2

Electrofacies of the Kockatea Shale

Electrofacies “A1” and “A”

These electrofacies belong at the top of the Kockatea Shale and show special gamma ray trends (Figure 5.1). “A1” displays an upward increasing gamma ray trend, whereas electrofacies of “A” has an upward decreasing trend. In some wells, the electrofacies of “A” is noticeably erratic.

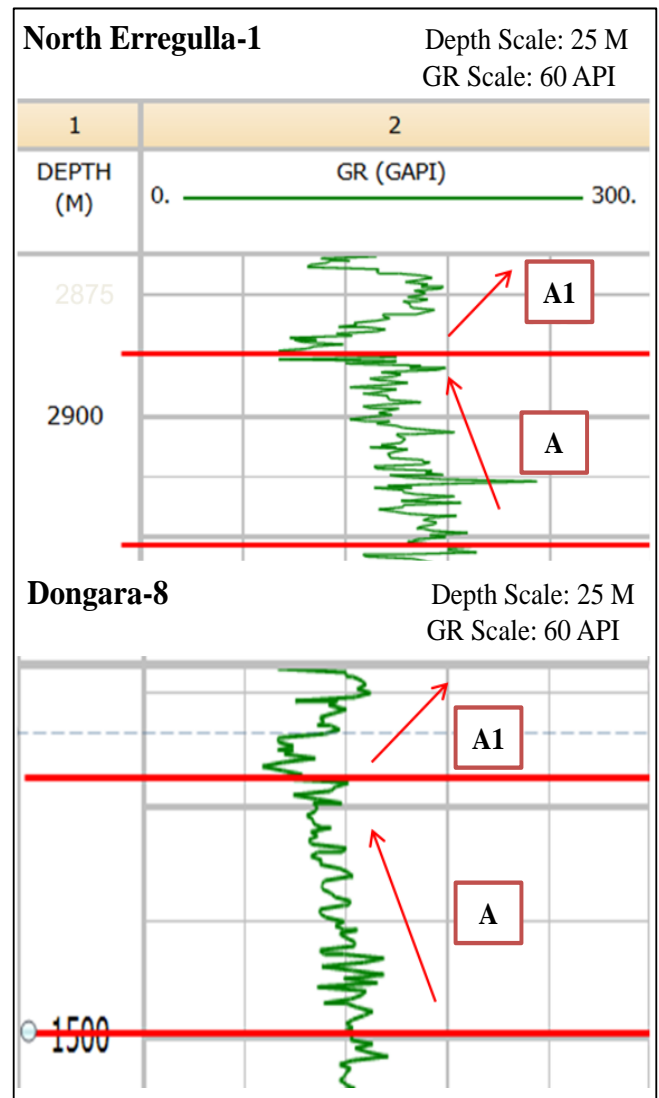
Lithofacies

The identified lithofacies for electrofacies of “A” are shaly-sandy interlaminated mudstone and sandstone. Electrofacies “A1” is mostly formed from sandstone

Claystone: Dark grey to brown grey, silty, trace mica, moderately hard, sub blocky to sub fissile.

Sandstone: Light grey, fine grained, grads to siltstone, trace mica, firm to moderately hard, well sorted, sub angular to sub rounded, poor porosity.

Note: The lithologies of intervals are derived from well completion reports of the wells.



Electrofacies “B”

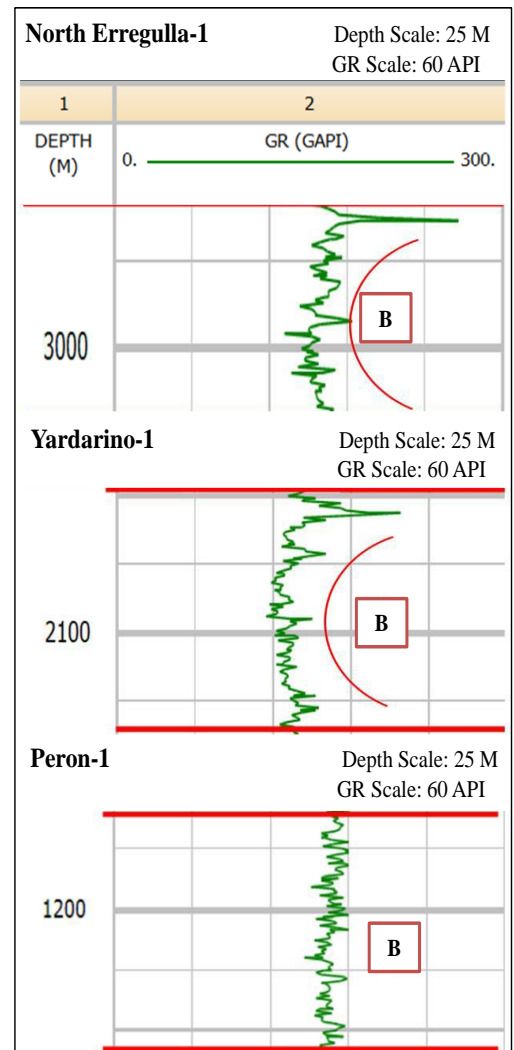
The electrofacies display an upward increasing trend on their upper parts, and it has ‘C’ shape (Figure 5.2). A spike can be seen on the top of electrofacies in some wells.

Lithofacies

General lithology is interbedded sandstone with claystone. Studying on the coincident cores with the electrofacies “C” shows mostly the lithofacies of siliceous mudstone and sandstone.

Claystone: Medium-dark grey to brown grey, silty, trace mica, increasing percentage with depth, moderately hard, sub blocky to sub fissile.

Sandstone: Light grey, fine-grained, grades to siltstone, trace mica, poor porosity, well sorted, sub angular to sub rounded, firm to moderately hard.



Electrofacies “C”

The lithofacies is formed from two parts; a decreasing upward trend on the lower parts of the curve and an increasing upward trend on the upper parts of the curve.

In general, there are no big fluctuations in the curves and the electrofacies displays a constant trend.

This electrofacies is thickened in some wells within the basin

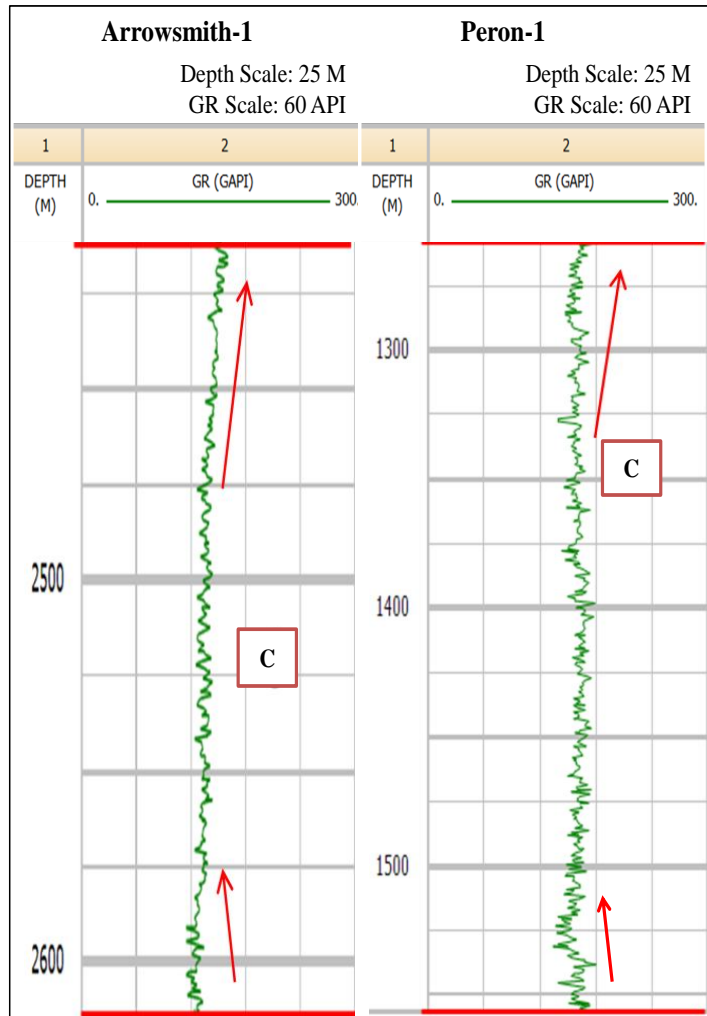
Lithofacies

Lithologically, the electrofacies is comprised of claystone with lesser sandstone in the upper section which decreases

downwards. In some wells, shale is constituent of the lower parts

Claystone: Med-dark grey, trace mica, scarcely trace limestone fragments, sub blocky to sub fissile-fissile, firm to moderately hard.

Sandstone: Light grey, fine-grained, trace mica, grads to siltstone, very poor porosity, well sorted, sub angular to sub rounded, firm to moderately hard.



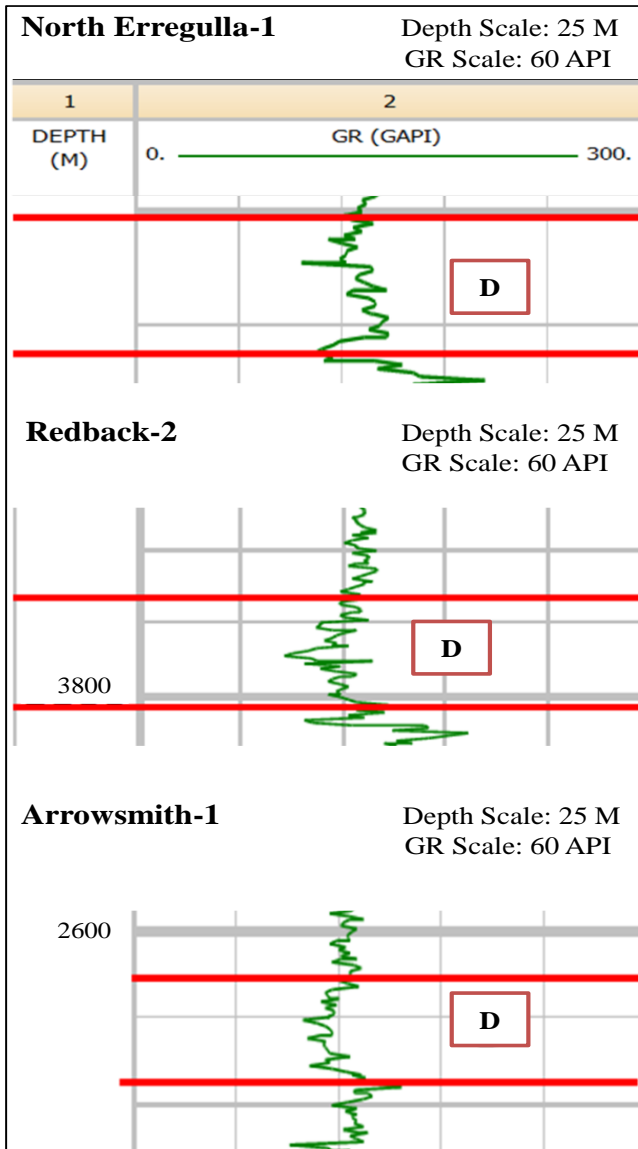
Electrofacies “D”

The electrofacies is mainly identified based on the sudden reduction in the amount of gamma ray/API counts.

Lithofacies

There is no core available for the North Erregulla-1. Electrofacies D in the Redback-2 is the response of lithofacies of fossiliferous mudstone and pyrite mudstone. The electrofacies is mainly formed from calcareous mudstone in the Arrowsmith-1.

Lithologically, the electrofacies contains claystone interbedded limestone. Limestone member in Redback-2 covers the Hovea Member. The low gamma ray may be due to the presence of calcite in the composition.



The claystone and limestone within electrofacies are as follows:

Claystone: Dark grey, partly silty, trace micro mica with minor pyrite, occasionally micro laminations of limestone, firm and sub fissile.

Limestone: Pale brown to greenish brown, trace glauconite, rare microcrystalline, minor trace pyrite, and firm.

Electrofacies “E”

The electrofacies is identified based on the upward increase at the lower part of the formation. This electrofacies is the lower part of Kockatea Shale in some wells.

The electrofacies is presented by a single spike of high gamma ray in wells of Strawberry Hill-1 and Dongara-8.

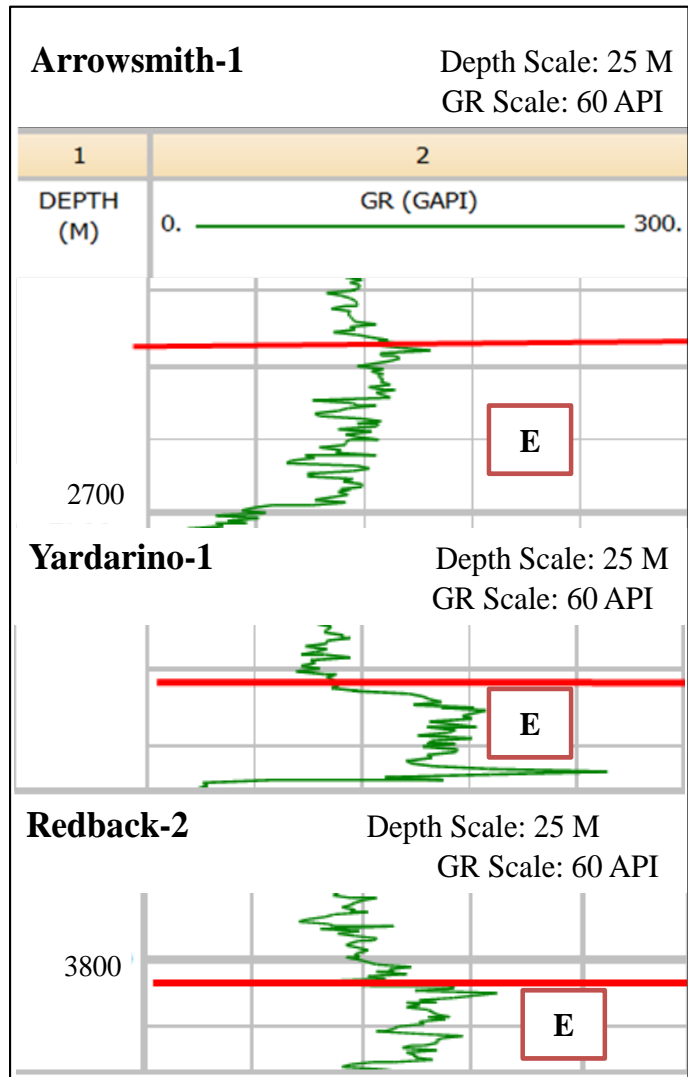
Lithofacies

There is not core available for the gamma ray response of electrofacies “E” in the wells of Arrowsmith-1 and Yardarino-1. Fossiliferous mudstone is dominantly presented in the cores of Redback-2 in the depth which electrofacies “E” is recognised.

Lithologically, the electrofacies is compound of shale/claystone and minor sandstone

Claystone: Dark grey-black, minor micro mica, occasionally silty with scarce pyrite, sub fissile to fissile, moderately hard.

Sandstone: Light to medium grey, fine-grained, calcareous cement; trace feldspar, silty/argillaceous matrix, moderately well sorted, sub angular to round, firm and poor porosity.



Appendix C.3

Electrofacies of the Carynginia Formation

Electrofacies of “A”

High gamma ray is seen for this electrofacies. The electrofacies has upward increasing trends and mostly forms the upper part of the Carynginia Formation.

Lithofacies

The Carynginia Formation in the Beekeeper -1 is mostly formed from limestone; however the high gamma ray value could be related to its component. There is no core available for the Woodada-1.

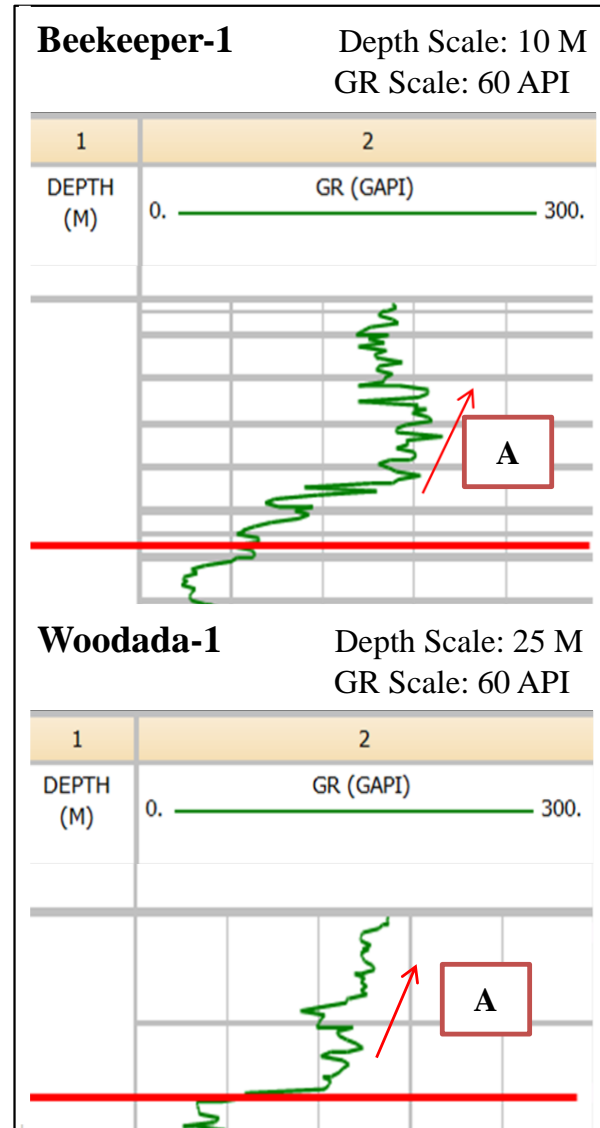
Lithologically, the electrofacies consists of shale/claystone with scarce interbedded limestone and sandstone.

Shale/claystone: Med-dark grey, very silty, trace pyrite, fine micaceous, hard to moderately hard, and sub fissile to fissile.

Sandstone: Greyish brown, very fine-grained, silty, rounded, hard.

Limestone: Greyish brown, light-dark grey, no visual porosity, fine grained to finely crystalline, calcarenitic.

Note: The lithologies of intervals are derived from well completion reports of the wells.



Electrofacies “B”

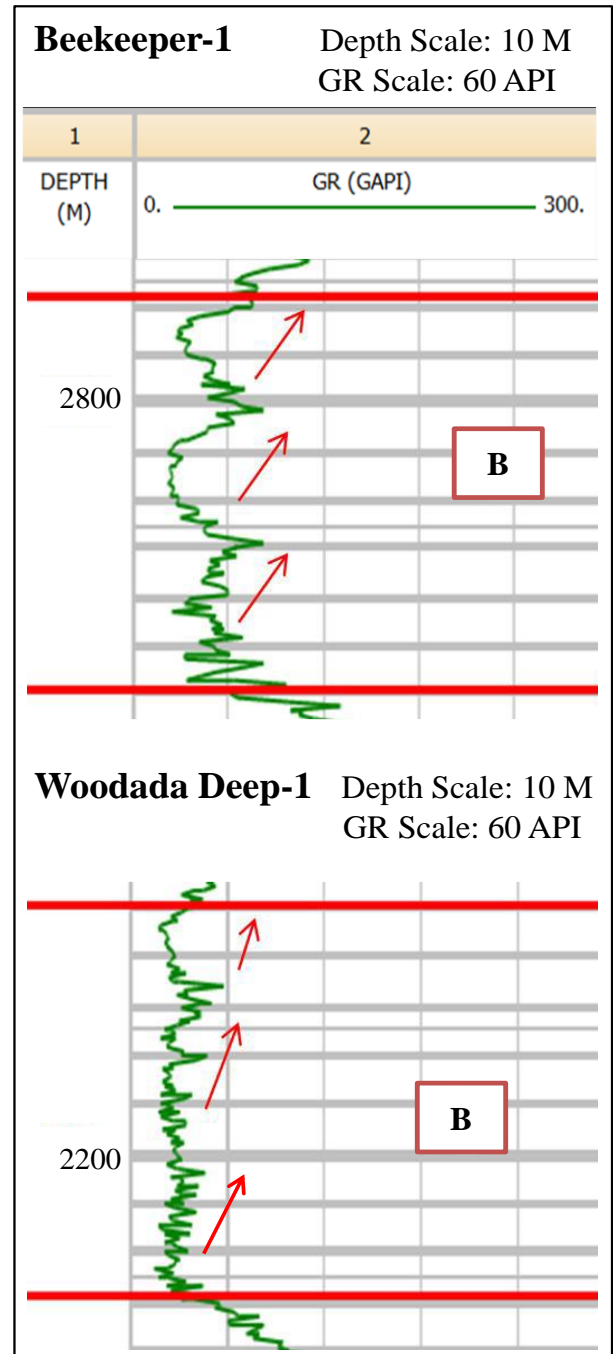
The electrofacies is determined based on its low gamma ray value, and it shows cycles of upward increasing trend. Electrofacies is related to the “Top limestone Member” of Carynginia Formation.

Lithofacies

The electrofacies is mainly formed from massive limestone lithology with thin interbeds of sandstone with minor shale.

Limestone: Various colours (cream to light brown mottled, white, and grey brown), calcarenitic, slightly pyritic, fossiliferous (bryozoan material constituting framework, traces of rugose coral fragments and brachiopods, minor dolomitization, hard and dense.

Sandstone: Without colour, light-grey, fine-medium grained, rarely coarse-grained, moderate to well sorted, sub angular to rounded.



Electrofacies “C”

The electrofacies formed from two parts, the low part has an increasing upward gamma-ray trend and the upper section has the upward decreasing gamma ray trend.

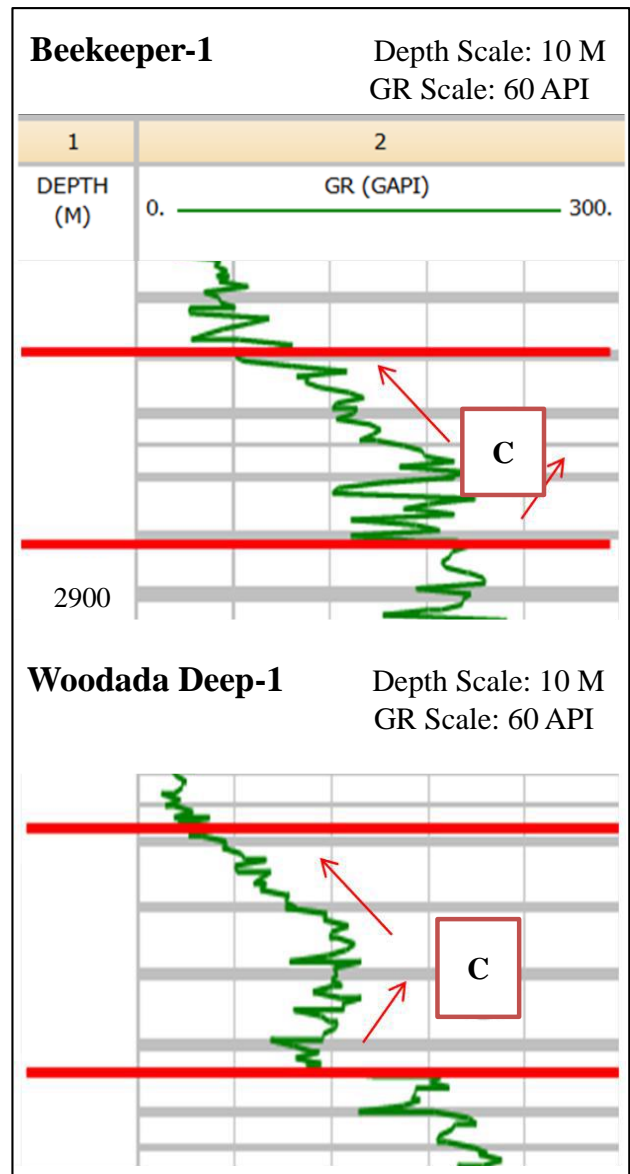
Lithofacies

There is no core available for this electrofacies in the Beekeeper-1 and Woodada Deep-1. However, there is some information about its composition in the reports which shows the electrofacies is mainly contain shale and siltstone.

Shale: Black, trace pyritic, blocky to sub fissile, slightly calcareous.

Siltstone: Dark grey-black, argillaceous, pyritic, firm to moderately hard

Sandstone: Light grey-grey, fine-grained, occasionally medium grained, moderately sorted, sub angular to sub rounded.



Electrofacies “D”

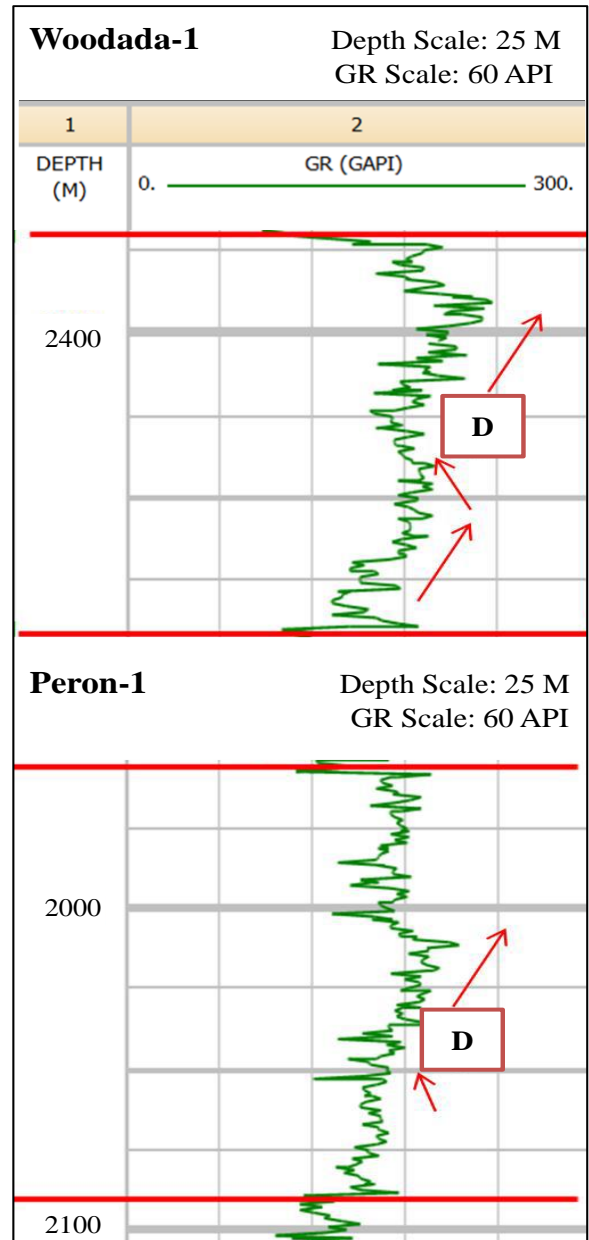
This electrofacies is comparatively thick, and shows an overall upward increasing trend. Nevertheless, some upward decreasing upward trend is presented in the middle of the electrofacies.

Lithofacies

There is no core data available for the Woodada-1 and Peron-1. Therefore, the information from well reports was used in order to realise the lithology of the electrofacies. The electrofacies consists of claystone/shale with slightly sandstone.

Claystone/shale: Medium dark grey-black, silty and grades to siltstone in part, slightly calcareous, minor micro mica, sub blocky to sub fissile, firm to moderately hard.

Sandstone: Medium grey, fine-grained, silty matrix, argillaceous, calcareous cement, firm to moderately hard, sub angular to sub rounded, poor visible porosity.



Electrofacies “E”

The electrofacies consists of both upward increasing and decreasing trends, and its shape is similar to the alphabet letter of “E”.

In some wells, there is a dramatic fluctuation in the electrofacies’ curve.

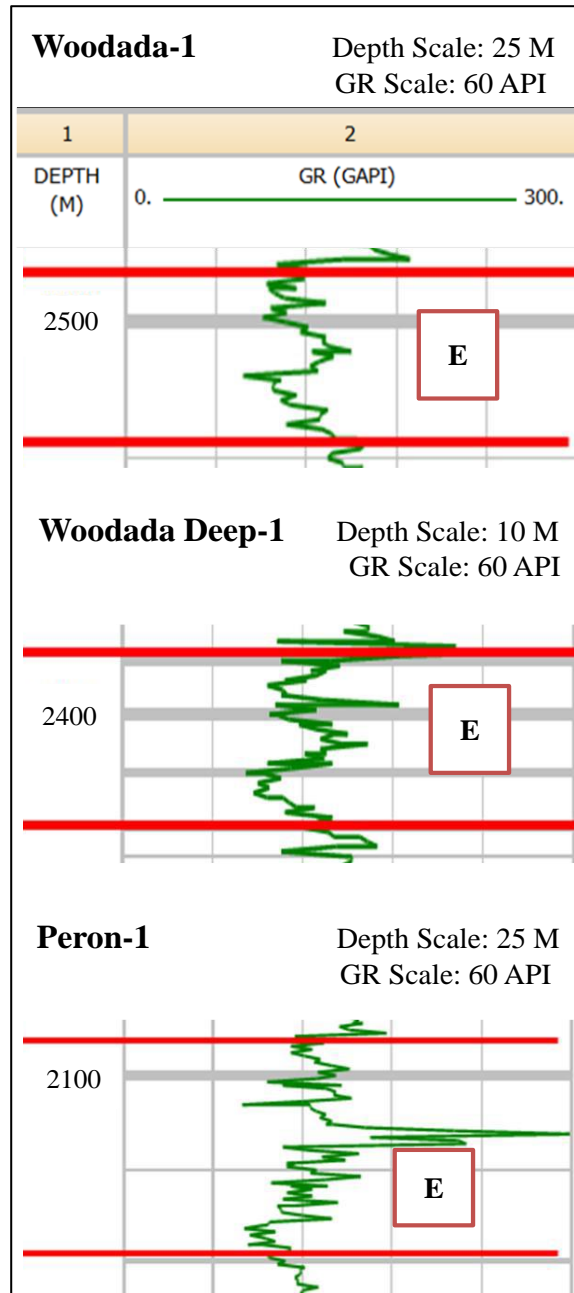
Lithofacies

There is no core data available for Woodada-1 and Peron-1. The lithofacies of bioturbated mudstone and fossiliferous mudstone are identified for the electrofacies “E” in the Woodada Deep-1.

Claystone and sandstone are components of the electrofacies. The presence of sandstone is possibly caused a reduction in the gamma ray value.

Claystone: Dark grey-black, silty, trace quartz inclusions, trace mica, sub blocky to sub fissile, soft to firm.

Sandstone: Light-medium grey, fine-grained with sporadically medium grains, trace lithics and mica, trace calcareous cement in part, siliceous cement, moderately sorted, sub angular to sub round, poor visible porosity and friable.



Electrofacies “F”

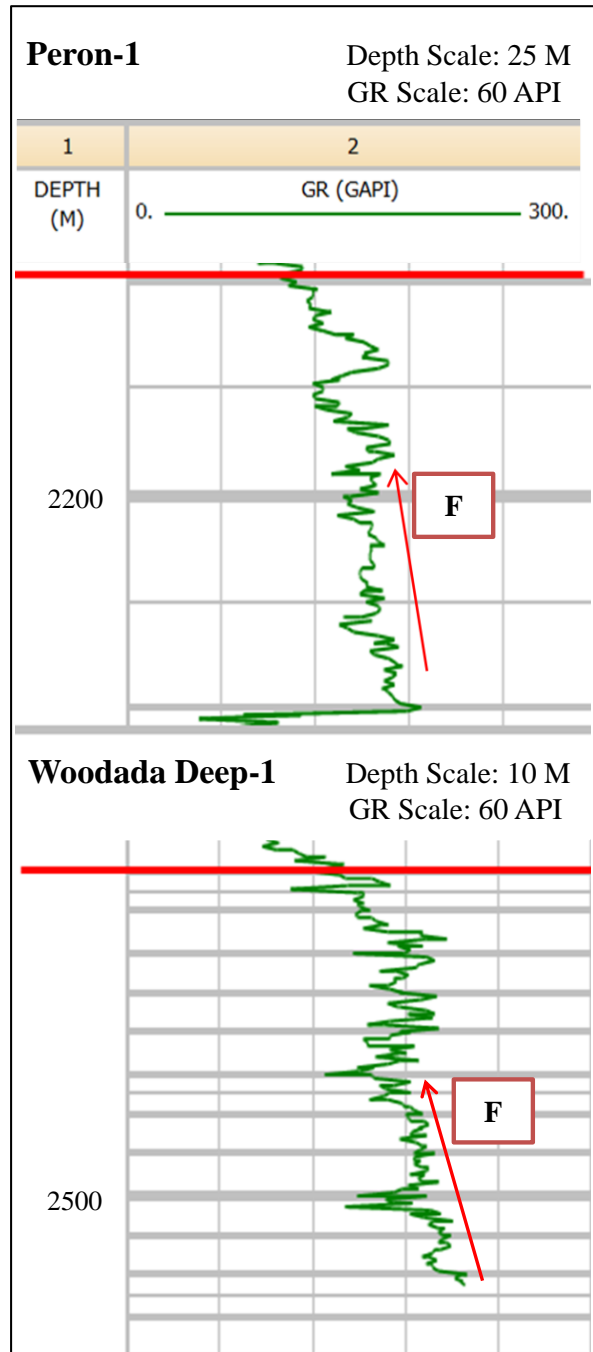
The electrofacies has the upward decreasing trend. The lithofacies is mostly in the lower part of Carynginia Formation. There are no measurements at these depths in the wells of Woodada-1, Beekeeper-1, and Indoon-1.

Lithofacies

There is no core data available for these depths at the wells of Peron-1 and Woodada deep-1. Lithologically, the electrofacies contains of clay stone with minor sandstone which their features described as follows

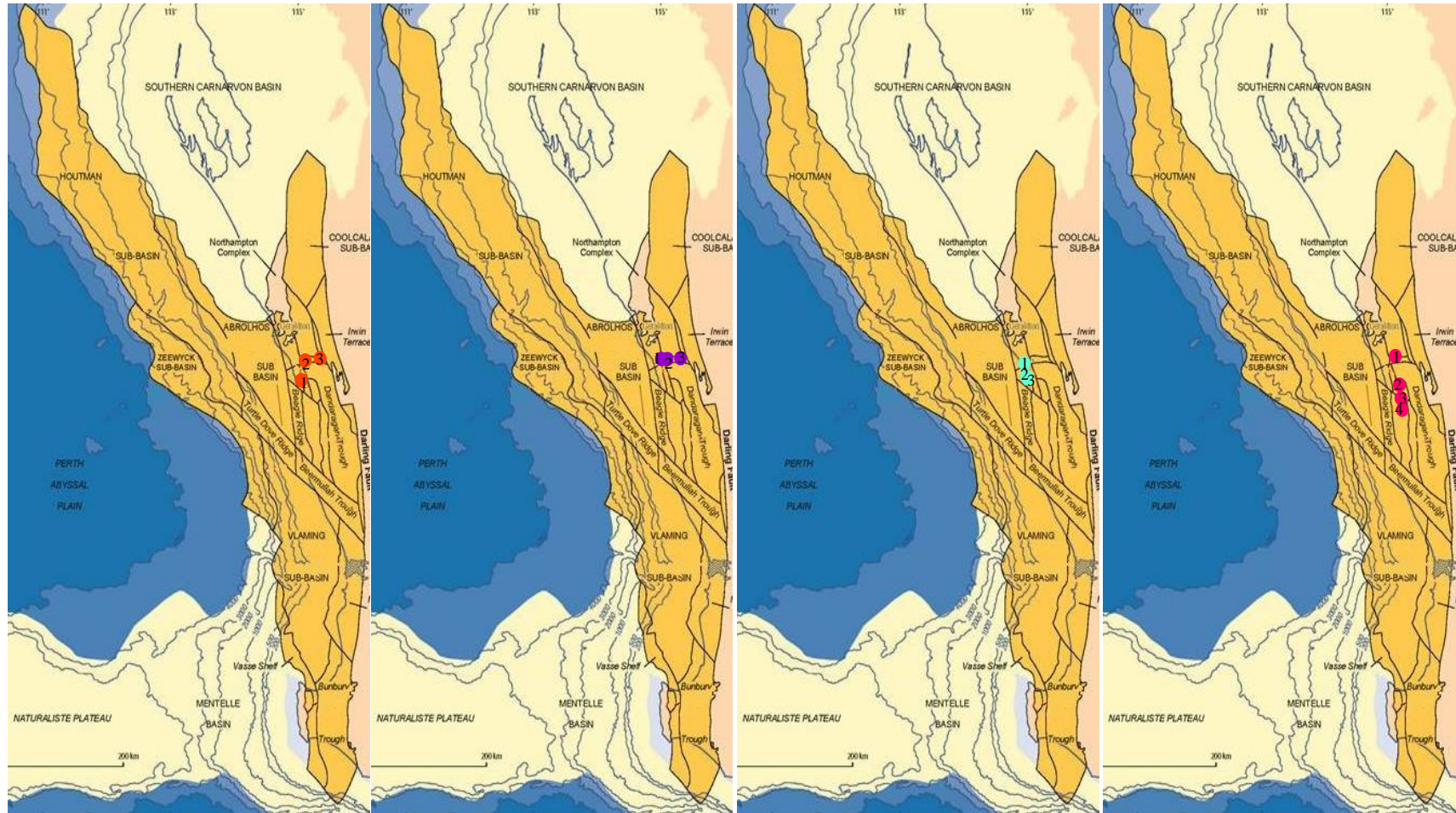
Claystone/shale: Grey-black, slightly calcareous, occasional micro mica, trace of quartz inclusion, silty in part, sub blocky to dominantly sub fissile, firm to moderately hard.

Sandstone: Light-medium grey, fine-grained, trace argillaceous matrix, siliceous cement, partly calcareous cement, well sorted, sub angular to sub round, poor visible porosity, firm to moderately hard.



Appendix C.4

Studied cross sections in the Kockatea Shale, Perth Basin



CS-A: (1) Robb-1 (2) Redback-2
(3) North Erregulla-1

CS-B: (1) Dongara-8 (2) Strawberry
Hill-1 (3) North Erregulla-1

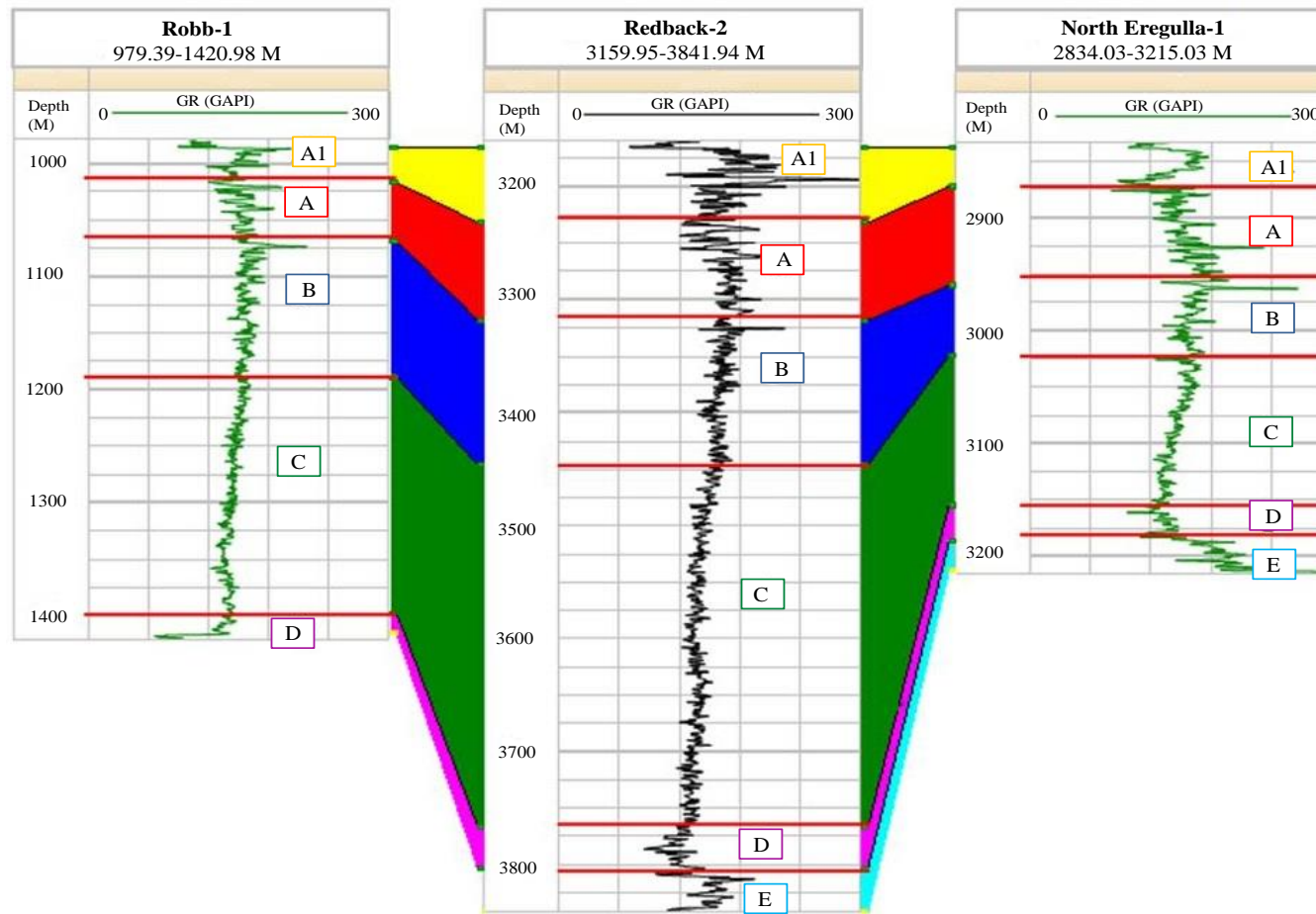
CS-C: (1) Jingemia-1 (2) Beharra-2
(3) Robb-1

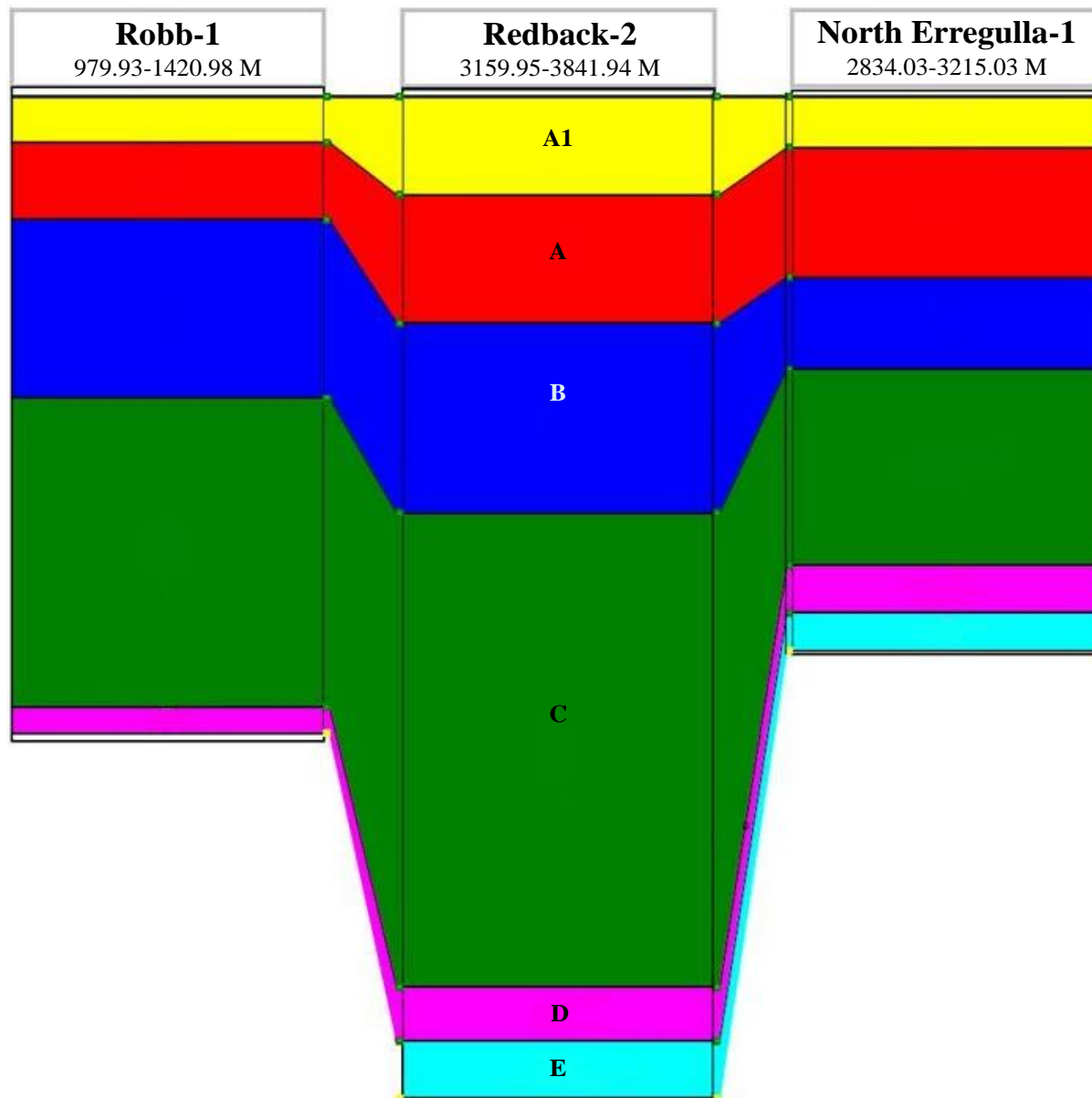
CS-D: (1) Yardarino-1 (2) Arrowsmith-1
(3) Woodada-1 (4) Peron-1

Appendix C.5

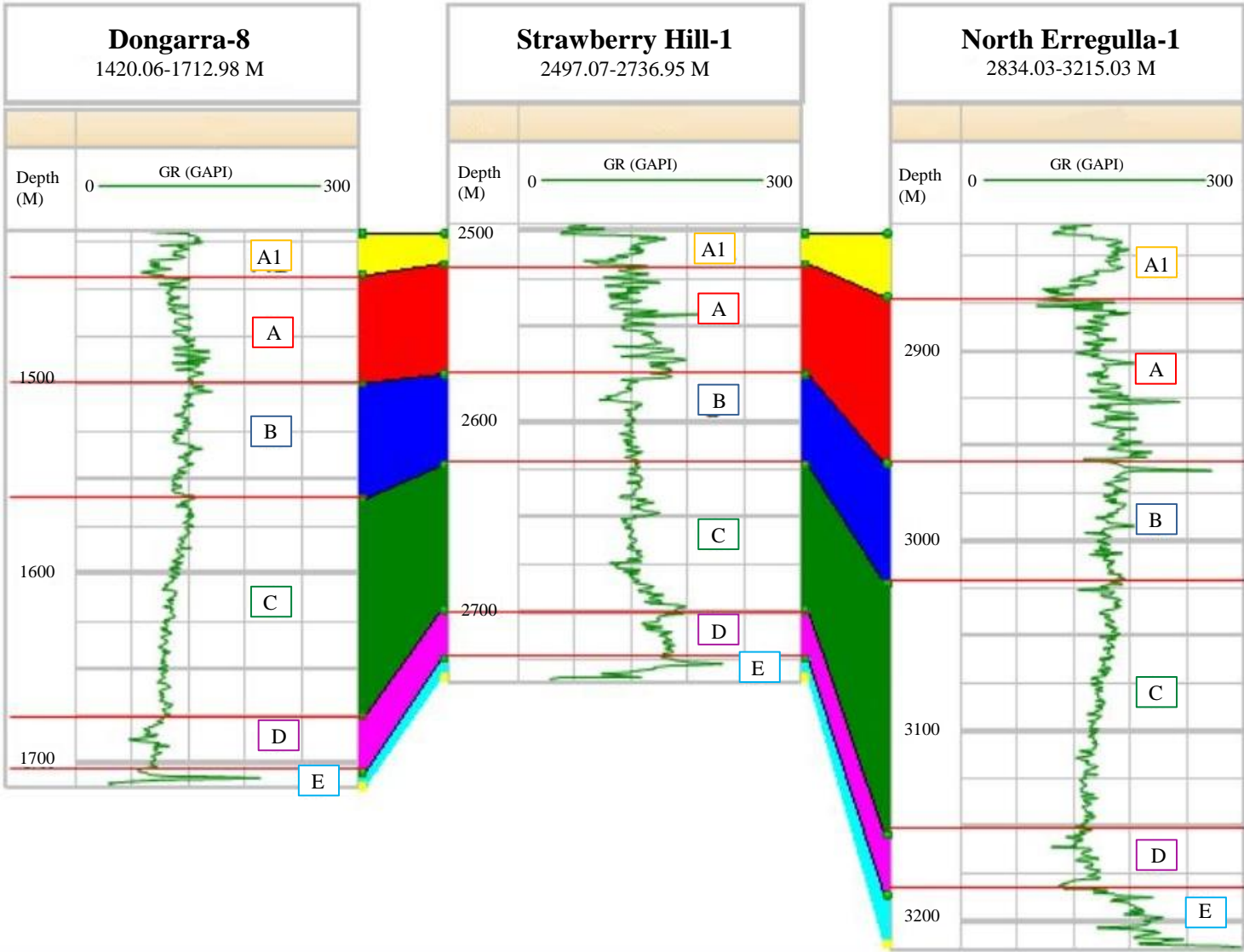
Correlation of the electrofacies in the Kockatea Shale across the Perth Basin

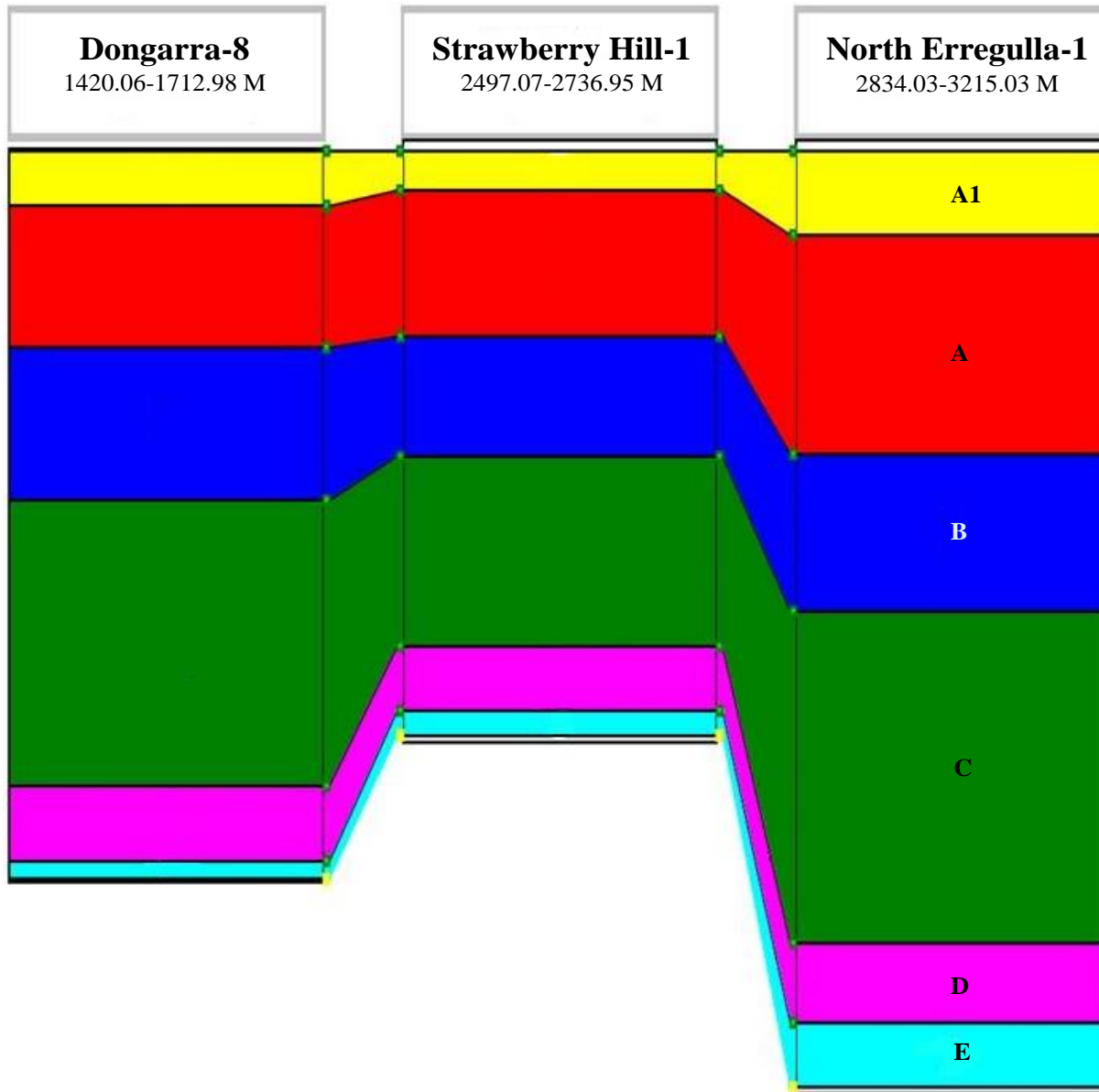
Cross Section-A



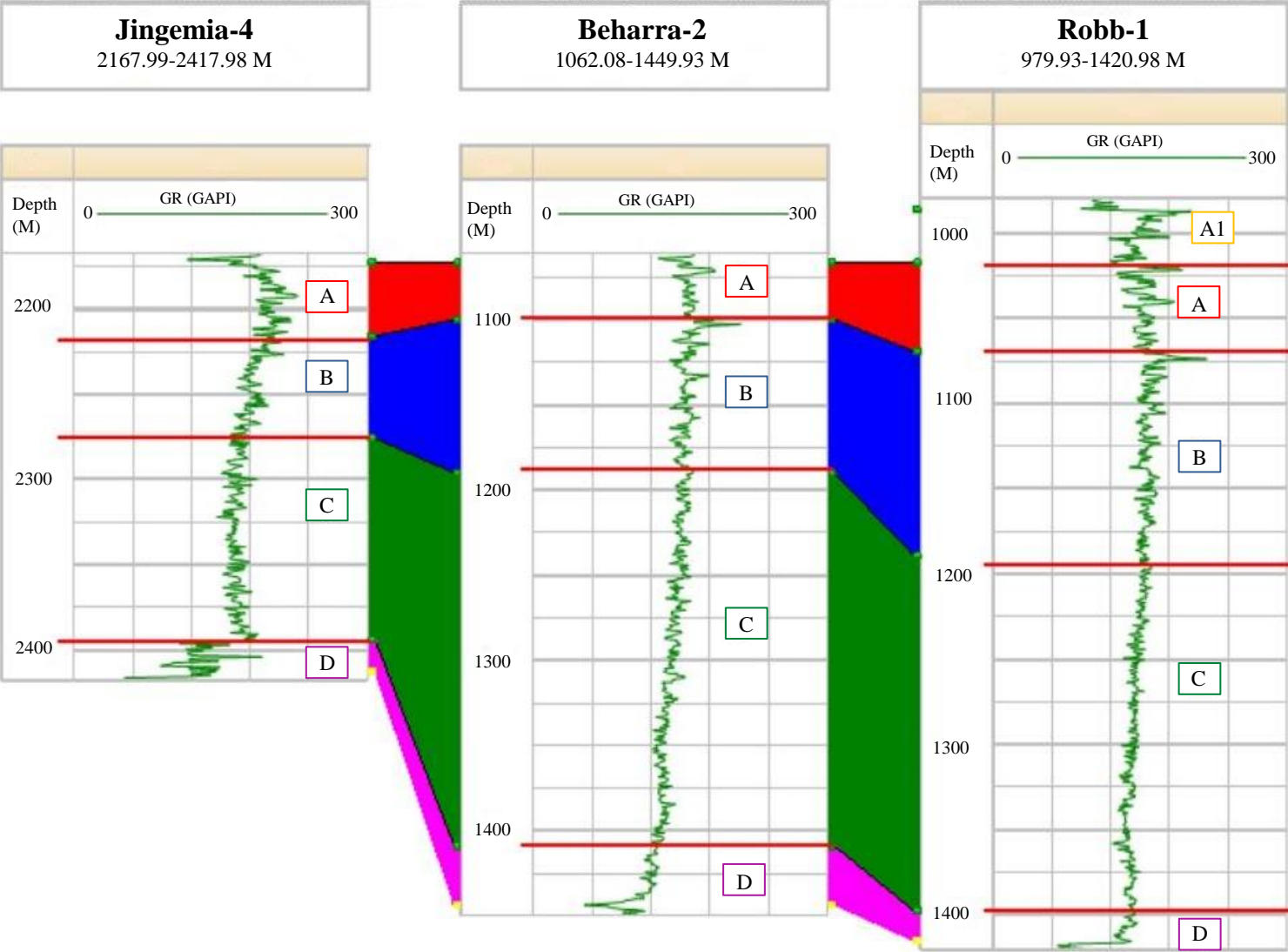


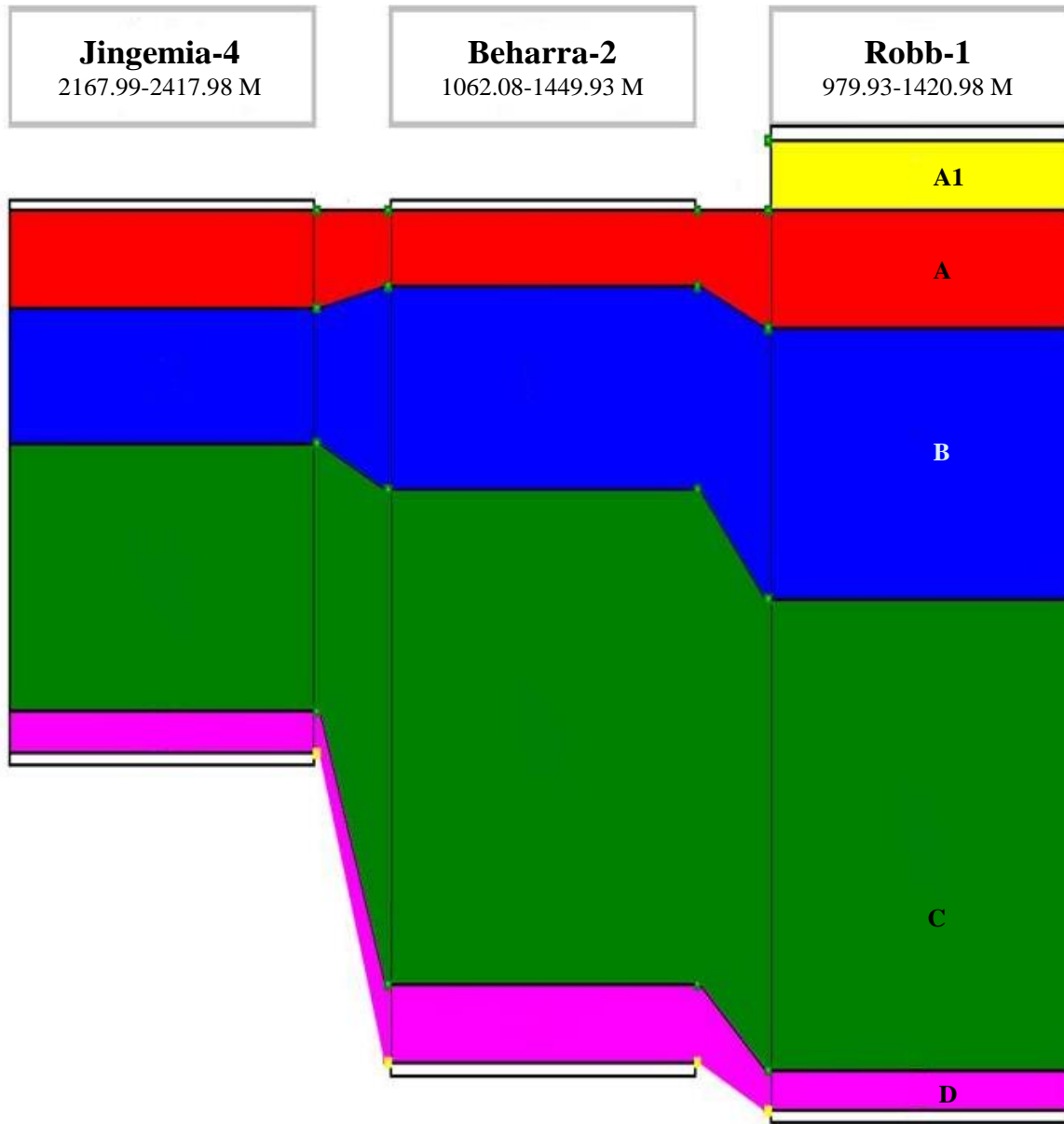
Cross Section-B



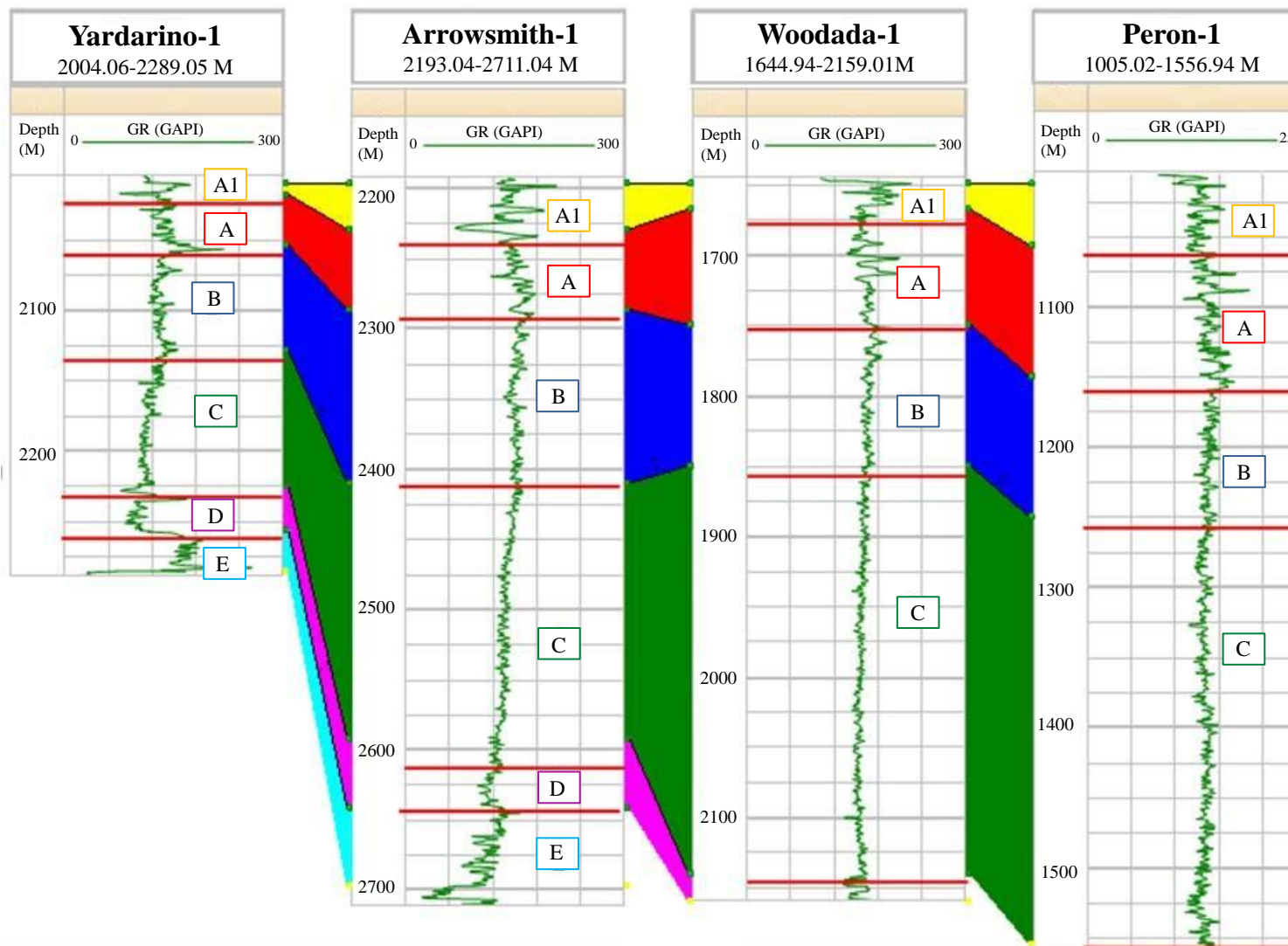


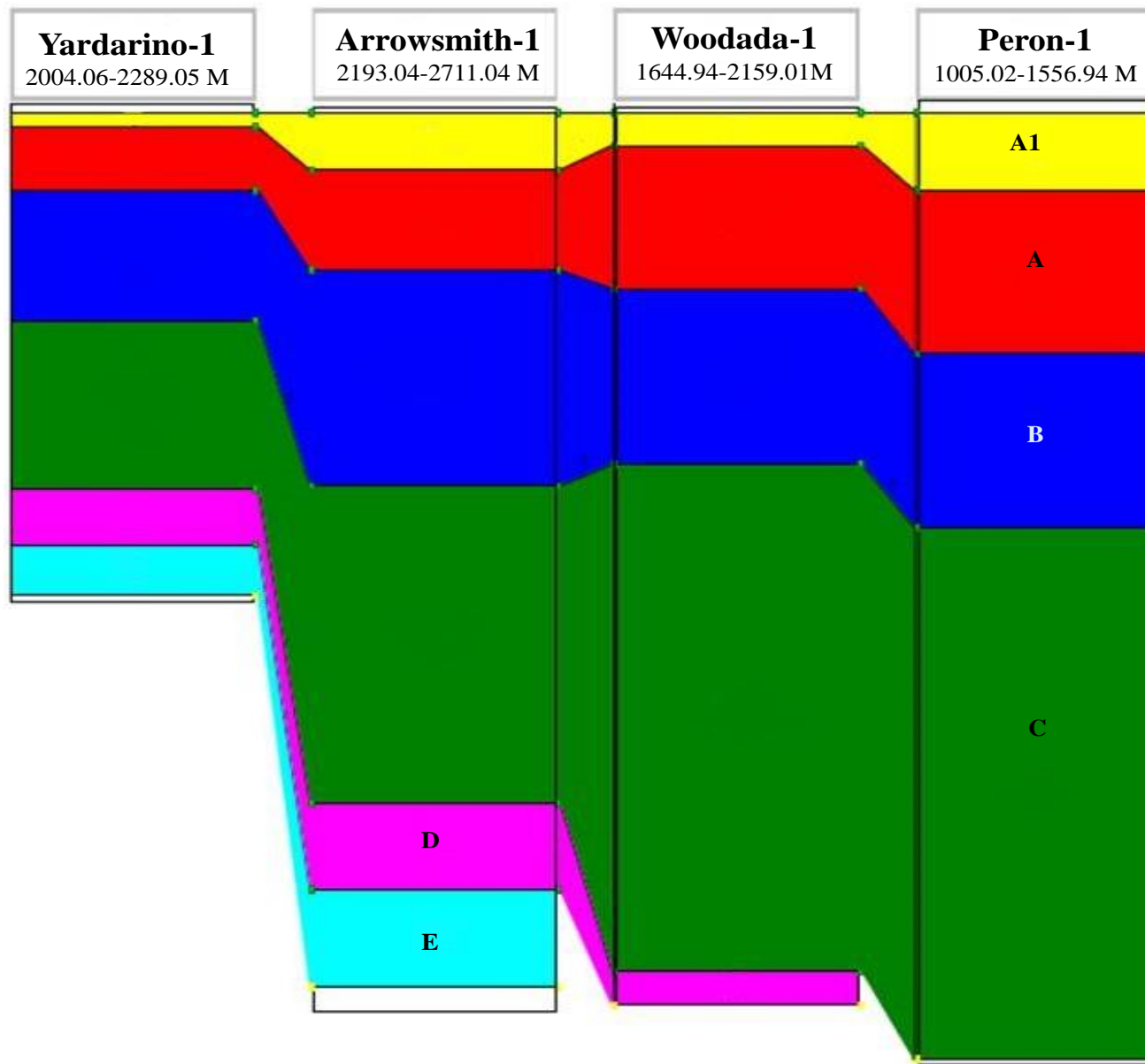
Cross section-C





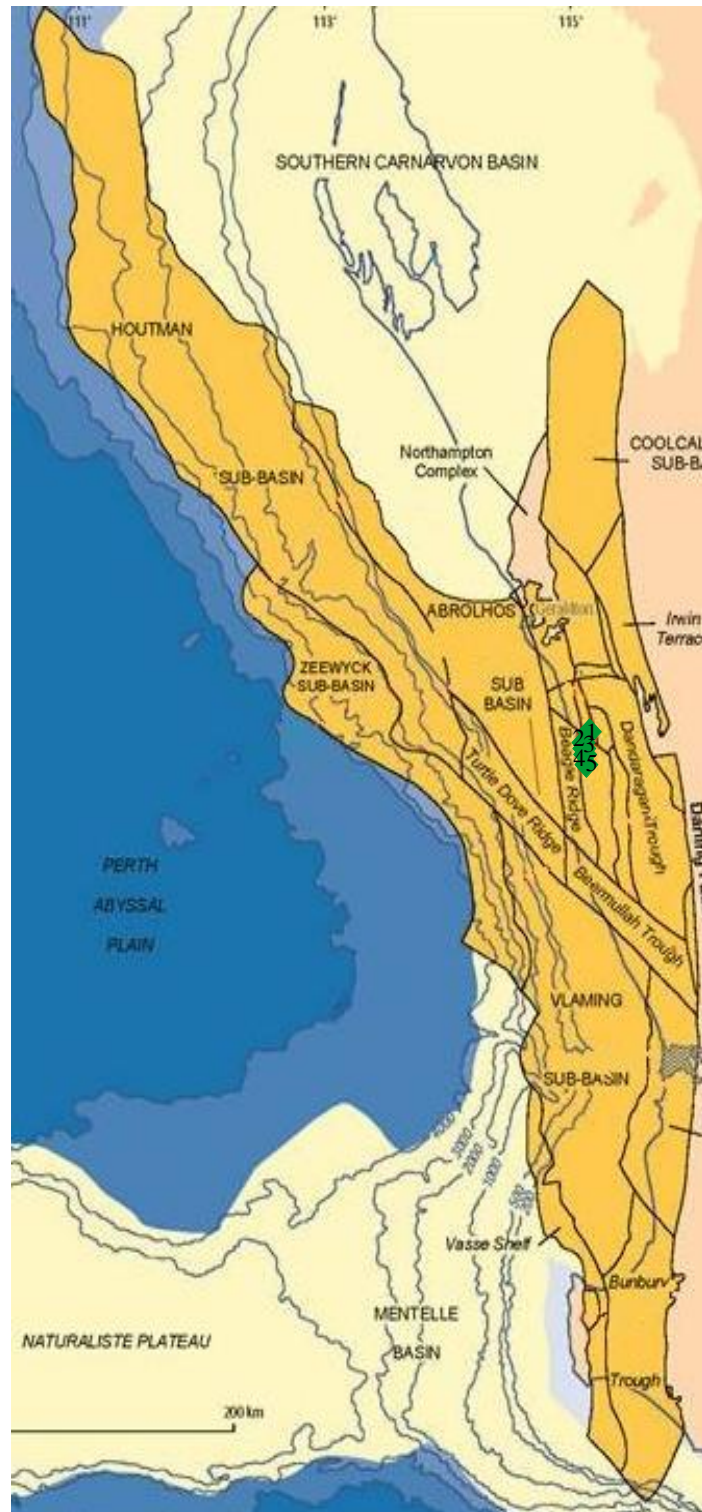
Cross section-D





Appendix C.6

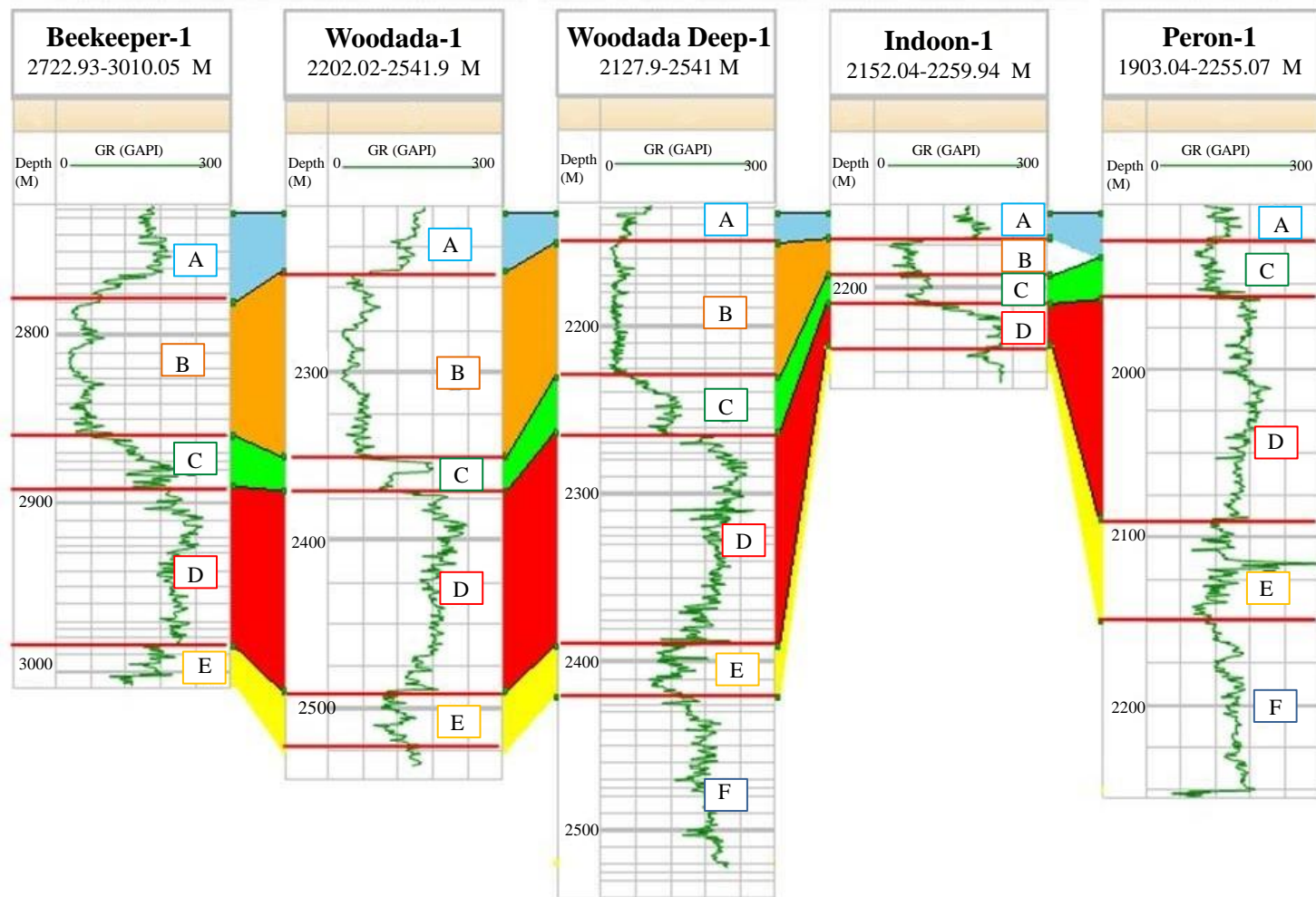
Studied cross section for the Carynginia Formation

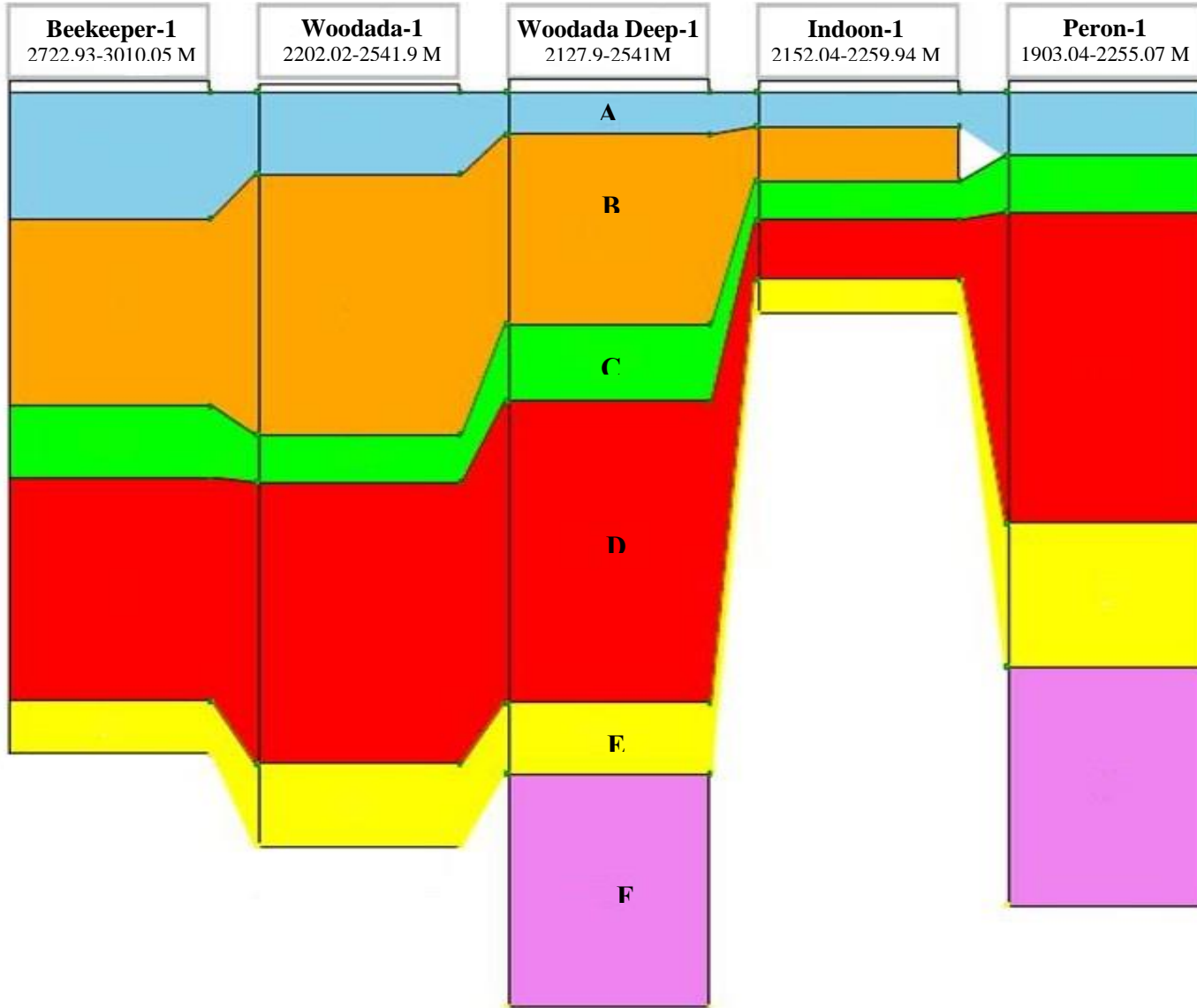


- (1) Beekeeper-1 (2) Woodada-1 (3) Woodada Deep-1
(4) Indoon-1 (5) Peron-1

Appendix C.7

Correlation of the electrofacies in the Carynginia Formation across the Perth Basin





Appendix C.8

TOC values of the Kockatea and the Carynginia formations in the Perth Basin, acquired by their geomechanical properties (Young's modulus and Poisson's ratio) from logs.

Well name	Formation	TOC-mean	Well Name	Formation	TOC-mean
Batavia-1	Kockatea	0.547	Batavia-1	Carynginia	3.237
Beharra-2	Kockatea	0.359	Beharra-2	Carynginia	0.819
Depot Hill-1	Kockatea	0.605	Depot Hill-1	Carynginia	1.927
Diamond Soak-1	Kockatea	0.389	Diamond Soak-1	Carynginia	F.T
Eurangoa-1	Kockatea	1.053	Eurangoa-1	Carynginia	4.307
Leander Reef-1	Kockatea	0.744	Leander Reef-1	Carynginia	F.T
Mondarra-1	Kockatea	0.404	Mondarra-1	Carynginia	0.173
Mt Horner-1	Kockatea	1.481	Mt Horner-1	Carynginia	12.281
Narlingue-1	Kockatea	0.202	Narlingue-1	Carynginia	4.241
Robb-1	Kockatea	0.524	Robb-1	Carynginia	F.T
South Turtle Dove 1B	Kockatea	0.359	South Turtle Dove 1B	Carynginia	0.375
Wittecarr-1	Kockatea	F.T	Wittecarr-1	Carynginia	0.652
Yardarino-1	Kockatea	3.166	Yardarino-1	Carynginia	1.046
Erregulla-1	Kockatea	0.466	Jurien-1	Carynginia	2.706
Geelvink-1A	Kockatea	0.407	Mt Adams-1	Kockatea	2.025
Mt Hill-1	Kockatea	1.751	North Erregulla-1	Kockatea	0.873
Strawberry Hill-1	Kockatea	1.219			

F.T: Fully Tracked